Biochemical properties of mutant GBA on alpha-synuclein metabolism

Laura Jane Smith

A thesis submitted for the degree of Doctor of Philosophy

Department of Clinical and Movement Neurosciences,

UCL Queen Square Institute of Neurology

University College London

2021

Declaration

I, Laura Jane Smith, confirm that the work presented in this thesis is my own. Where information has been derived from other sources, I confirm that this has been indicated in the thesis.

Abstract

Mutations in the *GBA1* gene are numerically the greatest risk factor for Parkinson disease (PD). The *GBA1* gene encodes for the lysosomal hydrolase enzyme, glucocerebrosidase (GCase), and mutations often lead to lysosomal impairment. The lysosome is important in the turnover of alpha-synuclein, the key hallmark for PD. The E326K mutation is one of the most common *GBA1* mutations and is proposed to have a minimal effect on GCase activity. Common mutations, L444P and N370S, are well documented loss of function mutations. It was hypothesised that *GBA1* mutations predispose patients to PD through influencing the relationship between GCase and alpha-synuclein, by altering the structural stability of GCase. The effect of the E326K mutation was characterised in human dermal fibroblasts, and demonstrated that it does not induce loss of GCase function, endoplasmic reticulum (ER) retention or ER stress, unlike L444P. Functional assays and proteolytic digestion analysis of recombinant GCase protein revealed minimal changes in stability across all mutants.

This was corroborated in undifferentiated and differentiated SH-SY5Y dopaminergic neuron-like cell lines over-expressing GCase variants. Undifferentiated SH-SY5Y also demonstrated a drastic increase in lipid droplet number and a modest increase of insoluble alpha-synuclein aggregates in E326K mutants. Differentiated SH-SY5Y neurons and human midbrain dopamine neurons differentiated from induced pluripotent stem cells were treated with alpha-synuclein pre-formed fibrils (PFF) to accelerate alpha-synuclein pathology. No change in aggregation was demonstrated by Homogeneous Time Resolved Fluorescence® (HTRF®) analysis in E326K neurons compared to control. In conclusion, the work presented here demonstrates that the E326K mutation

behaves differently to common loss of function mutations, however lipid dyshomeostasis and alpha-synuclein pathology is still evident.

Impact Statement

Mutations in the *GBA1* gene are numerically the greatest risk factor for Parkinson disease (PD). *GBA1*-associated PD (*GBA1*-PD) is indistinguishable from sporadic PD with wide spread alpha-synuclein pathology. However, it is often associated with an earlier age of onset and greater cognitive decline. The *GBA1* gene encodes for the lysosomal hydrolase enzyme, glucocerebrosidase (GCase), which cleaves glycosphingolipids. When in homozygous form, *GBA1* mutations cause the lysosomal storage disorder, Gaucher disease (GD). Mutations are characterised into mild and severe based on the level of residual activity of GCase. As not every GD patient develops PD, nor does every *GBA1* mutation carrier develop PD, a loss of GCase function cannot underlie the pathogenesis of *GBA1*-PD.

The E326K mutation occurs frequently, and does not cause clinical features of GD, yet increases risk for PD. The generally severe L444P mutation and generally mild N370S mutation were also included. The hypothesis that *GBA1* mutations lead to dysfunction of alpha-synuclein metabolism, through influencing its relationship with GCase was investigated. To do this the mechanisms underlying the E326K mutation were characterised in homozygous and heterozygous fibroblast cell lines, SH-SY5Y neuroblastoma cells and differentiated SH-SY5Y neurons. I identified that the E326K mutation does not work the same way as common loss of function mutations, L444P and N370S. There was also an absence of ER retention and ER stress. In neuroblastoma SH-SY5Y cell lines, I have demonstrated that the E326K mutation is associated with an alteration in lipid homeostasis, with a drastic increase in the accumulation of lipid droplets observed. In addition, SH-SY5Y cells with and without treatment with alpha-synuclein pre-formed fibrils were analysed to understand how alpha-

synuclein homeostasis was altered by *GBA1* mutations. I have shown that both E326K and L444P mutations lead to an increase in the presence of insoluble alpha-synuclein aggregates.

These findings have an impact for researchers working within the field of cell biology of *GBA1* mutations. The demonstration that the E326K mutation induces lipid metabolism alterations and alpha-synuclein pathology contributes to a growing body of literature that is concerned with uncovering the mechanisms contributing to the development of *GBA1*-PD. The dramatic increase in lipid droplets provide a novel insight into the underlying pathogenesis of the E326K mutation. The revelation that the level of insoluble alpha-synuclein aggregates in E326K cells was similar to that in the severe L444P cells contributes towards the plethora of literature showing alpha-synuclein is key in *GBA1*-PD pathogenesis. These findings link our research to disease relevant processes, and therefore may aid in the understanding of how *GBA1* mutations link to neurodegeneration.

The initial goal of this research was to unveil pathways that can be targeted for therapeutic intervention. The longer-term benefit would therefore be to patients affected by *GBA1*-PD. Communicating this research from academic to non-academic institutions will also be beneficial for all those directly and indirectly affected by the disease.

List of Abbreviations

AAV – Adeno-associated virus

AFM – Atomic force microscopy

ALP – Autophagy lysosomal pathway

ALR – Autophagic lysosomal reformation

ALS – Amyotrophic lateral sclerosis

ANT-2 – Adenine nucleotide translocator 2

ApoE – Apoliprotein E

ATP – Adenosine triphosphate

BBB – Blood-brain-barrier

BCA – Bicinchoninic acid

BDNF – Brain-derived neurotrophic factor

BiP – Binding immunoglobulin protein

BODIPY™ 493/503 – (4,4-Difluoro-1,3,5,7,8-Pentamethyl-4-Bora-3a,4a-Diaza-*s*-Indacene

BSA – Bovine serum albumin

Ca^{2+} - Calcium

Cas – CRISPR-associated protein

CBE - Conduritol B epoxide

cDNA – Complementary DNA

CHO – Chinese hamster ovary

CHOP – C/EBP Homologous Protein

CMA – Chaperone mediated autophagy

CMV - Cytomegalovirus

CNS – Central nervous system

COP – Coat protein complex

CRISPR – Clustered regularly interspaced short palindromic repeats

CSF- cerebrospinal fluid

CV – Column volumes

D2R – Dopamine receptor 2 subtype

D3R – Dopamine receptor 3 subtype

DAPI - 4′,6-diamidino-2-phenylindole

DAT – Dopamine transporter

DBS – Deep brain stimulation

dH_2O – Distilled H2O

DLB – Dementia with Lewy bodies

DMEM - Dulbecco's modified eagle media

DMSO – Dimethyl sulfoxide

DNA – deoxyribonucleic acid

DNJ – 1-deoxynojirimycin

DSG - Di(N-succinimidyl) glutarate

ECL – Electro-chemi-luminescence

eIF2-α – Eukaryotic initiation factor 2α

EM – electron microscopy

Endo H - Endoglycosidase H

ER – Endoplasmic reticulum

ERAD – ER-associated degradation

ERQC – ER quality control

ERT – Enzyme replacement therapy

FBS – Foetal bovine serum

FRET – Fluorescence resonance energy transfer

GAPDH - Glyceraldehyde 3-phosphate dehydrogenase

GBA1 – Glucocerebrosidase 1 gene

GBA1-PD – *GBA1*-associated PD

GBA2 – Non-lysosomal glucocerebrosidase gene

GBAP – GBA pseudogene

GCase - Acid-β-glucosidase enzyme

GD – Gaucher disease

GFP – Green fluorescent protein

GIRK2 – G-protein-regulated inward-rectifier potassium channel 2

GlcCer – Glucosylceramide

GlcSph – Glucosylsphingosine

GPNMB – Glycoprotein NMB

GSLs – Glycosphingolipids

HEK293 – Human embryonic kidney 293

HEPES – 4-(2-hydroxyethyl)-1-piperazineethanesulfonic acid

HMW – High molecular weight

HPLC – High-liquid performance chromatography

HRP – Horseradish peroxidase

HSP70 – Heat shock protein 70

HTRF – Homogenous time resolved fluorescence

iPSC – Induced pluripotent stem cell

IRE1 - Inositol-requiring enzyme 1

JNK – Jun N-terminal Kinase

Kb - Kilobase

kDa – kilodaltons

LAMP1- Lysosomal-associated membrane protein 1

LAMP2A – Lysosomal-associated membrane protein 2A

LB – Lysogeny broth

LC-MS – Liquid chromatography mass spectrometry

LIMP-2 – Lysosomal integral membrane protein type 2

LSD – Lysosomal storage disorder

M-Glu - 4-methylumbelliferyl-β-D-glucopyranoside

M6P - Mannose-6-phosphate

MeOH – Methanol

MPR – Mannose-phosphate receptor

MPTP - 1-methyl-4-phenyl-1,2,3,6-tetrahydropyridine

mRNA – Messenger RNA

N2a – Neuro 2A

NAC – Non-amyloid β component

NAD+ – Nicotinamide adenine dinucleotide

NADPH – Nicotinamide adenine dinucleotide phosphate

NaT – Sodium taurocholate

NEAA – Non essential amino acids

NGS – Normal goat serum

NMR – Nuclear magnetic resonance

OA – Oleic acid

OD – Optical density

OptiMEM – Opti-minimum essential medium

p-S129-alpha-synuckein – Phosphorylated alpha-synuclein

PBS – Phosphate-buffered saline

PBS-T – PBS-Tween

PC12 – Pheochromocytoma cell line

PCR – Polymerase chain reaction

PD – Parkinson disease

PERK – Protein kinase-like ER kinase

PFA – Paraformaldehyde

PFF – Pre-formed fibrils

PK – Proteinase K

RDP – Rabies derived peptide

rGBA – Recombinant GBA

RNA – Ribonucleic acid

RP – Reverse-phase

RPM – Revolutions per minute

SEM – Standard error of the mean

SNCA – Alpha-synuclein gene

SNpc - *Substantia nigra pars compacta*

SREBPS – Sterol regulatory element-binding proteins

SRP – Signal recognition particle

SRT – Substrate replacement therapy

TAGs – Triacylglycerols

TH – Tyrosine hydroxylase

ThS –Thioflavin S

ThT – Thioflavin T

TIM – Triosephosphate isomerase

TLRs – Toll-like receptors

Tm – Melting temperature

UPR – unfolded protein response

UPS – Ubiquitin proteosome system

Acknowledgements

It is my pleasure to thank my primary supervisor, Professor Anthony Schapira, for giving me the opportunity to study in his department, and for his consistent guidance and encouragement. Thank you for believing in me since I was an undergraduate student, and supporting me throughout my PhD.

I would like to express my thanks and appreciation to Dr Matt Gegg, for his commitment and dedication to my work. He has been a hands-on secondary supervisor and has provided me with consistent and insightful supervision. His expertise in the lab has been invaluable to me during my PhD and I truly believe I could not have gotten through the past 4 years without him.

I would also like to thank Dr David Chau, for all of his help and guidance throughout my time in the department.

I would like to extend my gratitude to Professor Vittorio Bellotti, Dr Guglielmo Verona and Dr Diana Canetti, who have offered insights and expertise in structural analyses. In particular, my thanks go to Dr Guglielmo Verona, who performed the purification of glucocerebrosidase and was instrumental to the execution of Chapter 4. He also generated alpha-synuclein pre-formed fibrils which were central to this study.

During my PhD, I have worked with many people. In particular, I would like to thank Miriam, Manuela, Soraya, Alyssa, Phil, John and Marco for being great friends and offering much entertainment and support throughout my PhD. I must also thank everyone in the Department of Clinical and Movement Neurosciences who have contributed toward generating a friendly and supportive research environment.

I cannot express how grateful I am to my Dad, Mam and brother, Daniel, who have been there for me over the past four years. It cannot be put in to words how appreciative I am to receive their consistent support and encouragement throughout my studies. I would also like to thank the rest of my family and all of my amazing friends; I could not have gotten through these last years without you all.

Thank you.

Table of Contents

List of Figures

List of Tables

1 General Introduction

1.1 Gaucher Disease

First described in 1882 by Phillippe Gaucher, Gaucher disease (GD) is the most common sphingolipidosis lysosomal storage disorder (LSD). GD is a rare, autosomal recessive disease. Among the general population, GD affects approximately 1 in every 50,000 live births. However, prevalence is higher among Ashkenazi Jews, with incidence increasing to approximately 1 in 800 live births (Horowitz et al., 1998, Charrow et al., 2000). The disease arises when mutations occur in the human glucocerebrosidase (*GBA1*) gene. This gene encodes for the lysosomal hydrolyse enzyme acid-β-glucosidase (GCase) (IUBMB enzyme nomenclature number EC 3.2.1.45). The role of GCase is to cleave glycosphingolipids (GSLs), glucosylceramide (GlcCer), into glucose and ceramide, and glucosylsphingosine (GlcSph), into glucose and sphingosine. GCase catalyses at optimal activity upon interacting with Saposin C, a co-factor, and negatively charged lipids (Grabowski et al., 1990).

Clinically, GD presents as the widespread accumulation of GlcCer and GlcSph within the lysosomes of many cell types, particularly macrophages, across several tissues and organs. These macrophages can infiltrate the spleen, liver and bone marrow leading to common GD-associated symptoms including thrombocytopenia, hepatosplenomegaly and anaemia. GD can be classified into three subtypes based upon the involvement of the central nervous system (CNS). Type 1 GD is the most common variant and can manifest at any age, this phenotype is normally referred to as non-neuronopathic as it doesn't usually have any CNS involvement. Types 2 and type 3 typically present a more severe clinical phenotype with disease onset occurring in early life and patients often dying young (Grabowski, 2008). These subtypes are often referred to as neuronopathic

as they affect the CNS. There is a wide spectrum of clinical manifestations across the entire GD subtypes, which suggests that there may be neurological involvement across the whole disease (Beavan et al., 2015).

Most mutations cause a reduction in GCase activity. Heterozygote carriers may retain up to 50% of the wild-type activity, with homozygotes having much lower activity (Alcalay et al., 2015). The exact pathogenesis of GD is still unclear; however, it is thought to involve mistrafficking of GCase protein, endoplasmic reticulum (ER) defects and lysosomal dysfunction.

The gold standard treatments for GD are enzyme replacement therapy (ERT) and substrate reduction therapy (SRT). ERT replaces GCase through administration of recombinant GCase enzymes, these enzymes often have modifications to their terminal mannose residues allowing for better targeting to and uptake into macrophages. SRT prevents the synthesis of GlcCer and GlcSph, helping to reduce substrate accumulation. Although successful, these therapies are unable to cross the blood-brain-barrier (BBB) and thus are ineffective against the neurological symptoms associated with GD, in particular type 2 and 3 (Maegawa et al., 2009).

1.2 Parkinson disease

Parkinson disease (PD) is the second most common neurodegenerative disorder. Over 1% of the population aged over 65 years are affected. The disease is characterised by the progressive loss of dopaminergic neurons in the *substantia nigra pars compacta* (SNpc) and the presence of intracellular proteinaceous inclusions, named Lewy bodies (Braak, 2017). PD patients exhibit a classic triad of motor symptoms including bradykinesia, rigidity and resting tremor. A spectrum of clinically significant non-motor symptoms has also been described. These

include cognitive decline, sleep disturbances, hyposmia and psychiatric symptoms (Balestrino and Schapira, 2020). It is suggested that at the onset of motor symptoms and PD diagnosis, dopamine neurons in the SNpc are reduced up to 60% (Marsden, 1990).

Lewy bodies are comprised of more than 300 proteins, with alpha-synuclein reported to be the most abundant (Spillantini et al., 1997, Wakabayashi et al., 2013, Shahmoradian et al., 2019). Electron microscopy (EM) analysis of alpha-synuclein reactive inclusions has revealed that Lewy bodies vary in morphology and heterogeneity. Within Lewy bodies there is an abundance of crowded membranous material, originating from vesicles and organelles; membrane and organelle fragments; lipids; alpha-synuclein and lysosomal and mitochondrial structures (Shahmoradian et al., 2019).

Braak et al., proposed a sequential model of Lewy body formation and deposition of alpha-synuclein (Braak et al., 2003). This starts at the dorsal motor nucleus of the glossopharyngeal and vagal nerves and anterior olfactory nucleus and then spreads progressively to involve the brain stem and the cortex (Braak et al., 2003).

The processes by which Lewy body pathology arises and their role in neurodegeneration remains elusive. The leading hypothesis suggests that intraneuronal alpha-synuclein first accumulates and aggregates, forming abnormal oligomers, which are then transformed into β-sheet rich amyloid fibrils. It is these fibrils that are the basis of Lewy bodies (Spillantini et al., 1998). The human alpha-synuclein sequence is highly conserved and can be divided into three regions: the N terminal, the non-amyloid β component (NAC) region and the C terminal. The N terminal region is thought to play a role in alpha-synuclein's

interaction with lipid membranes (Fusco et al., 2014). The NAC region is located at the central part of alpha-synuclein and is prone to forming β-sheet structures found in fibrils (El-Agnaf et al., 1998). The C terminal is a highly disordered and negatively charged region that is susceptible to post-translational modifications (Iyer and Claessens, 2019).

Whether alpha-synuclein oligomers or fibrils are the more toxic species remains unknown. Both have been shown to be toxic and it may be their differing sizes and shapes that lead to differences in reactivity and toxicity (Alam et al., 2019, Lashuel et al., 2013). Structural analysis studies suggest that oligomeric species and pre-fibril species are likely to represent the more toxic species leading to diseases (Chen et al., 2015). However, super-resolution and electron microscopy revealed that alpha-synuclein fibrils can affect the morphology and function of lysosomes in neural cells (Dilsizoglu Senol et al., 2021). A recent study in human induced pluripotent stem cell (iPSC)-derived neurons, rat primary cortical neurons and human neuroblastoma cells demonstrated that alpha-synuclein fibrils can have an immediate toxic effect due to the release of toxic oligomeric species (Cascella et al., 2021). Furthermore, incubation of Neuro 2A (N2a) cells with alpha-synuclein aggregates led to a retraction of neurite-like structures, lipid membrane damage and subsequent cytotoxicity (Melo et al., 2021). It also remains elusive whether Lewy body inclusions are toxic or if they are simply a marker of disease. However, in mice brains the areas affected by Lewy body inclusions show clear signs of dysfunction and degeneration (Luk et al., 2012).

Changes to conditions *in vitro*, including increasing protein concentrations, lead to alpha-synuclein assembling to form oligomers and fibrils (Lashuel et al., 2013). Once aberrant alpha-synuclein accumulates inside a cell it can either be degraded, deposited in inclusions such as Lewy bodies, or released into the

extracellular space. These processes may be related to failure of the cell to properly degrade alpha-synuclein. Alpha-synuclein is thought to be degraded by the autophagy-lysosomal pathway (ALP) (Cuervo et al., 2004, Martinez-Vicente and Cuervo, 2007). In human and mice brains with sporadic PD, there is evidence of autophagic and lysosomal dysfunction (Alvarez-Erviti et al., 2010, Dehay et al., 2010). This may lead to improper clearance of alpha-synuclein and its subsequent accumulation and aggregation. Another hypothesis arises from evidence of the uptake of extracellular alpha-synuclein fibrils by cells (Li et al., 2008, Kordower et al., 2008), which may propagate the spread of alpha-synuclein pathology and act as a template for misfolded, aggregated alpha-synuclein species.

The genetic link between alpha-synuclein and PD has also been studied extensively, with at least 30 mutations in the *SNCA* gene, the gene encoding the alpha-synuclein protein, found to cause PD. Several polymorphisms have been identified to lead to autosomal dominant forms of PD including point mutations such as A53T and A30P. Patients carrying the A53T mutation generally have an earlier age of onset and accelerated progression, whereas those with A30P are similar to sporadic PD (Schiesling et al., 2008). Biochemical studies have demonstrated that these mutations affect the *in vitro* mechanism of alpha-synuclein aggregation, with A53T aggregating more rapidly than A30P and wild-type alpha-synuclein, although the A30P variant aggregates more rapidly than wild-type (Li et al., 2001, Narhi et al., 1999). Expression of such variants in transgenic mice models highlights a toxic gain of function mechanism for mutated alpha-synuclein forms (Visanji et al., 2016). Although rare, point mutations in the *SNCA* gene are associated with high penetrance of PD. Additionally, multiplications of the *SNCA* locus are also associated with PD, including *SNCA*

duplications and triplications. These alterations correlate with disease severity, with patients harbouring *SNCA* triplications displaying a more severe phenotype than those with *SNCA* duplications (Cherian and Divya, 2020).

1.3 The link between *GBA1* mutations and Parkinson Disease

Towards the end of the 20th century, reports began to emerge associating GD and PD. This occurred because a number of type 1 GD patients developed parkinsonism (Turpin et al., 1988, McKeran et al., 1985). Since then, several large cohort studies have further investigated the link between *GBA1* mutations and the risk of developing PD (Bultron et al., 2010, Gan-Or et al., 2015, Sidransky et al., 2009, Tayebi et al., 2001). Further studies have indicated that approximately 5-10% of sporadic PD patients carry a *GBA1* mutation, with an overall odds ratio of 5.4 (Sidransky et al., 2009, Mata et al., 2008). This indicates that mutations in the *GBA1* gene are numerically the largest genetic risk factor for PD identified to date.

In the normal population, PD occurs in 3-4% of individuals. However, in type 1 GD patients this prevalence is increased. Carriers of *GBA1* mutations also harbour an increased risk of developing PD. Interestingly, there does not seem to be a difference between the risk associated with GD patients and carriers. It has been estimated that GD patients have a 9.1% chance of developing PD before age 80 years (Alcalay et al., 2014). Heterozygote *GBA1* mutation carriers are just as likely to develop PD before the age of 80, with a US study estimating 7.7% of carriers will develop PD (Anheim et al., 2012) and 15% in a UK cohort (McNeill et al., 2012). In one study of post mortem brains of PD patients, *GBA1* mutations were present in 12 of the 57 samples (21%) (Lwin et al., 2004). These were both homozygous and heterozygous mutations, further confirming that both types are associated with PD.

The frequency of *GBA1* mutations varies among different ethnic groups. In the European non-Ashkenazi Jewish population, it is 2.9-12%, whereas in the European Ashkenazi Jewish population it is 10-31%. This is much higher than in the general population, where <1% of healthy individuals are *GBA1* mutation carriers (Sidransky et al., 2009). In the Asian population, 1.8-8.7% of people have *GBA1* mutations, with 2.9-8% of North and South Americans having *GBA1* mutations (Migdalska-Richards and Schapira, 2016, Neumann et al., 2009).

It must be noted, however, that not every GD patient or *GBA1* mutation carrier will develop PD. Mutations in the *GBA1* gene do not cause a Mendelian form of PD, they are a genetic risk factor and increase the risk of developing PD 5-30-fold, depending on age, ethnicity and mutations included in analysis (Sidransky et al., 2009, Migdalska-Richards and Schapira, 2016, Lesage et al., 2011). Currently, studies are underway to assess prodromal symptoms of PD in large cohorts of *GBA1* mutation carriers to aid in earlier diagnosis and potentially allow researchers to predict who will go on to develop PD (Higgins et al., 2021). Furthermore, *GBA1* mutations have been associated with dementia with Lewy bodies (DLB), providing further evidence for a link between *GBA1* and alpha-synucleinopathies (Goker-Alpan et al., 2006, Mata et al., 2008).

1.4 *GBA1*-associated Parkinson disease pathology

GBA1-associated PD (*GBA1*-PD) is clinically non-distinguishable from sporadic PD, aside from an earlier age of onset (Sidransky et al., 2009, Lesage et al., 2011, Zhang et al., 2015, Gan-Or et al., 2010). On average, the onset of *GBA1*-PD is 5 years earlier than sporadic PD (Sidransky et al., 2009, Neumann et al., 2009, Gan-Or et al., 2008, Malek et al., 2018) and the onset of PD in GD patients is reported to be 5 years earlier than heterozygote *GBA1* carriers (Alcalay et al., 2014). Patients with *GBA1*-PD often have more advanced clinical decline, with a

greater risk for earlier and more prevalent cognitive impairment (Malek et al., 2018, Winder-Rhodes et al., 2013, Neumann et al., 2009, Sidransky et al., 2009, McNeill et al., 2012)

The pathology of *GBA1*-PD is identical to that of sporadic PD with nigrostriatal dopamine loss and the presence of deposits of aggregated alpha-synuclein in the form of Lewy bodies in the brainstem and cortex (Neumann et al., 2009, Westbroek et al., 2011, Goker-Alpan et al., 2006, Choi et al., 2011, Tayebi et al., 2003, Wong et al., 2004). Some reports suggest that brains from PD patients with *GBA1* mutations exhibit a more diffuse pattern of Lewy body distribution throughout the brain, compared to non-carriers (Nishioka et al., 2011). However, analysis of 33 PD patient brains disputed this and found no difference in Lewy body pathology between *GBA1*-PD and sporadic PD (Parkkinen et al., 2011).

Interestingly, in brain samples from 7 *GBA1* mutation carriers, who had a diagnosis of PD or Lewy body dementia, GCase was present in 32-90% of Lewy bodies, compared to non-mutation carriers where less than 10% of Lewy bodies were GCase positive (Goker-Alpan et al., 2010). A recent study also found that when analysing skin biopsies from PD patients, those with *GBA1* mutations had substantial intraneuronal alpha-synuclein deposits within sympathetic noradrenergic neurons (Isonaka et al., 2021). Further confirmation of a link between PD and the *GBA1* gene arose from a 2020 genome-wide association study. Analysis of the alpha-synuclein gene, *SNCA*, identified a polymorphism that was associated with an increased likelihood of developing PD in *GBA1* carriers (Blauwendraat et al., 2020). The same polymorphism was associated with accelerated motor decline in *GBA1*-PD patients, suggesting a role for alpha-synuclein in disease severity (Stoker et al., 2020a).

Much like sporadic PD, *GBA1*-PD exhibits the triad of cardinal motor symptoms (Goker-Alpan et al., 2008). However, it has been suggested that PD patients with *GBA1* mutations may present a worsened motor phenotype (Malek et al., 2018), and progression of motor symptoms may be more rapid in these individuals (Brockmann et al., 2015, Winder-Rhodes et al., 2013). Non-motor symptoms have been reported to be more common and severe in *GBA1*-PD compared to non-carriers. These include reduced cognition, depression, sleep disturbances and anosmia (Gan-Or et al., 2015, McNeill et al., 2012, Brockmann et al., 2011). A recent cohort study found that PD patients with *GBA1* mutations had earlier and more frequent onset of non-motor symptoms than those without *GBA1* mutations (Petrucci et al., 2020).

Cognitive decline is thought to develop sooner in PD patients with *GBA1* mutations (Brockmann et al., 2015, Zhang et al., 2015, Alcalay et al., 2012, Winder-Rhodes et al., 2013). Analysis of patients with homozygote or heterozygote *GBA1* mutations, but no clinical evidence of PD, revealed that these patients exhibit the prodromal features associated with *GBA1*-PD, including reduced cognition, olfaction and motor abnormalities (McNeill et al., 2012). A 2-year follow up study showed a deterioration of these symptoms (Beavan et al., 2015).

It has also been suggested that autophagic defects may contribute to the mechanisms associated with *GBA1*-PD (Magalhaes et al., 2016, Schöndorf et al., 2014) (see Chapter 1.8.2). This is similar to reports in other forms of familial PD including those with LRRK2 mutations (Orenstein et al., 2013) and ATP13A2 mutations (Usenovic et al., 2012).

1.5 Mutations in the *GBA1* gene

The *GBA1* gene is located on chromosome 1 (1q21) and is made up of 11 exons. The *GBA1* gene encodes for GCase, a lysosomal membrane-associated glycoprotein. To date, approximately 300 pathogenic mutations in the *GBA1* gene have been identified (Hruska et al., 2008, Beutler et al., 2004). These include substitutions, insertions, deletions and complex alleles. The most prevalent mutations are missense mutations. Some *GBA1* mutations arise from genetic rearrangements and deletions between the functional *GBA1* gene and a highly homologous pseudogene (*GBAP*). *GBAP* has the same orientation as *GBA1* and shares 96% exonic homology (Hruska et al., 2008). *GBAP* lacks large segments of deoxyribose nucleic acid (DNA) in introns 2, 4, 6 and 7, spanning 55 base pairs (Horowitz et al., 1989). Recombinant alleles are common in *GBA1* through cross-over between *GBA1* and *GBAP* (Dandana et al., 2016, Winfield et al., 1997, Sidransky et al., 2009).

The degree of PD pathogenicity associated with each individual *GBA1* mutation differs. Some mutations have been stratified into mild or severe mutations. The severity of a *GBA1* mutation is related to its effect on enzymatic activity and a recent study suggested that GCase activity in the blood of *GBA1*-PD patients inversely correlates with the clinical severity of the mutation (Huh et al., 2020). Severe mutations are associated with an earlier age of onset and greater odds ratio for developing PD compared to mild mutations (Gan-Or et al., 2015, Neumann et al., 2009, Lesage et al., 2011), and may be associated with a higher burden of symptoms and greater cognitive decline (Petrucci et al., 2020). PD odds ratios range between 2.84-4.94 for mild mutations and 9.92-21.29 for severe *GBA1* mutations (Gan-Or et al., 2015). Patients with severe *GBA1* mutations are also thought to be at a greater risk of dementia (Cilia et al., 2016).

Disease-causing mutations occur across the whole GCase protein (Smith et al., 2017) (see Figure. 1)**.** A summary of the penetrance of the most common *GBA1* mutations can be found in Table. 1. The L444P and N370S mutations are among the most common PD causing *GBA1* mutations, accounting for approximately 50% of *GBA1*-PD patients in the Ashkenazi Jewish population and 3% in the non-Ashkenazi Jewish population (Neumann et al., 2009, Sidransky et al., 2009). Both of these mutations have been associated with a loss of GCase activity *in vitro* (Grace et al., 1994, Horowitz et al., 2011, Montfort et al., 2004). The L444P mutation is referred to as a severe mutation as it generally causes a severe GD phenotype, with neurological involvement. This mutation has an odds ratio of 9.68 for PD (Sidransky et al., 2009), and is associated with higher diseases penetrance and a worse clinical phenotype. On the other hand, the N370S polymorphism is generally a milder variant, associated with a lower odds ratio for PD (3.30) compared to L444P (Sidransky et al., 2009). This mutation usually causes a mild, type 1 non-neuronopathic GD. However, this mutation has been associated with clinical heterogeneity. Individuals with the N370S genotype have presented a wide range of symptom severity, with some cases associated with early disease onset and severe clinical manifestation (Fairley et al., 2008, Zhang et al., 2012). According to one study, N370S alone is reportedly the most prevalent mutation in GD patients with early onset parkinsonism (Tayebi et al., 2003).

Some *GBA1* polymorphic variants like E326K are referred to as risk variants due to the observation that they do not present any clinical features of GD when homozygous, yet increase the risk for developing PD in both homozygous and heterozygous form (Duran et al., 2013, Chabas et al., 2005, Liou and Grabowski, 2012). The odds ratio for E326K and PD is between 1.5-1.99 (Ran et al., 2016,

Berge-Seidl et al., 2017, Huang et al., 2018, Stoker et al., 2020b). E326K is believed to be one of the most prevalent *GBA1* mutations in PD patients (Berge-Seidl et al., 2017, den Heijer et al., 2020, Ruskey et al., 2019). Patients carrying the E326K mutation have been associated with accelerated development of dementia and aggressive motor symptoms (Davis et al., 2016). A recent cohort study found that risk variants such as E326K were associated with rapid onset of severe clinical symptoms, similar to those caused by pathogenic *GBA1* mutations (Stoker et al., 2020b). Furthermore, metabolic and neuroimaging studies of E326K patients suggested a more severe PD disease pathology, and demonstrate similarities with DLB even in carriers with minimal cognitive decline (Greuel et al., 2020). In addition to E326K, another *GBA1* variant known as T369M has been identified to not cause GD in homozygous carriers, however whether this mutation is associated with PD remains controversial (Mallett et al., 2016).

Very little is known surrounding the effects of the E326K mutation. Generally, the E326K mutation reduces GCase activity to a lesser extent than other pathogenic *GBA1* mutations (Alcalay et al., 2015, Alcalay et al., 2020, Liou and Grabowski, 2012, Horowitz et al., 2011, Grace et al., 1999). A list of studies investigating the effect of the E326K mutation on GCase activity can be found in Table. 2. Interestingly, when in a compound heterozygote with another *GBA1* mutation, including L444P and N370S, there is almost complete loss of enzyme activity (Chabas et al., 2005, Liou and Grabowski, 2012). The fact that E326K does not cause GD suggests that the pathogenic mechanisms of *GBA1*-PD are distinct from those of GD.

Table 1. Penetrance of specific *GBA1* mutations in PD and non-PD patients and odds ratio for PD associated with each mutation.

Combined refers to the combined penetrance in PD and non-PD patients. (n.d) refers to no data.

	% Allele frequency			Odds ratio
	PD	**Non-PD**	**Combined**	
Risk variant				
E326K	1.67% – 19.4% [a-d]	1.03% – 1.97% [c,d]	2.8% – 3.88% [a,d]	1.57 – 3.2 [a,c-f]
Severe				
L444P	0.09% - 20.8% [a,b,d,e,g-o]	0.09% - 18% [d,g-l]	0.06% - 18.8% [a,d,g-i,k,l,o,p]	0.96 – 28.8 [e,g,h,p-r]
84GG	0.03% - 4% [g,h,l,s]	0.17% - 2.1% [g,h,s]	0.39% - 0.56% [g,h,s]	4.8 – 40.6 [g,h]
V349L	0.11% - 0.95% [g,h]	0.09% - 0.7% [g,h]	0.15% [g,h]	1.8 – 35.4 [g,h]
D409H	0.09% - 0.31% [i,l,m]	n.d	n.d	n.d
Mild				
N370S	0.03% - 54.5% [a,b,d,g-o,s,t]	0.048% - 67.5% [g-i,k-m,s,t]	0.08% -71.8% [a,d,g-l,k,l,o,p,s,t]	1.5 – 6.79 [d,g,h,n,p]
R496H	0.16% - 8.3% [g,h,j,s]	0.02% - 1.6% [g,h,j,s]	0.18% - 0.33% [g,h,j,s]	n.d

a. (Stoker et al., 2020b)
b. (Lwin et al., 2004)
c. (Huang et al., 2018)
d. (Duran et al., 2013)
e. (Ran et al., 2016)
f. (Berge-Seidl et al., 2017)
g. (Gan-Or et al., 2008)
h. (Gan-Or et al., 2015)
i. (Lesage et al., 2011)
j. (McNeill et al., 2012)
k. (Bultron et al., 2010)
l. (Rosenbloom et al., 2011)
m. (Neumann et al., 2009)
n. (Anheim et al., 2012)
o. (Mata et al., 2008)
p. (Sidransky et al., 2009)
q. (Chen et al., 2014)
r. (Zhao et al., 2016)
s. (Aharon-Peretz et al., 2004)
t. (Chetrit et al., 2013)

Table 2. The effect of the E326K *GBA1* mutation on GCase activity.

Study	Activity (% of non-*GBA1* mutation carriers)	Sample/expression system used
(Montfort et al., 2004)	42.7%	Recombinant GCase expressed in Sf9 cells
(Horowitz et al., 2011)	76%	Recombinant GCase expressed in HeLa cells
(Duran et al., 2013)	"lower limit of normal range"	White blood cells
(Lwin et al., 2004)	100%	E326K/+ human brain
(Liou and Grabowski, 2012)	42%	Recombinant GCase
(Alcalay et al., 2015)	82%	Dried blood spots
(Grace et al., 1999)	56-67%	Recombinant GCase expressed in Sf9 cells
(Malini et al., 2014)	54%	Recombinant GCase expressed in HEK293 cells
(Torralba et al., 2001)	26%	Recombinant GCase expressed in COS-1 cells
(Ron and Horowitz, 2005)	25-30%	Recombinant GCase expressed in HeLa cells
(Alcalay et al., 2020)	81.6%	Dried blood spots

1.6 Effect of *GBA1* mutations on enzyme activity and trafficking

1.6.1 Native GCase polypeptide processing and trafficking

Native GCase is a glycoprotein comprised of 497 residues and has a molecular weight between 59 and 69 kilodaltons (kDa) depending on post-translational modifications (Bergmann and Grabowski, 1989). It is synthesised and folded in the ER, and shuttled through the Golgi, where it undergoes glycosylation, and is subsequently trafficked to the lysosome (Ron et al., 2010) (Ron and Horowitz, 2005).

The mature GCase structure consists of three non-continuous domains, as shown in Figure. 1. (Dvir et al., 2003), with many important residues discussed in detail in a 2017 review (Smith et al., 2017). Domain I consists of an antiparallel β-sheet, with two disulphide bridges which may aid proper protein folding (Dvir et al., 2003). Domain II resembles an immunoglobulin fold made up of 8 β-sheets and domain III is comprised of a $(\beta/\alpha)_8$ triosephosphate isomerase (TIM) barrel. Domain III is also where the active site is located, which is comprised of a catalytic dyad surrounded by several key residues, all thought to be important in stabilisation and docking of the substrate (Lieberman, 2011, Dvir et al., 2003). Seven of these residues are aromatic and are likely to have a role in substrate recognition (Chi et al., 1999) and there are three free cysteines (residues 126, 248 and 342) which may be essential for preservation of an active enzyme (Liou et al., 2006).

Another important aspect of the GCase protein structure are the flexible loops. Loops 1, 2 and 3 cap the active site; each are mobile and able to adopt varying conformations in respect to each other (Kacher et al., 2008). The specific conformations adopted by loops 1 and 3 control the shape of the active site (Offman et al., 2011) and are important for the functionality of the GCase enzyme

and its pH optima. The optimal pH for GCase is around pH 5 (Liou et al., 2006), consistent with its lysosomal function (Lieberman et al., 2007). When in acidic conditions, there is a substantial rearrangement of Loop 3 from an extended to an alpha-helical conformation, allowing GCase to bind to its substrates (Lieberman et al., 2009, Lieberman et al., 2007). A further shift in Loop 2, upon substrate binding, alters hydrogen bonding allowing the active site to become more accessible (Lieberman et al., 2007). This suggests GCase may operate under an induced-fit mechanism.

The GCase protein contains a leader peptide of 39 amino acids, which is recognised by a signal recognition particle (SRP) (Koch et al., 2003). GCase enters the ER through a translocation pore (Halic and Beckmann, 2005) and once inside, the leader peptide is trimmed (Dalbey and Wickner, 1985) and GCase becomes ER-membrane associated (Aerts et al., 1986a). In the ER, GCase undergoes oligosaccharide chain alterations, with 4 *N*-linked glycan sequences (Asn-x-Ser/Thr) added to the protein at positions Asn 19, 59, 146 and 270. There is a fifth *N*-linked glycosylation site at Asn 462, however this site is not occupied (Berg-Fussman et al., 1993). Analysis of recombinant GCase protein revealed that glycosylation may be key for the functionality of the enzyme, as GCase is internalised by macrophages through their mannose residues (Tekoah et al., 2013).

Occupancy of these sites by *N*-linked oligosaccharide chains is thought to be required for the production of a fully functioning GCase enzyme (Grace and Grabowski, 1990). Crystallisation of recombinant GCase protein revealed that the residues surrounding the active site are much more disordered when the protein lacks *N*-linked glycosylation (Liou et al., 2006). When Asn 19 is not occupied, an inactive enzyme is produced. Asn 146 has a key role in maintaining the

thermostability of GCase, whereas a lack of *N*-linked glycosylation at Asn 270 and Asn 462 reduces activity due to their close proximity to the catalytic dyad (Berg-Fussman et al., 1993). A previous study using molecular dynamic simulations also reported that optimal GCase structural orientations are required in the catalytic dyad for the enzyme to function at full capacity and *N*-linked glycosylation may be crucial to generate such conformations (Souffrant et al., 2020).

If correctly folded, the GCase protein will exit the ER in a coat protein complex (COP) II vesicle and is trafficked toward the cis-Golgi cisternae (Kuehn et al., 1998). The vesicles dock to allow assembly of a SNARE complex for fusion of the membranes and delivery of GCase to the Golgi (Springer and Schekman, 1998). Upon receiving GCase, the Golgi complex initiates further processing of the *N*-linked glycans while the protein is in transit from the cis- to the trans-Golgi (Braulke and Bonifacino, 2009). Unlike other lysosomal hydrolases, GCase does not acquire a mannose-6-phosphate (M6P) mannose-phosphate receptor (MPR) and thus, it's *N*-linked glycans are subject to further modifications (Takasaki et al., 1984). These changes lead to a variety of GCase glycoforms, with differing molecular masses (Bendikov-Bar et al., 2013).

To aid in its transport through the ER and Golgi toward the lysosome, GCase binds to the lysosomal integral membrane protein type 2 (LIMP-2) (Reczek et al., 2007). Generally, the transport of lysosomal enzymes from the secretory pathway is governed by MPRs, however in MPR knock-out mice embryonic fibroblasts (MEFs), GCase trafficking was not disrupted confirming the enzyme is trafficked by LIMP-2, and in LIMP-2 knock out MEFs GCase protein levels and activity were significantly reduced, accompanied by a lack of lysosomal localisation (Reczek et al., 2007). GCase and LIMP-2 associate at the ER, at a neutral pH, and

dissociate in the acidic environment of the lysosome (Reczek et al., 2007). Within the LIMP-2 structure is a histidine residue at position 172 which may be required for GCase binding. It is thought that His 172 acts as a pH sensor to regulate the association and dissociation of the two proteins (Blanz et al., 2010). GCase and LIMP-2 are thought to interact via two hydrophobic helical interfaces. The regions responsible for this interaction include three helices in domain II of LIMP-2 and a conserved 11 amino acid sequence within the GCase structure (Zhao et al., 2014, Liou et al., 2014).

```
1                                                   50
ARPCIPKSFGYSSVVCVCNATYCDSFDPPTFPALGTFSRYESTRSGRRME
51                                 84GG             100
LSMGPIQANHTGTGLLLTLQPEQKFQKVKGFGGAMTDAAALNILALSPPA
101                                                 150
QNLLLKSYFSEEGIGYNIIRVPMASCDFSIRTYTYADTPDDFQLHNFSLP
151                                                 200
EEDTKLKIPLIHRALQLAQRPVSLLASPWTSPTWLKTNGAVNGKGSLKGQ
201                                                 250
PGDIYHQTWARYFVKFLDAYAEHKLQFWAVTAENEPSAGLLSGYPFQCLG
251                                                 300
FTPEHQRDFIARDLGPTLANSTHHNVRLLMLDDQRLLLPHWAKVVLTDPE
301                      E326K                      350
AAKYVHGIAVHWYLDFLAPAKATLGETHRLFPNTMLFASEACVGSKFWEQ
351                N370S                 V394L     400
SVRLGSWDRGMQYSHSIITNLLYHVVGWTDWNLALNPEGGPNWVRNFVDS
401   DV09H                                 L444P   450
PIIVDITKDTFYKQPMFYHLGHFSKFIPEGSQRVGLVASQKNDLDAVALM
451                                                 497
HPDGSAVVVVLNRSSKDVPLTIKDPAVGFLETISPGYSIHTYLWRRQ
```

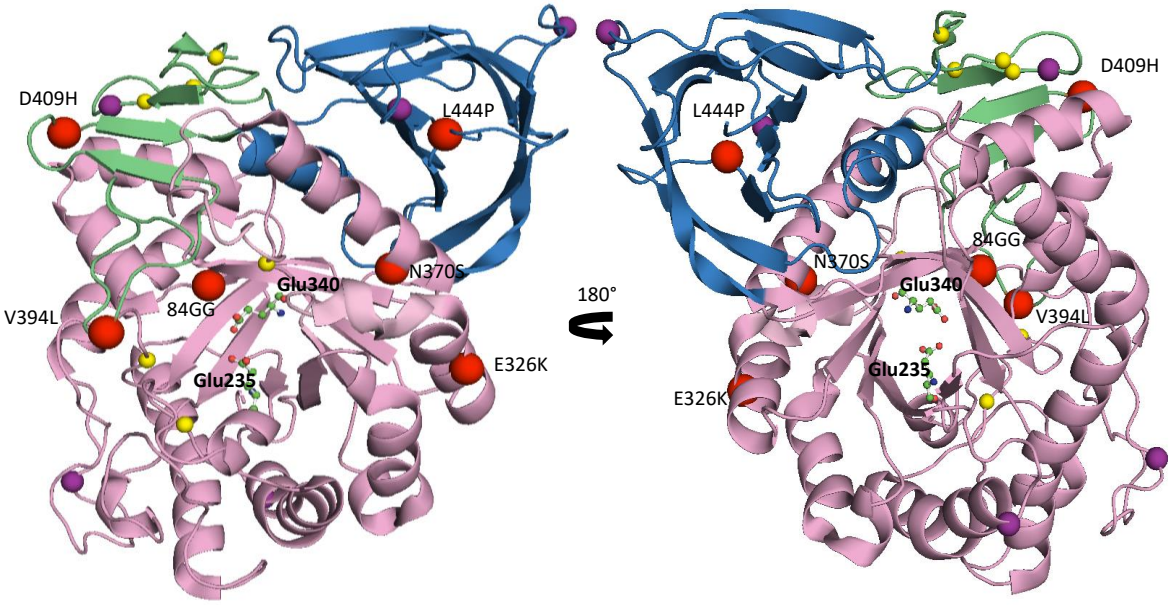

Figure 1. Crystal structure of glucocerebrosidase at pH 5.5 (PDB code 3GXI) created using PYMOL (http://www.pymol.org) and corresponding sequence.

Domain I is shown in green. Domain II is shown in blue. Domain III is shown in pink. The active site catalytic residues Glu 235 and Glu 340 are shown as ball-and-stick models or underlined in the sequence. The five *N*-linked glycosylation sites (Asn 19, Asn 59, Asn 146, Asn 270 and Asn 462) are shown as purple spheres or purple letters in the sequence. The free cysteine residues are shown as yellow spheres or yellow letters in the sequence. Six common *GBA1* mutations, L444P, N370S, E326K, 84GG, V934L and D409H are labelled as red spheres or red letters in the sequence.

1.6.2 Mutant GCase polypeptide processing and trafficking

Mutations in the *GBA1* gene can prevent proper processing and transport of GCase to the lysosome, with mutant GCase often retained in the ER (Schmitz et al., 2005, Zimmer et al., 1999, Ron and Horowitz, 2005). This is likely due to protein misfolding.

Aside from the N370S GCase protein, the X-ray structure of *GBA1* mutant proteins have not been resolved to accurately understand how they affect protein folding. The Asn 370 residue is located on the longest alpha-helix at the interface of domains II and III (Figure. 1.) (Smith et al., 2017), and may play a role in stabilising the conformation of the active site (Grace et al., 1994). Through hydrogen bond networks, Asn 370 stabilises loop 3 in the alpha-helical conformation required to accommodate the substrate. When a serine replaces the asparagine residue, GCase is misfolded and the distance between the residue and loop 3 increases. This results in destabilisation of loop 3 and impairs the ability of GCase to bind the substrate (Lieberman et al., 2007, Offman et al., 2011, Souffrant et al., 2020).

Although the X-ray structure of L444P is yet to be obtained, it is evident that the mutation occurs within domain II and is a considerable distance from the active site (Figure. 1.) (Smith et al., 2017), suggesting an important, yet unknown function for domain II. The substitution of leucine to proline is thought to cause rigidity in the protein backbone, potentially disrupting the hydrophobicity of the domain (Lieberman, 2011) which may influence protein folding. Furthermore, residues surrounding this mutation may interact with Saposin C, a GCase protein cofactor, with the L444P mutation potentially disrupting this (Atrian et al., 2008).

Polypeptides undergo ER quality control (ERQC) (Benyair et al., 2011). ERQC is integrated with stress response mechanisms, known as the unfolded protein response (UPR) (Liu and Ye, 2011), which prevents the exit of misfolded proteins into the secretory pathway by using recognition chaperones that interact with the peptide to sense correct folding. The UPR is initiated by the activation of stress sensors at the ER membrane, one of which is the double-stranded RNA-activated protein kinase-like ER kinase (PERK). The ER chaperone Grp78/binding immunoglobulin protein (BiP) recognises unfolded proteins in the ER lumen and activates PERK to transduce information about protein folding through controlling the expression of downstream transcription factors. Upon activation, PERK phosphorylates eukaryotic initiation factor 2α (eIF2-α), which then leads to an increase in the expression of the C/EBP Homologous Protein (*CHOP*) transcription factor in an attempt to reduce the overload of proteins at the ER (Mercado et al., 2013). Additional chaperones that have been shown to be important in regulating GCase folding in primary fibroblast models include Calnexin and heat-shock protein 70 (HSP70) (Ong et al., 2010, Fog et al., 2018).

If proteins are misfolded, they will undergo re-glycosylation, where glucose moieties are re-introduced to their *N*-linked glycans and enter the ERQC once again (Benyair et al., 2011, Parodi, 2000). If re-folding is unsuccessful, the misfolded protein will be re-translocated through the ER membrane to the cytoplasm where it is targeted by E3 ligases for polyubiquitination and degraded by proteasomes by the ubiquitin proteasome system (UPS) in ER-associated-degradation (ERAD) (Smith et al., 2011, Mercado et al., 2013).

Persistent presence of misfolded protein can saturate ERAD and lead to ER stress, activating the UPR in an attempt to protect the neuron (Colla et al., 2012a). This can eventually lead to apoptosis (Mercado et al., 2013).

Processing and trafficking of GCase protein is impaired in models of *GBA1* mutations. Endoglycosidase H (Endo H) analysis is a useful tool to distinguish between glycoproteins that have not reached the mid-Golgi and folded, processed, fully glycosylated mature protein. In wild-type fibroblast, the majority of GCase protein is endo H resistant, suggesting it has passed the mid-Golgi and is fully mature. Endo H analysis and immunocytochemistry in GD fibroblasts with L444P and N370S mutations demonstrate ER retention and an incompletely glycosylated GCase protein (Bendikov-Bar et al., 2011, Ron and Horowitz, 2005). Further studies have suggested that the extent of ER retention and improper processing may be correlated with GD disease severity (Bendikov-Bar et al., 2011, Bergmann and Grabowski, 1989, Beutler and Kuhl, 1986).

N-linked glycosylation has been proposed to play a role in the occurrence of the L444P mutation. Occupancy of Asn 19 stabilises regions 438-445 around the L444P mutation site, suggesting a lack of structural stability may influence mutations (Pol-Fachin et al., 2016). Targeting glycosylation therapeutically may aid in rescuing the instability of the L444P mutant protein.

Additionally, a plethora of evidence points toward ER stress accompanying *GBA1* mutations, with models demonstrating up-regulation of proteins involved with ERAD and UPR (Braunstein et al., 2018, Wang et al., 2011, Maor et al., 2013). In human dopamine neurons and *Drosophila* flies harbouring L444P and N370S mutations, the activation of ER stress pathways has been demonstrated (Fernandes et al., 2016, Sanchez-Martinez et al., 2016) (Schöndorf et al., 2014). Inhibition of GCase activity can elicit an ER stress response in neuroblastoma cells, indicating that enzyme activity may play a role independent of the presence of a pathogenic mutated protein (Kurzawa-Akanbi et al., 2012, Korkotian et al.,

1999). This suggests that ER stress may occur due to a combination of gain of function and loss of function mechanisms.

1.7 GCase activity and Parkinson Disease

Mutations in the *GBA1* gene can differentially affect GCase enzyme activity. Some mutations result in no residual activity, whereas others reduce activity (Grace et al., 1994, Liou et al., 2006, Alfonso et al., 2004). In GD, GCase activity is normally 10-20% of controls, whereas carriers can retain up to 50% (Migdalska-Richards and Schapira, 2016).

Post-mortem analysis of PD patient brains with heterozygous *GBA1* mutations, including L444P and N370S, revealed there is reduced GCase activity (Gegg et al., 2012). The greatest decrease, by 58%, was found in the SNpc. Analysis of the activity and expression of other lysosomal enzymes indicated that the decrease in GCase activity observed was specific and not due to a loss of lysosomal content or neuronal death. Analysis of activity in dried blood sports from patients carrying *GBA1* mutations, whether these be homozygote, heterozygote or compound heterozygote, revealed GCase activity was lower than non-carriers. Activity was at its lowest in homozygotes and compound heterozygotes (Alcalay et al., 2015).

In most cases, GCase activity does not correlate with disease severity, and the range of activity in severe and mild mutations may overlap (Sidransky, 2004). For example, the N370S mutation, which is normally associated with a mild GD phenotype, may exhibit lower activity than the severe L444P, N382K and G390R mutations (Liou et al., 2006, Montfort et al., 2004). Another clinical example of this is a study of a G202R homozygote infant with severe neuronopathic type III GD, who had only a slight reduction in enzyme activity (Zimmer et al., 1999).

In addition to *GBA1*-PD, GCase activity has been reported to be reduced in sporadic PD. In post-mortem brains of sporadic PD patients, a progressive and specific reduction in GCase activity in the SNpc and putamen has been reported with age (Huebecker et al., 2019, Rocha et al., 2015a, Gegg et al., 2012). In another study of PD and DLB brains, there was a significant decrease in GCase activity in the SNpc and frontal cortex, compared with controls. However, this was substantially lower (-40%) in those with *GBA1* mutations (Moors et al., 2019). Several other studies have also demonstrated a reduction in GCase activity in a number of brain regions, in PD brains with and without *GBA1* mutations (Murphy et al., 2014, Rocha et al., 2015a, Chiasserini et al., 2015). Measuring GCase activity in monocytes and lymphocytes from 48 PD patients revealed a significant reduction in enzymatic activity in monocytes with and without *GBA1* mutations. No difference was observed in lymphocytes (Atashrazm et al., 2018). Decreased activity has also been found in the cerebrospinal fluid (CSF) of PD patients with and without *GBA1* mutations (Parnetti et al., 2014), as well as in dried blood spots without *GBA1* mutations (Alcalay et al., 2015). The reports linking a reduction in GCase activity and protein level to sporadic PD confirm the relevance of GCase and its function to the wider PD population.

Importantly, in post-mortem brain tissue from healthy patients, the activity of GCase was diminished with ageing to a level comparable to that seen in *GBA1*-PD patients (Rocha et al., 2015a). *In vitro* studies also demonstrate a loss of GCase activity may occur with normal aging. In young and aged wild-type mice, reduced activity was reported in the ageing brain (Hallett et al., 2018). This may accelerate PD pathophysiology in vulnerable neurons.

1.8 Proposed mechanisms underlying *GBA1*-associated PD

A plethora of experimental data indicate there is a direct relationship between GCase and alpha-synuclein. However, the role of *GBA1* mutations in synucleinopathies remains largely unknown. Both loss of function and gain of function mechanisms have been proposed to influence PD risk and onset of *GBA1*-PD (Clark et al., 2007, Nichols et al., 2009), and it is thought that these two hypotheses are not mutually exclusive. An overview of the hypothesised mechanisms can be found in Figure. 2.

Many studies have indicated a loss of function in mutated GCase protein leading to PD pathology. Knock-out *GBA1* mouse models of severe neuronopathic GD exhibit rapid motor dysfunction associated with severe neurodegeneration and apoptotic cell death in the brain (Enquist et al., 2007). In GCase deficient *Drosophila* flies, there were severe lysosomal and autophagic defects, mitochondrial abnormalities, accumulation of GlcCer and locomotor deficits (Kinghorn et al., 2016). Another study demonstrated autophagic and proteasomal system defects, mitochondrial dysfunction and accumulation of alpha-synuclein in the brains of *GBA1* knock-out mice (Osellame and Duchen, 2013). Chemical inhibition of GCase activity using GCase-specific inhibitor, Conduritol B epoxide (CBE), in mice models demonstrates alpha-synuclein accumulation within nigral cell bodies and astroglia (Manning-Boğ et al., 2009). Alpha-synuclein accumulation was also present in neuroblastoma cell lines treated with CBE (Manning-Boğ et al., 2009). In CBE-treated human dopaminergic neurons, alpha-synuclein accumulation was accompanied by mitochondrial dysfunction and oxidative stress (Cleeter et al., 2013). In another mouse model, CBE-induced inhibition caused accumulation of alpha-synuclein in the SNpc, deficits in the autophagic and lysosomal pathways and lipid substrate accumulation (Rocha et

al., 2015c). Furthermore, in primary mouse neurons and PD patient fibroblasts with *GBA1* mutations, defects in the ALP were accompanied by alpha-synuclein accumulation. Impairments in the ALP were reversed by treatment with recombinant GCase protein, suggesting that a loss of GCase function was responsible for the pathology (Magalhaes et al., 2016).

As discussed above, reports that GCase activity is reduced in PD brains also support a loss of function hypothesis. Furthermore, *GBA1*-PD patients have been identified with null *GBA1* alleles, such as 84GG and IVS2+1G>A (Aharon-Peretz et al., 2004, Gan-Or et al., 2008, Clark et al., 2009). The loss of function hypothesis offers therapeutic targets for novel disease modifying agents, which may act by augmenting GCase activity or reducing substrate accumulation through other pathways. However, as only a minority of GD patients, whom have negligible levels of GCase activity, develop PD (Rosenbloom et al., 2011) and reports that GCase heterozygotes are at equal risk to homozygotes, this suggests that PD incidence cannot be related to activity. Further to this, mutations that do not reduce activity have been associated with PD, and there are mutations that do not cause GD but are risk factors for PD, such as E326K (Duran et al., 2013). Therefore, *GBA1*-PD pathogenesis must be more complex than a simple loss of function.

A toxic gain of function mechanism has therefore also been proposed. The majority of *GBA1* mutations are missense mutations and lead to the production of a misfolded GCase protein. This protein may be retained in the ER, leading to the activation of ERAD (Ron and Horowitz, 2005). Prolonged activation and retention may induce apoptosis and neuronal stress (Stoker et al., 2018). Moreover, it has been suggested that GCase protein may directly interact with

alpha-synuclein and influence its aggregation (Sidransky and Lopez, 2012, Yap et al., 2011).

It may be that the mechanisms in which *GBA1* mutations predispose to PD is multifaceted, with several elements important. As not all mutations are associated with equal risk of PD, it may be that different pathogenic mechanisms are more pronounced in carriers of different mutations. It is important to note that these hypotheses do not explain why the majority of GD patients or *GBA1* mutation carriers do not develop PD.

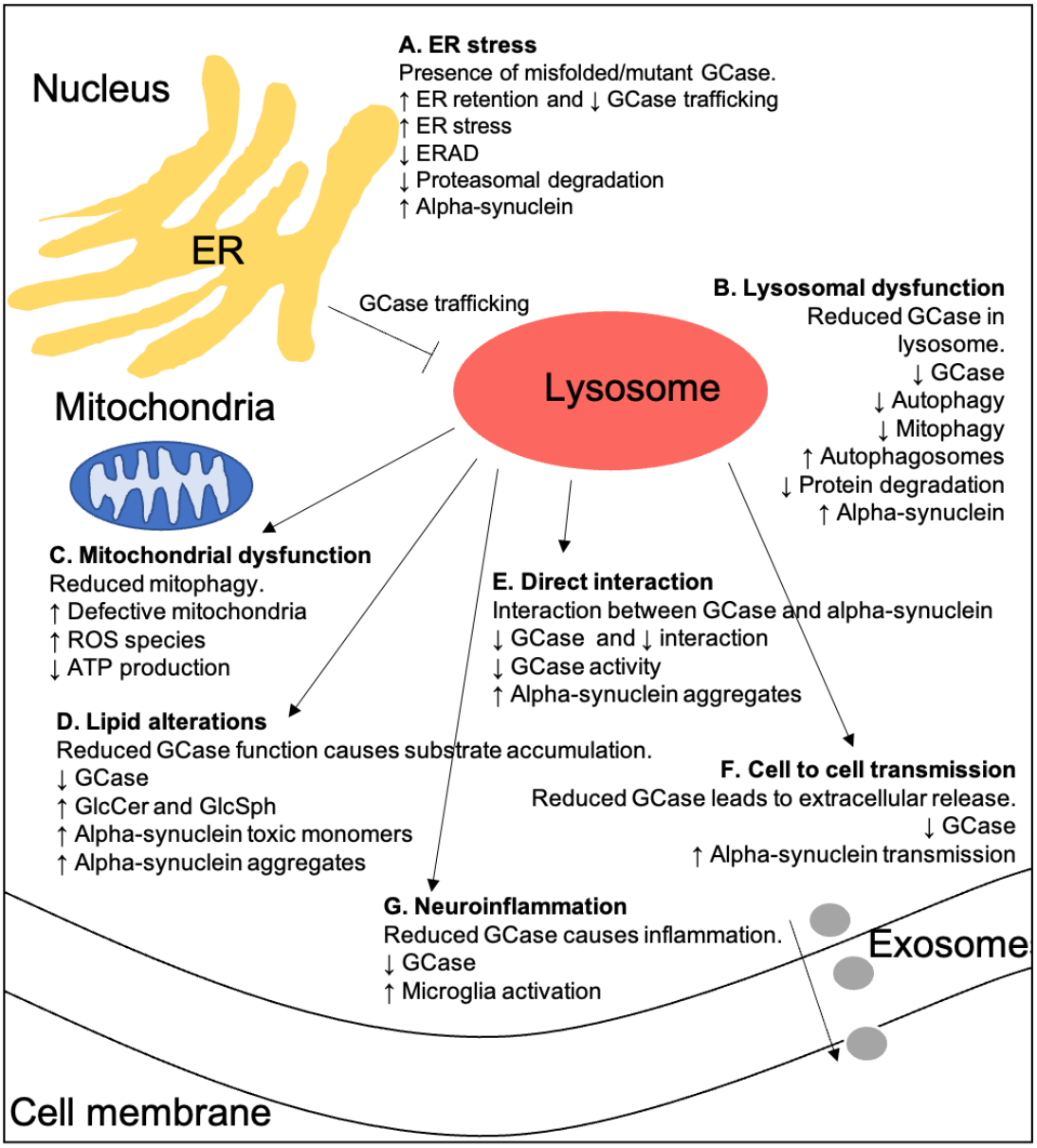

Figure 2. Schematic demonstrating proposed hypotheses for role of GCase in alpha-synuclein pathology.

A) Presence of misfolded, mutated GCase protein causes protein to be retained in the ER and not trafficked to the lysosome. Persistent ER retention leads to ER stress and reduces proteasomal degradation and ERAD pathways leading to increased accumulation of alpha-synuclein. **B)** Reduced GCase in the lysosome through improper GCase trafficking, degradation or presence of inactive GCase enzyme leads to lysosomal dysfunction. This impairs the autophagy-lysosomal pathway of protein and organelle clearance and leads to defective autophagy, mitophagy and protein degradation which causes a build-up of alpha-synuclein. **C)** Lysosomal dysfunction caused by reduced GCase can lead to defective clearance of mitochondria through mitophagy. This causes a build-up of damaged mitochondria, increased ROS species and oxidative stress and reduced ATP production. **D)** Reduced GCase function may cause an accumulation of lipid substrates. This can alter the lipid composition of cells

and influence lipid membrane fluidity and integrity, which can affect alpha-synuclein binding and induce aggregation. **E)** A direct interaction may occur between GCase and alpha-synuclein, which is reduced when the GCase protein level is reduced. The interaction is inhibitory so reduces GCase activity further. Mutations may reduce the affinity for this interaction and lead to alpha-synuclein pathology. **F)** Cell to cell transmission of alpha-synuclein may be how synucleinopathies propagate their pathology. Reduced GCase levels and activity can increase the exosome-mediated extracellular release of alpha-synuclein. The released alpha-synuclein can be taken up by neighbouring cells and act as a template to induce the toxic conversion of endogenous alpha-synuclein into aggregates. **G)** Reduced GCase or substrate accumulation can lead to activation of microglia and neuroinflammation.

1.8.1 Reduced GCase activity and alpha-synuclein

Mutations in the *GBA1* gene have been reported to cause a reduction in enzymatic activity (Montfort et al., 2004, Sidransky et al., 2009, Grace et al., 1994). Several mutations occur in and around the active site, which commonly cause GD, and ultimately destabilise the active site and thus likely diminish or reduce GCase activity. As discussed above, in post-mortem brains and CSF from *GBA1*-PD patients there is evidence of reduced GCase activity (Gegg et al., 2012, Parnetti et al., 2014). Homozygote and compound heterozygote patients exhibit low activity compared to controls, with carriers demonstrating intermediate activity (Alcalay et al., 2015). To date, there is no evidence of a correlation between GCase activity and *GBA1*-PD risk.

There is a vast array of experimental data providing evidence for a link between GCase activity and alpha-synuclein. Analysis of GCase activity in post-mortem brains from PD and *GBA1*-PD patients demonstrate a decrease in GCase protein and activity which correlates with alpha-synuclein pathology (Gundner et al., 2019). In mouse models of GD, and thus with little to no activity, there is evidence of alpha-synuclein accumulation in the brain (Cullen et al., 2011, Fishbein et al., 2014, Sardi et al., 2011, Xu et al., 2014, Xu et al., 2011, Ginns et al., 2014). In midbrain-like organoids, decreased GCase activity coupled with increased wild-type alpha-synuclein expression results in the accumulation of insoluble alpha-synuclein β-sheet rich aggregates and Lewy body inclusions (Jo et al., 2021). Inhibition of GCase activity with CBE demonstrates increased alpha-synuclein accumulation in cell and mouse models (Manning-Boğ et al., 2009, Cleeter et al., 2013). Knock-down of the *GBA1* gene in cell models also influences alpha-synuclein homeostasis (Mazzulli et al., 2011). Furthermore, GCase knockdown

in *Drosophila* fly models demonstrates increased alpha-synuclein aggregation and dopaminergic neuronal loss (Abul Khair et al., 2018).

Enhancing GCase activity in animal models can rescue alpha-synuclein pathology (Sardi et al., 2013). Over-expression of wild-type GCase protein, which subsequently led to an increase in GCase activity, in human embryonic kidney 293 (HEK293) cells expressing A53T mutant alpha-synuclein and pheochromocytoma cell line (PC12) expressing wild-type alpha-synuclein, induced a reduction in alpha-synuclein levels (Cullen et al., 2011). Conversely, the same was not observed in mesencephalic MES23.5 cells expressing wild-type alpha-synuclein (Cullen et al., 2011). Furthermore, in human dopamine neurons harbouring heterozygous mutations for L444P and N307S there was a significant elevation in alpha-synuclein levels (Schöndorf et al., 2014), which can be rescued through lentiviral administration of wild-type GCase (Woodard et al., 2014). It has also been proposed that there may be a reciprocal relationship between GCase and alpha-synuclein as over-expression of alpha-synuclein results in decreased GCase activity in cell models (Yang et al., 2016, Mazzulli et al., 2011). One study also suggested that pathogenic fibrillar forms of alpha-synuclein may induce a time-dependant reduction in GCase activity in primary neurons and transgenic mice treated with CBE (Henderson et al., 2020).

Further supporting this loss of function hypothesis, reports suggest that reduced activity correlates with alpha-synuclein accumulation in cell models and post-mortem brain tissue (Bae et al., 2015, Murphy et al., 2014). In addition to alpha-synuclein accumulation, GCase deficient HEK293 cells exhibit impaired extracellular secretion of alpha-synuclein, exacerbating intracellular accumulation (Kim et al., 2018a).

Although these studies provide a link between reduced GCase activity and alpha-synuclein pathology, other studies have failed to demonstrate this. In mesencephalic cells, expression of mutant GCase protein increased alpha-synuclein levels with no effect on activity (Cullen et al., 2011). In CBE-treated neuroblastoma cells or primary rat cortical neurons, there was no evidence of alpha-synuclein accumulation (Dermentzaki et al., 2013). In another study, a reduction to 50% GCase activity was not sufficient to cause PD-like pathology in mouse models of *GBA1*-PD (Sardi et al., 2011). Furthermore, there was no difference in alpha-synuclein pathology in iPSC-derived dopamine neurons carrying homozygote or heterozygote *GBA1* mutations, although GCase activity was significantly lower in homozygotes (Schöndorf et al., 2014). Interestingly, in primary neurons and transgenic mouse models treated with CBE, GCase inhibition did not lead to an increase in total alpha-synuclein or formation of alpha-synuclein pathology. Inhibition of GCase activity, however, did enhance pre-existing alpha-synuclein pathology, leading to elevation of pathogenic phosphorylated alpha-synuclein (p-S129-alpha-synuclein) (Henderson et al., 2020). This finding was not neuron specific.

Considering that *GBA1* mutation carriers are as likely to develop PD as homozygotes, even though they retain more activity (McNeill et al., 2012, Alcalay et al., 2015, Aharon-Peretz et al., 2004), and that most GD patients do not develop PD (Rosenbloom et al., 2011) even though GCase activity is very low, one would believe activity is not solely responsible for PD onset.

1.8.2 Autophagic-lysosomal pathway dysfunction and alpha-synuclein

Balance between the synthesis and degradation of molecules and organelles is critical for cellular homeostasis and proper cell function. This is controlled by the ALP which is the cells major mechanism of protein clearance and organelle

turnover (Klionsky and Emr, 2000). Neurons are particularly vulnerable to alterations in the ALP (Nixon, 2013), and mutations in this pathway are linked to synucleinopathies (Dehay et al., 2013). There are three types of autophagic pathways including macroautophagy, microautophagy, and chaperone-mediated autophagy (CMA). There are several key acid hydrolases within the lysosome to help with degradation, including GCase, and when there is defective function there is impaired clearance (Westbroek et al., 2011).

Macroautophagy is critical to neuronal survival and the integrity of pre-synaptic structures (Blanz and Saftig, 2016). This process degrades macromolecules, such as proteins and lipids, in addition to larger structures such as aggregated proteins and damaged organelles (Parzych and Klionsky, 2014). To do so, cargo for degradation is sequestered into autophagosomes and delivered to the lysosome to form autophagolysosomes which are subsequently degraded by lysosomal hydrolases (Kinghorn et al., 2016). On the other hand, CMA involves a chaperone complex that specifically identifies and degrades soluble monomeric proteins in the cytosol. Once bound, the chaperone transports the substrate protein to the lysosome where the substrate binds to the lysosomal-associated membrane protein 2a (LAMP2A) receptor. Next, a translocation complex is formed, and the proteins cross the lysosomal membrane to be degraded (Cuervo and Wong, 2013, Parzych and Klionsky, 2014).

Proper function of the ALP is critical for the regulation of alpha-synuclein homeostasis as both macroautophagy and CMA play a role in the degradation of alpha-synuclein (Cuervo et al., 2004, Martinez-Vicente and Cuervo, 2007). Both of these processes are reported to be impaired in PD (Alvarez-Erviti et al., 2010, Cuervo et al., 2004) and several studies have reported ALP dysfunction in *GBA1*-

PD. The degree of ALP defects is comparable between homozygotes and heterozygotes (Magalhaes et al., 2016, Schöndorf et al., 2014).

Defective ALP has been reported in *GBA1*-PD patient brains (Gegg et al., 2012) and in GD and *GBA1*-PD patient iPSC-derived or adipose stem cell-derived neurons (Fernandes et al., 2016, Yang et al., 2017, Schöndorf et al., 2014). Several cell and animal models of *GBA1* mutations demonstrate ALP dysfunction (Fernandes et al., 2016, Bae et al., 2015, Klionsky and Emr, 2000) (Rocha et al., 2015c). In patient fibroblasts with *GBA1* mutations, there is impaired lysosomal recycling. This may mean the neuron is unable to maintain the pool of fully-functioning lysosomes required for adequate clearance of proteins such as alpha-synuclein (Magalhaes et al., 2016). Efficient autophagy relies on fully functioning lysosomes and lysosomal enzymes, including GCase (Wong and Krainc, 2017), which may explain why autophagic defects are so prevalent in *GBA1* mutants. Pharmacological inhibition of GCase or silencing of *GBA1* mRNA results in decreased lysosomal protein turnover and ALP dysfunction in many neuronal cell models (Bae et al., 2015, Dermentzaki et al., 2013, Mazzulli et al., 2011, Osellame et al., 2013). Knockdown of *GBA1* led to defective ALP in neuroblastoma cells and rodent brains (Du et al., 2015, Mazzulli et al., 2011, Magalhaes et al., 2016). It has also been reported that impaired autophagic and proteasomal pathways, as a result of GCase deficiency, can lead to the accumulation of dysfunctional mitochondria (Osellame et al., 2013, Cleeter et al., 2013).

Impaired ALP may influence alpha-synuclein pathology. A vast amount of experimental data in models of *GBA1* mutations or GCase deficiency point to a correlation between increased alpha-synuclein accumulation and ALP dysfunction (Mazzulli et al., 2011, Rocha et al., 2015c, Manning-Boğ et al., 2009,

Cleeter et al., 2013, Xu et al., 2011, Bae et al., 2015, Cullen et al., 2011). Impaired autophagic and lysosomal mechanisms are evident in *GBA1* mutant iPSC-derived neurons (Schöndorf et al., 2014, Fernandes et al., 2016), PD brains (Alvarez-Erviti et al., 2010) and GCase knock-out cells (Du et al., 2015) was accompanied by alpha-synuclein aggregation, possibly due to impaired degradation. In neural crest stem cell derived dopaminergic neurons, heterozygous N370S *GBA1* mutations and subsequent reduction in GCase activity was found to be required for Cathepsin D function. Cathepsin D is a lysosomal aspartic endo-protease involved in the degradation and removal of monomeric alpha-synuclein from neurons. Treatment of these neurons with ERT or chaperone drugs to increase GCase activity rescued Cathepsin D protein and activity, restoring ALP function and reducing alpha-synuclein levels (Yang et al., 2020b). Chemical inhibition of autophagy also leads to the accumulation of alpha-synuclein aggregates (Klucken et al., 2012). Furthermore, in cortical neurons from L444P/WT mice, the half-life of alpha-synuclein was increased by more than 70% compared to cells from WT/WT littermates (Fishbein et al., 2014), suggesting deficient turnover. *In vitro* studies have demonstrated that activation of autophagy can reduce deposits of alpha-synuclein (Spencer et al., 2009).

In order for cells to maintain their full complement of lysosomes, there is a process called autophagic lysosome reformation (ALR). This follows termination of macroautophagy. It is believed that protolysosomal tubules extrude from autophagolysosomes which mature into functional lysosomes to restore lysosomal number (Li et al., 2016). This process is dependent on mTOR activity, a reduction in which is evident in models of GCase deficiency (Magalhaes et al., 2016, Kinghorn et al., 2016). These models exhibit impaired ALR, inhibition of macroautophagy flux and increased alpha-synuclein levels.

A bidirectional loop has been proposed to explain the relationship between *GBA1* mutations, alpha-synuclein and the lysosome (Mazzulli et al., 2011). *GBA1* mutations may result in reduced GCase activity and subsequent lysosomal dysfunction, which leads to the accumulation of GSL substrates and alpha-synuclein. This accumulation of alpha-synuclein may impede the transport of newly synthesised GCase from the ER to the lysosome. This further exacerbates dysfunction of lysosomes and autophagic-mediated turnover of alpha-synuclein, leading to more accumulation of alpha-synuclein (Mazzulli et al., 2011). Alpha-synuclein then aggregates and builds-up more, further inhibiting GCase trafficking. This feedback loop can eventually cause neuronal cell death (Balestrino and Schapira, 2018). Supporting evidence for the bidirectional loop comes from a study demonstrating that over-expression of alpha-synuclein in cortical neurons results in an increase in the immature ER form of GCase, with a reduction in the levels of post-ER fully glycosylated GCase protein (Mazzulli et al., 2011). Interestingly, increased levels of immature GCase forms have been reported in L444P mutants, suggesting defective trafficking in these cells (Khanna et al., 2010, Arrant et al., 2019). In mouse neurons alpha-synuclein over-expression disrupts the ER to Golgi trafficking of autophagic machinery (Cuervo et al., 2004), which can interfere with proper alpha-synuclein degradation. Furthermore, impaired GCase trafficking can contribute to reduced activity and lysosomal dysfunction even in the absence of a *GBA1* mutation (Wong and Krainc, 2016). However, how different GCase alterations directly or indirectly affect the autophagic pathway and subsequent pathology is yet to be revealed.

1.8.3 Cell-to-cell transmission of alpha-synuclein

Alpha-synuclein may be able to propagate and spread progressively throughout the brain via cell-to-cell transmission. In 2003, Braak et al., suggested that the

spread of alpha-synuclein aggregates followed a caudo-rostral pattern in sporadic PD (Braak et al., 2003). This finding gave rise to the hypothesis that alpha-synuclein monomers or aggregates may spread from cell-to-cell by the uptake and release of aggregation-prone alpha-synuclein species. In human PD brains, the possibility of neuron-to-neuron transmission of misfolded alpha-synuclein has been demonstrated (Li et al., 2008, Kordower et al., 2008). In these studies, naïve transplanted embryonic stem cells were grafted into PD brains and follow-up analysis showed the appearance of aggregated alpha-synuclein in the graft cells. This suggests that aggregation-prone alpha-synuclein was directly transmitted from the host neurons to the graft neurons, and points towards a prion-like mechanism for alpha-synuclein pathology.

It remains unknown as to how alpha-synuclein spreads from cell-to-cell, however studies point towards exosome-mediated release in a calcium-dependant manner (Emmanouilidou et al., 2010, Lee et al., 2005). Interestingly, the amount of alpha-synuclein released into the extracellular space appears to correlate with the levels of intracellular alpha-synuclein (Reyes et al., 2015). This suggests that release of alpha-synuclein may be a way in which the cell responds to override abnormal alpha-synuclein levels. Further evidence supporting the hypothesis of alpha-synuclein seeding comes from analysis of human plasma and CSF, where alpha-synuclein monomers and oligomers can be detected in both PD patients and healthy controls (Borghi et al., 2000, El-Agnaf et al., 2003). A recent study also found that the alpha-synuclein species in exosomes from PD patients was more pathogenic than those from healthy controls, with the ratio of oligomeric and p-S129-alpha-synuclein to total alpha-synuclein being higher (Zheng et al., 2021). Similarly, in extracellular vesicles from PD patients, alpha-synuclein

concentration was significantly higher when compared to DLB patients and healthy controls (Stuendl et al., 2021).

Aggregate prone alpha-synuclein may be taken up into neighbouring cells and act as a template to promote the misfolding of endogenous alpha-synuclein, ultimately leading to the formation of Lewy bodies (Brundin et al., 2008). In a mouse model over-expressing human alpha-synuclein, 15% of grafted mouse cortical neuronal stem cells exhibited alpha-synuclein inclusions after four weeks (Desplats et al., 2009). In another study, 5% of grafted dopaminergic neurons in the striatum of mice over-expressing alpha-synuclein exhibited alpha-synuclein pathology including monomers, oligomers and fibrils after 6 months (Hansen et al., 2011). *In vitro* studies demonstrate that exogenous application of recombinant alpha-synuclein pre-formed fibrils (PFF) can induce the recruitment of endogenous soluble able-synuclein into insoluble pathological aggregates in cells over-expressing alpha-synuclein (Hansen et al., 2011, Luk et al., 2009, Volpicelli-Daley et al., 2011). In mouse cortical neurons or human dopaminergic neurons, treatment with PFF induced endogenous alpha-synuclein to become insoluble and phosphorylated at Ser129 to a greater extent than treatment with monomeric alpha-synuclein. (Gegg et al., 2020). This may then lead to alterations in synaptic function and neuronal cell death.

Many studies have investigated the link between *GBA1* mutations and alpha-synuclein transmission. In a transgenic mouse model expressing human alpha-synuclein, control and GCase knock-out SH-SY5Y cells were grafted into the hippocampus. An increase in alpha-synuclein transmission was observed in cells lacking GCase. Ectopic expression of wild-type GCase protein reversed the effects of GCase depletion on alpha-synuclein transmission (Bae et al., 2014), providing evidence of a role for GCase in alpha-synuclein propagation.

Furthermore, in iPSC-derived dopamine neurons from N370S heterozygote patients, ER stress and defective autophagic-lysosomal clearance led to elevated extracellular alpha-synuclein levels (Fernandes et al., 2016).

Alpha-synuclein and protein aggregates can be packaged into extracellular vesicles and released into the extracellular space. Inhibition of lysosomal function in neuroblastoma cells over-expressing wild-type alpha-synuclein demonstrated a marked increase in exosome-mediated alpha-synuclein release and transmission (Alvarez-Erviti et al., 2011b). In *GBA1*-PD fibroblasts with L444P or N370S mutations, defective GCase activity promotes extracellular vesicle release (Cerri et al., 2021). In *GBA1* deficient *Drosophila* flies, accelerated protein aggregation has been demonstrated to coincide with increased spread of protein aggregations between cells through dysregulated extracellular vesicles (Jewett et al., 2021). The same study also suggested that wild-type GCase can be packaged in to extracellular vesicles and trafficked between cells, and that it may be this mechanism that contributes to reducing the spread of protein aggregates in an organism.

Analysis of *GBA1* knock-out *Drosophila* flies demonstrated defects in the autophagic turnover and abundance of proteins associated with exosome release, suggesting *GBA1* mutations may increase extracellular secretion of protein aggregates (Thomas et al., 2018). Co-cultures of primary mouse cortical neurons treated with CBE demonstrated that a GCase deficiency increased alpha-synuclein fibril release, which was higher when treated with PFFs, providing further evidence for a prion-like pathology (Gegg et al., 2020). In another study, over-expression of mutant GCase protein in primary mouse cortical neurons resulted in an increase in intracellular alpha-synuclein oligomers, accompanied by an increase in the release of brain exosomes and transmission

of exosome-associated alpha-synuclein oligomers. Wild-type GCase over-expression led to a significant decrease in exosome secretion in these cells. Chronic inhibition of GCase in alpha-synuclein mutant mice also led to a marked increase in exosome-mediated secretion of alpha-synuclein oligomers (Papadopoulos et al., 2018). Interestingly, accumulation of GlcCer may influence the generation of distinct pathological forms of α-synuclein (Suzuki et al., 2018), which have been shown to be capable of pathogenic templating in human dopamine neurons (Taguchi et al., 2017) and may propagate the spread of alpha-synuclein pathology.

1.8.4 ER stress and alpha-synuclein

Mutations in the *GBA1* gene may lead to the production of a misfolded protein, which can be retained in the ER to induce ER stress (Fernandes et al., 2016, Maor et al., 2013, Ron and Horowitz, 2005). There is mounting evidence from cell and animal models pointing towards a gain of function mechanism for *GBA1* mutations that involve ER retention and activation of the pathways associated with ER stress, including ERAD and the UPR (Wang et al., 2011, Maor et al., 2013, Braunstein et al., 2018, Fernandes et al., 2016, Sanchez-Martinez et al., 2016, Schöndorf et al., 2014). Different *GBA1* mutations have demonstrated variable degrees of ER retention and protein degradation (Ron and Horowitz, 2005). The extent of ER stress may correlate with disease severity, as fibroblasts derived from patients with the severe L444P mutation display extensive ERAD (Bendikov-Bar et al., 2011). This may be due to more severe conformational changes occurring, affecting protein stability. If more mutant GCase protein is retained in the ER, less protein is translocated to the lysosome and thus may have more severe consequences. Interestingly, an inhibition of the ERAD process was found to rescue native folding of mutant GCase through upregulation

of the UPR. This too was found to correlate with disease severity as the rescue was more efficient in L444P GD-patient derived fibroblasts than N370S (Wang et al., 2011).

Accumulation of alpha-synuclein has also been linked to ER dysfunction. Evidence of ER stress has been exhibited in several models of synucleinopathies (Colla et al., 2012a, Colla et al., 2012b). Intracellular alpha-synuclein accumulation can elicit an ER stress response (Heman-Ackah et al., 2017, Cooper et al., 2006). In N370S iPSC-derived dopaminergic neurons, mutant protein induced ER stress and dysfunction which led to elevated extracellular alpha-synuclein release (Fernandes et al., 2016). Alpha-synuclein can also interact with the ER chaperone BiP, inducing its activation and the UPR pathway (Bellucci et al., 2011) and thus interfere with proper protein folding, potentially exacerbating misfolding. Abnormal UPR has also been reported in DLB human brain samples. This correlated with alpha-synuclein pathology (Baek et al., 2016).

The current literature surrounding *GBA1* mutations and the ER suggest that early intervention to alleviate ER stress may be an attractive therapeutic avenue to explore to treat *GBA1*-PD.

1.8.5 Disruption in lipid metabolism and alpha-synuclein

Dysfunction of cellular lipid homeostasis may underlie PD pathology. Lipid homeostasis is necessary for synaptic plasticity and neuronal function (Farmer et al., 2020). The pathological fibrilisation of alpha-synuclein is thought to be strongly mediated by physiological interactions between alpha-synuclein and lipids. An amphipathic alpha-helical domain in the N terminal of alpha-synuclein is proposed to mediate its binding to phospholipid membranes. It is believed that alpha-synuclein exists physiologically as a disordered, free monomer and an

alpha-helix-rich membrane-bound form (Lee et al., 2002, Davidson et al., 1998). Balance between these two structural states plays a key role in the kinetics of the pathogenic aggregation of alpha-synuclein. A previous study using solution state nuclear magnetic resonance (NMR) proposed that GCase can directly inhibit lipid-induced aggregation by binding to the C terminal of alpha-synuclein, causing its dissociation from lipids at the N terminal. The same mechanism was also shown to destabilise mature fibrils (Barber et al., 2018). However, it remains debatable whether the binding of lipids to alpha-synuclein promotes or prevents aggregation. A 2003 study reported that binding of alpha-synuclein to lipid membranes may propagate aggregation (Lee et al., 2002), however a recent study demonstrated that binding of alpha-synuclein to lipid membranes may slow down fibril elongation (Kurochka et al., 2021).

Lipid membrane fluidity is essential for efficient binding of alpha-synuclein (Galvagnion et al., 2016). If aberrant lipid homeostasis occurs, this may alter lipid membrane composition or fluidity and binding of alpha-synuclein to lead to subsequent neurotoxicity (Farfel-Becker et al., 2014, Ginns et al., 2014). Furthermore, alpha-synuclein aggregates may interact with lipid membranes, leading to membrane damage and toxicity (Melo et al., 2021). Alterations to lipid composition have been reported in PD brains, including changes in levels of fatty acids and lipid raft content (Fabelo et al., 2011). Changes in membrane fluidity could greatly affect alpha-synuclein degradation as membrane dynamics are required for macroautophagy and CMA (Gegg and Schapira, 2018). It is important to note that changes in cellular lipid composition may affect membranes differently depending on their lipid content. For example, the plasma membrane has a high cholesterol and sphingolipid content, whereas the ER and mitochondrial membranes has high glycerophospholipid content and thus

changes may differ in response to specific lipid changes (Harayama and Riezman, 2018).

Several cell and animal models of GCase deficiency have reported an accumulation of its GSL substrates, GlcCer and GlcSph (Sardi et al., 2011, Sardi et al., 2017, Nagata et al., 2017, Schöndorf et al., 2014, Orvisky et al., 2002, Farfel-Becker et al., 2014, Rocha et al., 2015c, Xu et al., 2011, Hallett et al., 2018). In a *GBA1*-PD mouse model, reducing GSL levels improved cognitive symptoms (Sardi et al., 2017). Fibroblasts from WT/L444P PD patients demonstrated a significant increase in GSLs compared to healthy controls and sporadic PD patients, which correlated with decreased GCase activity. Lipids extracted from these fibroblasts can accelerate the aggregation of recombinant alpha-synuclein, due to a higher content of short-chain lipids (Galvagnion et al., 2020). Excess GSLs can alter lipid membrane composition, leading to changes in membrane fluidity and curvature. Decreased membrane fluidity has been reported in type 1 GD fibroblasts, induced by increases in GSL levels. (Varela et al., 2016). The GCase substrate GlcCer has been reported to accumulate in lipid rafts, stabilising GSL-enriched liquid domains (Hein et al., 2008, Varela et al., 2016).

It is important to note that the presence of GSL accumulation was not evident in the putamen and cerebellum of *GBA1*-PD brains (Gegg et al., 2015) or in the primary motor cortex of *GBA1*-PD patients (Clark et al., 2015). However, there is evidence of GlcCer and GlcSph accumulation in PD and neuropathic GD brains (Rocha et al., 2015a, Huebecker et al., 2019, Nilsson and Svennerholm, 1982, Orvisky et al., 2002). In sporadic PD brains, there was decreased GCase activity but no change in GlcCer levels (Boutin et al., 2016). Interestingly, the distribution among the different GlcCer species was different compared with controls in

N370S dopamine neurons (Fernandes et al., 2016). This suggests that perhaps specific GlcCer isoforms have different roles in PD pathology, rather than just an accumulation of all GlcCer species.

A direct link between GSL accumulation and alpha-synuclein fibrilisation has also been suggested. Accumulation of GlcCer has been shown to stabilise toxic alpha-synuclein oligomers in primary cortical neurons and human iPSC-derived neurons (Mazzulli et al., 2011). In human neurons, GlcCer and GlcSph were shown to trigger the formation alpha-synuclein oligomers, which are capable of acting as a seed to propagate alpha-synuclein pathology (Taguchi et al., 2017). GlcCer has recently been reported to self-assemble into an amyloid-like fibrillar aggregate *in vitro*, exhibiting a twisted ribbon-like structure, capable of inducing alpha-synuclein aggregation and oligomer stabilisation in acidic condition (Paul et al., 2021). In GCase mutant human midbrain neurons, GlcCer has been reported to trigger the conversion of alpha-synuclein monomers in to a structurally distinct high molecular weight (HMW) species. This HMW species had unique structural properties consistent with pathogenic alpha-synuclein fibrils (Zunke et al., 2018). Reducing the levels of GSLs reversed this conversion. A similar rescue was observed in mice models of synucleinopathy, where inhibition of the synthesis of GlcCer and its metabolites was seen shown to decrease alpha-synuclein pathology (Sardi et al., 2017).

Over the last decade, it has been proposed that alpha-synuclein exists in a dynamic equilibrium between physiological soluble, monomers and soluble, tetramers and multimers. These physiological HMW species are less prone to aggregation, whereas monomers readily assemble into pathogenic alpha-synuclein insoluble oligomers (Bartels et al., 2011). Saturated fatty acids are thought to stabilise physiological alpha-synuclein tetramers, whereas

unsaturated fatty acids shift the equilibrium towards monomeric alpha-synuclein (Fanning et al., 2019). Changes to GSL composition has also been associated with a shift away from tetrameric alpha-synuclein species. In GCase knock-out SH-SY5Y neuroblastoma cells, L444P/WT primary cortical neurons and N370S/WT iPSC-derived human dopamine neurons there was a shift toward increased monomeric species. This shift was rescued by reducing GSL synthesis (Kim et al., 2018b), suggesting that GlcCer may destabilise aggregate-resistant physiological tetramer/multimers increasing the number of free monomers capable of oligomerising. Furthermore, in alpha-synuclein mutant mice, over-expression of wild-type GCase protein and subsequent reduction in GSL levels rescued the shift towards monomeric alpha-synuclein, likely through an increase in lipid turnover (Glajch et al., 2021).

A deficiency in GCase has not only been associated with increases in GSL levels, but also with alterations in the composition of other lipids species (Westbroek et al., 2011). This may be relevant as changes in levels of hydrolysed triacylglycerols (TAGs) and GSLs (particularly GM1 and GM3); binding to acidic phospholipid vesicles and ordered regions of lipid membranes may enhance the conversation of monomeric alpha-synuclein into toxic aggregates (Alecu and Bennett, 2019, Martinez et al., 2007). Further to this, an increase in total ceramide level has been reported the serum of *GBA1*-PD patients (Guedes et al., 2017), and in Lewy body dementia patients elevation of ceramide levels has been observed independent of *GBA1* mutation status (Kurzawa-Akanbi et al., 2021). In the SNpc of PD brains (Moloney et al., 2018) and brains from GD patients (Murugesan et al., 2018), the marker of lipid-induced stress, glycoprotein NMB (GPNMB) is selectively elevated. GPNMB is a glycoprotein involved in tissue damage and inflammation. It is mainly associated with astrocytes, microglia and

macrophages. Furthermore, CBE-induced lysosomal dysfunction in mice led to an increase in GPNMB levels which were similar to that seen in the PD brain (Moloney et al., 2018). This presents further evidence for a primary role for lipids in *GBA1*-PD degeneration.

Experimental data suggests there may be specific cell types that present a selective vulnerability to lipid alterations. Studies using human brains contain a mixture of neurons and glia, and it may be that substrate accumulation is cell specific. This highlights the difficulty of determining lipid alterations where small changes may be difficult to detect in certain cell types. Furthermore, it could be that subtle changes in subcellular localisation of the substrate or alterations to the distribution of species that may affect alpha-synuclein metabolism.

1.8.6 Direct interaction between GCase and alpha-synuclein

GCase has been found to be an important component of Lewy bodies (Goker-Alpan et al., 2010). This may arise through a direct, physical interaction between the GCase and alpha-synuclein proteins. This interaction has been reported both in solution and via the lipid membrane, both occurring only in acidic conditions (Yap et al., 2011, Yap et al., 2013b). At the membrane surface of intralysosomal vesicles, the membrane-bound alpha-helical form of alpha-synuclein was shown to interact with GCase, forming a membrane-bound complex which inhibits the activity of GCase (Yap et al., 2013b). Saposin C, a GCase activator protein, can bind and induce the release of alpha-synuclein from GCase reversing the inhibition (Yap et al., 2013a). In alpha-synuclein knock-out mice, there was a 35% increase in GCase activity, with no effect on overall enzyme level or lysosomal number, further supporting the inhibitory effect of alpha-synuclein (Fishbein et al., 2014). These studies are however *in vitro* so the same may not occur physiologically.

Further *in vitro* investigations into the GCase-alpha-synuclein membrane-bound complex have revealed that GCase binds to the membrane lipid bilayer, partially inserting itself with the active site at a specific position. To do this the flexible loops within the GCase structure surrounding the active site are rearranged, this may potentially alter the active site position and prevent substrate access (Yap et al., 2015). In addition to this, upon GCase binding the alpha-synuclein protein is lifted up from the membrane, which may alter the helical residues within the protein. This movement may expose a portion of alpha-synuclein to lysosomal proteases, perhaps enhancing its degradation (Yap et al., 2015). Interestingly, analysis of this interaction in the presence of the N370S mutation revealed a reduction in the binding affinity of GCase to alpha-synuclein (Yap et al., 2011). This suggests that GCase may have a protective mechanism, which may involve preventing aggregation or inducing alpha-synuclein degradation upon binding.

However, as the majority of the research is from one source it is difficult to say with certainty that there is enough evidence to support a physical interaction. Furthermore, little is known about how the formation of this complex would influence alpha-synuclein turnover and stability.

1.8.7 Mitochondrial dysfunction and neuroinflammation

Mitochondria play a central role in energy production by oxidative phosphorylation. However, they are also heavily involved in other cellular processes including regulation of calcium homeostasis, membrane potential, apoptosis and stress response (Schapira and Gegg, 2011). Impairment of mitochondrial function is thought to play a key role in PD pathogenesis (Schapira et al., 1990, Schapira et al., 1989, Schapira, 2008), and some studies have investigated the link between GCase and mitochondrial dysfunction. In homozygous *GBA1* mutant mice, there was a significant reduction in adenosine

triphosphate (ATP) production and oxygen consumption suggesting defective mitochondria (Xu et al., 2014). Knock-out of the *GBA1* gene in another mouse model demonstrated mitochondrial dysfunction and an accumulation of fragmented mitochondria (Osellame et al., 2013). Inhibition of GCase activity in neuroblastoma cell lines can also lead to oxidative stress and defective mitochondria (Cleeter et al., 2013). In *GBA1* deficient *Drosophila* flies, mitochondrial abnormalities including reduced ATP levels, large mitochondria and increased sensitivity to oxidative stress was observed in the brain (Kinghorn et al., 2016). This was accompanied by severe lysosomal defects and impaired autophagic flux. Although the cause of mitochondrial dysfunction in PD remains unclear, this suggests a role for impaired ALP-mediated clearance of damaged mitochondria. Impaired mitochondrial clearance has also been demonstrated in iPSC-derived dopamine neurons from *GBA1* mutation carriers and *Drosophila* fly models; this was accompanied by changes in nicotinamide adenine dinucleotide (NAD+) metabolism and restoring this prevented dopamine neuron loss and motor decline in flies (Schöndorf et al., 2018). Furthermore, it has also been proposed that the pathogenic accumulation of alpha-synuclein can render dopamine neurons more susceptible to mitochondrial dysfunction induced by 1-methyl-4-phenyl-1,2,3,6-tetrahydropyridine (MPTP) in an L444P/WT mouse model (Yun et al., 2018).

Neuroinflammation has also been associated with PD pathogenesis (Tansey and Goldberg, 2010) and *GBA1* mutations. In serum from GD patients, higher concentrations of inflammatory markers have been reported compared to controls (Allen et al., 1997). In animal models of GCase deficiency there is considerable neuroinflammation including activation of microglia, upregulation of inflammatory cytokines and higher levels of immune markers in the plasma

(Mistry et al., 2010, Vitner et al., 2014, Keatinge et al., 2015). It may be that neuroinflammation arises as a result of substrate accumulation within neurons that can activate microglia (Vitner et al., 2012, Enquist et al., 2007). Neuroinflammation is also exhibited in mice treated with CBE (Rocha et al., 2015c). Experiments have also suggested a link between alpha-synuclein and microglial activation (Alvarez-Erviti et al., 2011a, Zhang et al., 2005, Lee et al., 2010). It is thought that secreted alpha-synuclein may be able to bind directly to Toll-like receptors (TLRs) on the microglia and activate them resulting in neuroinflammation (Kim et al., 2013, Thome et al., 2016). As mentioned above, GCase deficient neurons have increased alpha-synuclein secretion (Chapter 1.8.3). This extracellular alpha-synuclein may also be taken up by microglia and astrocytes to be degraded (Cavaliere et al., 2017, Loria et al., 2017), however if these cells are GCase deficient then alpha-synuclein degradation may be defective through improper ALP function (see Chapter 1.8.2) and thus contribute to the spread of alpha-synuclein pathology.

1.9 Treatment for *GBA1*-associated Parkinson Disease

Currently, all treatment for PD is symptomatic and no drug is able to exert a neuroprotective or neurorestorative effect. Patients with *GBA1*-PD are thought to respond to dopaminergic therapy the same way as sporadic PD patients (Ziegler et al., 2007, Neumann et al., 2009). However, some studies report a less efficacious response (Tayebi et al., 2003). Deep brain stimulation (DBS) may also be efficacious in alleviating symptoms in *GBA1*-PD patients. In a 2013 study, 17% of PD patients who had a positive clinical effect following DBS were *GBA1* mutation carriers (Angeli et al., 2013).

The link between the *GBA1* gene and PD has now opened a new avenue for therapy, with GCase as a novel target. The current treatments for GD are enzyme

ERT and SRT. ERT works by administering active, recombinant GCase protein to the cells to increase GCase protein and activity. These cannot cross the BBB and thus are ineffective in treating *GBA1*-PD. SRT works to reduce the accumulation of GCase substrate by inhibiting the biosynthesis of GlcCer and GlcSph (Shemesh et al., 2015). A potent, brain-penetrant inhibitor of GlcCer synthase, GZ667161, has been shown to decrease the levels of lipid substrates in a GD mouse model and alpha-synuclein aggregation in mice models of synucleinopathies (Sardi et al., 2017).

Another avenue being pursued is the use of gene therapy to treat *GBA1*-PD. Adeno-associated virus (AAV) mediated expression of human recombinant GCase in the hippocampus of a pre-symptomatic mouse model of GD has been shown to be effective in reducing alpha-synuclein pathology (Sardi et al., 2011). Further studies in a symptomatic GD mouse model and in a transgenic mouse model over-expressing alpha-synuclein, show that when virus-encoding human recombinant GCase was injected into the CNS there was increased GCase expression and activity which lead to a reduction in the levels of substrate and alpha-synuclein aggregates (Sardi et al., 2013). The same was exhibited by AAV-mediated increased in GCase levels in rodent PD models (Rocha et al., 2015b)

Of recent, focus has been on the development of small-molecule chaperones to treat *GBA1*-PD. These drugs improve GCase activity by binding to mutated GCase in the ER, at a neutral pH, to facilitate correct folding. The chaperone-GCase complex is then trafficked to the lysosome, where the complex dissociates at an acidic pH. The residual activity in the GCase protein can then hydrolyse GlcCer and GlcSph (Jung et al., 2016)

A number of small-molecule chaperone candidates have been identified as potential treatments for *GBA1*-PD, including already known drugs such as ambroxol and isofagomine (Maegawa et al., 2009, Shanmuganathan and Britz-McKibbin, 2011) and newly discovered chaperones (Patnaik et al., 2012, Aflaki et al., 2016). In fibroblasts and neurons with *GBA1* mutations, these drugs have demonstrated efficacy in increasing GCase protein level, activity and aid in trafficking of mutant GCase to the lysosome (Shanmuganathan and Britz-McKibbin, 2011, Maegawa et al., 2009, Patnaik et al., 2012, McNeill et al., 2014, Bendikov-Bar et al., 2013, Sanchez-Martinez et al., 2016, Aflaki et al., 2016, Yang et al., 2017). Both ambroxol and isofagomine have been shown to successfully reduce ER stress and improve symptoms in *GBA1* mutant *Drosophila* flies (Maor et al., 2016, Sanchez-Martinez et al., 2016, Suzuki et al., 2015).

Further studies in *in vitro* and *in vivo* disease models have demonstrated the ability of ambroxol to not only increase GCase activity, but also reduce alpha-synuclein pathology (Sanchez-Martinez et al., 2016, Yang et al., 2017, Migdalska-Richards et al., 2016, Migdalska-Richards et al., 2017a, Magalhaes et al., 2018). Trials investigating the safety of ambroxol in humans are now underway. In type 1 GD patients, ambroxol was safely tolerated and exerted a positive effect on GCase (Zimran et al., 2013). In a recent single-centre, open-label, noncontrolled clinical trial with *GBA1*-PD and sporadic PD patients treated with increasing doses of the drug, ambroxol was well tolerated and safe. It was found that ambroxol successfully crosses the BBB and enters the CSF where it alters GCase activity (Mullin et al., 2020). This suggests that there is successful target engagement of ambroxol on GCase. The next step would be to perform a larger trial and study the efficacy of ambroxol in treating *GBA1*-PD and idiopathic PD.

1.10 Aims and objectives

In this work, it is hypothesised that mutations in the *GBA1* gene associated with a greater risk for PD, cause more neuronal cell dysfunction through influencing the interaction between GCase and alpha-synuclein. To address this hypothesis, the E326K, L444P and N370S mutations have been investigated. A key aim was to characterise the E326K mutation and identify if this results in loss of function or gain of function mechanisms. I sought to understand the relationship between GCase and alpha-synuclein and investigate how *GBA1* mutations affect this. Mutation-induced effects on the GCase secondary structure will aid the understanding of how the mutations induce the downstream effects on GCase and alpha-synuclein homeostasis. To assess this, the objectives were planned to:

1. Characterise the effect of E326K, L444P and N370S *GBA1* mutations on GCase activity, expression and cellular localisation using patient fibroblast cells.
2. Study how E326K, L444P and N370S *GBA1* mutations effect GCase protein stability. For this objective, recombinant *GBA1* protein with the wild-type, E326K, L444P and N370S genotype was partially purified from HEK293 cells using size-exclusion chromatography and the effect of pH and temperature on protein stability was analysed.
3. Investigate the effect of E326K, L444P and N370S *GBA1* mutations on alpha-synuclein levels and pathology. To do this, SH-SY5Y cells over-expressing wild-type, E326K, L444P and N370S protein were differentiated into dopaminergic neurons and data corroborated in iPSC-derived midbrain dopamine neurons.

2 Materials and Methods

2.1 Chemicals and reagents

Unless otherwise stated, all chemicals and reagents were purchased from Thermofisher, Merck Millipore or Abcam.

2.2 Antibodies

Table 3. Antibodies used in this project

Antibody Name	Immunogen and epitope	Species	Western Blot or Dot Blot Dilution	Immunofluorescence Dilution
Anti-GBA clone 2e2, AP1140 (Millipore)	Recombinant human GBA protein, AA 146-236 (outside of mutation sites)	Mouse, mAb	1/1000	1/200
Anti-GRP78 BiP, ab21685 (Abcam)	Mouse GRP78 BiP, epitope AA 600 to the C-terminus	Rabbit, pAb	1/1000	n/a
MJFR1, ab138501 (Abcam)	Recombinant full-length human alpha-synuclein, epitope AA 118-123	Rabbit, mAb	1/1000	n/a
LAMP-1/CD107a, NB120-19294 (Novus)	Synthetic peptide corresponding to AA 407-416 of human LAMP1	Rabbit, mAb	1/1000	n/a
eIF2α, 9722 (Cell Signaling)	Human eIF2α protein	Rabbit, pAb	1/2000	n/a
Phospho-eIF2α (Ser51), 9721 (Cell Signaling)	Human eIF2α protein when phosphorylated at Ser51	Rabbit, pAb	1/2000	n/a
Recombinant Anti-ALIX [EPR23653-32], ab275377 (Abcam)	Recombinant ALIX fragment	Rabbit, mAb	1/1000	n/a
Anti-Flotillin 1 antibody, ab41927 (Abcam)	Synthetic peptide corresponding to Human Flotillin 1, AA 1-100	Rabbit, pAb	1/1000	n/a
His-Tag (D3I10) XP (Cell Signaling)	6xHis-tag fused to either the amino or carboxyl terminus of targeted proteins in transfected cells	Rabbit, mAb	1/1000	1/250
Calnexin, ab22595 (Abcam)	Human Calnexin epitope AA 550 to the c-terminus	Rabbit, pAb	n/a	1/500
Cathepsin D [ERP3057Y], ab75852 (Abcam)	Human Cathepsin D epitope AA 350 to the c-terminus	Rabbit, mAb	1/2000	1/150
Glucosylceramide RAS_0100 (Glycobiotech)	Human Glucosylceramide	Rabbit	1/500-1/1000	1/100
Recombinant Anti-Alpha-synuclein aggregate antibody [MJFR-14-6-4-2] – Conformation-Specific ab209538 (Abcam)	Recombinant full-length alpha-synuclein aggregate	Rabbit, mAb	1/1000	n/a
Beta III Tubulin (TU-2) ab7751 (Abcam)	Class III beta-tubulin specific for neurons epitope AA 441-448	Mouse, mAb	1/4000	1/500
PSD95 (D27E11) XP (Cell Signaling)	Human PSD95	Rabbit, mAb	1/1000	n/a

Tyrosine Hydroxylase ab112 (Abcam)	Full length SDS denatured tyrosine hydroxylase	Rabbit, pAb	n/a	1/100
Beta-actin, ab8227 (Abcam)	Human beta-actin, epitope AA 1-100	Rabbit, pAb	1/4000-1/500	n/a
Anti-Rabbit HRP (Dako)	n/a	n/a	1/3000	n/a
Anti-Mouse HRP (Dako)	n/a	n/a	1/3000	n/a
Anti-Mouse Alex-Fluor 488 (Invitrogen)	n/a	n/a	n/a	1/300 – 1/500
Anti-Rabbit Alex-Fluor 568 (Invitrogen)	n/a	n/a	n/a	1/300 – 1/500

2.3 Plasmid preparation

Recombinant expression constructs and plasmids were generated by Dr David Chau (Department of Clinical and Movement Neurosciences, Queen Square Institute of Neurology, UCL). Two constructs were generated: PCR1 containing the full-length wild-type *GBA1* complementary DNA (cDNA) and PCR2 containing the full-length wild-type *GBA1* cDNA with a c-terminal 6xHis-tag and a thrombin cleavage site. A schematic of the constructs is in Figure. 3. Constructs were ligated into the pcDNA3.1 vector. This is a mammalian expression vector with a cytomegalovirus (CMV) promotor region, ampicillin bacterial resistance and neomycin/G418 selectable marker (Figure. 4.).

For plasmid amplification, 10 ng of with PCR1 or PCR2 plasmid was transformed into MAX Efficiency DH10B e-coli competent cells. Cells were plated on to agar plates with 150 µg/µl ampicillin and incubated at 37°C overnight. Individual colonies were selected and inoculated in 5 mL lysogeny broth (LB) with 150 µg/µl ampicillin for at 37°C with 225 revolutions per minute (RPM) shaking overnight. After incubation, cells were pelleted by centrifugation at 8000 RPM for 5 minutes.

Plasmid DNA was isolated using QIAprep spin Miniprep Kit (Qiagen #27104) and the concentration and purity was determined by Nanodrop analysis (see below chapter 2.3). The insert sequence was confirmed by Sanger sequencing (Source Bioscience) with custom designed primers (Eurofins Genomics). This was ran at

least twice. The primers used were GP551, GP555, GP556 and reverse primers GP601, GP602 and GP552 diluted to 3.2 pmol/µl. A list of primers and their sequences can be found in Table. 4. Figures 5. and 6. illustrate where each primer binds to and reads human *GBA1* cDNA sequence. For large scale plasmid preparation, 150 mL LB medium was inoculated with sequence verified clones and grown overnight at 37°C with 225 RPM shaking. The culture was pelleted at 4000 for 10 minutes and plasmid DNA was isolated by endotoxin-free plasmid Maxi Kit (Qiagen #12362).

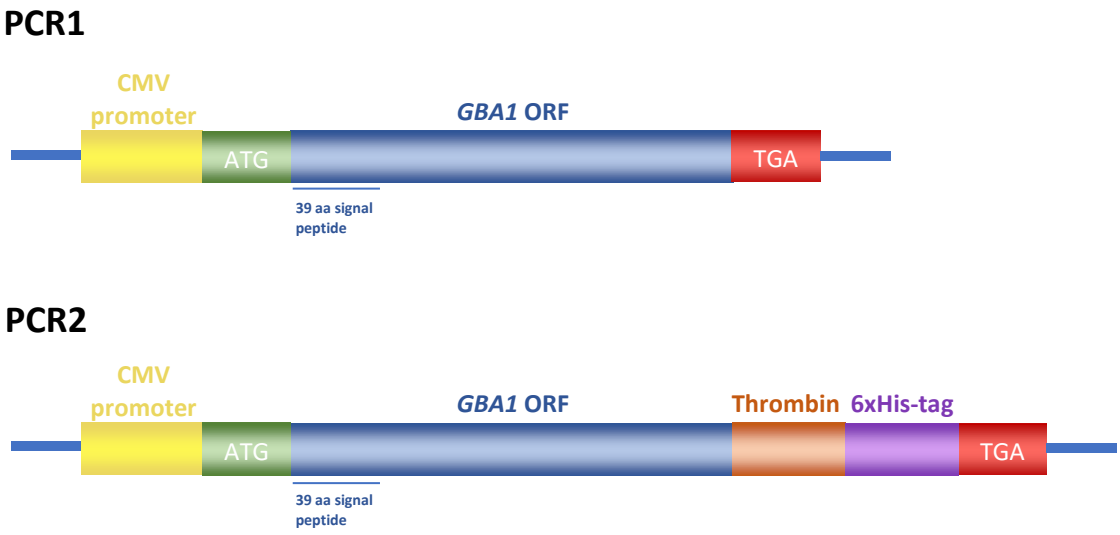

Figure 3. Schematic of PCR1 and PCR2 constructs.
Constructs contain the CMV promoter, ATG start codon and TGA terminating codon. PCR1 construct contains the full-length wild-type *GBA1* cDNA OFR. PCR2 construct contains the full-length wild-type *GBA1* cDNA ORF with a c-terminal 6xHis-tag and a thrombin cleavage site.

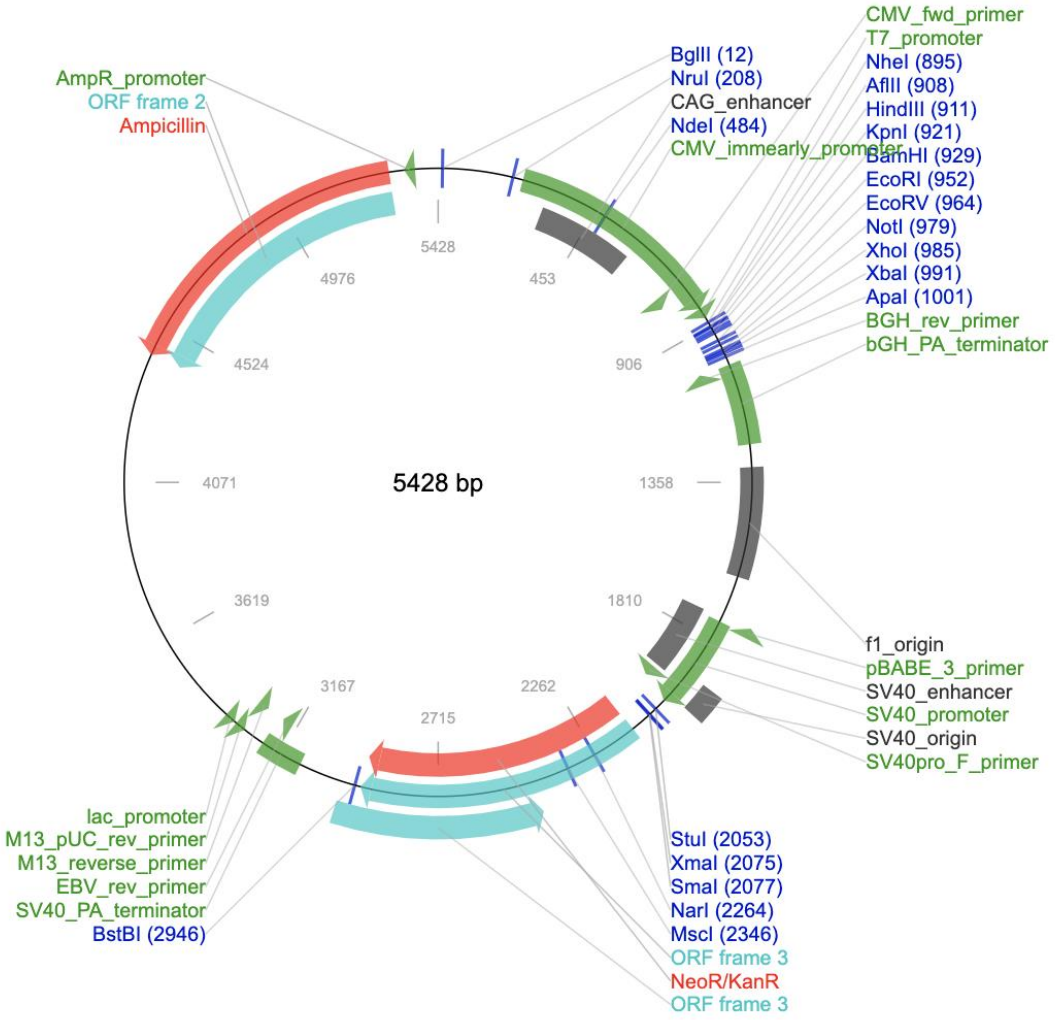

Figure 4. Map of pcDNA3.1(+) vector.

Mammalian expression vector with the CMV promotor. 5428 base pairs in size with high expression level. Restriction sites include NotI and XbaI. Bacterial resistance is ampicillin. Mammalian selectable marker is Neomycin/G418. Schematic sourced from www.addgene.org.

Table 4. List of primers used to sequence *GBA1* cDNA

Primer name	Sequence
GP551	CAA CAC CAT GCT CTT TGC CTC
GP552	CGC CAC AGG TAG GTG TGA ATG
GP554	GGA AAG TGA GTC ACC CAA ACC
GP555	CAG CCA GAA CAG AAG TTC CAG
GP556	CTG AGC ACA AGT TAC AGT TCT GG
GP601	CGA TTT AAG TAG CAA ATT TTG GG
GP602	GAC ATT GTG GTG AGT ACT GTT GG

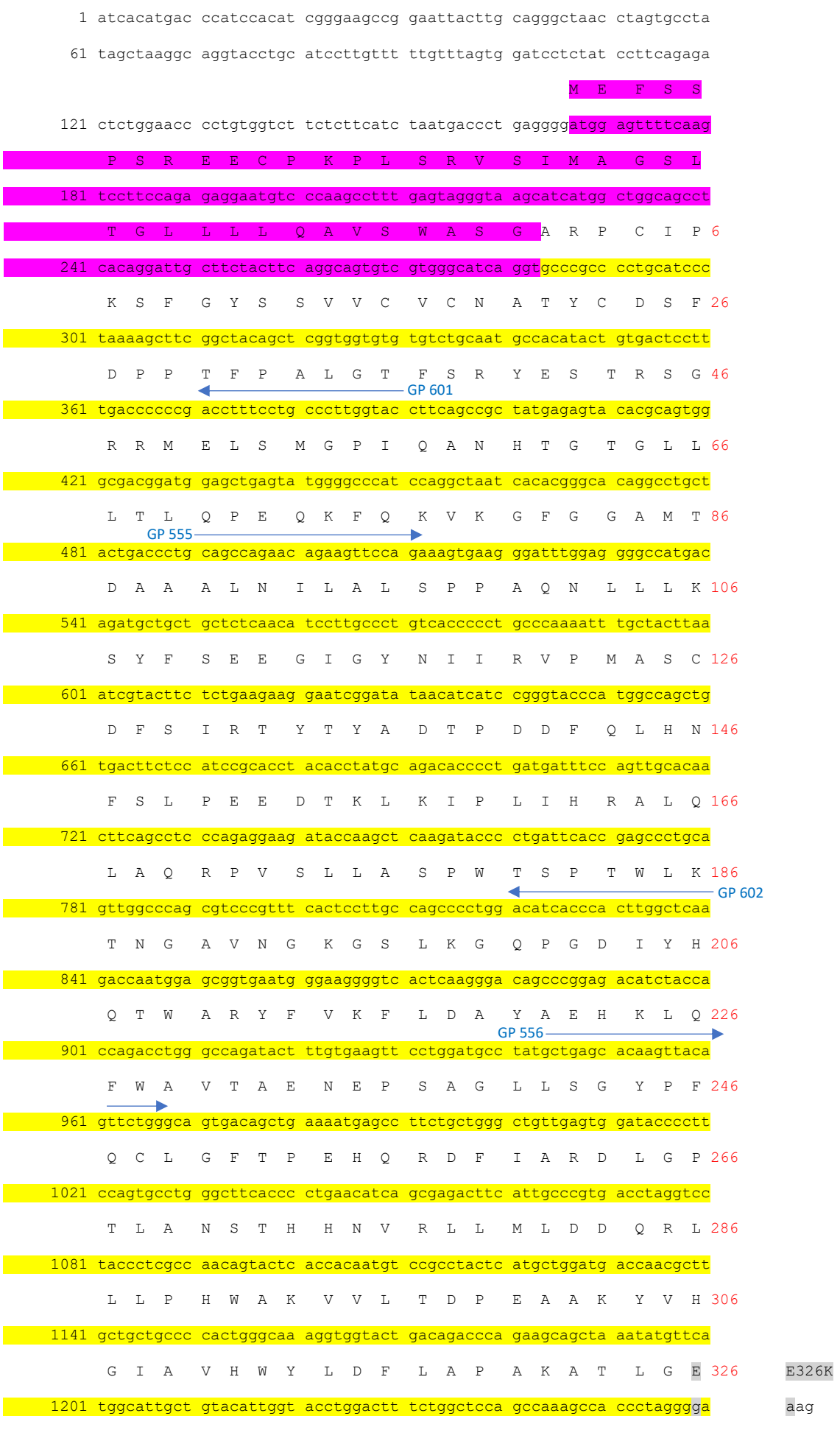
1 atcacatgac ccatccacat cgggaagccg gaattacttg cagggctaac ctagtgccta
61 tagctaaggc aggtacctgc atccttgttt ttgtttagtg gatcctctat ccttcagaga
M E F S S
121 ctctggaacc cctgtggtct tctcttcatc taatgaccct gaggggatgg agttttcaag
P S R E E C P K P L S R V S I M A G S L
181 tccttccaga gaggaatgtc ccaagccttt gagtagggta agcatcatgg ctggcagcct
T G L L L L Q A V S W A S G A R P C I P 6
241 cacaggattg cttctacttc aggcagtgtc gtgggcatca ggtgcccgcc cctgcatccc
K S F G Y S S V V C V C N A T Y C D S F 26
301 taaaagcttc ggctacagct cggtggtgtg tgtctgcaat gccacatact gtgactcctt
D P P T F P A L G T F S R Y E S T R S G 46
GP 601
361 tgacccccccg acctttcctg cccttggtac cttcagccgc tatgagagta cacgcagtgg
R R M E L S M G P I Q A N H T G T G L L 66
421 gcgacggatg gagctgagta tggggcccat ccaggctaat cacacgggca caggcctgct
L T L Q P E Q K F Q K V K G F G G A M T 86
GP 555
481 actgaccctg cagccagaac agaagttcca gaaagtgaag ggatttggag gggccatgac
D A A A L N I L A L S P P A Q N L L L K 106
541 agatgctgct gctctcaaca tccttgccct gtcacccccct gcccaaaatt tgctacttaa
S Y F S E E G I G Y N I I R V P M A S C 126
601 atcgtacttc tctgaagaag gaatcggata taacatcatc cgggtaccca tggccagctg
D F S I R T Y T Y A D T P D D F Q L H N 146
661 tgacttctcc atccgcacct acacctatgc agacacccct gatgatttcc agttgcacaa
F S L P E E D T K L K I P L I H R A L Q 166
721 cttcagcctc ccagaggaag ataccaagct caagataccc ctgattcacc gagccctgca
L A Q R P V S L L A S P W T S P T W L K 186
GP 602
781 gttggcccag cgtcccgttt cactccttgc cagcccctgg acatcaccca cttggctcaa
T N G A V N G K G S L K G Q P G D I Y H 206
841 gaccaatgga gcggtgaatg ggaaggggtc actcaaggga cagcccggag acatctacca
Q T W A R Y F V K F L D A Y A E H K L Q 226
GP 556
901 ccagacctgg gccagatact ttgtgaagtt cctggatgcc tatgctgagc acaagttaca
F W A V T A E N E P S A G L L S G Y P F 246
961 gttctgggca gtgacagctg aaaatgagcc ttctgctggg ctgttgagtg gataccccttt
Q C L G F T P E H Q R D F I A R D L G P 266
1021 ccagtgcctg ggcttcaccc ctgaacatca gcgagacttc attgcccgtg acctaggtcc
T L A N S T H H N V R L L M L D D Q R L 286
1081 taccctcgcc aacagtactc accacaatgt ccgcctactc atgctggatg accaacgctt
L L P H W A K V V L T D P E A A K Y V H 306
1141 gctgctgccc cactgggcaa aggtggtact gacagaccca gaagcagcta aatatgttca
G I A V H W Y L D F L A P A K A T L G E 326 E326K
1201 tggcattgct gtacattggt acctggactt tctggctcca gccaaagcca ccctagggga aag

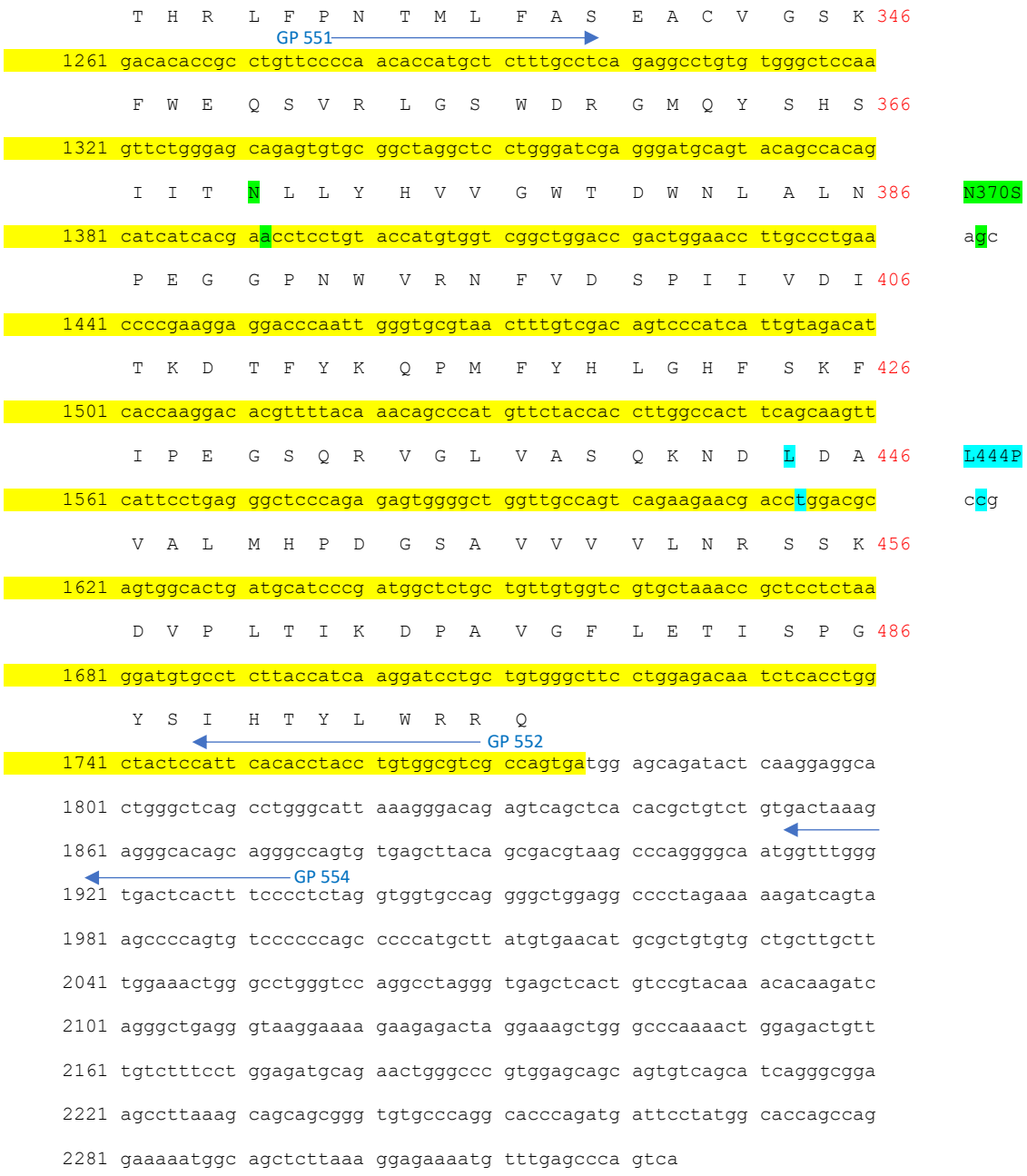

Figure 5. Human *GBA1* gene cDNA sequence.

Purple base pairs and nucleotides indicate the 39 amino acid signal peptide. Yellow base pairs and nucleotides indicate *GBA1* cDNA sequence. The E326K, N370S and L444P mutations are demonstrated in grey, green and blue respectively. Binding of primers GP551, GP552, GP554 GP555, GP556, GP601 and GP602 are shown in blue or by arrows.

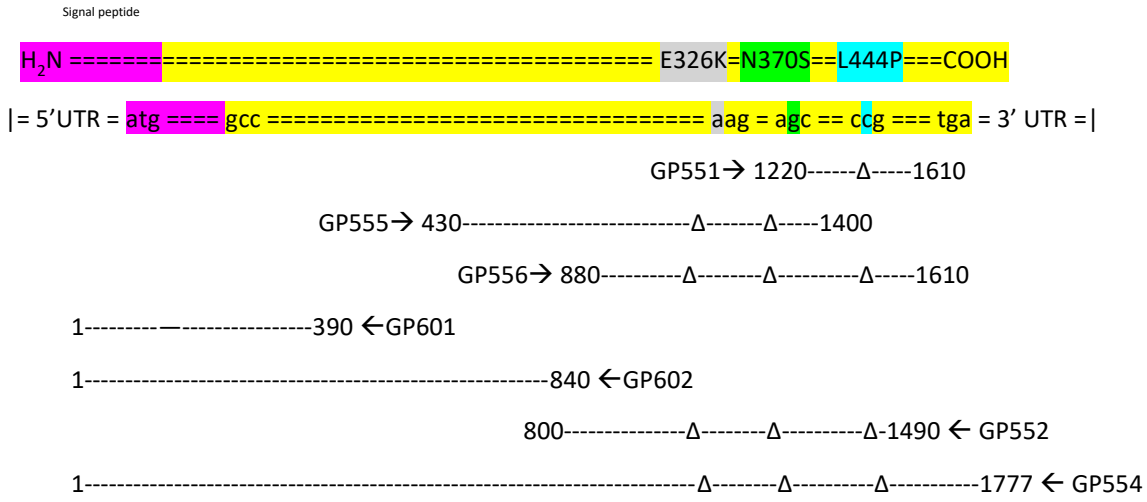

Figure 6. Primers used to sequence GBA1 cDNA and their binding position and reading frame.

Forward primers include: GP551 spanning base pairs 1220 – 1610; GP555 spanning base pairs 430 – 1400 and GP556 spanning base pairs 880 – 1610. Reverse primers bind and read the following sections of cDNA: GP601 base pairs 1 – 390; GP602 spans base pairs 1 – 840; GP552 which reads base pairs 800 – 1490 and GP544 spans base pairs from 1777. Δ indicates the site of each mutation. Use of these primers ensure each mutation site is sequenced three times, and the full *GBA1* cDNA sequence is read a minimum of twice.

2.4 Nanodrop analysis

To assess DNA or ribonucleic acid (RNA) concentrations, 1.5 μL of eluted plasmid DNA or RNA was pipetted onto the Nanodrop pedestal. Absorbance at 260 nm (A260) was read to assess DNA or RNA concentration. DNA and RNA purity was assessed by analysing the ratio between A260/A280. For pure DNA or RNA, this ratio is greater than 1.8.

2.5 Site directed mutagenesis

Site directed mutagenesis was carried out according to manufacturer's guidelines (Agilent Technologies QuikChange II Site-Directed Mutagenesis Kit #200521). Mutagenesis was used to introduce E326K, L444P or N370S mutations into PCR1 and PCR2. Primers for mutagenesis were generated using the Agilent Technologies QuikChange Primer Design online software (Table. 5.). To summarise, 20 ng template DNA was mixed with 5 μL reaction butter, 125 ng of forward and reverse primers containing the desired mutation, 1 μL PfuTurbo, 1 μL dNTPs and made up to 50 μL with distilled H_2O (dH_2O). The reaction was cycled for 12 cycles (55°C anneal, 1 minute; 68°C extension 1 min / kilobase (kb) plasmid) and then digested for 2 hours at 37°C with Dpn1. 1 μl of the digested DNA was transformed into MAX Efficiency DH5α Competent cells and colonies were selected, expanded in LB media and plasmid isolated using the QIAprep spin Miniprep Kit (Qiagen #27104) or the endotoxin-free plasmid Maxi Kit (Qiagen #12362). Amplified plasmid was sequenced by SourceBioscience to confirm the presence of desired mutations as shown in Figures. 7. and 8.

Table 5. Primers used in site directed mutagenesis of *GBA1* cDNA.

Mutated base pairs are in bold and underlined.

Mutation	Forward Primer	Reverse Primer
L444P	AGTCTTCTTGCTGG**G**CCTGCGTCACCGTG	TCAGAAGAACGACC**C**GGACGCAGTGGCAC
E326K	CGGTGGGATCCC**T**TCTGTGTGGCGG	GCCACCCTAGGG**A**AGACACACCGCC
N370S	GGTGTCGTAGTAGTGCT**C**GGAGGACATGGTACA	CCACAGCATCATCACGA**G**CCTCCTGTACCATGT

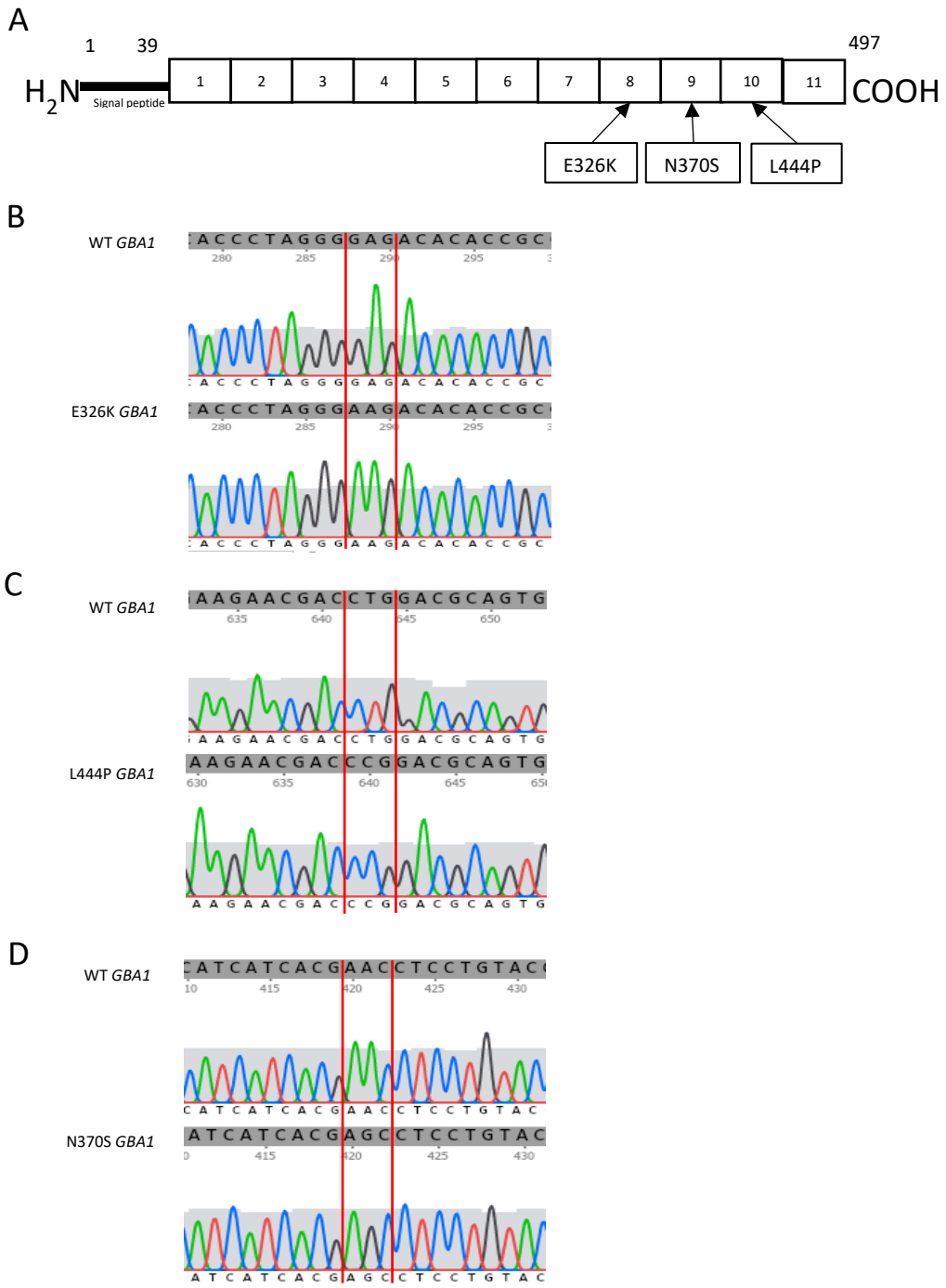

Figure 7. Site directed mutagenesis in full-length *GBA1* cDNA and sequencing chromatogram.

A) Schematic of *GBA1* cDNA with 11 exons. Arrows show the location of E326K, L444P and N370S mutations. **B)** Site-directed mutagenesis was performed in wild-type *GBA1* cDNA to a single nucleotide G>A to give E326K mutation. Chromatogram from Sanger sequencing with GP566 primer confirms nucleotide substitution. **C)** Site-directed mutagenesis was performed in wild-type *GBA1* cDNA to a single nucleotide T>C to give L444P mutation. Chromatogram from Sanger sequencing with GP566 primer confirms nucleotide substitution. **D)** Site-directed mutagenesis was performed in wild-type *GBA1* cDNA to a single nucleotide A>G to give N370S mutation. Chromatogram from Sanger sequencing with GP566 primer confirms nucleotide substitution.

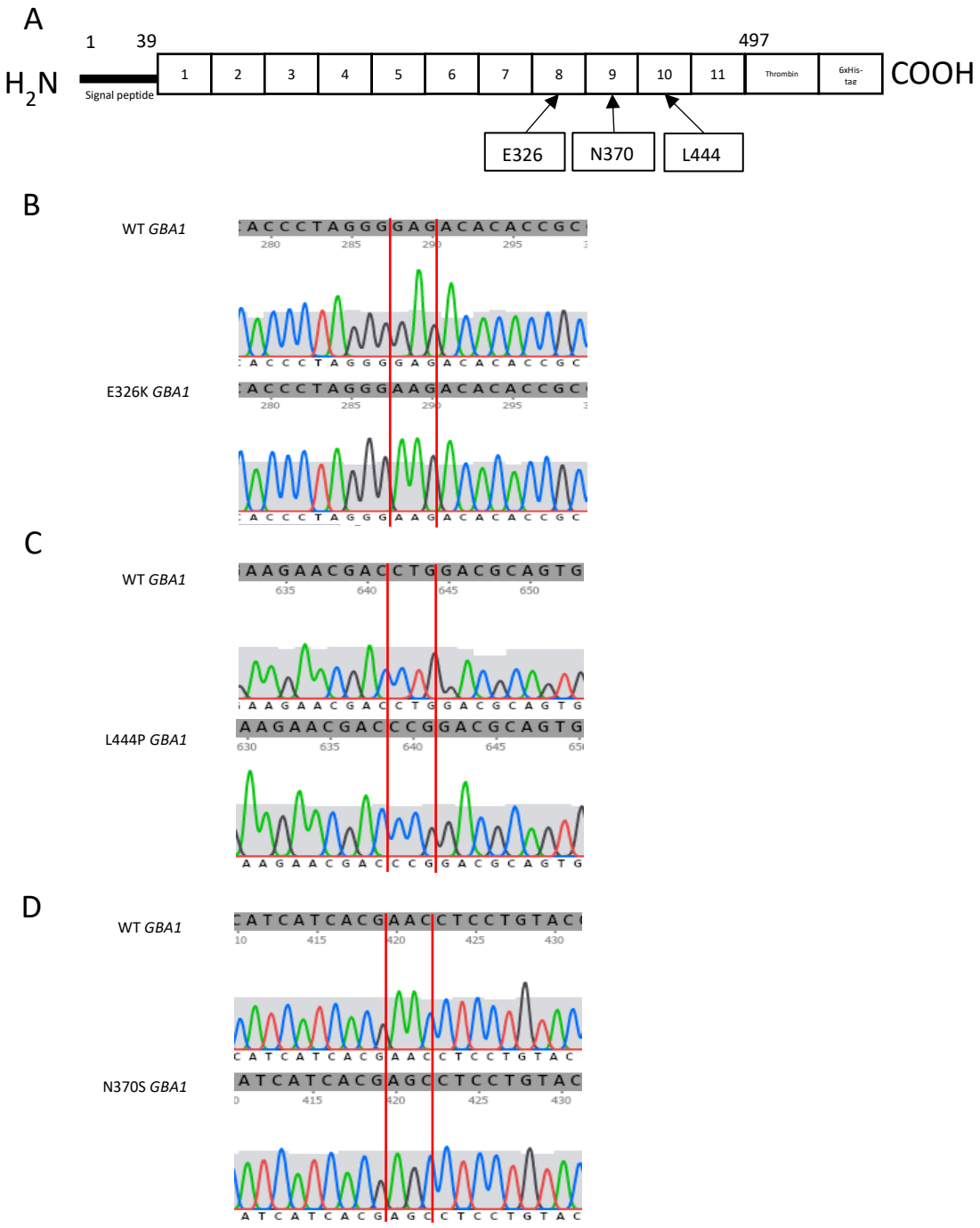

Figure 8. Site directed mutagenesis in full-length *GBA1* cDNA with c-terminal 6xHis-tag and sequencing chromatogram.

A) Schematic of *GBA1* cDNA with 11 exons. Arrows show the location of E326K, L444P and N370S mutations. **B)** Site-directed mutagenesis was performed in wild-type *GBA1* cDNA to a single nucleotide G>A to give E326K mutation. Chromatogram from Sanger sequencing with GP566 primer confirms nucleotide substitution. **C)** Site-directed mutagenesis was performed in wild-type *GBA1* cDNA to a single nucleotide T>C to give L444P mutation. Chromatogram from Sanger sequencing with GP566 primer confirms nucleotide substitution. **D)** Site-directed mutagenesis was performed in wild-type *GBA1* cDNA to a single nucleotide A>G to give N370S mutation. Chromatogram from Sanger sequencing with GP566 primer confirms nucleotide substitution.

2.6 Cell lines

Most human fibroblast cell lines were taken from the Schapira laboratory cell line bank and had been previously made. All patients and controls included in the study gave informed consent and the collection of skin biopsies was approved by the Royal Free Research Ethics Committee (REC number 10/H0720/21). Cell lines GM10905 and GM20272 were purchased from Coriell Institute cell repository. NDS00203 was purchased from NINDS Stem Cell Catalogue. Human iPSCs were derived from fibroblasts from the Schapira laboratory cell bank.

Parental SH-SY5Y cells were obtained from the European Collection of Authenticated Cell Cultures at passage 12. Parental HEK293 cells were taken from the Schapira laboratory cell bank.

2.7 Fibroblast cell culture

Patient fibroblast cells were cultured in Dulbecco's modified eagle media (DMEM) 4500 (mg/L) growth medium supplemented with Glutamax, 10% foetal bovine serum (FBS), non-essential amino acids (NEAA: 0.1 mM of: glycine, L-alanine, L-asparagine, L-aspartic acid, L-glutamic acid, L-proline and L-serine) and penicillin/streptomycin antibiotic cocktail (50ng/ml) at 37°C and 5% CO_2. See Table. 6. for list of fibroblast cell lines used in this study. Cell lines were harvested 48h after replenishing media at around 80% confluency using trypsin digestion. Cells were washed once in phosphate-buffered saline (PBS) and trypsin was added (0.25% trypsin in Versene). Following an incubation of 5 minutes at 37°C and 5% CO_2, the plates were tapped to detach cells. The trypsin was neutralised in 3 volumes of normal growth medium. For continued culturing, a fraction of cells was transferred to a falcon tube and pelleted for 5 minutes at 1000 RPM (200 x *g*). Pellets were resuspended in the appropriate volume of normal medium and split into new plates. If required, cells were counted prior to seeding using the C-

Chip NanoEnTek DHC-N01 counter. Cell line stocks were generated by resuspending cell pellets in 1 mL of freezing medium (10% dimethyl sulfoxide (DMSO) in FBS). Cells were frozen initially at -80°C and transferred to liquid nitrogen for long term storage.

Table 6. Fibroblast lines utilised in this study.

Cell line	GBA genotype	Phenotype	Gender	Age
KMI	WT/WT	Unaffected	F	58
SCO	WT/WT	Unaffected	M	53
ROK	WT/WT	Unaffected	F	73
7301	WT/WT	Unaffected	Unknown	Teenager
LB	WT/WT	Unaffected	Unknown	Infant
GM10915	L444P/L444P	Type I GD	M	7
GM20272	L444P/L444P	Type II GD	M	Child
EK	WT/E326K	PD	M	50
NDS00203	E326K/E326K	PD	M	52
IPE	N370S/N370S	GD	F	58
SAL	N370S/N370S	GD	M	76

2.8 SH-SY5Y cell culture

SH-SY5Y neuroblastoma cells were cultured in a 1:1 mixture of Ham's F-12 and DMEM growth medium supplemented with 10% FBS, non-essential amino acids (NEAA: 0.1 mM of: glycine, L-alanine, L-asparagine, L-aspartic acid, L-glutamic acid, L-proline and L-serine) and penicillin/streptomycin antibiotic cocktail (50ng/ml) at 37°C and 5% CO_2. SH-SY5Y lines ectopically expressing GCase protein coupled to G418 selection marker were routinely cultured in 400 μg/mL G418. Growth under these conditions ensured stable expression of GCase protein. See Table. 7. For the list of SH-SY5Y lines used in this study. For routine culture, cells were passaged at around 80% confluency using trypsin digestion. Culture medium was removed from cells, centrifuged at 1000 RPM (200 x *g*) for 5 minutes to remove floating cells and stored at -80°C for analysis. Cells were washed once in PBS and trypsin was added (0.25% trypsin in Versene). Following an incubation of 2 minutes, the plates were tapped to detach cells. The trypsin was neutralised in 9 volumes of normal growth medium. For continued culturing, a fraction of cells was transferred to a falcon tube and pelleted for 10 minutes at 1000 RPM (200 x *g*). Pellets were resuspended in the appropriate volume of normal medium and split into new plates. If required, cells were counted prior to seeding using the C-Chip NanoEnTek DHC-N01 counter. Cell line stocks were generated by resuspending cell pellets in 1 mL of freezing medium (10% DMSO in FBS). Cells were frozen initially at -80°C and transferred to liquid nitrogen for long term storage.

Table 7. SH-SY5Y lines generated in this project.

Cell Line Name	Genotype	Tag
Wild-type 3 (WT3)	Wild-type	No tag
Wild-type 4 (WT4)	Wild-type	No tag
WTH4	Wild-type	C-terminal 6xHis-tag
E326K 3	E326K	No tag
E326K 6	E326K	No tag
E326K H-5	E326K	C-terminal 6xHis-tag
L444P 3 (L4P3)	L444P	No tag
L444P 5 (L4P5)	L444P	No tag
L444P H-4	L444P	C-terminal 6xHis-tag
N370S 2	N370S	No tag
N370S 3	N370S	No tag
N370S H-1	N370S	C-terminal 6xHis-tag

2.9 HEK293 cell culture

Human embryonic kidney 293 (HEK293) cells were cultured in DMEM 4500 (mg/L) growth medium supplemented with Glutamax, 10% FBS, non-essential amino acids (NEAA: 0.1 mM of: glycine, L-alanine, L-asparagine, L-aspartic acid, L-glutamic acid, L-proline and L-serine) and penicillin/streptomycin antibiotic cocktail (50ng/ml) at 37°C and 5% CO_2. HEK293 lines ectopically expressing GCase protein coupled to G418 selection marker were routinely cultured in 2.5 mg/mL G418. Growth under these conditions ensured stable expression of GCase protein. See Table. 8. for list of HEK293 cell lines used in this study. Cell lines were harvested 48h after replenishing media at around 80% confluency using trypsin digestion. Cells were washed once in PBS and trypsin was added (0.25% trypsin in Versene). Following an incubation of 5 minutes at 37°C and 5% CO_2, the plates were tapped to detach cells. The trypsin was neutralised in 3 volumes of normal growth medium. For continued culturing, a fraction of cells was transferred to a falcon tube and pelleted for 5 minutes at 1000 RPM (200 x *g*). Pellets were resuspended in the appropriate volume of normal medium and split into new plates. If required, cells were counted prior to seeding using the Ch-Chip NanoEnTek DHC-N01 counter. Cell line stocks were generated by resuspending cell pellets in 1 mL of freezing medium (10% DMSO in FBS). Cells were frozen initially at -80°C and transferred to liquid nitrogen for long term storage.

Table 8. HEK293 lines generated in this project.

Cell Line Name	Genotype	Tag
WT-293	Wild-type	C-terminal 6xHis-tag
E326K-293	E326K	C-terminal 6xHis-tag
L444P-293	L444P	C-terminal 6xHis-tag
N370S-293	N370S	C-terminal 6xHis-tag

2.10 Stable transfection of SH-SY5Y cells

SH-SY5Y cells were transfected with the pcDNA3.1 vector containing PCR1 or PCR2 harbouring wild-type, E326K, L444P or N370S *GBA1* mutations (see chapter 2.2 and 2.4). 24 hours prior to transfection, SH-SY5Y cells were plated at $2.5x10^5$ cells per well in a 12 well plate. A liposome-DNA mix was made using 2 µL XtremeGENE and 2 µg DNA in Opti-minimum essential medium (Opti-MEM). The mixture was vortexed and incubated at room temperature for 15 minutes. Following this, the mixture was added dropwise to the adherent cells growing in complete medium. Cells were transfected with either PCR1 plasmid containing wild-type, L444P, E326K and N370S GBA or PCR2 (C-terminal 6xHis-tag) plasmid containing wild-type, L444P, E326K and N370S GBA cDNA. A mock transfection, containing no DNA was performed in parallel. Cells were incubated for 72 hours before replacing the medium with fresh growth medium, supplemented with 400 µg/ml G418 antibiotics and incubated at 37°C and 5% CO_2 for selection. Growth medium with selection reagent was replaced every 2-3 days. After ensuring all mock transfections had died, colonies from the transfected cells were selected with sterile cloning cylinders. Colonies were transferred to 6 well plates and maintained in growth medium containing G418. Once confluent, cells were trypsinised and expanded into a $10mm^2$ dish in 10 mL normal growth media. Clones were frozen down or pelleted for characterisation.

2.11 Stable transfection of HEK293 cells

HEK293 cells were transfected with the pcDNA3.1 vector containing PCR2 harbouring wild-type, E326K, L444P or N370S *GBA1* mutations (see chapter 2.2 and 2.4). 24 hours prior to transfection, HEK293 cells were plated in a $10mm^2$ dish in normal growth media at 20×10^5 cells. After ensuring cells were at 40% confluency, HEK293 cells were transfected using Superfect Transfection

Reagent (Qiagen #301305). The administration of DNA to Superfect reagent was in a 1:9 ratio. Cells were transfected with PCR2 (C-terminal His-tag) plasmid containing wild-type, L444P, E326K and N370S GBA cDNA. A mock transfection, containing no DNA was performed in parallel. Cells were treated with normal growth medium, supplemented with 2.5 mg/ml G418 antibiotics, 25mM 4-(2-hydroxyethyl)-1-piperazineethanesulfonic acid (HEPES) and 0.1mM Amphotericin B for selection and incubated at 37°C and 5% CO_2. Cells were trypsinised and counted using the C-Chip NanoEnTek DHC-N01 counter and seeded into 96 well plates at a density of one cell per. Cells were again treated with normal growth medium, supplemented with 2.5 mg/ml G418 antibiotics, 25mM HEPES and 0.1mM Amphotericin B for selection and incubated at 37°C and 5% CO_2. The selection medium was changed every 3 days. After 14 days, wells with a single colony were washed once with PBS, trypsinised and transferred to a 6 well plate in 2mL selection medium. Once confluent cells were again trypsinised and expanded into a 10mm^2 dish in 10 mL normal growth medium, where they were harvested for continued growth, or to generate pellets for further analysis.

2.12 Differentiation of SH-SY5Y cells

Cells were differentiated in to human dopaminergic neurons, as described previously (Gegg et al., 2020). Prior to seeding, 6 well plates were coated with 1mL/well poly-L-ornithine solution (0.01 % (wt/vol); Sigma Cat #P4957-50ML) for 1 hour at room temperature. Following one wash with PBS, plates were air dried and coated in 2 µg/ml fibronectin and 1 µg/ml laminin in PBS for 1 hour. Plates were aspirated immediately before seeding. SH-SY5Y cells were grown to 80-90% confluence in a 10mm^2 dish in 10 mL normal growth medium and were passaged with 1 mL trypsin. The reaction was stopped with 9 volumes of growth

medium. Cells were pelleted at 200 x *g* for 10 minutes and resuspended in differentiation medium (Neurobasal media supplemented with 1X B-27™, 30 µM retinoic acid, 10 ng/mL brain-derived neurotrophic factor (BDNF) and penicillin/streptomycin antibiotic cocktail (50ng/ml)). Cells were counted using the C-Chip NanoEnTek DHC-N01 counter and seeded at 4.5 x 10^5 cells/mL. Differentiation medium was changed every 2-3 days, keeping light exposure to a minimum. Cells should be differentiated by 10 days. After 10 days culture medium was removed from cells, centrifuged at 200 x *g* for 5 minutes to remove floating cells and stored at -80°C for analysis. Cells were washed in PBS and trypsinised with 100 µL trypsin. The reaction was stopped with 9 volumes of differentiation medium and cells pelleted at 200 x g for 10 minutes. Pellets were resuspended in PBS and centrifuged again at 200 x *g* for 10 minutes. Supernatant was discarded, and cells were stored at -80°C for analysis.

2.13 Induced pluripotent stem cell derived midbrain dopamine neurons

Midbrain dopamine neurons were generated from iPSCs by Dr Matt Gegg, using the floor plate protocol of Kriks et al., (Kriks et al., 2011).

Table 9. Midbrain dopamine neurons lines generated in this project.

Cell line	GBA genotype	Phenotype	Gender	Age
MNO	WT/WT	Unaffected	F	53
EK	E326K/WT	PD	M	50
KTI	N370S/WT	PD	F	55

2.14 Preparation of cell pellets

2.14.1 Obtaining dry cell pellets

Cells were harvested by trypsination, followed by neutralisation in the appropriate volume of growth medium. Cells were pelleted at 200 *x g* for 10 minutes. The cell pellet was washed with 1 mL PBS and pelleted at 200 x *g* for 10 minutes in microfuge tubes. The supernatant was discarded, and the dry cell pellet was stored at -80°C until analysis.

2.14.2 Triton X 100 extraction of cell pellets

For protein analysis, cell pellets were solubilised in 1% (v/v) Triton X 100 in PBS pH 7.4, containing 1 X protease and phosphatase inhibitors (Halt) on ice with vortexing for 15 minutes. The lysate was centrifuged at 17,000 x *g* for 10 minutes at 4°C in a microfuge. The supernatant containing extracted proteins was aliquoted and stored at -80°C or used for bicinchoninic acid (BCA) assay analysis (Chapter 2.13.4).

2.14.3 Probe sonication of cell pellets

For some protein analyses, cell pellets were lysed by probe sonication. Pellets were resuspended in dH_2O supplemented with 1 X protease and phosphatase inhibitors (1x) (Halt). The lysate was sonicated using the Soniprep 150 instrument for 15-30 seconds. Cell lysate was stored at -80°C or used for BCA analysis.

2.14.4 BCA assay

Bovine serum albumin (BSA) standards of known protein concentrations (0.05 – 1.0 μg/μl) and Triton X 100 cell lysates were diluted in dH_2O and pipetted into clear bottomed 96 well plates to final volumes of 50 μL. 50 μL of BCA reagent (50:1 ratio of A:B) was added to the wells. The plate was incubated at 37°C in a humidified atmosphere for 30 minutes. Absorbance was read at 562 nm on a

plate reader (Bio-Rad). BSA standards of known protein concentrations were plotted against absorbance at 562 nm using Excel and sample protein concentration was interpolated from the standard curve by linear regression.

2.15 SDS-PAGE and Western blotting

Triton X 100 fibroblast and SH-SY5Y cell lysates containing 10 – 30 µg of protein were added to 4 X NuPage™ sample buffer and 10 X NuPage™ reducing agent and diluted in dH_2O to a consistent final volume. Samples were heated for 10 minutes at 70°C and loaded alongside 5 µL Precision Plus Protein™ molecular weight standard (Bio-Rad #1610374) onto 4-12% NuPage™ gels. Samples were electrophoresed at 200 V (Bio-Rad power pack) for 45 minutes for SH-SY5Y cells or 60 minutes for fibroblast cells in NuPage™ MES sodium dodecyl sulphate (SDS) running buffer. Proteins were transferred onto PVDF membranes at 30 V for 1 hour in Towbin buffer (25 mM Tris, 190 mM glycine, 20% MeOH) using the XCell transfer system. For HEK293 cells, lysates containing 10 – 30 µg of protein were added to either 4 X Bolt™ sample buffer and 10 X Bolt™ reducing agent. For analysis of untransfected HEK293 cells, 90 µg of protein was loaded. Samples were heated for 10 minutes at 70°C and loaded alongside 5 µL SeeBlue™ Plus2 pre-stained protein standard onto Bolt™ 8% bis-tris protein gels. Gels were run for 45 minutes at 165 V in 1X Bolt™ MOPS SDS running buffer. Proteins were transferred onto PVDF membranes at 23 V for 1 hour in Bolt™ transfer buffer.

Membranes containing transferred proteins were blocked for 1 hour with 10% milk diluted in PBS by rolling at room temperature. Primary antibodies (Table. 3.) were added to 5% milk diluted in PBS and incubated with the membrane on a roller for 1-2 hours at room temperature or overnight at 4°C. Membranes were washed for 5 minutes with 0.4% PBS-Tween (PBS-T), the wash was repeated 2

more times. The membranes were then incubated with horseradish peroxidase (HRP)-conjugated secondary antibodies in 5% milk PBS for 1 hour at room temperature. Following the incubation, membranes were washed as before with an additional final 5minute wash in PBS. Membranes were incubated with 2 mL GE Healthcare Amersham™ electro-chemi-luminescence (ECL)™ Prime Western Blotting Detection Reagent for 5 minutes and excess reagent drained. Blots developed using the Bio-Rad ChemiDoc imaging system (Bio-Rad) using the 'chemi' protocol with signal accumulation mode, calibrated to the signal intensities. Molecular weight protein standard markers were captured using the 'colorimetric' protocol.

Western blots were analysed using ImageLab software (Bio-Rad). Protein abundance was quantified by densitometry analysis of band intensity.

2.16 Dot blotting

Nitrocellulose membrane (PerkinElmer PROTRAN, 0.45 µm pore size) was assembled into BioRad dot blot apparatus and washed twice with PBS. Samples of cell lysate or medium were loaded in duplicate or triplicate onto the nitrocellulose membrane and vacuum was applied. The membrane was washed twice with PBS followed by blocking with BlockACE (BioRad) for 1 hour at room temperature. The membrane was incubated overnight at 4°C with primary antibody in BlockACE and washed twice with 0.4% PBS-T. Secondary antibody in BlockACE was incubated with the membrane at room temperature for 1 hour. The membrane was washed three times with 0.4% PBS-T with an additional final 5 minute wash in PBS. Membranes were developed and imaged in the same manner as for western blotting (section 2.14). Dot blots were analysed using ImageLab software (Bio-Rad). Protein abundance was quantified by

densitometry analysis of the dots and the mean of each duplicate or triplicate calculated.

2.17 Quantitative real-time PCR for mRNA analysis

Total RNA was extracted from dry cell pellets using the RNAeasy kit (Qiagen), per manufacturer's instructions. Concentration and purity of RNA was determined using the Nanodrop (see section 2.3). 600 ng RNA was converted to cDNA with the QuantiTect reverse transcription kit (Qiagen) as per manufacturer's instructions. Quantitative real-time polymerase chain reaction (PCR) reactions were performed using the QuantiTect SYBR Green kit (Qiagen). To summarise, 2 μL cDNA, 10 μL SYBR Green, 7 μL RNAse free dH_2O and 1 μL 20 μM forward and reverse primers was added to each well. A mock mixture using 2 μL RNAse free dH_2O instead of cDNA was used as a blank. See Table. 10. for primers used (Eurofins Genomics) as previous (Gegg et al., 2012, Alvarez-Erviti et al., 2013). For the PCR reaction activation was at 95°C for 10 minutes. Following this was 40 cycles of denaturing at 94°C for 15 seconds; annealing at 58°C for 30 seconds and extension at 72°C for 30 seconds. Fold-change in gene expression was calculated using the ΔC_T method, based on biological reference samples and glyceraldehyde 3-phoshate dehydrogenase (GAPDH) messenger RNA (mRNA) levels for normalisation. All results obtained were from the evaluation of two technical duplicates of three independent experiments.

Table 10. Primers used for analysis of gene expression by quantitative real-time PCR.

Primer	Forward Primer	Reverse Primer
GBA1	TGCTGCTCTCAACATCCTTGCC	TAGGTGCGGATGGAGAAGTCAA
SNCA	GCCAAGGAGGGAGTTGTGGCTGC	CTGTTGCCACACCATGCACCACTCC
TH	GCGGTTCATTGGGCGCAGG	CAAACACCTTCACAG
CHOP	ACCAAGGGAGAACCAGGAAACG	TCACCATTCGGTCAATCAGAGC
GAPDH	GAAGGTGAAGGTCGGAGT	GAAGATGGTGATGGGATTTC

2.18 Fluorescence microscopy

For analysis of coverslips a Zeiss Axioplan microscope fitted with an LED illumination unit (QImaging wLS) with red, green and blue filters was used. Images were captured using Micro-Manager software. Exposure settings were adjusted and the same threshold was used throughout image capturing. Images were analysed using ImageJ software.

2.19 Immunofluorescence microscopy

Cells were plated onto coverslips in 12 well plates and incubated at 37°C at 5% CO_2 until ready for analysis. Coverslips were removed from each well and fixed in pre-warmed (37°C) 4% paraformaldehyde (PFA) (SantaCruz) in PBS at room temperature for 20 minutes. Permeabilisation of the cells was carried out by incubation with pre-chilled 100% methanol (MeOH) at -20°C for 15 minutes. After washing once with PBS, coverslips were blocked in 10% normal goat serum (NGS) diluted in PBS for 45 minutes at 37°C in a humidified atmosphere. After aspirating the NGS, coverslips were incubated with primary antibody (Table. 3.) diluted in 2% NGS diluted in PBS for 45 minutes at 37°C in a humidified atmosphere. The cells were washed once with PBS and once with 2% NGS diluted in PBS. Following the washes, the coverslips were incubated with Alexa

Fluor (488 and 568) conjugated secondary antibodies in 2% NGS diluted in PBS for 45 minutes at 37°C in a humidified atmosphere. Cells were washed once with PBS and coverslips were mounted onto glass slides with 1 μg/mL 4′,6-diamidino-2-phenylindole (DAPI) CitiFluor and sealed with nail polish for later analysis by fluorescence microscopy (see section 2.17).

2.20 GCase activity assay

Triton X 100 cell pellets with a protein concentration of between 0.2 mg/ml and 2 mg/ml were added to clear bottom 96 well plates. For determining the activity of recombinant protein, samples were made to a final volume of 10 µL with a concentration between 0.2 μg/ml and 200 μg/ml. Wells with PBS alone acted as a blank to measure background fluorescence. GCase activity was determined by the hydrolysis of 5mM 4-methylumbelliferyl-β-D-glucopyranoside (M-Glu) in McIlvaine buffer at pH 5.4 in the presence of 22mM sodium taurocholate (NaT). NaT inhibits cytosolic glucocerebrosidase 2 (*GBA2*) and activates lysosomal *GBA1* (Wenger et al., 1978). Additionally, the assay was performed at pH 4.5 in the absence of NaT. The pharmacological irreversible GCase inhibitor, CBE (Kuo et al., 2019) was administered at a final concentration of 1 mM to confirm assay specificity. The assay was incubated at 37°C for 1 hour (Wenger et al., 1978) and stopped by adding 0.25 M glycine at pH 10.4. Fluorescence was measured at excitation 365 nm and emission 450 nm on Cytation-1 plate reader (Bio-Tek). 4-methylumbelliferone fluorescence (1 nmol) was used as a standard of known fluorescence.

Enzyme activities were calculated by subtracting the background fluorescence from the mean fluorescence for a given cell lysate. This was then divided by the fluorescence of the 4-methylumbelliferone standard to give activity in

nmol/hour/ml. This was divided by the total protein concentration, determined by a BCA assay, to calculate the activity in nmol/hour/mg.

2.21 Lysosomal hydrolase activity assay (β-galactosidase and β-hexosaminidase activity assay)

The activity of β-Galactosidase and β-Hexosaminidase was assayed in cell lysates using the substrates 4-Methylumbelliferyl β-D-galactopyranoside (1mM) and 4-Methylumbelliferyl N-acetyl-β-D-glucosaminide (2mM), respectively, in a sodium citrate buffer (pH 4.1). Plates were incubated at 37°C in a humidified atmosphere for 30 minutes and the reaction stopped by the addition of 0.25 M glycine at pH 10.4. Fluorescence was measured and enzyme activities calculated as above for the GCase activity assay (Chapter 2.19).

2.22 Statistics

Graphs were made using Microsoft Excel or GraphPad Prism version 9.3.1 and are expressed as MEAN ± standard error of the mean (SEM). Statistical significance was determined by one-way ANOVA and Tukey's post hoc test using Origin 2017 software or GraphPad Prism version 9.3.1, or by linear mixed-effects model fit by REML using R version 3.6.2.

3 Biology of *GBA1* E326K mutation

3.1 Introduction

The common *GBA1* mutations, L444P and N370S, account for 1.01 – 15.3% of *GBA1* carriers (Sidransky et al., 2009, Neumann et al., 2009) and have been studied extensively. Both are associated with PD, with the severe L444P mutation associated with an odds ratio of 0.96-28.8 and the mild N370S mutation associated with an odds ratio of 1.5-6.79 (see Table. 1.) (Sidransky et al., 2009, Aharon-Peretz et al., 2005, Clark et al., 2007, Gan-Or et al., 2015, Gan-Or et al., 2008, Ran et al., 2016, Duran et al., 2013). Evidence suggests that they may work via both loss of function (Grace et al., 1994, Sanchez-Martinez et al., 2016, Schöndorf et al., 2014) and gain of function (Sanchez-Martinez et al., 2016, Ron and Horowitz, 2005, Maor et al., 2013) mechanisms. The E326K mutation is one of the most prevalent PD causing *GBA1* mutations, with a carrier frequency of 1.3 – 7.57% (Duran et al., 2013, Stoker et al., 2020b, Huang et al., 2018). However, very little is known regarding the mechanisms underlying E326K pathology. This mutation is non-pathogenic for GD when homozygous, presenting no clinical features of GD, however when in a compound heterozygote with a GD-causing mutation, E326K contributes to GD severity (Duran et al., 2013, Chabas et al., 2005, Liou and Grabowski, 2012). Although not associated with GD, both E326K carriers and homozygotes are at an increased risk for PD, with the odds ratio calculated at 1.5-3.2 (Table. 1.) (Ran et al., 2016, Berge-Seidl et al., 2017, Huang et al., 2018, Stoker et al., 2020b).

Several groups have attempted the biochemical characterisation of E326K (McNeill et al., 2014, Chabas et al., 2005, Liou and Grabowski, 2012, Horowitz et al., 2011, Montfort et al., 2004), however compared to L444P and N370S, very little is known about the pathways involved in E326K pathology. A summary of

previous studies investigating the effect of the E326K mutation on GCase activity can be found in Table. 2. The aim of this study was to characterise whether the E326K mutation is a loss of function or a gain of function mutation. As this mutation does not cause GD, it suggests that the underlying mechanisms for *GBA1*-PD may be different to those of GD. The key outcome was to understand the effect of the E326K mutation on GCase protein levels, function and localisation. Utilising L444P and N370S mutations allows comparison to both mild and severe mutations. Analysis of the cellular mechanisms involved in all three mutations may increase understanding of the pathways involved in an individual mutation's predisposition to PD.

It may be that the mechanism in which *GBA1* mutations predispose to PD is multifaceted, with several elements important. As not all mutations are associated with equal risk of PD, it may be that different pathogenic mechanisms are more pronounced in carriers of different mutations.

3.2 Materials and Methods

3.2.1 Chemicals and reagents

Unless otherwise stated, all chemicals and reagents were purchased from ThermoFisher, Merck Millipore and Abcam.

3.2.2 Antibodies

Table 11. Antibodies used in chapter 3.

Antibody Name	Immunogen and epitope	Species	Western Blot or Dot Blot Dilution	Immunofluorescence Dilution
Anti-GBA clone 2e2, AP1140 (Millipore)	Recombinant human GBA protein, AA 146-236 (outside of mutation sites)	Mouse, mAb	1/1000	1/200

Anti-GRP78 BiP, ab21685 (Abcam)	Mouse GRP78 BiP, epitope AA 600 to the C-terminus	Rabbit, pAb	1/1000	n/a
eIF2α, 9722 (Cell Signaling)	Human eIF2α protein	Rabbit, pAb	1/2000	n/a
Phospho-eIF2α (Ser51), 9721 (Cell Signaling)	Human eIF2α protein when phosphorylated at Ser51	Rabbit, pAb	1/2000	n/a
Beta-actin, ab8227 (Abcam)	Human beta-actin, epitope AA 1-100	Rabbit, pAb	1/4000-1/500	n/a
LAMP-1/CD107a, NB120-19294 (Novus)	Synthetic peptide corresponding to AA 407-416 of human LAMP1	Rabbit, mAb	1/1000	n/a
Calnexin, ab22595 (Abcam)	Human Calnexin epitope AA 550 to the c-terminus	Rabbit, pAb	n/a	1/500
Cathepsin D [ERP3057Y], ab75852 (Abcam)	Human Cathepsin D epitope AA 350 to the c-terminus	Rabbit, mAb	1/2000	1/150
Glucosylceramide RAS_0100 (Glycobiotech)	Human Glucosylceramide	Rabbit	1/500-1/1000	1/100
Anti-Rabbit HRP (Dako)	n/a	n/a	1/3000	n/a
Anti-Mouse HRP (Dako)	n/a	n/a	1/3000	n/a
Anti-Mouse Alex-Fluor 488 (Invitrogen)	n/a	n/a	n/a	1/300 – 1/500
Anti-Rabbit Alex-Fluor 568 (Invitrogen)	n/a	n/a	n/a	1/300 – 1/500

3.2.3 Fibroblast cell culture

Culturing of fibroblasts was carried out as described in Chapter 2.7. A list of fibroblast cell lines used in this study can be found in Table. 6.

3.2.4 Sequencing of fibroblasts

To confirm the genome of the fibroblast lines, genome sequencing was performed. Total RNA was isolated from fibroblasts using the RNAeasy kit (Qiagen), according to the manufacturer's instructions and eluted in RNase and DNase free water. The concentration of RNA was determined using a Nanodrop, as described in Chapter 2.3. Following this, 600 ng RNA was converted to cDNA

with the QuantiTect reverse transcription kit (Qiagen) as per manufacturer's instructions. Using the Promega GoTaq Polymerase kit (M300), PCR for genotyping was made using 5 μL 5X Green GoTaq Reaction Buffer, 1.25 μL of each primer (0.5 μM), 0.125 μL GoTaq Polymerase, 0.5 μL of cDNA and 16.4 μL RNase/DNase free H_2O. PCR was set with an initial activation step at 95°C for 2 minutes. This was followed by 30 cycles of complete denaturing of all double stranded DNA at 95°C for 30 seconds, primer annealing at 63°C for 30 seconds and extension at 72°C for 30 seconds. After this, a final extension step was set at 72°C for 5 minutes.

To assess whether the correct DNA product was made, DNA was run on 1% agarose gel alongside 5 μL Precision Plus Protein™ molecular weight standard (Bio-Rad #1610374). Visualisation of a single band around 550 kb was considered positive for the *GBA1* amplicon. DNA was sent for Sanger sequencing by SourceBioscience using primers as listed in Table. 12. Sequences were analysed using SnapGene software, and representative chromatograms are shown in Figure. 9.

Table 12. Primers used to sequence fibroblasts.

	Primers	Sequence
Wild-type	GP551	CAA CAC CAT GCT CTT TGC CTC CGC
	GP552	CAC AGG TAG GTG TGA ATG
	GP554	GGA AAG TGA GTC ACC CAA ACC
	GP556	CTG AGC ACA AGT TAC AGT TCT GG
E326K	GP551	CAA CAC CAT GCT CTT TGC CTC CGC
	GP552	CAC AGG TAG GTG TGA ATG
L444P	GP554	GGA AAG TGA GTC ACC CAA ACC
	GP556	CTG AGC ACA AGT TAC AGT TCT GG
N370S	GP554	GGA AAG TGA GTC ACC CAA ACC
	GP556	CTG AGC ACA AGT TAC AGT TCT GG

A

WT/WT (Cell line SCO)

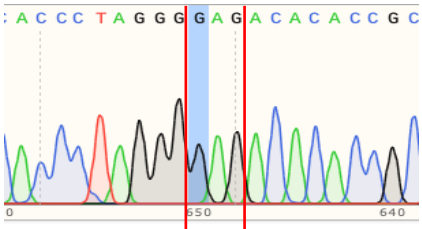

E326K/WT (Cell line EK)

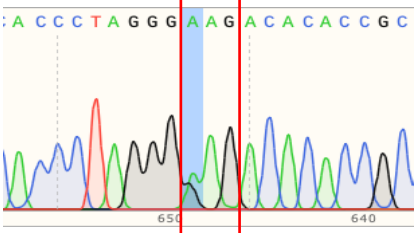

E326K/E326K (Cell line NDS200203)

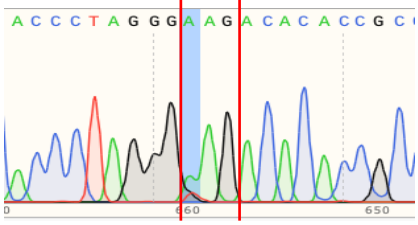

B

WT/WT (Cell line SCO)

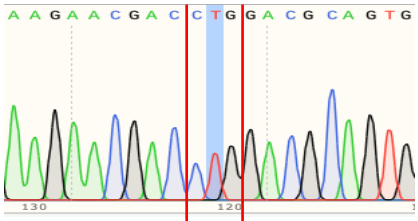

L444P/L444P (Cell line GM20272)

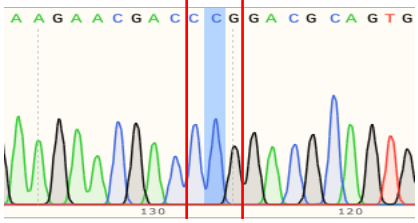

C

WT/WT (Cell line SCO)

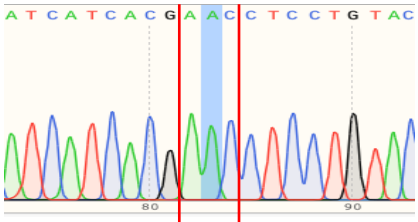

N370S/N370S (Cell line IPE)

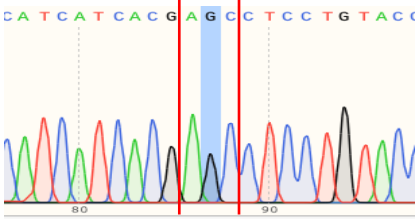

Figure 9. Chromatogram from Sanger sequencing of fibroblast cell lines.

A) Chromatograms for homozygous wild-type fibroblast line SCO, heterozygous E326K fibroblast line EK and homozygous E326K fibroblast line NDS200302 showing E326K mutation. **B)** Chromatograms for homozygous wild-type fibroblast line SCO and homozygous L444P fibroblast line GM20272 showing L444P mutation. **C)** Chromatograms for homozygous wild-type fibroblast line SCO and homozygous N370S fibroblast line IPE showing N370S mutation.

3.2.5 Western blotting

Samples for western blotting were generated as described in Chapter 2.14. Western blotting was performed as described in Chapter 2.15 using the NuPAGE™ equipment. Antibodies used for fibroblast western blot analysis is listed in Table. 11.

3.2.6 mRNA analysis

Analysis of mRNA levels of *GBA1, CHOP* and *GAPDH* was performed as described in Chapter 2.17. A list of primers used in Table. 10.

3.2.7 GCase activity assay

Cell lysates for GCase activity analysis were generated as described in Chapter 2.13. *In vitro* GCase protein activity assay was performed at pH 5.4 with NaT and pH 4.5 as described in Chapter 2.20.

3.2.8 Lysosomal hydrolase activity assay (β-galactosidase and β-hexosaminidase activity assay)

Cell lysates for analysis of β-Galactosidase and β-Hexosaminidase activity analysis were generated as described in Chapter 2.14. *In vitro* β-Galactosidase and β-Hexosaminidase enzyme activity assay was performed at pH 4.1 as described in Chapter 2.21.

3.2.9 Endo H analysis

To study the subcellular localisation and transport of GCase mutants, the processing of its *N*-linked glycans was monitored by performing Endo H and PNGase F digestions. Endo H cleaves only high mannose structures and hybrid structures, whereas PNGase F hydrolyses nearly all type of *N*-linked glycan chains from glycoproteins. Fibroblast cell lysates were generated and protein concentration measured using the BCA assay, as described in Chapter 2.14.

Digestions were performed according to the manufacturer's instructions (New England BioLabs #P0702L and #P0704S). For wild-type, E326K and N370S mutant lines, 20 µg of total protein was denatured with 1X Glycoprotein Denaturing Buffer at 100°C for 10 minutes. For L444P mutants 60 µg of total protein was denatured. Following this, denatured protein sample was incubated for 2 hours at 37°C, with either Endo H or PNGase F, alongside 1X GlycoBuffer 3 or GlycoBuffer 2, respectively. Reactions were stopped by adding to 4 X NuPage™ sample buffer and 10 X NuPage™ reducing agent to each sample. Digestion was analysed by western blotting, as described in Chapter 2.15 and immunoblotted with anti-GBA antibody (Millipore) (Table. 11.).

3.2.10 Immunofluorescence microscopy

3.2.10.1 Cathepsin D and Calnexin Immunofluorescence

To visualise the subcellular localisation and transport of GCase mutants, cells were stained with Cathepsin D, a lysosomal marker, and calnexin, an ER marker. Fibroblast cell lines were plated onto coverslips in 12 well plates and incubated at 37°C at 5% CO_2 until ready for analysis. Immunofluorescence was performed as described in Chapter 2.19. Cells were stained with either anti-Cathepsin D antibody (Abcam) and anti-GBA antibody (Millipore) or anti-Calnexin antibody (Abcam) and anti-GBA antibody (Millipore). More information on the antibodies can be found in Table. 11. Coverslips were analysed by fluorescence microscopy as described in Chapter 2.18.

3.2.10.2 GlcCer Immunofluorescence

The level of GlcCer lipids in fibroblast cells was investigated by staining fibroblast cell lines with anti-Glucosylceramide RAS_0100 (Glycobiotech) antisera and analysing by immunofluorescence microscopy. Immunofluorescence staining was performed as per manufacturer's instructions (Brade et al., 2000). Cells were

plated onto coverslips in 12 well plates and incubated at 37°C at 5% CO_2 until ready for analysis. Coverslips were removed from each well and fixed in pre-warmed (37°C) 4% PFA (SantaCruz) in PBS at room temperature for 20 minutes. Permeabilization of the cells was carried out by incubation with pre-chilled 100% MeOH at -20˚C for 15 minutes. Coverslips were blocked in 10% NGS diluted in PBS for 1 hour at 37°C in a humidified atmosphere. After aspirating NGS, coverslips were washed twice in 0.1% PBS-T. Coverslips were incubated with antisera (Table. 11.) diluted in 3% NGS diluted in PBS for 1 hour at 37°C in a humidified atmosphere. The cells were washed four times with 0.1% PBS-T and once with 3% NGS diluted in PBS. Following the washes, the coverslips were incubated with Alexa Fluor 488 conjugated secondary antibodies in 3% NGS diluted in PBS for 1 hour at 37°C in a humidified atmosphere. Cells were washed six times with 0.1% PBS-T and coverslips were mounted onto glass slides with 1 μg/mL DAPI CitiFluor and sealed with nail polish for later analysis by fluorescence microscopy (see section 2.18).

3.2.11 Dot blotting

The level of GlcCer lipids in fibroblast cells was investigated using the anti-Glucosylceramide RAS_0100 (Glycobiotech) antisera and dot blotting. As a positive control, C18-Glucosyl(β)ceramide (d18:1/18:0) powder (Avanti #860547) was solubilised in chloroform and diluted to the desired concentration in spotting buffer (CHCl3 (250): MeOh (500): 50mM HCl (200): Ponceau Red (20)). C18-Glucosyl(β)ceramide (d18:1/18:0) was added to the dot blot in decreasing dilutions to produce a standard curve. Fibroblast cell lysates were generated as described in Chapter 2.14. Dot blotting was then performed as described in Chapter 2.16. In an attempt to reduce non-specific staining, the protocol provided

by the manufacturer was also followed (Brade et al., 2000). However, this protocol did not produce improved results.

3.2.12 Real time GCase assay

Lysosomal GCase activity, but not ER and Golgi-resident GCase activity, can be measured in live cells by using a substrate that is taken up into acidic vesicles only, where it fluoresces upon catalysis with GCase (Mazzulli et al., 2016). Cells were grown in 24 well plates until 70-90% confluent. For 24 hours prior to analysis, some wild-type cells were treated with 10 μM CBE to inhibit GCase. When confluent, cells were washed with PBS and loaded with 400 μg/mL PFB-FDGluc (5-Pentafluorobenzoylamino) Fluorescein Di-β-D-Glucopyransoside (ThermoFisher) in Opti-MEM for 1 hour at 37°C. Cells were washed three times and incubated in Opti-MEM. Fluorescence (excitation, 488 nm; emission, 520 nm) was measured over 90 minutes at 37°C with a fluorescent plate reader. After the experiment, Opti-MEM was aspirated and cells collected, pelleted and lysed in 1% (v/v) Triton X 100 in PBS as described in Chapters 2.14.1 and 2.14.2. The total protein concentration of each well was calculated with the BCA assay (chapter 2.14.4). CBE-sensitive initial rate was calculated and normalised to protein concentration in the well. Cells were measured in triplicates.

3.3 Results

3.3.1 No significant reduction in GCase protein and gene expression levels in E326K mutant fibroblasts

To investigate the effect of the E326K mutation on GCase protein level, western blotting was employed to measure the levels of intracellular GCase protein in fibroblast cell lines from different patients (Figure. 10A.). All three bands on the blot were quantified and band densities added together for analysis. For all analyses in this chapter, results were pooled for wild-type controls, L444P/L444P

and N370S/N370S lines. Data is normalised to WT/WT controls which was set at 1. Quantitative analysis of the GCase immunoblot revealed that the level of GCase protein was not significantly reduced in E326K heterozygous and homozygous fibroblasts compared to healthy controls. The level of GCase protein reduced from 1 in WT/WT controls to 0.86 ± 0.4 and in homozygotes to 0.97 ± 0.35, however this was not significant ($p>0.05$). Fibroblasts homozygous for L444P and N370S mutations exhibited a marked reduction in GCase protein level. In L444P/L444P fibroblasts, GCase protein level dropped to 0.020 ± 0.11 (****$p<0.0001$ vs WT/WT). This was also significantly reduced when compared to E326K heterozygous fibroblasts (****$p<0.0001$) and E326K homozygous fibroblasts (****$p<0.0001$). In N370S/N370S fibroblast cell lines, GCase protein was reduced to 0.18 ± 0.17 of control cell lines (****$p<0.001$). Similar to L444P fibroblasts, this reduction was significantly lower than E326K heterozygous fibroblasts (***$p<0.001$) and E326K homozygous fibroblasts (***$p<0.001$). There was no significant difference between L444P and N370S fibroblasts. Due to the young age of the L444P homozygous fibroblast lines (Table. 6.), analysis was repeated with age-matched healthy control fibroblasts (LB and 7301 cell lines) (Figure. 10B.). As L444P results in a severe clinical outcome, patients often have a short lifespan (Sidransky, 2012) which makes obtaining age-matched cell lines difficult. The level of GCase protein level was similar between adult (1 ± 0.25) and young controls (0.87 ± 0.034). In this experiment, analysis showed that the L444P/L444P fibroblast GCase protein was significantly lower than both aged and young control fibroblasts at 0.03 ± 0.11 (***$p<0.001$). There was no difference between the GCase protein level of aged and young control cells.

Quantitative PCR analysis of GCase mRNA levels in the different fibroblast cell lines revealed a similar pattern to *GBA1* protein level analysis (Figure. 10C.).

Data is normalised against WT/WT control. Compared to control lines, cell lines harbouring heterozygous and homozygous E326K mutations express similar levels of GCase mRNA transcript. WT/WT control cells were expressed as 1, with heterozygous E326K lines exhibiting 0.96 ± 0.48 *GBA1* mRNA expression level and homozygous E326K lines exhibiting 0.89 ± 0.41 GCase mRNA expression. GCase mRNA expression was significantly reduced in fibroblasts homozygous for L444P (0.12 ± 0.09) compared to WT/WT (****$p<0.0001$), E326K heterozygotes (****$p<0.0001$) and E326K homozygotes (***$p<0.001$). In fibroblasts homozygous for N370S *GBA1* mRNA levels were reduced to 0.19 ± 0.15, which was significantly lower than WT/WT (****$p<0.0001$), E326K heterozygotes (***$p<0.001$) and E326K homozygotes (**$p<0.01$).

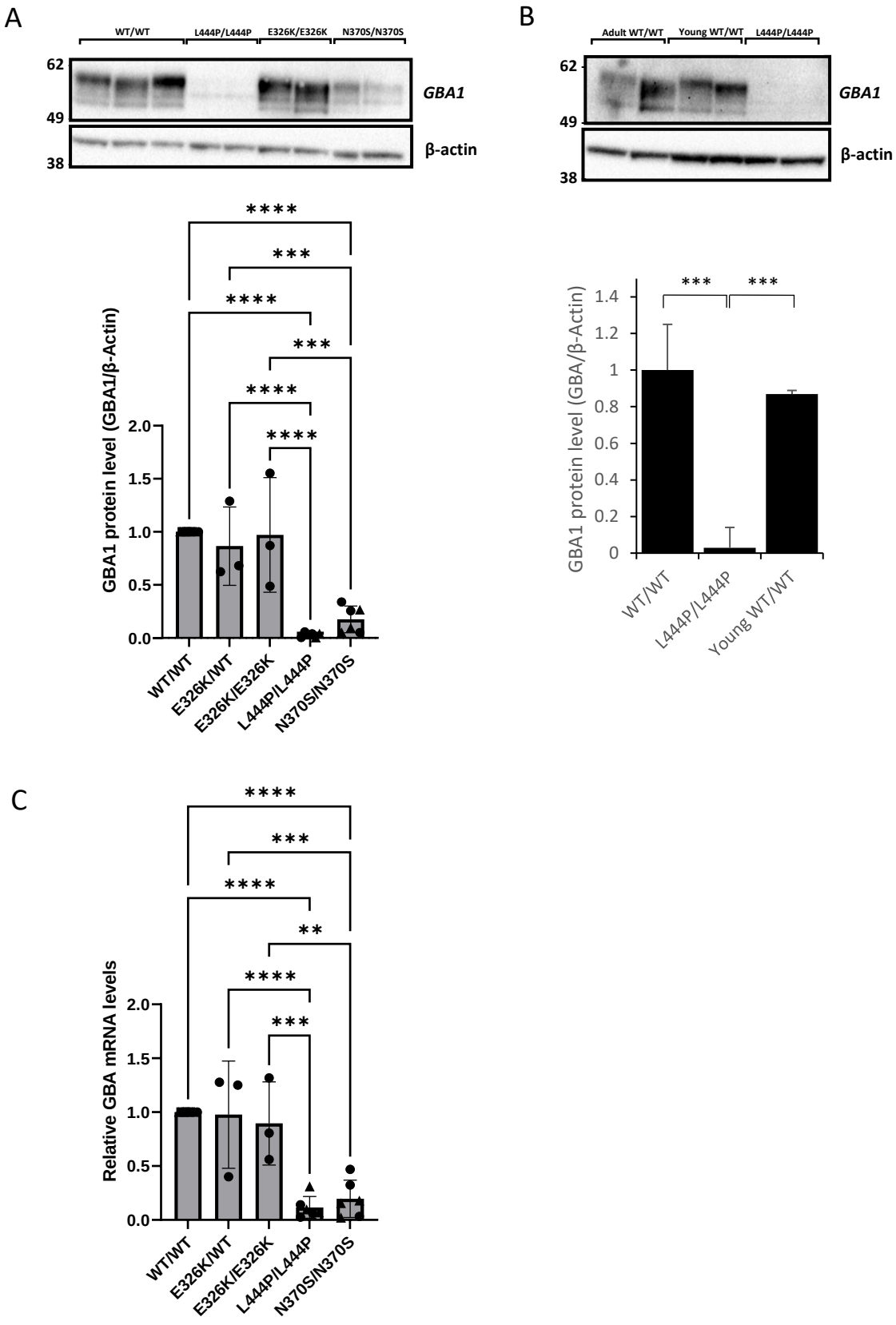

Figure 10. GCase protein level and expression in patient-derived fibroblasts.

A) Immunoblot and quantification for GCase protein level in fibroblasts normalised to WT/WT control fibroblast, which was set at 1. Cell lines used: WT/WT (SCO, KMI, ROK); E326K/WT (EK); E326K/E326K (NDS00203); L444P/L444P (GM10915; GM20272);

N370S/N370S (IPE, SAL). For quantification, band density for each cell line was calculated and expressed as the mean for each genotype. Three technical repeats. Graph made using GraphPad Prism showing mean and error bars show SEM. Each cell line for each genotype depicted as a different symbol. Statistical test used was one way ANOVA with Tukey post-hoc analysis (***p<0.001, ****p<0.0001). **B)** Immunoblot and quantification for GCase protein level in adult and young control fibroblasts normalised to WT/WT control fibroblasts, which was set at 1. For quantification, band density for each cell line was calculated and expressed as the mean for each genotype. Graph shows mean and error bars show SEM. Cell lines used: WT/WT (SCO, KMI, ROK); L444P/L444P (GM10915; GM20272); Young WT/WT (7301, LB). Three technical repeats. Statistical test used was one way ANOVA with Tukey post-hoc analysis (***p<0.001). **C)** Quantification of GCase mRNA levels in patient fibroblasts normalised to WT/WT control fibroblasts, which was set at 1. Cell lines used: WT/WT (SCO, KMI, ROK); E326K/WT (EK); E326K/E326K (NDS00203); L444P/L444P (GM10915; GM20272); N370S/N370S (IPE, SAL). For each experiment, two biological replicates were used for each cell line. For quantification, *GBA* expression for each cell line was calculated and expressed as the mean for each genotype. Three technical repeats were performed. Graph made using GraphPad Prism showing mean and error bars show SEM. Each cell line for each genotype depicted as a different symbol. Statistical test used was one way ANOVA with Tukey post-hoc analysis (**p<0.01, ***p<0.001, ****p<0.0001). Cells used were between passage 5-11 and results were replicated across passages.

3.3.2 No significant reduction in GCase enzymatic activity in E326K mutant fibroblasts

To assess the effect of E326K mutations on GCase function, enzyme activity in fibroblast total cell lysates was measured. Enzyme activity is described as the catalytic ability of an enzyme, usually calculated as moles of substrate converted per unit time (Gomes and Rocha-Santos, 2019). GCase activity was measured at pH 5.4 with 22 mM NaT and at pH 4.5 with 2 mM deoxynojirimycin (DNJ), a *GBA2* inhibitor (Boot et al., 2007). At pH 5.4, *GBA1* activity is specifically measured as NaT is both an inhibitor of *GBA2* and a co-factor for *GBA*, similar to Saposin C *in vivo* (Berger et al., 2015). To confirm the specificity of the enzyme assay to GCase activity, 1 mM CBE was administered to fibroblast cell lysates (Figure. 11.). This resulted in complete abolition of GCase activity detected by the assay in fibroblasts homozygous for wild-type and L444P, confirming the specificity of the assay. Activity in the mutant fibroblasts has been normalised against controls. At pH 5.4, the activity of E326K was similar to control fibroblasts (Figure. 12A.). Healthy wild-type control activity was expressed as 1 nmole/hr/mg and E326K heterozygotes was 0.99 ± 0.59 nmole/hr/mg. There was a reduction in E326K homozygotes to 0.63 ± 0.2 nmole/hr/mg, but this was not significant. In L444P homozygous cells, there was a marked reduction in activity at pH 5.4 to 0.04 ± 0.09 nmole/hr/mg (****$p<0.0001$). This was significantly reduced compared to E326K heterozygotes (****$p<0.0001$) and homozygotes (*$p<0.05$). In fibroblasts homozygous for the N370S mutation, GCase activity was reduced to 0.067 ± 0.02 nmole/hr/mg at pH 5.4 (****$p<0.0001$). This was significantly lower than E326K heterozygotes (****$p<0.0001$) and homozygotes (****$p<0.0001$). A similar pattern was observed at pH 4.5 (Figure. 12C.). There was a slight reduction in activity in both E326K heterozygotes (68.1 ± 19.37%) and

homozygotes (81.71 ± 12.47%). In L444P/L444P fibroblasts, activity dropped to 5.93 ± 1.27% of controls and in N370S/N370S fibroblasts activity was 17.1 ± 12.32% % of control cells (****p<0.0001). These were both significantly lower than the activities expressed in E326K heterozygous and homozygous fibroblasts (****p<0.0001).

Again, GCase activity analysis was repeated with age-matched control fibroblasts for L444P cell lines at pH 5.4 (Fig. 12B) and pH 4.5 (Fig. 12D). There was a slight drop in GCase activity in young control fibroblasts at pH 5.4, however the homozygous L444P fibroblast activity was still significantly reduced (*p<0.05). At pH 4.5, there was minimal alterations between young and aged controls and the activity in L444P fibroblasts was significantly lower than both (*p<0.05). This indicates a lack of activity arises specifically from the L444P mutation.

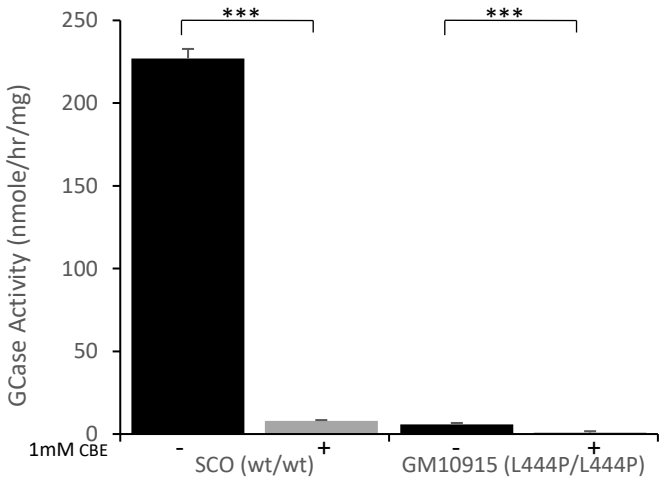

Figure 11. Confirmation of specificity of GCase activity assay in fibroblasts.
GCase activity assay with M-Glu was performed at pH 5.4 with NaT in the presence of 1mM CBE inhibitor. (-) denotes no CBE. (+) denotes CBE administration. Cell lines used: WT/WT (SCO); L444P/L444P (GM10915). Two biological replicates and three technical repeats. Statistical test used was one way ANOVA with Tukey post-hoc analysis (***p<0.001). Graph shows mean and error bars show SEM. Cells used were between passage 5-11 and results were replicated across passages.

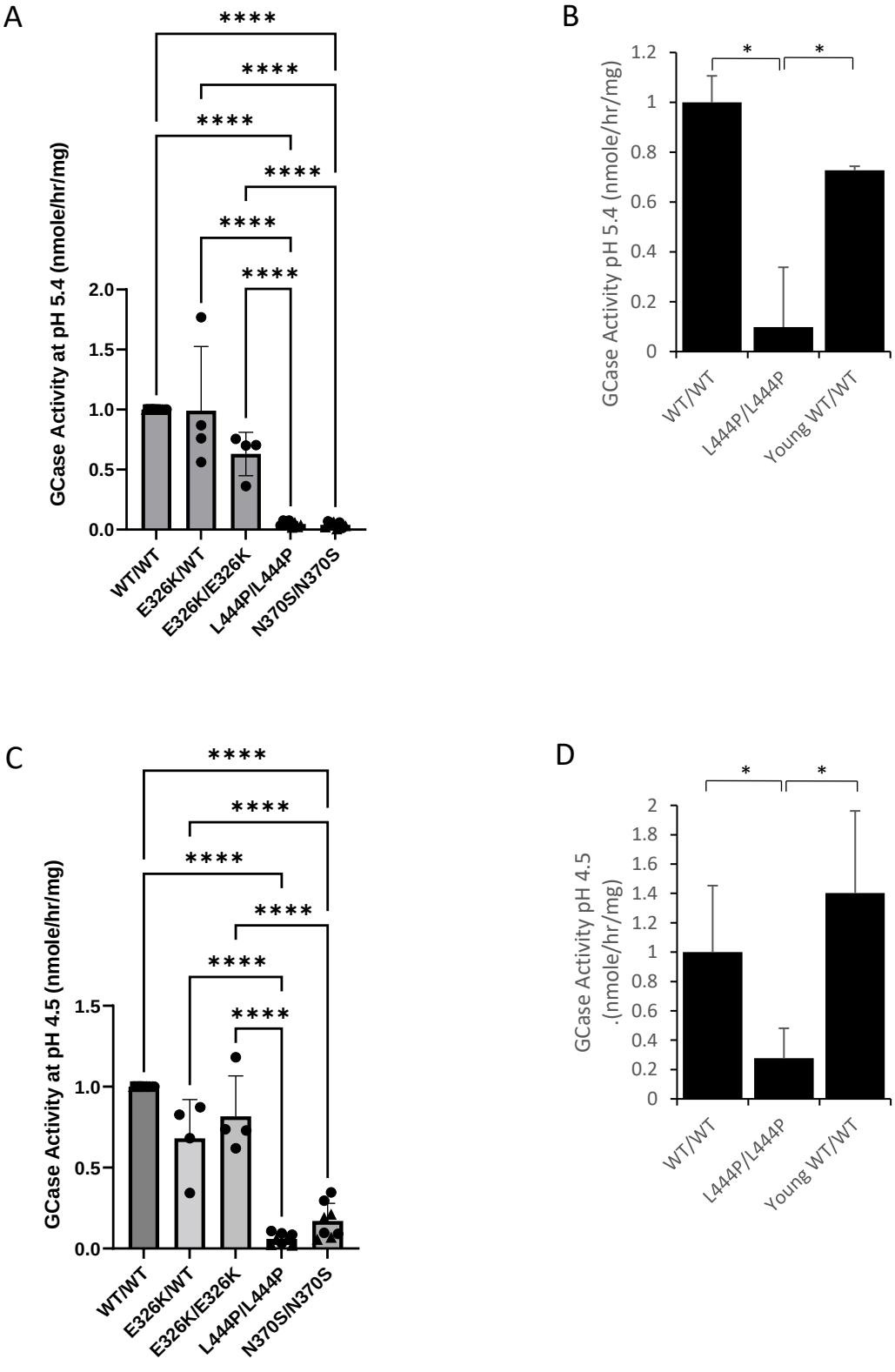

Figure 12. GCase enzyme activity in patient-derived fibroblasts.

GCase activity assay with M-Glu was performed at both pH 5.4 with NaT and pH 4.5 on fibroblast cell lysates. Cells used were between passage 5-11 and results were replicated across passages. All data normalised to WT/WT control fibroblasts, which was set at 1. For each experiment, two biological replicates were used for each cell line. For quantification, GCase activity for each cell line was calculated and data expressed as

the mean of each genotype. **A)** GCase activity in nmole/hr/mg in fibroblasts measured at pH 5.4. Cell lines used: WT/WT (SCO, KMI, ROK); E326K/WT (EK); E326K/E326K (NDS00203); L444P/L444P (GM10915; GM20272); N370S/N370S (IPE, SAL). Two biological replicates and four technical repeats. Graph made using GraphPad Prism showing mean and error bars show SEM. Each cell line for each genotype depicted as a different symbol. Statistical test used was one way ANOVA with Tukey post-hoc analysis (****$p<0.0001$). **B)** GCase activity in nmole/hr/mg in fibroblasts measured at pH 5.4 in adult and young controls. Cell lines used: WT/WT (SCO, KMI, ROK); L444P/L444P (GM10915; GM20272); Young WT/WT (7301, LB). Two biological replicates and four technical repeats. Graph shows mean and error bars show SEM. Statistical test used was one way ANOVA with Tukey post-hoc analysis (*$p<0.05$). **C)** GCase activity in nmole/hr/mg in fibroblasts measured at pH 4.5. Cell lines used: WT/WT (SCO, KMI, ROK); E326K/WT (EK); E326K/E326K (NDS00203); L444P/L444P (GM10915; GM20272); N370S/N370S (IPE, SAL). Two biological replicates and four technical repeats. Graph made using GraphPad Prism showing mean and error bars show SEM. Each cell line for each genotype depicted as a different symbol. Statistical test used was one way ANOVA with Tukey post-hoc analysis (****$p<0.0001$). **D)** GCase activity in nmole/hr/mg in fibroblasts measured at pH 4.5 in adult and young controls. Cell lines used: WT/WT (SCO, KMI, ROK); L444P/L444P (GM10915; GM20272); Young WT/WT (7301, LB). Two biological replicates and four technical repeats. Graph shows mean and error bars show SEM. Statistical test used was one way ANOVA with Tukey post-hoc analysis (*$p<0.05$). Error bars show SEM.

3.3.3 Lysosomal content and function unaltered in E326K mutant fibroblasts

To assess the effect of the E326K mutation on lysosomal content and function, the lysosomal machinery in GCase mutant fibroblasts was analysed. The overall endo-lysosomal content of the cells was measured by immunoblotting for the lysosomal marker lysosomal-associated membrane protein 1 (LAMP1) (Figure. 13A.). Analysis of LAMP1 levels did not reveal any significant changes in LAMP1 protein in homozygous and heterozygous E326K fibroblasts compared to healthy controls (*$p<0.05$). Similarly, no significant changes in LAMP1 levels were seen in fibroblasts homozygous for L444P and N370S mutations. Further analysis revealed that LAMP1 levels were not significantly altered in young healthy controls compared to adult healthy controls (Figure. 13B.). There was no significant difference between young control fibroblasts and fibroblasts homozygous for L444P mutations.

To investigate overall lysosomal function, enzyme activity assays were performed to measure the activity of two other lysosomal hydrolases, β-galactosidase and β-Hexosaminidase (Figure. 14A.). There were no significant changes in the activity of both lysosomal enzymes in E326K heterozygous and homozygous fibroblasts compared to healthy controls (Figure. 14A. and 14B.). Furthermore, no significant alterations in β-galactosidase and β-Hexosaminidase activities were seen across all cell lines. Again, activity was measured in young healthy control fibroblasts to age-match the L444P homozygous cells (Figure. 14C. and 14D.). Compared to adult controls which exhibited 1 ± 0.01 nmole/0.5hour/mg of β-galactosidase activity, young controls exhibited 0.65 ± 0.06 nmole/0.5hour/mg activity (**$p<0.001$). This was similar to the activity in L444P/L444P fibroblasts 0.70 ± 0.09 nmole/0.5hour/mg (**$p<0.001$ vs adult control). The activity of β-

Hexosaminidase was also reduced compared to adult controls, however this was not significant. Healthy adult control fibroblasts had β-Hexosaminidase activity of 1 ± 0.13 nmole/0.5hour/mg. This was reduced 0.87 ± 0.11 nmole/0.5hour/mg in young adult controls, which was comparable to L444P/L444P fibroblasts (0.82 ± 0.16 nmole/0.5hour/mg). This reduction is likely due to the young age of the fibroblast.

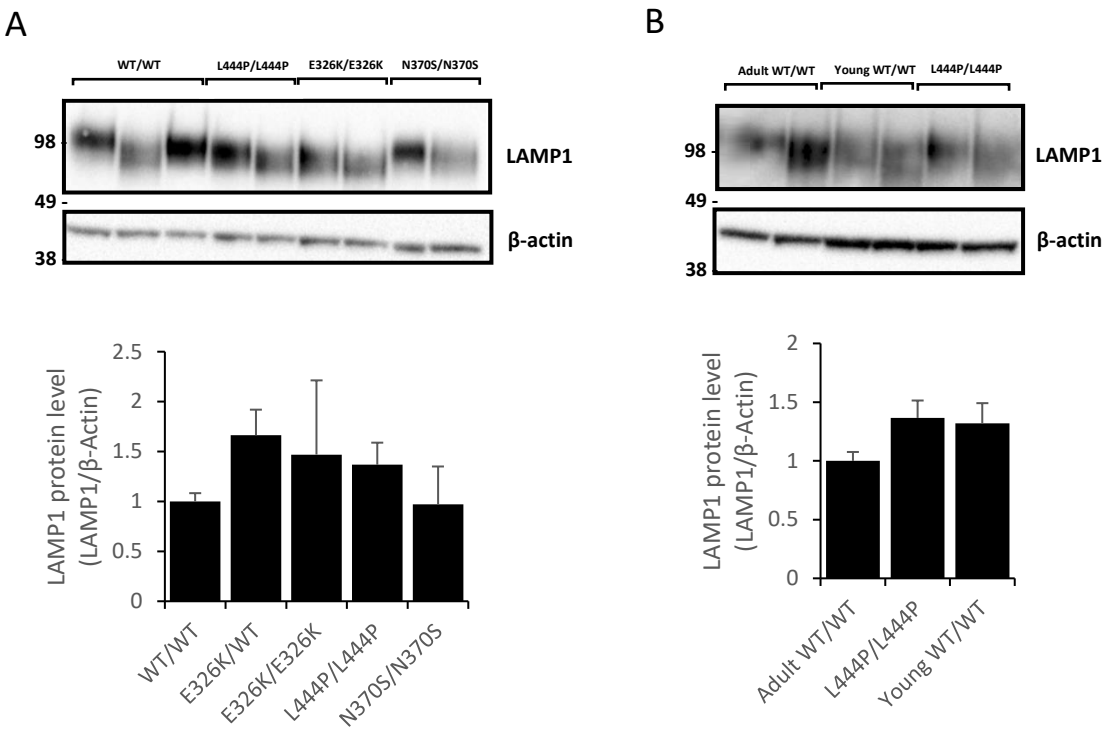

Figure 13. Lysosomal content in patient-derived fibroblasts.

LAMP1 levels were measured via western blot to assess the overall endo-lysosomal content of the fibroblasts. For quantification, band density for each cell line was calculated and data expressed as the mean for each genotype, normalised to WT/WT fibroblast controls, which was set at 1. **A)** Immunoblot and quantification for LAMP1 protein level in fibroblasts. Cell lines used: WT/WT (SCO, KMI, ROK); E326K/WT (EK); E326K/E326K (NDS00203); L444P/L444P (GM10915; GM20272); N370S/N370S (IPE, SAL). Three technical repeats. **B)** Immunoblot and quantification for LAMP1 protein level in adult and young control fibroblasts. Cell lines used: WT/WT (SCO, KMI, ROK); L444P/L444P (GM10915; GM20272); Young WT/WT (7301, LB). Three technical repeats. Statistical test used was one way ANOVA with Tukey post-hoc analysis. Graphs show mean and error bars show SEM.

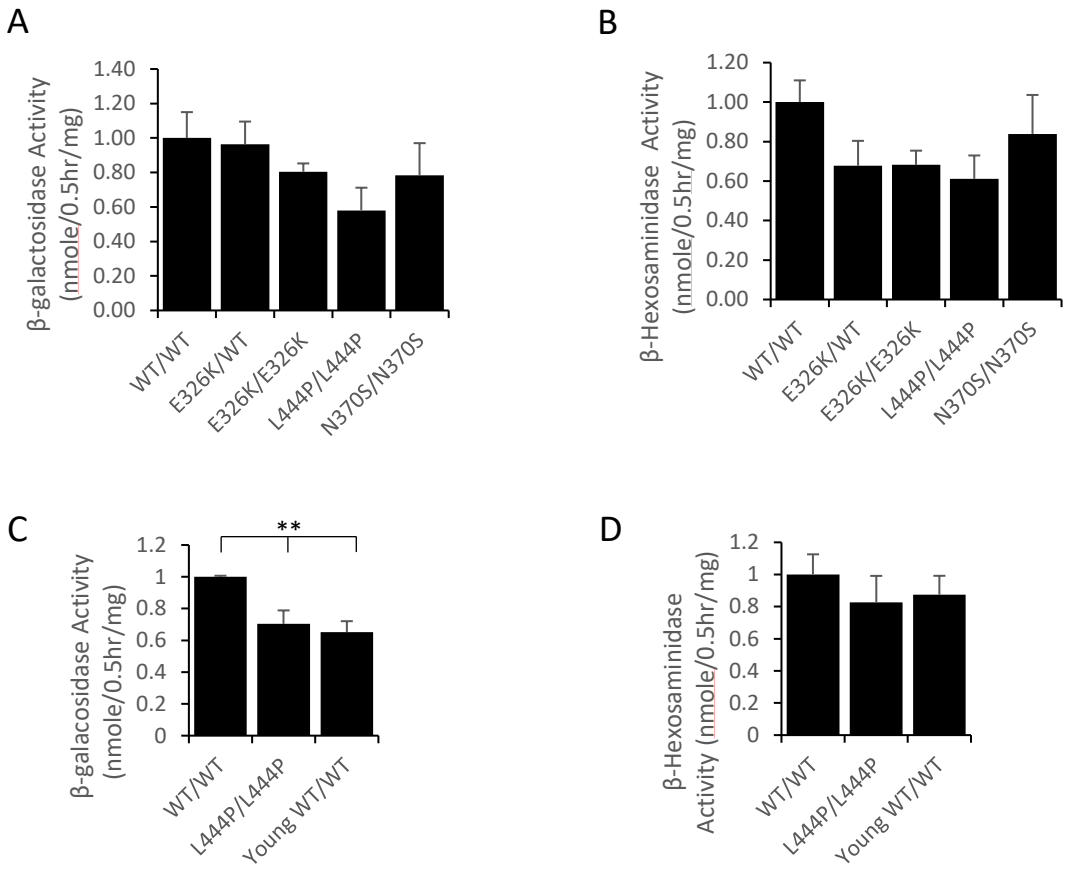

Figure 14. Lysosomal function in patient-derived fibroblasts.

The activities of lysosomal hydrolases, β-galactosidase and β-Hexosaminidase were measured to assess overall lysosomal function in fibroblasts. All data normalised to WT/WT control fibroblasts, which was set at 1. For each experiment, two biological replicates were used for each cell line. For quantification, activity for each cell line was calculated and data expressed as the mean of each genotype. **A)** β-galactosidase activity in nmole/0.5hr/mg in fibroblasts measured at pH 4.1. Cell lines used: WT/WT (SCO, KMI, ROK); E326K/WT (EK); E326K/E326K (NDS00203); L444P/L444P (GM10915; GM20272); N370S/N370S (IPE, SAL). Two biological replicates and four technical repeats. **B)** β-Hexosaminidase activity in nmole/0.5hr/mg in fibroblasts measured at pH 4.1. Cell lines used: WT/WT (SCO, KMI, ROK); E326K/WT (EK); E326K/E326K (NDS00203); L444P/L444P (GM10915; GM20272); N370S/N370S (IPE, SAL). Two biological replicates and four technical repeats. **C)** β-galactosidase activity in nmole/0.5hr/mg in in adult and young controls measured at pH 4.1. Cell lines used: WT/WT (SCO, KMI, ROK); L444P/L444P (GM10915; GM20272); Young WT/WT (7301, LB). Two biological replicates and four technical repeats. **D)** β-Hexosaminidase activity in nmole/0.5hr/mg in in adult and young controls measured at pH 4.1. Cell lines used: WT/WT (SCO, KMI, ROK); L444P/L444P (GM10915; GM20272); Young WT/WT (7301, LB). Two biological replicates and four technical repeats. Statistical test used was one way ANOVA with Tukey post-hoc analysis (**p<001). Graphs show mean and error bars

show SEM. Cells used were between passage 5-11 and results were replicated across passages.

3.3.4 E326K mutant fibroblasts do not exhibit ER retention

The different glycosylation patterns of GCase, as it passes through the secretory pathway, can be utilised to assess the proportion of GCase that is trapped in the ER. To investigate the effect of the E326K mutation on GCase protein ER retention, I studied the processing of its *N*-linked glycans by performing glycoprotein digestion with Endo H and PNGase F enzymes. Endo H is a recombinant glycosidase that cleaves only high mannose structures and hybrid oligosaccharides from *N*-linked glycoproteins, whereas PNGase F is an amidase that cleaves between the innermost GlcNac and asparagine residues of oligosaccharides from *N*-linked glycoproteins (Maley et al., 1989) (Figure. 15.). GCase is transcribed and translated in the ER, where it undergoes protein folding. It is in the ER and through transit through the Golgi where the GCase protein undergoes post-translational modifications through the addition of *N*-linked glycan chains (Braulke and Bonifacino, 2009). This leads to a variety of GCase glycoforms, with differing molecular masses between 59 – 69 kDa (Bendikov-Bar et al., 2013).

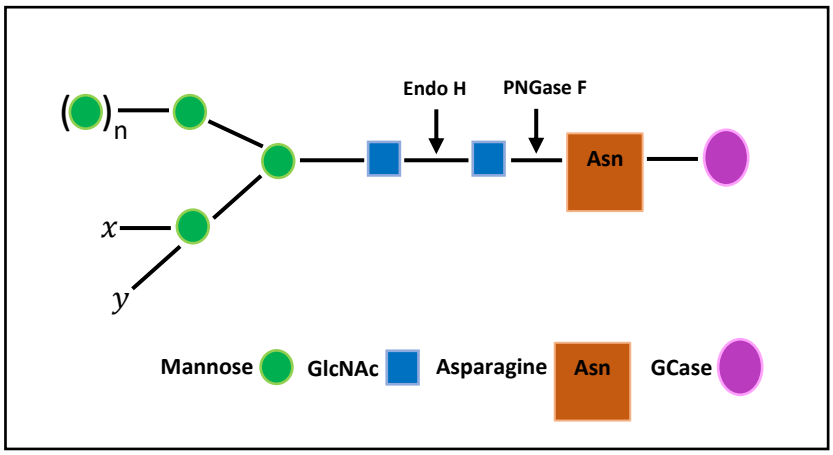

Figure 15. Illustrative diagram showing the cleave site of both Endoglycosidase H and PNGase F enzymes in the GCase glycoprotein.

The immunoblot of Endo H treated fibroblast cell lysate (Figure. 16A.) and quantification (Figure. 16B.) demonstrate that the L444P homozygote protein is the only one to induce significant ER retention of GCase protein (*p<0.05). Data is normalised against WT/WT healthy control cell lines. The GCase protein resolves as 3 bands after treatment, with the lower exposure blot showing two higher molecular weight bands likely to be mature protein. For analysis, wild-type fibroblasts were digested by PNGase F as a positive control for unglycosylated GCase (red asterisk). As this enzyme cleaves all *N*-linked glycans, this is the most immature form of GCase protein. The corresponding ER-resident bands in the mutant cell lines are marked with a black asterisk. This band is absent in wild-type cell lines. To quantify the retention of mutant GCase protein, the density of the ER-resident band was divided by the density of the two mature GCase bands (Figure. 16B.). Homozygous L444P cells exhibited significant ER retention of mutant GCase protein, with the Endo H sensitive fraction of GCase increasing from 1 ± 0.15 in healthy controls to 5.42 ± 1.93 (*p<0.05). This was also significantly higher than in N370S homozygous cell lines (1.52 ± 0.38). Both E326K heterozygous and homozygous fibroblasts did not exhibit altered fractions of ER-retained GCase protein compared to healthy controls or mutant lines.

To further investigate the effect of the E326K *GBA1* mutation on ER retention of mutant GCase protein, immunofluorescence analysis was performed by staining the fibroblast cell lines for GCase protein (green) and calnexin (red) (Figure. 17.). As calnexin acts as an endogenous ER marker, this analysis allows us to qualitatively analyse the amount of GCase that is retained within the ER and not transported through the cell for further maturation before reaching the lysosome. When mutant GCase protein is retained in the ER, the GCase and calnexin stain will co-localise. Staining of both GCase and calnexin was above background, as

shown by the secondary antibody only control, suggesting staining is specific to GCase and calnexin. In wild-type control cells, GCase accumulates in punctate structures in cell periphery and does not co-localise with calnexin, indicative of no ER retention. A similar observation is seen in E326K homozygous and heterozygous lines, as well as N370S homozygous lines. On the other hand, homozygous L444P fibroblast cell lines display a more diffuse GCase stain which is not associated with punctate structures and does not accumulate in a perinuclear pattern. In these cells, GCase does co-localise with calnexin, suggesting ER retention.

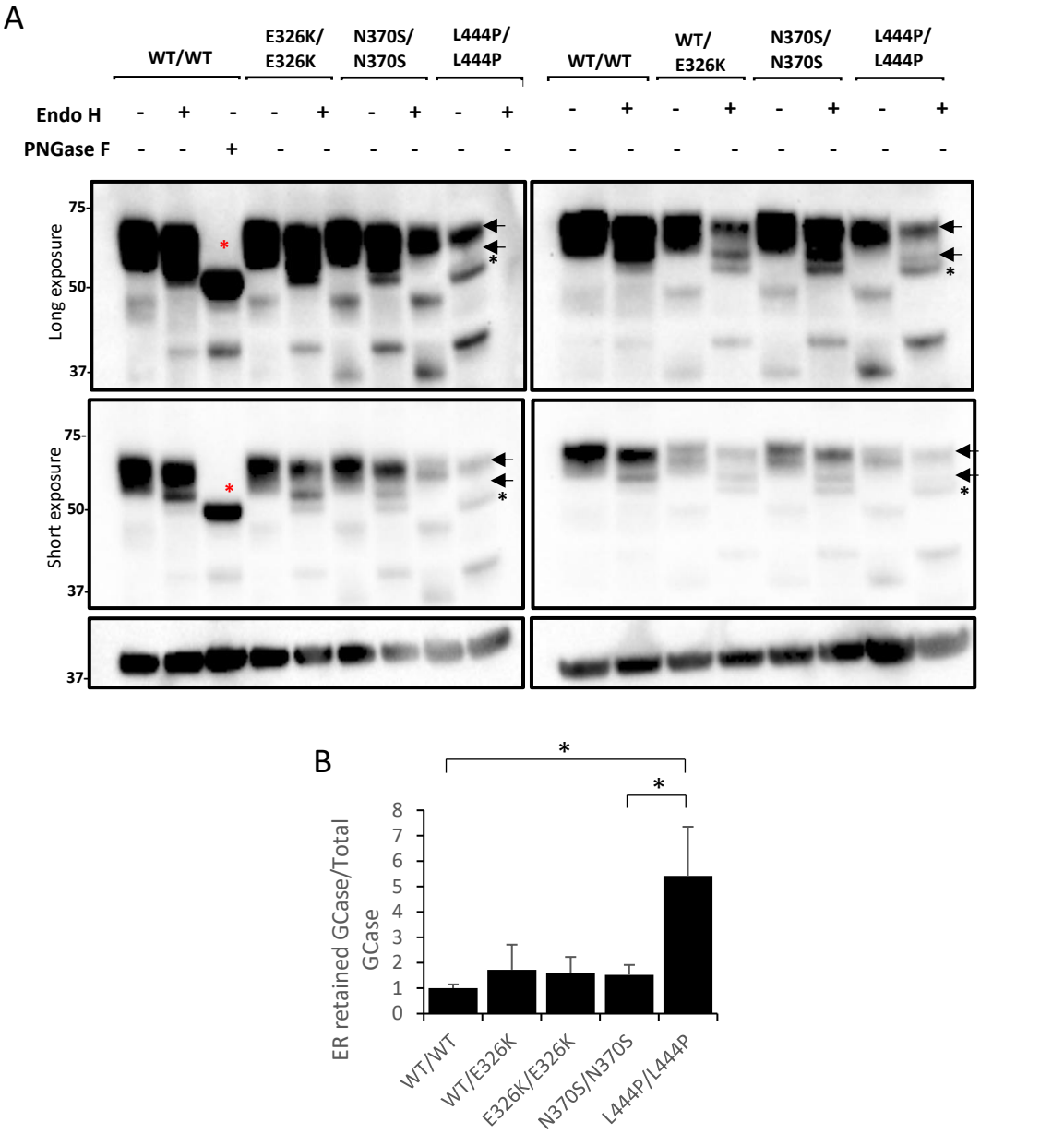

Figure 16. ER retention of GCase in patient-derived fibroblasts by Endo H analysis. **A)** Fibroblast cell lysates (20 µg of WT, E326K and N370S mutants and 70 µg of L444P mutants) were treated with or without endoglycosidase-H (Endo H) and GCase protein species analysed by Western blot. A higher concentration of L444P cell lysate was required to visualise bands on the gel. Cell lines used: WT/WT (SCO, ROK); E326K/WT (EK); E326K/E326K (NDS00203); L444P/L444P (GM10915; GM20272); N370S/N370S (IPE, SAL). SCO WT/WT cell lysate (20 µg) was treated with Peptide-N-Glycosidase F (PNGase F) as a positive control. Figure shows blots at long and short exposure. The two normal species of GCase detected in fibroblasts are indicated by arrows. An additional lower molecular weight band was observed, indicating ER retained GCase, in L444P/L444P fibroblasts following endo-H treatment (black *asterisk*). The WT/WT cell line treated with PNGase exhibited a lower molecular weight band, indicating a GCase species with no glycosylation (red *asterisk*). **B)** Quantitative analysis of Endo H digestion

displayed as the density of bands for ER resident GCase divided by the density of bands for total GCase protein, normalised to β-actin band density. Three technical repeats. Graph shows mean and error bars show SEM. Statistical test used was one way ANOVA with Tukey post-hoc analysis (*$p<0.05$). Cells used were between passage 5-11 and results were replicated across passages.

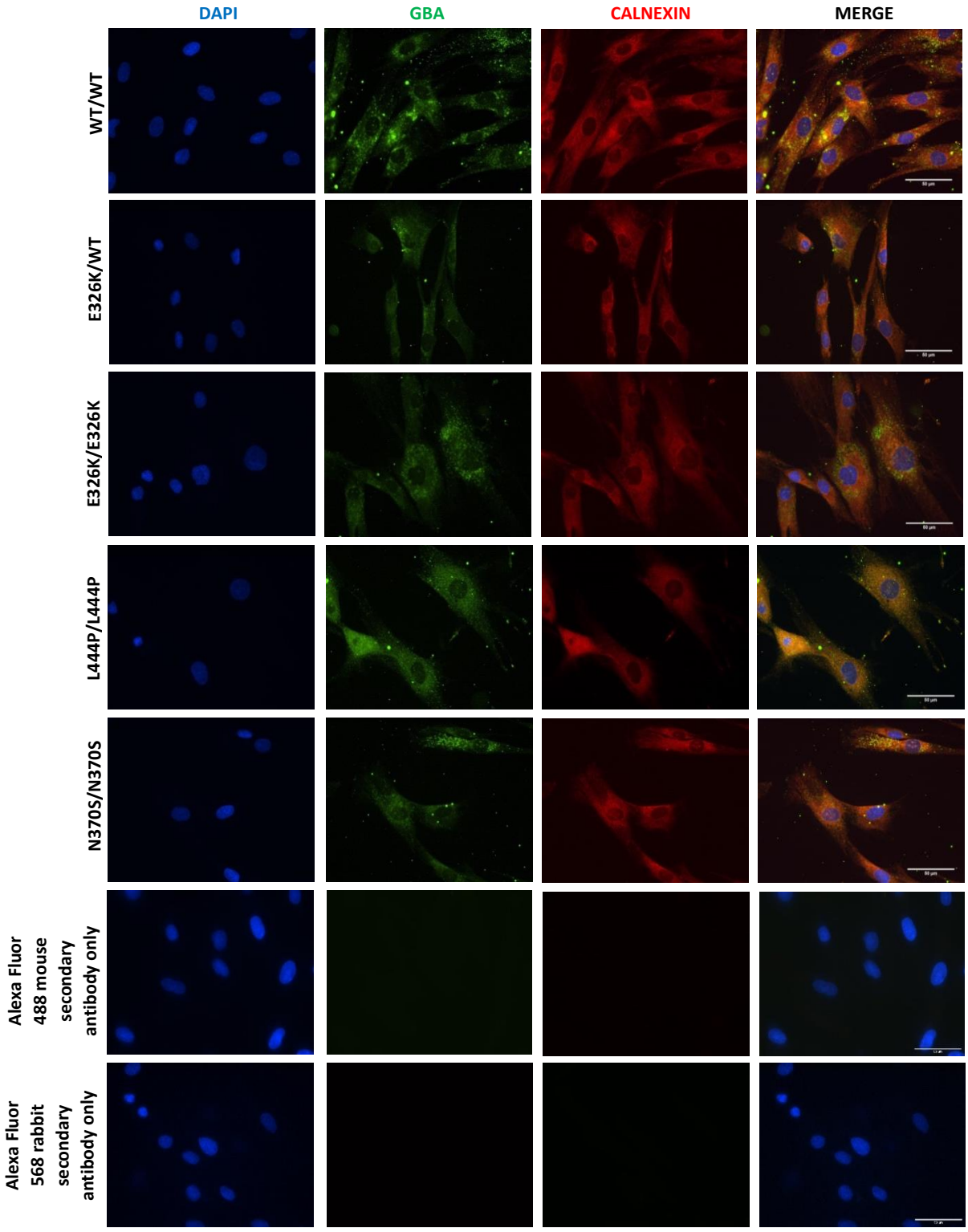

Figure 17. ER retention of GCase in patient-derived fibroblasts by immunofluorescence analysis.

Cell lines were analysed by immunofluorescence with anti-*GBA1* (green) and anti-Calnexin (red) antibodies, with DAPI for nuclei staining (blue). Representative lines of each genotype shown (WT/WT (SCO); E326K/WT (EK); E326K/E326K (NDS00203); L444P/L444P (GM20272); N370S/N370S (IPE). Secondary antibody only controls

shown in bottom two panels; WT/WT SCO cell line. Cells used were between passage 5-11 and results were replicated across passages. Scale bar is 50 µm.

3.3.5 The E326K mutation does not significantly alter GCase lysosomal translocation

To further analyse the subcellular localisation of mutant GCase protein, the effect of *GBA1* mutations on the lysosomal translocation of GCase protein was investigated. Following its processing through the ER and Golgi apparatus, GCase binds to LIMP-2 for translocation to the lysosome to carry out its function as a lysosomal hydrolase enzyme (Reczek et al., 2007). For qualitative analysis of GCase trafficking to the lysosome, immunofluorescence analysis was performed by staining the fibroblast cell lines for GCase protein (green) and cathepsin D (red) (Figure. 18A.). Cathepsin D is a lysosomal protease, and acts as an endogenous lysosomal marker, and allows us to visualise whether mutant GCase has been trafficked correctly to the lysosome. When mutant GCase protein is properly trafficked to the lysosome, there will be marked co-localisation between GCase and cathepsin D. Staining of both GCase and cathepsin D was above background, as shown by the secondary antibody only control, suggestive staining is specific. Similar to healthy wild-type controls, E326K homozygous and heterozygous cell lines show GCase accumulating in punctate structures in the cell periphery, which morphologically resemble lysosomes and co-localise with cathepsin D, indicative of proper trafficking of mutant GCase protein to the lysosome. The same is also seen in N370S homozygous cell lines. Conversely, in L444P homozygous cell lines GCase staining is reduced and does not follow the same pattern. There is a drastic reduction of GCase and cathepsin D co-localisation in these cells, suggesting improper trafficking of L444P mutant protein to the lysosome. In addition to immunofluorescence, western blotting was also utilised to measure the levels of cathepsin D protein across the cell lines (Figure. 18B.). Immunoblotting and quantification of cathepsin D protein level

revealed no significant changes across the different *GBA1* mutations, although L444P caused a small increase.

Lysosomal GCase activity can be measured alone, without measuring ER and Golgi-resident GCase, in live cells by using a substrate that is only taken up in to acidic vesicles, and fluoresces upon catalysis with GCase (Mazzulli et al., 2016). After loading of substrate, there is a linear increase in fluorescent product up to 45 minutes, after which GCase enzymatic activity plateaus (Figure. 19A.). This plateau is likely the depletion/release of substrate from late endosomes and lysosomes over time. Therefore, the initial linear rate of enzyme activity was calculated between time 0 and time 45 minutes. Lysosomal GCase activity is abolished in wild-type fibroblast cells treated with 1 mM CBE, a GCase specific inhibitor. The initial rate equation of lysosomal GCase activity for each cell line is shown in Figure. 19B. When compared to healthy wild-type controls, which had an initial rate equation of y=18403371x, E326K homozygotes exhibited a similar initial linear rate of enzyme activity, with an equation of y=16823338x. On the other hand, E326K heterozygote cell lines had a slower initial rate of GCase enzyme activity, with an initial rate equation of y=11332758x. Cell lines harbouring the N370S homozygous mutation also have a lower initial rate of GCase enzyme activity, with an initial rate equation of y=71268687x. In L444P/L444P cells GCase activity was similar to that of CBE-treated wild-type controls, which was abolished, and the initial rate equation was y=0x.

A

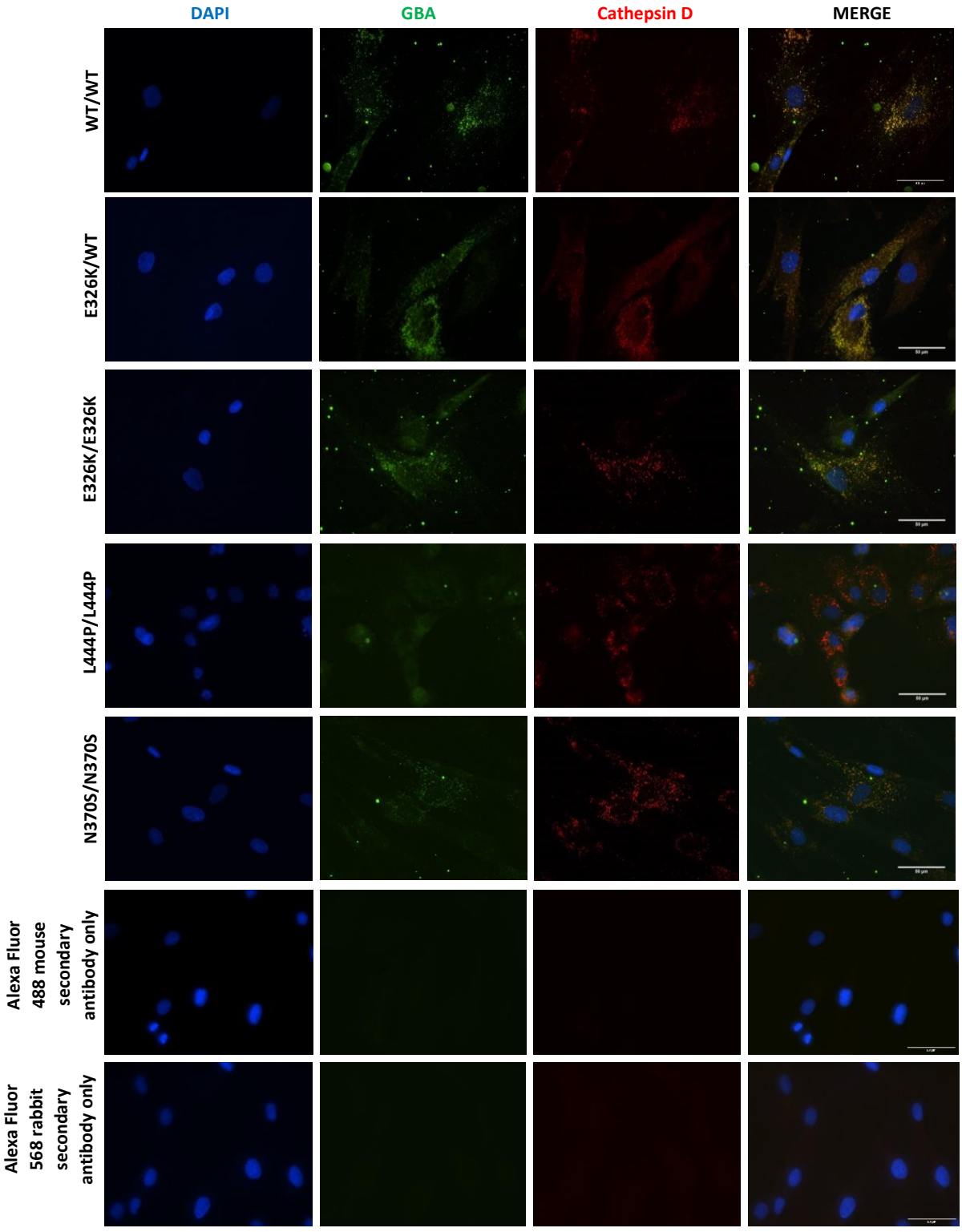
DAPI
GBA
Cathepsin D
MERGE
WT/WT
E326K/WT
E326K/E326K
L444P/L444P
N370S/N370S
Alexa Fluor 488 mouse secondary antibody only
Alexa Fluor 568 rabbit secondary antibody only

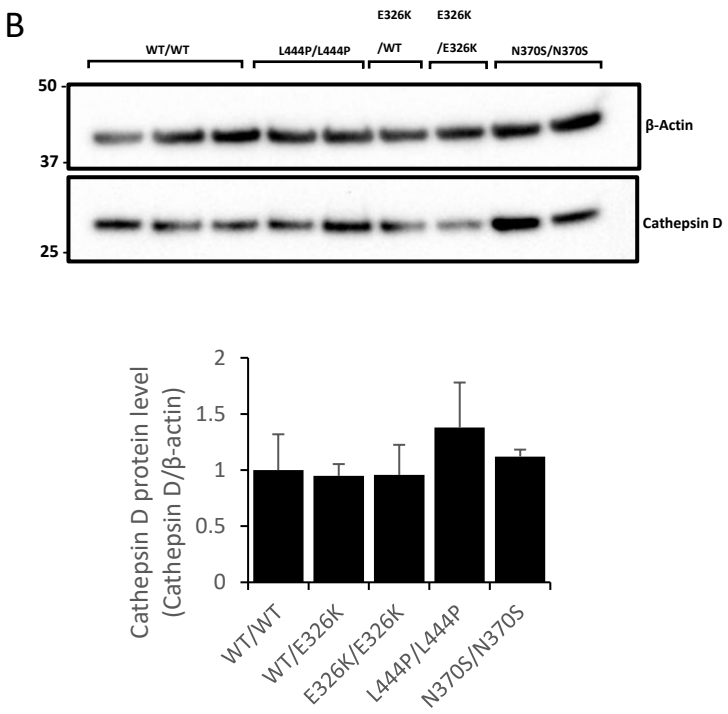

Figure 18. Lysosomal translocation of active GCase in patient-derived fibroblasts

A) Fibroblast cell lines were analysed by immunofluorescence with anti-*GBA1* (green) and anti-Cathepsin D (red) antibodies, with DAPI for nuclei staining (blue). Representative lines of each genotype shown (WT/WT (SCO); E326K/WT (EK); E326K/E326K (NDS00203); L444P/L444P (GM20272); N370S/N370S (IPE). Secondary antibody only controls shown in bottom two panels; WT/WT SCO cell line. Scale bar is 50 µm. **B)** Immunoblot and band density quantification of Cathepsin D protein level in fibroblasts. For quantification, data was normalised to WT/W, which was set at 1. Band density for each cell was calculated and data expressed as mean of each genotype. Cell lines used: WT/WT (SCO, KMI, ROK); E326K/WT (EK); E326K/E326K (NDS00203); L444P/L444P (GM10915; GM20272); N370S/N370S (IPE, SAL). Three technical repeats. Graph shows mean and error bars show SEM. Cells used were between passage 5-11 and results were replicated across passages. Statistical test used was one way ANOVA with Tukey post-hoc analysis.

A

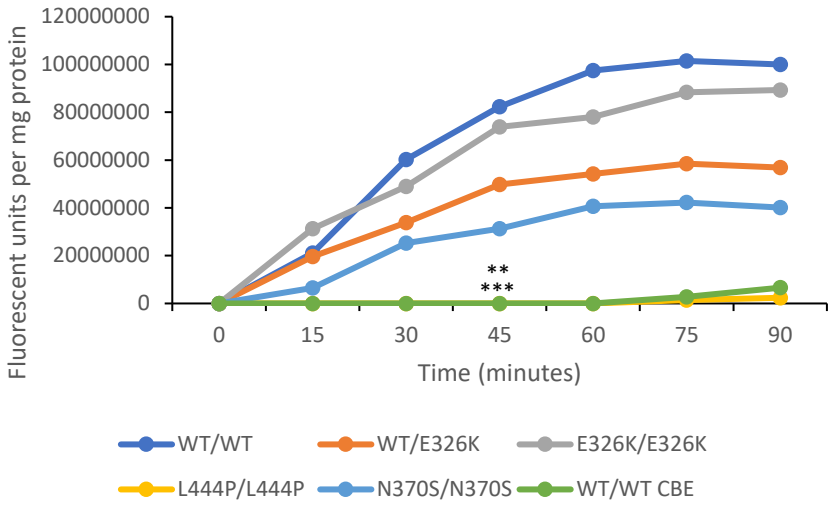

B

Genotype	Linear trendline equation (y=mx)
WT/WT	y=18403371x
WT/E326K	y=11332758x
E326K/E326K	y=16823338x
L444P/L444P	y=0x
N370S/N370S	y=7128687x
WT/WT + CBE	y=0x

Figure 19. Activity of lysosomal GCase.

A) Fibroblast cell lines were incubated with PFB-FDGluc substrate for 1 hour at 37°C. Following washing, fluorescence was measured every 15 minutes for 90 minutes. Cell lines used: WT/WT (SCO, KMI, ROK); E326K/WT (EK); E326K/E326K (NDS00203); L444P/L444P (GM10915; GM20272); N370S/N370S (IPE). **B)** The initial linear rate of each reaction was calculated between time 0 and time 45 minutes and initial rate equations displayed in the table. Two biological repeats and three technical repeats. Statistical test used was one way ANOVA with Tukey post-hoc analysis. WT/WT vs. L444P/L444P ***p<0.001; WT/WT vs. WT/WT + CBE **p<0.01; E326K/E326K vs. L444P/L444P *p<0.05. Cells used were between passage 5-11 and results were replicated across passages.

3.3.6 E326K mutant fibroblasts do not exhibit ER stress

To investigate the effect of the E326K mutation on ER stress, levels of intracellular markers of ER stress in patient fibroblasts were measured and compared this to healthy controls. GRP78, also known as BiP, is a central regulator for ER stress (Lee, 2005). BiP protein levels are increased during ER stress. Quantitative analysis of BiP immunoblots reveal that there is no significant change in BiP levels in E326K mutants (Figure. 20A.). Data was normalised to healthy wild-type controls, which was set at 1 ± 0.15. BiP protein level in E326K heterozygous fibroblasts was 0.97 ± 0.22 and in E326K homozygous fibroblasts was 0.83 ± 0.13. There is an increase in BiP protein levels in fibroblasts homozygous for the L444P mutation, reaching 1.36 ± 0.27, however this was not significant. In N370S homozygous fibroblasts, there was a reduction in BiP levels to 0.75 ± 0.19 and again, this was not significant when compared to controls. There were no significant alterations in BiP protein level between all mutations.

The effect of E326K mutations on the expression level of the *CHOP* transcription factor was investigated next. *CHOP* plays an important role in ER stress-induced apoptosis and may be up-regulated in response to prolonged activation of the UPR (Hu et al., 2018). Quantitative PCR of *CHOP* transcript levels (cycle threshold value between 25-28) showed that although there were no significant changes compared to controls, homozygous L444P fibroblast cell lines had increased *CHOP* expression from 1 ± 0.37 to 2.97 ± 1.01 (Figure. 20B.). In heterozygous E326K fibroblasts there was an increase in *CHOP* expression to 1.64 ± 0.81, however in homozygous E326K fibroblasts there was a reduction in *CHOP* expression to 0.65 ± 0.29. A reduction in N370S homozygotes compared to healthy control was also observed (0.12 ± 0.06). These changes were not

significant. In addition to this, I attempted to quantify the levels of *CHOP* protein by western blot, however this was undetectable.

To further analyse ER stress, changes in the levels of phosphorylated eIF2α were assessed via western blot. When ER stress occurs, this leads to PERK phosphorylation and activation, which leads to phosphorylation of eIF2α (Leitman et al., 2014). This method was unable to resolve bands corresponding to phosphorylated eIF2α (Figure. 20C.) and therefore could not continue with this part of the analysis.

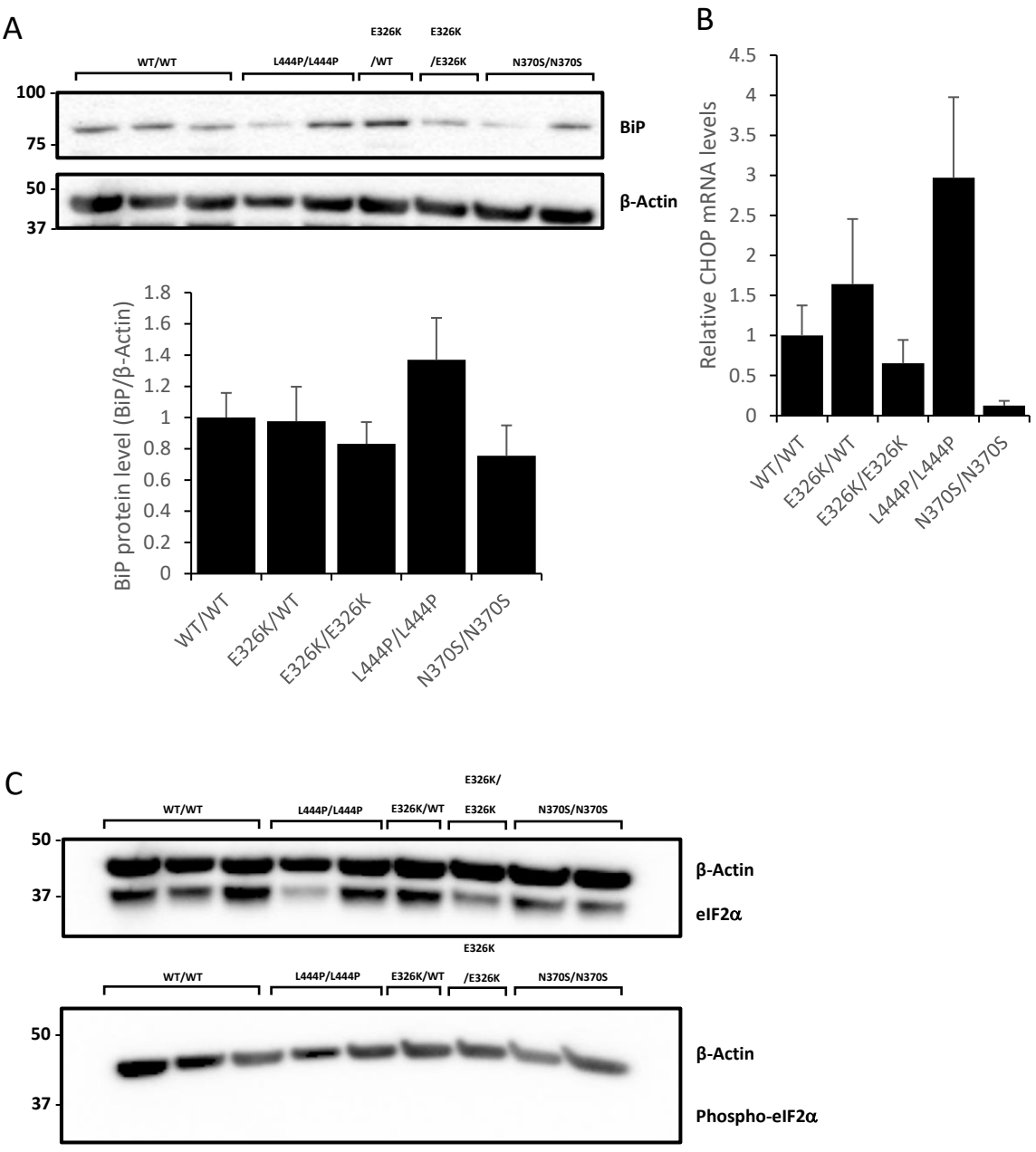

Figure 20. ER stress in patient-derived fibroblasts.

A) Immunoblot and band density quantification of BiP protein level in fibroblasts normalised to WT/WT control fibroblasts, which was set at 1. For quantification, band density for each cell line was calculated and data expressed as a mean of each genotype. Cell lines used: WT/WT (SCO, KMI, ROK); E326K/WT (EK); E326K/E326K (NDS00203); L444P/L444P (GM10915; GM20272); N370S/N370S (IPE, SAL). Three technical repeats. **B)** Quantification of *CHOP* mRNA levels in patient fibroblasts normalised to WT/WT control fibroblasts, which was set at 1. Cell lines used: WT/WT (SCO, KMI, ROK); E326K/WT (EK); E326K/E326K (NDS00203); L444P/L444P (GM10915; GM20272); N370S/N370S (IPE, SAL). For each experiment, two biological replicates were used for each cell line. For quantification, *CHOP* expression for each cell

line was calculated, pooled and averaged for each genotype. Three technical repeats. **C)** Immunoblot of the levels of eIF2α and phosphorylated eIF2α protein level in patient-derived fibroblast cell lines. Cell lines used: WT/WT (SCO, KMI, ROK); E326K/WT (EK); E326K/E326K (NDS00203); L444P/L444P (GM10915; GM20272); N370S/N370S (IPE, SAL). Three technical repeats. Graphs show mean and error bars show SEM. Statistical test used was one way ANOVA with Tukey post-hoc analysis (*$p<0.05$). Cells used were between passage 5-11 and results were replicated across passages.

3.3.7 Investigation of GlcCer lipid alterations in mutant fibroblasts

To study the effect of E326K, L444P and N370S *GBA1* mutations on lipid homeostasis, I attempted to characterise the changes in the levels of the glycosphingolipid substrate, GlcCer. The primary function of GCase is to hydrolase glycosphingolipids at the lysosome, and when there is improper function, this may lead to their accumulation (Varela et al., 2016, Rocha et al., 2015c). For this analysis, the anti-GlcCer antisera from Glycobiotech was utilised (Brade et al., 2000). First, a dot blot was performed (Figure. 21A) with C18 Glucosyl(ß) Ceramide (d18:1/18:0) lipids as a standard and fibroblast cell lysate. The C18 Glucosyl(ß) Ceramide (d18:1/18:0) lipids failed to produce a linear dilution curve, and fibroblast cell lysates exhibited similar levels of non-specific binding on the membrane and therefore no conclusion could be made. Next, immunofluorescence analysis was performed by staining the fibroblast cell lines for GlcCer lipids (green) using the same antisera (Figure. 20B.). Unfortunately, the same problem occurred with significant non-specific binding. The anti-sera stained the whole cell body, including the nucleus and there were no differences observed across the different mutant lines.

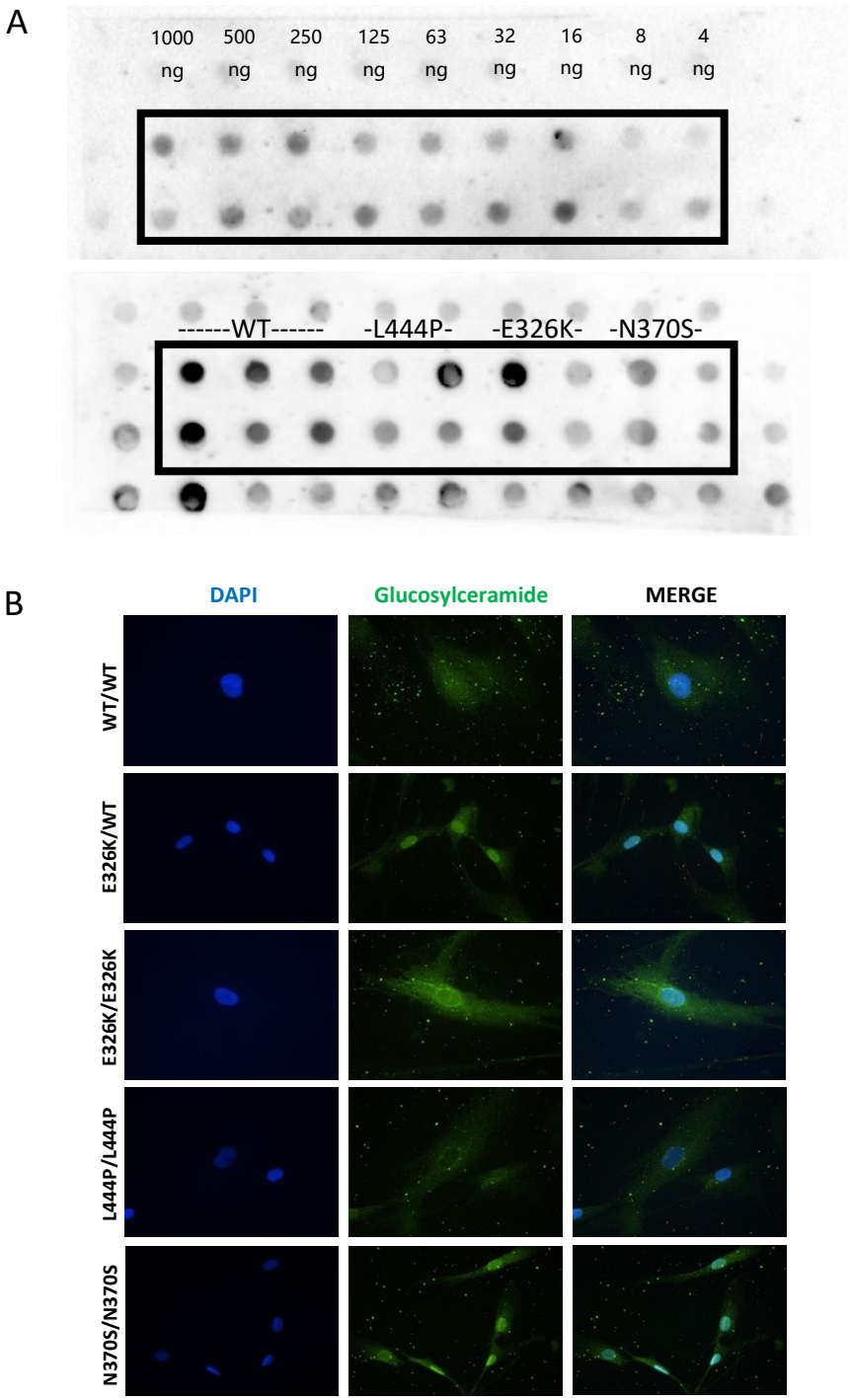

Figure 21. Lipid analysis in patient-derived fibroblasts.

A) C18 Glucosyl(ß) Ceramide (d18:1/18:0) lipids (0-1000 ng/ml) and fibroblast cell lysates samples were loaded on a dot blot, vacuum applied and membranes immunoblotted with anti-GlcCer antisera antibody. The top blot shows the dilution curve for C18 Glucosyl(ß) Ceramide (d18:1/18:0) lipids with decreasing concentrations loaded. The bottom blot is patient-derived fibroblasts blotted in duplicates. Cell lines used: WT/WT (SCO, KMI, ROK); E326K/WT (EK); E326K/E326K (NDS00203); L444P/L444P (GM10915; GM20272); N370S/N370S (IPE, SAL). Unable to detect GlcCer via dot blot as the antibody non-specifically binds to membrane. Two biological replicates and two technical repeats. **B)** Fibroblast cell lines were analysed by immunofluorescence with

anti-GlcCer antisera antibody (green) and DAPI for nuclei staining (blue). Representative lines of each genotype shown (WT/WT SCO; E326K/WT EK; E326K/E326K NDS00203; L444P/L444P GM10915; N370S/N370S IPE. Cells used were between passage 5-11 and results were replicated across passages.

3.4 Discussion

This study was designed to investigate the effect of the E326K *GBA1* PD risk variant on GCase protein levels, function and localisation, whilst simultaneously comparing to the known pathogenic variants, L444P and N370S. The results demonstrate that unlike L444P and N370S, the E326K mutation does not induce a significant loss of GCase function. Nor does it lead to retention of mutant GCase in the ER and subsequent failure of lysosomal translocation and an elevation of ER stress markers, unlike L444P. These results support the hypothesis that different mutations in *GBA1*-PD may act via different mechanisms. A summary of the main findings in this chapter can be found in Table. 13.

Patient-derived primary fibroblast cell lines were chosen as the model system (Table. 6.). These cells allow analysis of endogenous GCase protein and have been used previously to attempt to dissect PD pathogenesis (Sanchez-Martinez et al., 2016, McNeill et al., 2014, Collins et al., 2017, Auburger et al., 2012, Teves et al., 2018, Ambrosi et al., 2014). Homozygous mutations were selected for analysis of wild-type, L444P and N370S as it is assumed that any pathogenesis caused by the mutation will be more severe when in homozygous form. Both homozygous and heterozygous E326K cell lines were utilised as the biochemical effect of E326K was suspected to be mild and this allowed comparison between the two genotypes. It is important to note that the E326K fibroblast lines used in this study are a model of *GBA1*-PD, derived from PD patients, whereas the L444P and N370S homozygote cells are derived from GD patients. Another limitation of this model is that fibroblasts are not neuronal and the level of alpha-synuclein expression is too low for adequate investigations in to the relationship between *GBA1* mutations and alpha-synuclein pathology (Hoepken et al., 2008).

Furthermore, the L444P homozygous cell lines and young WT/WT cell lines were taken from a different cohort to the other fibroblast lines. This may introduce variability within phenotypes in cells harbouring the same genotype due differential handling. If fibroblast cells are handled differently or improperly, this may introduce an element of stress to the cells which may have a subsequent effect on ER stress or mitochondrial function, thus it is important to consider this when drawing conclusions. Differential handling of fibroblast cell lines may explain the heterogeneity described in phenotypes, for example one study demonstrated variable degrees of ER trapping of GCase in type 1 N370S fibroblasts (Ron and Horowitz, 2005). Furthermore, it may explain why specific *GBA1* mutations are associated with UPR activation in some studies, whereas in others they are not. In N370S heterozygous fibroblast cells, one study demonstrated UPR activation (Sanchez-Martinez et al., 2016), whereas in other studies the levels of UPR makers were unchanged (Maor et al., 2013, Braunstein et al., 2018). Ideally, aged control fibroblasts from both cohorts would have been used in the present study.

Mutation	*GBA1* expression	GCase protein level	GCase activity	Lysosomal content	ER retention	ER stress
E326K	-	-	-	-	-	-
L444P	↓ ****	↓ ****	↓ ****	-	↑ *	-
N370S	↓ ****	↓ ****	↓ ****	-	-	-

Table 13. Summary of main findings in Chapter 3.

Arrows indicate either an increase (↑) or decrease (↓) compared to wild-type. (-) indicates no significant change compared to wild-type. (*p<0.05; **p<0.01; ***p<0.001; ****p<0.0001).

3.4.1 The E326K variant does not behave in the same way as common loss-of-function pathogenic *GBA1* mutations

Few groups have attempted the biochemical characterisation of the E326K GCase mutant protein. In this study, fibroblast cells from PD patients who are heterozygous and homozygous for E326K did not have a significant reduction in GCase protein (Figure. 10A.) or mRNA transcript level (Figure. 10C.), suggesting that the E326K mutation does not influence transcription of the *GBA1* gene nor is it misfolded and degraded by ERAD. This is supported by another study in E326K homozygous fibroblast cells, where GCase protein level was not significantly reduced (~80% of control) and no change in E326K GCase mRNA transcript was found (McNeill et al., 2014). In this study, both heterozygous and homozygous E326K cell lines had significantly higher protein level compared to N370S and L444P cells. Protein expression levels were reflected in GCase activity at both pH 5.4 and pH 4.5. Neither homozygous or heterozygous E326K fibroblasts exhibit a significant reduction in GCase activity, suggesting little effect on GCase function. Interestingly, activity was higher in the E326K homozygous line at pH 5.4, compared to heterozygotes which had higher activity at a pH 4.5, suggesting the zygosity of the E326K mutation may influence the pH optima.

These findings are supported by previous literature that demonstrate the E326K variant retains over half of its activity in a variety of cell models expressing recombinant GCase (54 – 60.9%) (Malini et al., 2014, Grace et al., 1999, Horowitz et al., 2011) and in dried blood spots (82.2%) (Alcalay et al., 2015). Conversely, several other studies have found that the E326K mutation does induce a marked reduction in GCase activity to around 25% – 42.7% of control (Ron et al., 2005, McNeill et al., 2014, Torralba et al., 2001, Chabas et al., 2005, Liou and Grabowski, 2012). Furthermore, some studies suggest that the E326K mutation

is a modifier variant rather than a pathogenic variant, as it causes a marked reduction in GCase function when in a compound heterozygote (Chabas et al., 2005, Liou and Grabowski, 2012), which may explain why activity is not reduced. However, as most of these studies used human cell lines expressing plasmid, bacterial or viral vectors harbouring mutant GCase, it is difficult to accurately compare to diseased protein from patients with homozygous and heterozygous mutations. As this study investigated the biology of endogenous E326K in patient-derived cells this should be more translatable to human disease.

As there is little literature surrounding the effect of E326K on GCase protein and expression level, the L444P and N370S mutations were also investigated. These mutations not only act to confirm the validity of the results, but also allow comparisons to a generally severe (L444P) and a generally mild (N370S) pathogenesis. A plethora of studies have investigated the biology of the L444P and N370S mutations, demonstrating both loss of function and gain of function mechanisms (Alfonso et al., 2004, Grace et al., 1994, Grace and Grabowski, 1990, Ohashi et al., 1991, McNeill et al., 2014, Migdalska-Richards et al., 2017b, Lieberman et al., 2007, Yun et al., 2018, Sanchez-Martinez et al., 2016, Schöndorf et al., 2014, Fernandes et al., 2016, Garcia-Sanz et al., 2017, Maor et al., 2013, Bendikov-Bar et al., 2011, Ron and Horowitz, 2005). First, it was confirmed that the L444P homozygous mutation induced a significant reduction in GCase protein level (Figure. 10A.) and activity (Figure. 12.). This corroborates previous reports from patient-derived fibroblast studies, where heterozygous and homozygous L444P mutations lead to a marked reduction in GCase protein level (McNeill et al., 2014, de la Mata et al., 2015, Sanchez-Martinez et al., 2016) and activity (Mu et al., 2008, Patnaik et al., 2012, McNeill et al., 2014, Cerri et al.,

2021, Sanchez-Martinez et al., 2016, Bendikov-Bar et al., 2011, de la Mata et al., 2015, Galvagnion et al., 2020).

Next, the effect of the N370S mutation was investigated. A loss of function mechanism was anticipated, as previously reported. Fibroblast studies have demonstrated a loss of GCase protein (Sanchez-Martinez et al., 2016, McNeill et al., 2014, Garcia-Sanz et al., 2017, Ron and Horowitz, 2005) and activity in cells harbouring the N370S mutation (Mu et al., 2008, Patnaik et al., 2012, McNeill et al., 2014, Cerri et al., 2021, Sanchez-Martinez et al., 2016, Garcia-Sanz et al., 2017, Ron and Horowitz, 2005). As expected, our findings demonstrate that in the homozygous form the N370S mutation leads to a significant reduction in GCase protein level (Figure. 10A.) and activity (Figure. 12.).

GCase mRNA expression level was 11.7% of control in L444P homozygous fibroblasts (Figure. 10C.). This is corroborated by a previous study in L444P/WT fibroblasts (Sanchez-Martinez et al., 2016). In N370S fibroblasts, transcript level was 18.6% of control cells, which is different to a previous report in heterozygous fibroblasts where mRNA levels were unchanged (Garcia-Sanz et al., 2017), however this is likely due to our cells being homozygous. It is unclear why the there is a reduction in transcript levels in L444P and N370S cells, however missense mutations in other genes have also been associated with reduced transcript levels, possibly by altering mRNA folding (Harries et al., 2004). In addition, L444P transcript levels were higher than protein levels (2.8% of control). Therefore, it can been hypothesised that any transcribed protein is being misfolded and degraded by ERAD, as previously reported in L444P fibroblasts (Ron and Horowitz, 2005).

It was also anticipated that the changes induced by the N370S mutation would not be as severe as those caused by the L444P mutation, due to the observation that the N370S mutation is generally associated with a milder disease phenotype (Sidransky and Lopez, 2012). This was true of the fibroblast cell models in this study, where although both mutations significantly reduced GCase protein, expression and activity, the reduction was more severe in L444P cells. This has also been demonstrated previously in heterozygous fibroblasts (Sanchez-Martinez et al., 2016). Importantly, these changes were significantly lower than both control and E326K cells, providing further evidence that the E326K mutation does not act as a loss of function mutation.

There were no obvious changes in lysosomal content and overall function in mutant fibroblasts. Several markers were used to assess this including the level of LAMP1 protein and the activity of lysosomal hydrolases (Figure. 13. and 14.). These methods were chosen as they have been performed previously to assess lysosomal content and function in models of *GBA1* deficiency. In a past study, LAMP1 protein levels were measured to give insight into lysosomal content in *GBA1* deficient primary cortical neurons and demonstrated no change (Magalhaes et al., 2016). To improve this in the future, live cells could be stained with LysoTracker or Lyso ID to visualise lysosomes via confocal microscopy (Kinghorn et al., 2016, Magalhaes et al., 2016). If the lysosomes present as enlarged or abnormal this is suggestive of lysosomal defects. In addition, other lysosomal protein levels could be measured including cathepsin D and LIMP2. To assess total lysosomal function, the activity of two other lysosomal hydrolases, β-galactosidase and β-Hexosaminidase, were measured. Previous studies suggest that a *GBA1* deficiency may affect their activities. In heterozygous *GBA1* mutant MEFs and *GBA1* knockout MEFs, β-galactosidase activity was increased,

whereas β-Hexosaminidase activity was increased only in heterozygous cells (Magalhaes et al., 2016). Additionally, in aged *GBA1* deficient *Drosophila,* β-galactosidase activity was increased compared to age-matched controls (Kinghorn et al., 2016). This approach has also been used in human brains. In *GBA1*-PD patient brains, no change was observed in β-Hexosaminidase activity compared to control or sporadic PD brains (Gegg et al., 2012). Conversely, in the brain of sporadic PD patients, a reduction in both β-galactosidase and β-Hexosaminidase activity was observed, compared to healthy controls (Huebecker et al., 2019). A more sensitive method would be to measure the intracellular lysosomal activity using commercially available assays. These involve using a lysosome-specific, self-quenched substrate that is taken up selectively by the lysosome and produces a fluorescence signal upon degradation, which is proportional to the overall lysosomal activity. Cathepsin D activity can also be sensitively measured using commercially available kits, as done previously in *GBA1* mutant neurons (Yang et al., 2020b). Furthermore, an image-based protocol has recently been described involving fluorescent lysosome tracers to analyse and quantify lysosomal functions including cathepsin D activity, GCase activity and lysosomal pH (Albrecht et al., 2020). This may provide a more sensitive and accurate measure of total lysosome function.

3.4.2 *GBA1* mutations may influence lipid metabolism in cells

Alterations in lipid metabolism seem to play a role in *GBA1*-PD neurodegeneration. There have been several studies linking a GCase deficiency to GSL accumulation (Sardi et al., 2011, Sardi et al., 2017). Human dopamine neurons harbouring the L444P and N370S mutation have been shown to have altered GSL composition, including increased GlcCer levels (Taguchi et al., 2017, Schöndorf et al., 2014, Fernandes et al., 2016). It is important to note that the

presence of these lipids in *GBA1*-PD is debatable (Gegg et al., 2015, Huebecker et al., 2019)

A recent study in L444P/L444P fibroblasts demonstrated increased GSL levels correlated with decreased GCase activity (Galvagnion et al., 2020), and in CBE-treated cells and mice, there was evidence of GlcCer accumulation (Varela et al., 2016, Rocha et al., 2015c). As L444P fibroblasts in this study exhibited a drastic reduction in GCase activity and the real-time lysosomal GCase assay suggested that L444P homozygotes had similar activity to CBE treated controls (Figure. 19.), it was hypothesised that there would be significant GlcCer accumulation. As previous literature also suggests that N370S homozygotes exhibit GlcCer accumulation (Schöndorf et al., 2014), it was also anticipated that this would evident in N370S fibroblasts however to a lesser extent than L444P as there was more residual activity. GlcCer accumulation was not expected to be evident in E326K fibroblasts due to minimal change in activity. Unfortunately, the antisera against GlcCer produced non-specific binding across the dot blot membrane and the C18 Glucosyl(ß) Ceramide (d18:1/18:0) lipid standard failed to produce a linear dilution curve, suggesting that any signal was not specific to GlcCer and thus I was unable to clearly analyse the levels. It also failed to work for immunofluorescence analysis.

Future analysis should include using thin-layer chromatography. This technique allows the separation of polar neutral lipids and is an effective method for resolution of GlcCer species, allowing their separation from galactosylceramide (Ogawa et al., 1988). Thin-layer chromatography has been performed previously to analyse changes in GlcCer levels in *GBA1* deficient mouse brain, liver and spleen (Yildiz et al., 2013). Using this method, an increase in GlcCer was observed in all three tissues.

Ideally, lipidomic analysis of the fibroblasts should be performed to analyse the entire lipid profile. Lipids have previously been extracted from fibroblasts and subjected to liquid chromatography mass spectrometry and thin-layer chromatography and mass spectrometry to analyse changes in GSLs (Galvagnion et al., 2020, Fuller et al., 2008, Raju et al., 2015). This is a much more sensitive approach and allows alterations in all lipid species to be analysed, as well as total levels. It would also allow identification of long and short chain sphingolipids, the latter of which have been associated with accelerating alpha-synuclein pathology (Galvagnion et al., 2020). Further to this, mass spectrometry would allow analysis of the distribution of GlcCer species. This has been reported to be altered in N370S human dopamine neurons (Fernandes et al., 2016), and may shed further light on the subcellular localisation of active GCase protein.

3.4.3 The E326K variant does not influence GCase ER retention and ER stress, unlike L444P

Aberrant trafficking of mutant GCase may contribute to the activation of UPR and ER stress. Several studies have demonstrated a link between *GBA1* mutations and retention in the ER in fibroblasts (Bendikov-Bar et al., 2011, Ron and Horowitz, 2005, Wang et al., 2011, McNeill et al., 2014). The intracellular fate of mutant GCase was followed by first monitoring the processing of its *N*-linked glycans by subjecting the fibroblasts to Endo H digestion. This allows one to follow the trafficking of mutant GCase, as the removal of the final three mannose residues is performed in the Golgi. Therefore, it enables one to distinguish between glycoproteins that are retained in the ER and those that have passed through the Golgi and are mature (Bendikov-Bar et al., 2011). PNGase F digestion was also performed on a control fibroblast to act as a reference for unglycosylated GCase protein.

GCase that is heavily misfolded and becomes trapped in the ER contains *N*-linked glycans that are sensitive to cleavage by Endo H. The results in this study demonstrate evidence of ER retention in L444P homozygous fibroblasts, in which the vast majority of GCase protein was Endo H sensitive (Figure. 16A. and 16B.). On the contrary, control fibroblasts and those harbouring the E326K and N370S variants had only a small fraction of Endo H sensitive GCase protein (Figure. 16A. and 16B.) These findings are in line with previous studies demonstrating that L444P mutant protein is retained in the ER in fibroblasts (McNeill et al., 2014, Bendikov-Bar et al., 2011), however they are not supported by reports that E326K and N370S mutants lead to ER retention in fibroblasts (McNeill et al., 2014, Garcia-Sanz et al., 2017). This could be explained by the hypothesis that disease severity may correlate with ER retention of GCase. For example, in one study patients with the same N370S genotype exhibited differential Endo H sensitive fractions of GCase, with severe type 1 GD at 80-85% and mild type 1 GD at 45% of total GCase protein (Ron et al., 2005). Another fibroblast study also demonstrated that in N370S homozygotes, the amount of Endo H sensitive protein differs between cell lines (Schmitz et al., 2005). Therefore, in this study it may be that the patients from whom N370S/N370S fibroblasts were taken from had a mild phenotype.

The retention of mutant GCase in the ER was also analysed qualitatively by immunofluorescence (Figure. 17.). The results suggest that fibroblasts harbouring E326K and N370S mutations display little ER localisation, suggestive of no retention. In the ER. Whereas, L444P GCase is strongly localised to the ER and indicates this mutant is retained in the ER (Figure. 17.). Although these results confirm the Endo H analysis, it is important to note that the calnexin stain is more diffuse than expected and the staining pattern did not resemble previous

papers where calnexin is expressed in punctate and tubular-like structures in control fibroblasts (Garcia-Sanz et al., 2017, Matsui et al., 2013). In one study, fibroblasts with *GBA1* mutations exhibited a more diffuse calnexin staining pattern, suggesting a more disordered ER network, however, I was unable to accurately identify punctate and tubular structures in this calnexin staining. This is likely due to the fluorescence microscope used, resulting in low resolution images. Ideally, immunofluorescence would be performed using laser confocal microscopy. Another limitation also arises with the inability to use these images to accurately quantify the co-localisation of GCase with calnexin, something that could be overcome by using laser confocal microscopy. Co-localisation can be quantified using Pearson's correlation co-efficient, which measures the pixel-by-pixel covariance in the signal levels of two images and can provide an accurate and quantitative measurement of co-localisation in images from confocal microscopy (Dunn et al., 2011).

In addition, lysosomal trafficking of GCase has been shown to be defective in GCase mutant cells (Wang et al., 2011, Thomas et al., 2021, Schmitz et al., 2005, Tan et al., 2014, Sanchez-Martinez et al., 2016). This was examined in the fibroblasts by immunofluorescence and analysis of lysosomal GCase activity (Figure. 18). As expected, cathepsin D stained as small punctate structures in the periphery, which morphologically resemble lysosomes (Matsui et al., 2013). This co-localised with GCase, which is accumulated in punctate lysosomal structures, indicative of proper trafficking. The same observation occurs in fibroblasts harbouring E326K and N370S mutations. Conversely, in L444P fibroblasts the GCase staining pattern is reduced and is more diffuse, with little co-localisation with cathepsin D. Again, a limitation of this experiment is that quantification was not possible with these images. However, these qualitative results, coupled with

the findings that L444P is retained in the ER and that real-time lysosomal GCase activity is similar in L444P homozygotes to that of CBE-treated control cells (Figure. 19.), suggests that the L444P protein is likely to be heavily misfolded and unstable and does not reach the lysosome.

As expected from the data demonstrating an absence of significant GCase ER retention in E326K and N370S cells, immunofluorescence analysis revealed that the majority of these mutants were trafficked to the lysosome. Analysis of real-time lysosomal GCase activity reveals minimal changes in E326K homozygotes (Figure. 19.). This supports the findings that total GCase activity is not reduced. Interestingly, lysosomal GCase activity in E326K heterozygotes was reduced compared to control. This provides further evidence that the zygosity of the E326K mutation may influence the pH optima of GCase activity. As there is little to no literature investigating the E326K mutation, the work presented here is novel. Surprisingly, in N370S homozygous fibroblasts there was a marked reduction in real-time lysosomal GCase activity. This is likely to be a more sensitive measure than qualitative immunofluorescence analysis and suggests that some of the N370S protein that is being trafficked to the ER is likely to be inactive. Although this data fits with previous findings that fibroblasts harbouring the L444P mutation exhibit a reduction in mutant GCase lysosomal trafficking (Tan et al., 2014, Schmitz et al., 2005, Wang et al., 2011), it does not corroborate previous studies that show the N370S protein is not trafficked to the lysosome (Thomas et al., 2021, Steet et al., 2006, Sanchez-Martinez et al., 2016).

Protein trafficking has been analysed previously using confocal scanning microscopy (Hara et al., 2014, Halaban et al., 2000). This could be a future prospective for analysis of GCase trafficking by staining for calnexin, LAMP1/cathepsin D and GCase. Confocal scanning microscopy also allows Z-

stack imaging to create 3-dimensional images to better visualise the ER and lysosomal network (Saberianfar et al., 2016) and allows for more accurate visualisation of the intracellular localisation of proteins. Another more sensitive method for assessing the intracellular localisation of proteins is to perform subcellular fractionation to isolate the ER and lysosomal fractions. This technique separates cellular compartments using properties such as density, size and shape. It is primarily carried out using differential centrifugation in a highly viscous media. Subcellular fractionation has been previously utilised to evaluate the intracellular localisation of L444P mutant GCase protein in fibroblasts through performing GCase activity assays on each fraction (Wang et al., 2011). Repeating this analysis on fibroblasts harbouring the E326K mutation in homozygous and heterozygous form would provide more specific data as to the subcellar localisation of mutant GCase and demonstrate how effective trafficking is in these fibroblasts. This would also provide further insight into the fraction of fully active mutant GCase protein that is reaching the lysosome in these cells.

Another avenue to pursue in the future would be to examine the effect of molecular chaperones on mutant GCase trafficking in the fibroblasts. Such drugs are thought to bind to mutant GCase in the ER, where they facilitate correct folding and trafficking to the lysosome (Jung et al., 2016), and have demonstrated the ability to rescue GCase protein level, activity and lysosomal translocation in models of *GBA1*-PD (Shanmuganathan and Britz-McKibbin, 2011, Maegawa et al., 2009, Patnaik et al., 2012, McNeill et al., 2014, Bendikov-Bar et al., 2013, Sanchez-Martinez et al., 2016, Aflaki et al., 2016, Yang et al., 2017). Furthermore, the molecular chaperones isofagomine and ambroxol have been shown to increase the lysosomal pool of GCase in L444P fibroblasts, mice and *Drosophila* models (Khanna et al., 2010, Sanchez-Martinez et al., 2016). This

may shed more light on the trafficking of E326K and N370S cells. If administration of chaperones increases the real-time lysosomal GCase activity in these cells it would suggest improper trafficking and a degree of ER retention.

Most *GBA1* mutations are missense mutations and are thought to cause misfolding of mutant protein (Hruska et al., 2008), which may underlie ER retention of mutant GCase. Persistent presence of misfolded protein in the ER can lead to ER stress. A plethora of evidence points towards ER stress accompanying *GBA1* mutations (Wang et al., 2011, Maor et al., 2013, Braunstein et al., 2018, Fernandes et al., 2016, Ron and Horowitz, 2005, Sanchez-Martinez et al., 2016, Schöndorf et al., 2014). Although there was no evidence of ER retention in E326K fibroblasts, it was anticipated that the mutant may exert a toxic gain of function through inducing ER stress. These results suggest that neither homozygous or heterozygous E326K mutations elicit an ER stress response. There was minimal change observed in both BiP protein level and *CHOP* transcript level in these cells (Figure. 20.). Coupled with the lack of reduction in GCase levels and activity, these results suggest that the E326K mutation does not induce significant misfolding. There are no previous studies investigating ER stress and E326K to corroborate these findings, however the L444P and N370S data can be used to validate the fibroblast model.

As expected from previous studies in L444P homozygous and heterozygous fibroblasts (Maor et al., 2013, Bendikov-Bar et al., 2011), the L444P fibroblasts exhibited an in ER stress markers (Figure. 20A and 20B.). Conversely, N370S fibroblasts did not elicit an ER stress response. This is similar to findings in heterozygous fibroblasts, where L444P led to an increase in BiP and *CHOP* but N370S did not (Sanchez-Martinez et al., 2016), and in a fibroblast study where N370S heterozygotes lines express variability in BiP expression (Kilpatrick et al.,

2016). This does not fit with other findings in N370S homozygous fibroblasts where expression of BiP and *CHOP* were increased (Maor et al., 2013, Braunstein et al., 2018). From this, it can be concluded that it is likely that the UPR is cell line specific, and various other factors may influence its activation including differential handling of the cells.

I also attempted to characterise the phosphorylation of eIF2-α but I was unable to detect this in these fibroblasts via western blot (Figure 20C.). *CHOP* is also not detectable by western blot in these fibroblasts. This is likely due to the levels being below the limit of detection, and as *CHOP* is increased downstream of eIF2-α activation (Mercado et al., 2013) one would expect that you would not be able to detect either. This was unexpected as the ratio of phosphorylated eIF2-α to total eIF2-α levels has been measured previously in GD fibroblasts harbouring N370S and L444P mutations (Braunstein et al., 2018). Again, the lack of phosphorylated eIF2-α in the fibroblasts used in this study may arise due to the activation of the UPR being cell line specific. Furthermore, as the extent of ERAD has been shown to correlate with GD disease severity (Ron and Horowitz, 2005), it may be that activation of the eIF2-α specific pathway in UPR is also related to disease severity and this may explain the discrepancies seen between the fibroblasts in this study and the previous 2018 study. For future studies, the inositol-requiring enzyme 1 (IRE1) pathway could be investigated. Likewise to PERK, IRE1 is a ER-stress sensing and transducing protein. Activation of IRE1 specifically mediates the splicing and activation of the Xbp1 gene, which is then translated in to a protein that translocates into the nucleus and activates UPR related genes (Yoshida et al., 2001). An elevation in Xbp1 gene splicing has been reported in GD fibroblasts, including those homozygous for L444P and N370S

(Maor et al., 2013). Measuring the levels of Xbp1 gene splicing would provide further data to corroborate the BiP and *CHOP* analyses in this study.

As a more sensitive approach to investigate ER stress, a future prospective would be to investigate calcium (Ca^{2+}) homeostasis in these fibroblasts. Disturbances to the cellular levels of Ca^{2+} may reduce the protein folding capacity of the ER, leading to ER stress and eventual apoptosis (Berridge et al., 2000). Dysregulation of ER and lysosomal Ca^{2+}, and increased vulnerability to stress responses, has been observed in fibroblasts derived from patients with *GBA1* mutations (Kilpatrick et al., 2016). Small molecule proteostasis regulators, that increase the levels of ER Ca^{2+} concentration in fibroblasts, have been shown to enhance the folding, trafficking and function of L444P and N370S GCase (Ong et al., 2010, Mu et al., 2008). The effect of E326K mutations on Ca^{2+} homeostasis should be measured in the future using live-cell imaging and epifluorescence microscopy with fluorescent Ca^{2+} indicators, as previous (Kilpatrick et al., 2013).

3.4.4 Additional future studies

Another avenue to explore in the future would be to investigate how the E326K mutation affects mitochondrial function in fibroblasts. Mitochondrial dysfunction, including reduced ATP levels, oxidative stress, abnormal mitochondrial dynamics and impaired mitophagy has been demonstrated in models of GCase deficiency (Osellame et al., 2013, Kinghorn et al., 2016) and in *GBA1* mutant neurons (Schöndorf et al., 2018). The Seahorse XF Analyser is a tool that could be utilised in the future to measure the oxygen consumption rate and extracellular pH in cells to provide information on mitochondrial function, oxidative stress and metabolic dysfunction (Leung and Chu, 2018). This instrument is able to provide fast real-time analysis of metabolism in cells and could provide insight into the contribution of mitochondrial dysfunction in the pathogenesis of E326K, L444P and N370S

mutations in fibroblasts. Such methods have been used to demonstrate defective mitochondrial respiration as measured by decreased ATP production and decreased oxygen consumption rate in isolated mitochondria from a GD mouse model (Dasgupta et al., 2015) and *GBA1* mutant human dopamine neurons (Kim et al., 2021).

3.5 Conclusion

In this chapter I have demonstrated that in both heterozygous and homozygous form, the E326K *GBA1* mutation does not act via a loss of function mechanism. There were minimal changes in E326K GCase protein level, mRNA transcript level and activity compared to wild-type controls. This was also significantly elevated compared to L444P and N370S, which are well documented loss of function mutations. There are also no apparent changes in ER stress, ER retention and lysosomal trafficking in E326K mutants, suggesting that the presence of the mutated protein in the ER does not initiate a gain of function pathological mechanism this way.

4 *GBA1* mutations and protein stability

4.1 Introduction

GBA1 mutations occur across the entire GCase protein structure (Smith et al., 2017). Aside from those in and around the active site, which may cause conformational changes to alter the structure of the active site and reduce enzyme activity, mutations may affect structural stability. A proteins stability is defined by its capacity to retain its active structural conformation when exposed to adverse environmental conditions, such as increases in temperature or changes in pH levels (Suplatov et al., 2015). Structural stability is important for enzymatic function, subcellular trafficking and potentially protein interactions. An enzyme's pH stability or thermostability is closely linked to its overall structural stability and is important for function (Xia et al., 2016, Ward and Moo-Young, 1988). The major forces involved in maintaining the active conformation of an enzyme are hydrogen bonds and hydrophobic effects (Yeoman, 2010).

GBA1 mutations may affect the stability of the GCase protein, and thus lead to its degradation through the UPR and ERAD (Ron and Horowitz, 2005, Bendikov-Bar et al., 2011). This is supported by the findings in this study demonstrating that the L444P mutant protein is associated with ER retention and initiates the UPR and ER stress response in fibroblasts (see Chapter 3.). Previous studies have reported that the two most common *GBA1* mutations, L444P and N370S, occur far from the active site and likely work by destabilising the mature GCase structure leading to its degradation (Lieberman et al., 2007). As analysis of the crystal structure of N370S (Wei et al., 2011), coupled with molecular dynamic simulations (Offman et al., 2010), showed that the N370S protein is virtually indistinguishable to native GCase and yet activates degradation pathways (Fernandes et al., 2016), this suggests that it is a lack of protein stability that

induces this degradation. The N370S mutation has also been reported to shift the GCase protein pH optima from 4.5 to 6.5 (Steet et al., 2006), again suggesting altered protein stability. The L444P mutation occurs in the hydrophobic core of domain III (Lieberman, 2011). This substitution induces domain rigidity and disrupts the domains hydrophobicity, which may subsequently affect protein stability. Studies have found that the L444P mutation results in an unstable enzyme with little to no residual activity (Grace et al., 1994, Pastores and Hughes, 1993, Grace et al., 1991). No investigations into the E326K variant's structure have been undertaken however, as this mutation occurs on the surface of domain III it may influence GCase protein interactions or binding (Malini et al., 2014).

N-linked glycosylation is thought to confer an enzyme's stability. Interestingly, in GCase this post-translational modification induces local conformational stability in residues across the entire protein. Without proper glycosylation, the GCase enzyme is not functional (Tekoah et al., 2013, Berg-Fussman et al., 1993). Asn 19, in particular, has been reported to be required for a fully functioning catalytic dyad, whereas Asn 146 is thought to play a role in GCase thermostability (Berg-Fussman et al., 1993). Occupation of the first glycosylation site at Asn 19 stabilises regions 438-335, which surrounds the L444P mutation site. Occupation of this glycosylation site may affect the stability of the catalytic dyad in the active site. Glycosylation at sites Asn 59 and Asn 270 have also been shown to be involved in reducing the flexibility of GCase protein structure (Pol-Fachin et al., 2016). This demonstrates a potential link between enzymatic stability in individual GCase mutants and cellular pathology.

The aim of this chapter was to investigate how *GBA1* mutations affect GCase protein stability to influence its behaviour within the cell. This information will give insight into how individual *GBA1* mutations affect the protein at the structural level

to influence pathogenesis. To do this, recombinant GCase protein with a c-terminal 6xHis-tag, harbouring the E326K, L444P and N370S *GBA1* mutations, was expressed in HEK293 cells. I aimed to purify recombinant GCase protein by Ni-NTA agarose affinity chromatography and size-exclusion chromatography; this is the preferred method of purifying proteins containing a 6x-His tag (Spriestersbach et al., 2015).

4.2 Materials and Methods

4.2.1 Chemicals and reagents

Unless otherwise stated, all chemicals and reagents were purchased from ThermoFisher, Merck Millipore and Abcam.

4.2.2 Antibodies

Table 14. Antibodies used in Chapter 4.

Antibody Name	Immunogen and epitope	Species	Western Blot Dilution	Immunofluorescence Dilution
Anti-GBA clone 2e2, AP1140 (Millipore)	Recombinant human GBA protein, AA 146-236 (outside of mutation sites)	Mouse, mAb	1/1000	1/200
His-Tag (D3I10) XP (Cell Signaling)	6xHis-tag fused to either the amino or carboxyl terminus of targeted proteins in transfected cells	Rabbit, mAb	1/1000	1/250
Beta-actin, ab8227 (Abcam)	Human beta-actin, epitope AA 1-100	Rabbit, pAb	1/4000-1/500	n/a
Anti-Rabbit HRP (Dako)	n/a	n/a	1/3000	n/a
Anti-Mouse HRP (Dako)	n/a	n/a	1/3000	n/a
Anti-Mouse Alex-Fluor 488 (Invitrogen)	n/a	n/a	n/a	1/300 – 1/500
Anti-Rabbit Alex-Fluor 568 (Invitrogen)	n/a	n/a	n/a	1/300 – 1/500

4.2.3 HEK293 cell culture

HEK293 cells were cultured as described in Chapter 2.9. A list of HEK293 cell lines generated in this study is in Table. 8.

4.2.4 Stable transfection of HEK293 cells

HEK293 cells were stably transfected to express c-terminal 6xHis-tag wild-type, E326K, L444P and N370S GCase protein as described in Chapter 2.11.

4.2.5 Western blotting

For analysis of HEK293 cells, cell lysates were generated as described in Chapter 2.14. Western blotting was performed as described in Chapter 2.15 using the Bolt™ instruments. For analysis of GCase protein, Cerezyme® was used as a reference. Cerezyme® was courtesy of Prof. Derralyn Hughes, LSD Disease Clinic, Royal Free Hospital. For analysis of His protein, recombinant human *GBA1* (rGBA) protein (R&D Systems) was used as a reference. This recombinant *GBA1* is produced in Chinese Hamster Ovary (CHO) cells and includes a c-terminal 6xHis-tag and the 39 amino-acid leader peptide, which will be cleaved from our constructs during processing (Grabowski et al., 1989). It runs higher (~65KDa) than our *GBA1* construct (59kDa) due to the addition of the 39 amino acid leader peptide. A list of antibodies used for analysis listed in Table. 14.

To assess protein in the fractions following size-exclusion chromatography and affinity chromatography, 5-45 µL of each fraction was added to 4 X Bolt™ sample buffer and 10 X Bolt™ reducing agent and diluted in dH_2O to a consistent final volume. 0.01 – 1 µg Cerezyme® was loaded as a positive control. Samples were loaded alongside 5 µL SeeBlue™ Plus2 pre-stained protein standard on to onto Bolt™ 8% bis-tris protein gels. Gels were run for 45 minutes at 165 V in 1X Bolt™

MOPS SDS running buffer and membranes transferred and imaged as described in Chapter 2.15.

4.2.6 Gel electrophoresis and Coomassie

For visualisation of proteins in samples, 5-45 µL of each fraction was added to 4 X Bolt™ sample buffer and 10 X Bolt™ reducing agent and diluted in distilled H_2O to a consistent final volume. 0.01 – 1 µg Cerezyme® was loaded as a positive control. Samples were loaded alongside 5 µL SeeBlue™ Plus2 pre-stained protein standard on to onto Bolt™ 8% bis-tris protein gels. Gels were ran for 45 minutes at 165 V in 1X Bolt™ MOPS SDS running buffer. Coomassie Brilliant Blue stain was added to the gel and incubated for at least 2 hours at room temperature whilst shaking. Ultrapure water replaced the stain and the gel was shaken until clear to visualise each protein band using a light box.

4.2.7 mRNA analysis

Analysis of mRNA levels of *GBA1* and *GAPDH* was performed as described in Chapter 2.17. A list of primers used can be found in Table. 10.

4.2.8 GCase activity assay

The activity of recombinant GCase protein and in HEK293 cells was assessed through a fluorescent GCase activity assay as described in Chapter 2.20.

4.2.9 Lysosomal hydrolase activity assay (β-galactosidase and β-hexosaminidase activity assay)

The activity of β-Galactosidase and β-Hexosaminidase was assayed in cell lysates as described in Chapter 2.21.

4.2.10 Size-exclusion chromatography

Dry pellets of stable HEK293 cell lines were obtained and lysed in 1% (v/v) Triton X 100 in PBS pH 7.4, containing 1X protease and phosphatase inhibitors (Halt) as described in Chapter 2.14. Size-exclusion chromatography was performed by Dr Guglielmo Verona, National Amyloidosis Centre – Wolfson Drug Discovery Unit, Department of Inflammation, Division of Medicine, Faculty of Medical Sciences, UCL. Briefly, 100 μL of cell lysate was loaded onto a Superdex 200 10/300 GL (Column Volume 24ml; GE Healthcare) connected to a ÅKTA Explorer FPLC system (GE Healthcare). UV signal at 280 nm was monitored using the software PrimeView (GE Healthcare). The column was previously equilibrated with 2 column volumes (CV) of 100 mM Ammonium Bicarbonate, pH 8, and was eluted at 0.5 ml/min over a volume of 44 ml. Automatic fraction collection was set to 0.5 ml per fraction.

4.2.11 Affinity chromatography

To obtain pure GCase protein, affinity chromatography was performed by Dr Guglielmo Verona using a pre-packed 5ml HisTrap FF crude affinity chromatography column (GE Healthcare) connected to a ÅKTA Prime FPLC system (GE Healthcare). UV signal at 280 nm was monitored using the software PrimeView (GE Healthcare). 2 ml of cell lysate was loaded onto the column, previously washed and equilibrated with 20 mM Potassium Phosphate, 10 mM Imidazole, 150 mM NaCl, 0.1% Triton, pH 8. The unbound fraction was collected and loaded a second time in order to ensure maximum binding. The column was then washed with 2 CV (10 ml) of 20 mM Potassium Phosphate, 15 mM Imidazole, 150 mM NaCl, 10mM Beta-mercaptoethanol, 0.1% Triton, pH 8, to remove any non-specific bound molecules. The unbound fraction was collected for further analysis. Finally, the column was eluted with 20 mM Potassium

Phosphate, 250 mM Imidazole, 150 mM NaCl, 10mM Beta-mercaptoethanol, 0.1% Triton, pH 8. UV signal at 280 nm was followed in order to decide when to stop the sample collection. To remove imidazole, samples were dialysed for 1 cycle over-night against 20 mM Potassium Phosphate, 150 mM NaCl, 10mM Beta-mercaptoethanol, 0.1% Triton, pH 8 at 4°C in the dark, and stored at 4°C to be analysed within 2 days.

4.2.12 Thermostability analysis

To assess the effect of *GBA1* mutations on protein thermostability, fractionated cell lysate following size-exclusion chromatography was subjected to increasing temperatures and GCase activity analysed. Following size-exclusion chromatography, samples containing wild-type, E326K, L444P and N370S GCase protein were diluted in PBS to give a 0.0012 μg/μL concentration. For analysis at acidic pH, solutions were made up in 8 separate tubes containing 5 μL 0.0012 μg/μL recombinant GCase protein (0.06 μg/μL final concentration); 5 μL PBS; 5mM M-Glu in McIlvaine buffer at pH 5.4 in the presence of 22mM NaT. For analysis at neutral pH, solutions were made up in 8 separate tubes containing 5 μL 0.0012 μg/μL recombinant GCase protein (0.06 μg/μL final concentration); 5 μL PBS; (M-Glu) in McIlvaine buffer at pH 7.4 in the presence of 22mM NaT. For both acidic and neutral conditions, one tube was heated at the following temperatures for 30 minutes: 37°C, 40°C, 45°C, 50°C, 55°C, 60°C and 70°C. Following this the reaction was stopped by adding 0.25 M glycine at pH 10.4. Samples were transferred to 96 well plates and measured in triplicates. Fluorescence was measured at excitation 365 nm and emission 450 nm. 4-methylumbelliferone fluorescence (1 nmol) was used as a standard of known fluorescence.

4.2.13 pH stability

To assess the effect of *GBA1* mutations on pH stability, fractionated cell lysate following size-exclusion chromatography was incubated in acidic and neutral conditions for an extended time period and GCase activity analysed at frequent timepoints. Following size-exclusion chromatography, samples containing wild-type, E326K, L444P and N370S GCase protein were diluted in PBS to give a 0.0012 μg/μL concentration. For each genotype, acidic and neutral conditions were used. In a polypropylene tube a solution was made containing 0.1 μg/μL recombinant *GBA1* protein, PBS, and McIlvaine buffer containing NaT at either pH 5.4 or pH 7.4. Samples were heated at 37°C on a heat block and aliquots removed for analysis at minutes 1, 2, 3, 4, 5, 10, 20, 30, 40, 50 and 60. Aliquots were incubated with 5 mM M-Glu for 30 minutes and the reaction stopped with 0.25 M glycine at pH 10.4. Each sample was transferred to 96 well plates and measured in triplicates. Fluorescence was measured at excitation 365 nm and emission 450 nm. 4-methylumbelliferone fluorescence (1 nmol) was used as a standard of known fluorescence.

4.2.14 Trypsin digestion patterns

Trypsin is one of the most commonly used proteolytic enzymes in proteomics. It is used to digest proteins into smaller peptides by cleaving the c-terminal side of lysine and arginine amino acid residues (Vandell and Limbach, 2010). If a protein is less stable, one would expect it to be more flexible and unstructured and therefore more easily digestible by trypsin. To assess the effect of *GBA1* mutations on protein stability each sample was subjected to trypsin digestion, following from size-exclusion chromatography. This was performed by Dr Guglielmo Verona. The concentration of samples containing wild-type, E326K, L444P and N370S *GBA1* protein was diluted to 0.001 μg/μL. GCase protein was

incubated with Trypsin at a ratio of 1:20 (Trypsin:*GBA1*) in 150 mM McIlvaine buffer at pH 5.4 and heated at 37°C for 2 hours. An aliquot of sample was taken at time points 0, 2, 5, 10, 20, 30, 60 and 120 minutes. To stop the reaction, sample buffer containing 0.02 M Tris, 2 mM EDTA, 5% SDS, 0.05% bromophenol blue, 5% glycerol, pH 8 was added at a ratio of 1:1 to the sample, which was then boiled at 100°C for 5 minutes. Western blot analysis was performed with anti-GBA antibody (Millipore) as described in Chapter 4.2.5.

4.3 Results

4.3.1 C-terminal 6xHis-tag does not interfere with GCase enzyme activity

The c-terminal of an enzyme may be involved in enzymatic activity, and the addition of a 6xHis-tag to this domain may hinder the function of the enzyme (Sabaty et al., 2013). To assess whether the addition of a c-terminal 6xHis-tag interfered with recombinant GCase activity, a GCase assay was performed at both pH 5.4 and pH 4.5 (Figure. 22A.) on untransfected HEK293 cells, HEK293 cells expressing wild-type GCase with a c-terminal 6xHis-tag and HEK293 cells expressing untagged wild-type GCase. Compared to untransfected HEK293 cells, both the tagged and untagged cells exhibited significantly increased GCase activity at pH 5.4 and pH 4.5 (**$p<0.01$), confirming the over-expression of GCase. There was no significant difference between the activity of tagged GCase and untagged GCase at either pH, confirming that a c-terminal 6xHis-tag does not interfere with activity. There were also no significant differences in the activity levels of β-galactosidase and β-Hexosaminidase across the cell lines (Figure.22B.).

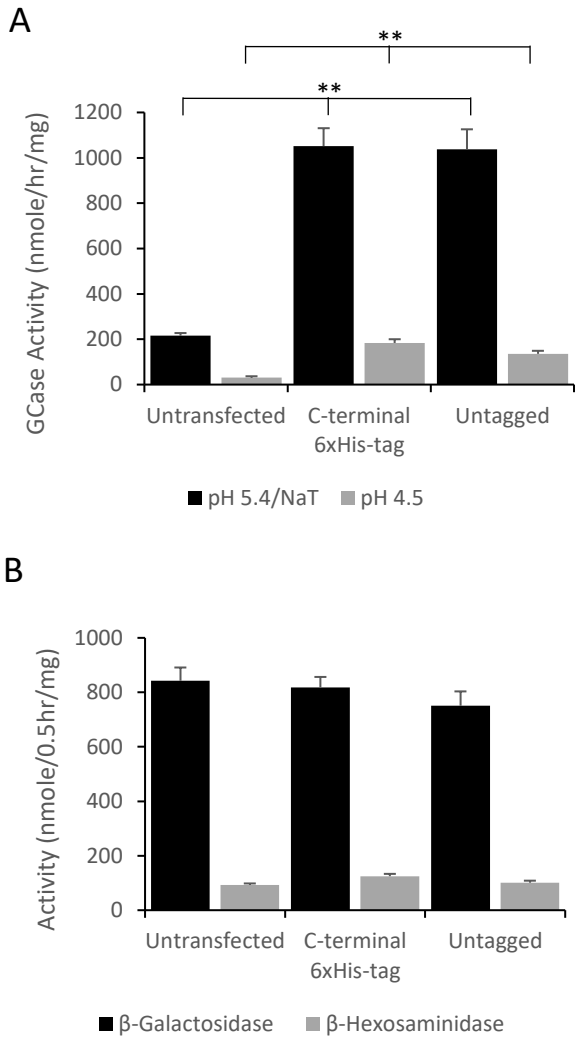

Figure 22. Effect of c-terminal 6xHis-tag on GCase activity in HEK293 cells.

A) GCase activity assay in nmole/hr/mg in untransfected HEK293 cells and HEK293 cells expressing recombinant GCase at pH 5.4 with NaT and at pH 4.5. **B)** β-galactosidase and β-Hexosaminidase activity in nmole/0.5hr/mg in untransfected HEK293 cells and HEK293 cells expressing recombinant GCase measured at pH 4.1. One cell line used for each sample. Two biological replicates with three technical repeats. Graph shows mean and error bars show SEM. Statistical test used was one way ANOVA with Tukey post-hoc analysis (**$p<0.01$).

4.3.2 Successful over-expression of GCase protein in HEK293 stable cell lines

In order to characterise the over-expression of recombinant GCase with a c-terminal 6xHis-tag in HEK293 stable cell lines, protein and expression levels of GCase and His protein were measured. Quantification of the GCase immunoblot (Figure. 23A.) revealed that all stably transfected clones exhibited significantly higher GCase protein compared to untransfected cells (wildtype and L444P ***p<0.001; E326K *p<0.05; N370S **p<0.01). Cerezyme® was utilised as a positive control running at 59 kDa. All data is normalised to untransfected cells at 1 ± 0.02. In wild-type cells, GCase protein level was 21.2 ± 3.8. In the mutant lines expressing L444P, E326K and N370S the GCase protein level was 8.4 ± 2.01, 4.1 ± 0.2 and 7.4 ± 1.15, respectively. Quantification of the His immunoblot (Figure. 23B.) also demonstrated a marked increase in His protein in stable cell lines compared to untransfected HEK293 cells (**p<0.01). Recombinant GCase with a c-terminal 6xHis-tag was utilised as a control. The rGBA protein runs higher (~65kDa) than our GCase constructs (59kDa) as it includes the 39 amino acid leader peptide. All data is normalised to untransfected cells at 1 ± 0.03. For wild-type GCase cells, His protein level was 13.7 ± 3.04. In L444P mutant cells His protein was 5.4 ± 0.72, in E326K cells His protein was 4.01 ± 0.58 and in N370S cells His protein levels were 6.5 ± 1.18. This was expected to be lower than quantification with the anti-GBA antibody as the anti-His antibody does not bind endogenous GCase.

To further the analysis of recombinant c-terminal tagged GCase protein quantitative PCR was used to measure GCase transcript levels (Figure. 23C.). Data is normalised to untransfected cells, which is set at 1 ± 0.2. All transfected cell lines exhibit a significant increase in GCase transcript levels. Wild-type

HEK293 cells had increased expression to 5.26 ± 1.19 (*p<0.05) and L444P and N370S increased to 8.22 ± 3.1 (***p<0.05) and 8.25 ± 3.29 (*p<0.05), respectively. The E326K cell lines exhibit the lowest increase in GCase transcript reaching 3.09 ± 0.31 (*p<0.05).

To complete the characterisation of the HEK293 over-expressing stable cell lines, immunofluorescence was performed to qualitatively analyse the expression of GCase and His protein (Figure. 23D.). Compared to untransfected HEK293 cells, all stable clones exhibited higher expression of GCase and His protein.

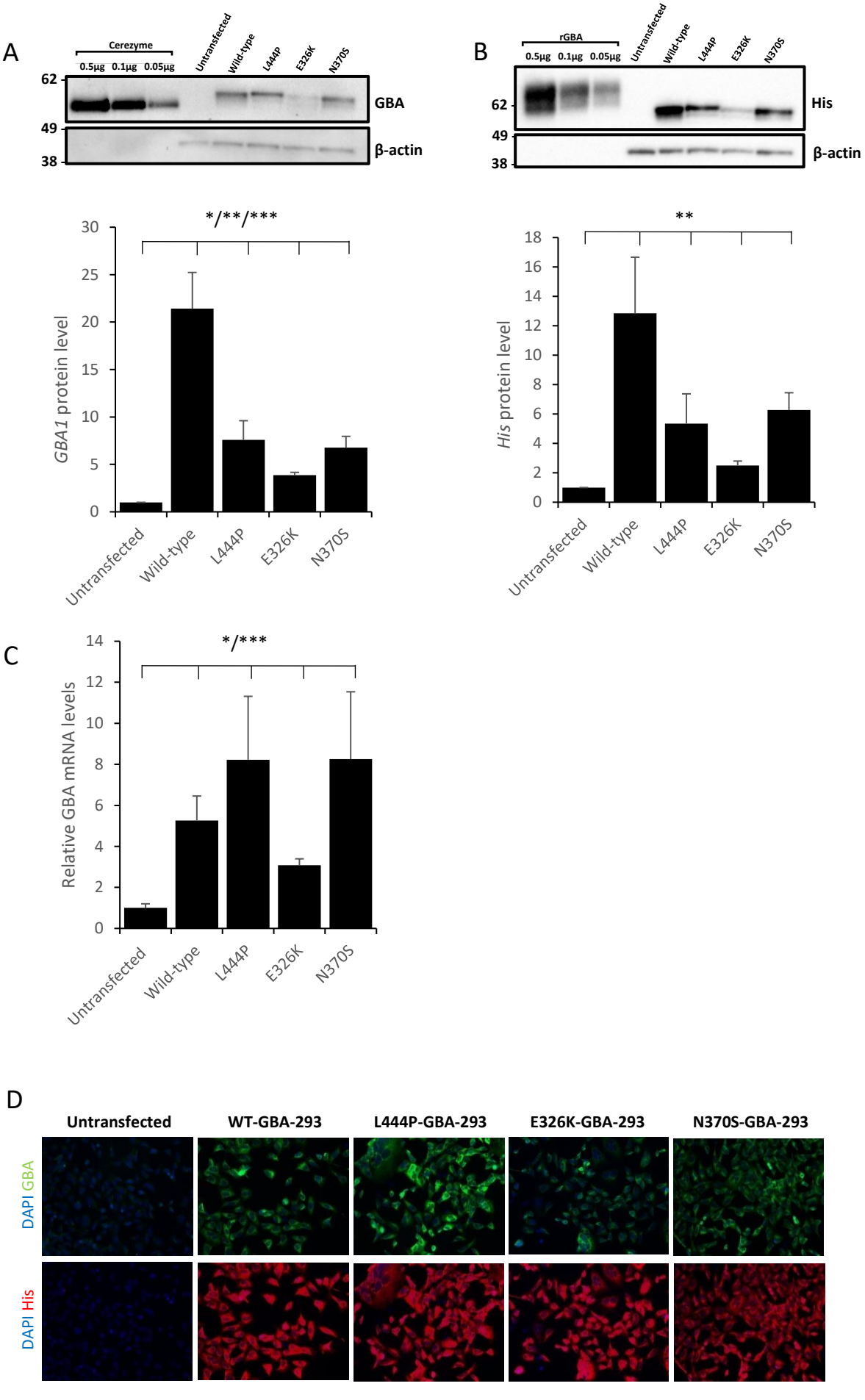
A
Cerezyme
0.5µg 0.1µg 0.05µg
Untransfected
Wild-type
L444P
E326K
N370S
62
49
38
GBA
β-actin
B
rGBA
0.5µg 0.1µg 0.05µg
Untransfected
Wild-type
L444P
E326K
N370S
62
49
38
His
β-actin
*/**/***
GBA1 protein level
30
25
20
15
10
5
0
Untransfected
Wild-type
L444P
E326K
N370S
**
His protein level
18
16
14
12
10
8
6
4
2
0
Untransfected
Wild-type
L444P
E326K
N370S
C
*/***
Relative GBA mRNA levels
14
12
10
8
6
4
2
0
Untransfected
Wild-type
L444P
E326K
N370S
D
Untransfected
WT-GBA-293
L444P-GBA-293
E326K-GBA-293
N370S-GBA-293
DAPI GBA
DAPI His

Figure 23. Characterisation of GCase over-expression in HEK293 cells stably transfected with 6xHis-tagged GCase constructs.

A) *GBA1* immunoblot and quantification in untransfected HEK293 cell lines and HEK293 stable cell lines. One cell line used for each genotype. Cerezyme® used as positive control. Band density quantified and data is normalised to untransfected HEK293 cells. Three technical repeats. Graph shows mean and error bars show SEM. Statistical test used was one way ANOVA with Tukey post-hoc analysis (*p<0.05, **p<0.01, ***p<0.001). Wild-type vs. untransfected *p<0.05; L444P vs. untransfected *p<0.05; E326K vs. untransfected *p<0.05; N370S vs. untransfected *p<0.05. **B)** *His* immunoblot and quantification in untransfected HEK293 cell lines and HEK293 stable cell lines. One cell line used for each genotype. Recombinant *GBA1* with c-terminal 6xHis-tag used as positive control. Band density quantified and data is normalised to untransfected HEK293 cells. Three technical repeats. Graph shows mean and error bars show SEM. Statistical test used was one way ANOVA with Tukey post-hoc analysis (*p<0.05, **p<0.01, ***p<0.001). Untransfected vs. stable cell lines **p<0.01. **C)** Quantification of *GBA1* mRNA levels in HEK293 stable lines normalised against untransfected HEK293 cells. One cell line used for each genotype. Two biological replicates and three technical repeats. Graph shows mean and error bars show SEM. Statistical test used was one way ANOVA with Tukey post-hoc analysis (*p<0.05, ***p<0.001). Wild-type vs. untransfected *p<0.05; L444P vs. untransfected *p<0.05; E326K vs. untransfected ***p<0.001; N370S vs. untransfected *p<0.05. **D)** Individual clones for each genotype were selected and analysed by immunocytochemistry with anti-*GBA* (green) and anti-*His* antibodies (red), with DAPI for nuclei staining (blue).

4.3.3 Optimisation of c-terminal 6xHis-tagged GCase purification

As there is not much literature demonstrating purification of recombinant GCase from HEK293 cells using affinity chromatography, the protocol was first optimised. First, the efficacy of lysing HEK293 cells stably transfected with wild-type GCase by probe sonication or in 1% (v/v) Triton X 100 lysis buffer was assessed. Affinity chromatography was performed and aliquots collected of the cell lysate (input), unbound fraction and the eluted fraction. Immunoblotting with anti-*GBA* antibody (Figure. 24A.) and quantification (Figure. 24B.) demonstrates the amount of recombinant GCase protein recovered. Input for both conditions is set at 100%. For probe sonication, 10% of protein was lost in the unbound fraction and 25% was recovered in the eluted fraction. When cells were lysed with 1% Triton X 100 buffer, 2% of GCase protein is unbound with an overall recovery of 55% in the eluate.

Samples were run on gel electrophoresis and stained with Coomassie Brilliant Blue (Figure. 24C.). This allows visualisation of individual polypeptides within a sample and suggests that the eluate is purely GCase. Next, a GCase activity assay was performed at pH 5.4 and at pH 4.5 (Figure. 24D.) At both pH, cells lysed in Triton X 100 exhibited significantly higher GCase activity compared to those lysed by probe sonication (*$p<0.05$). To complete optimisation, I wanted to confirm that GCase protein remained active in each buffer used for affinity chromatography at pH 5.4 and pH 4.5 (Figure. 24E.). At both pH, activity was abolished in the presence of increasing concentrations of imidazole. At pH 5.4 activity dropped from 4323 ± 492 nmole/hr/mg to 136 ± 75 at 10 mM imidazole, and was undetectable at 100 mM and 200 mM imidazole. Similarly, at pH 4.5 GCase activity was also undetectable at 100 mM and 200 mM imidazole, and dropped from 2647 ± 329 nmole/hr/mg to 74 ± 12 at 10 mM imidazole.

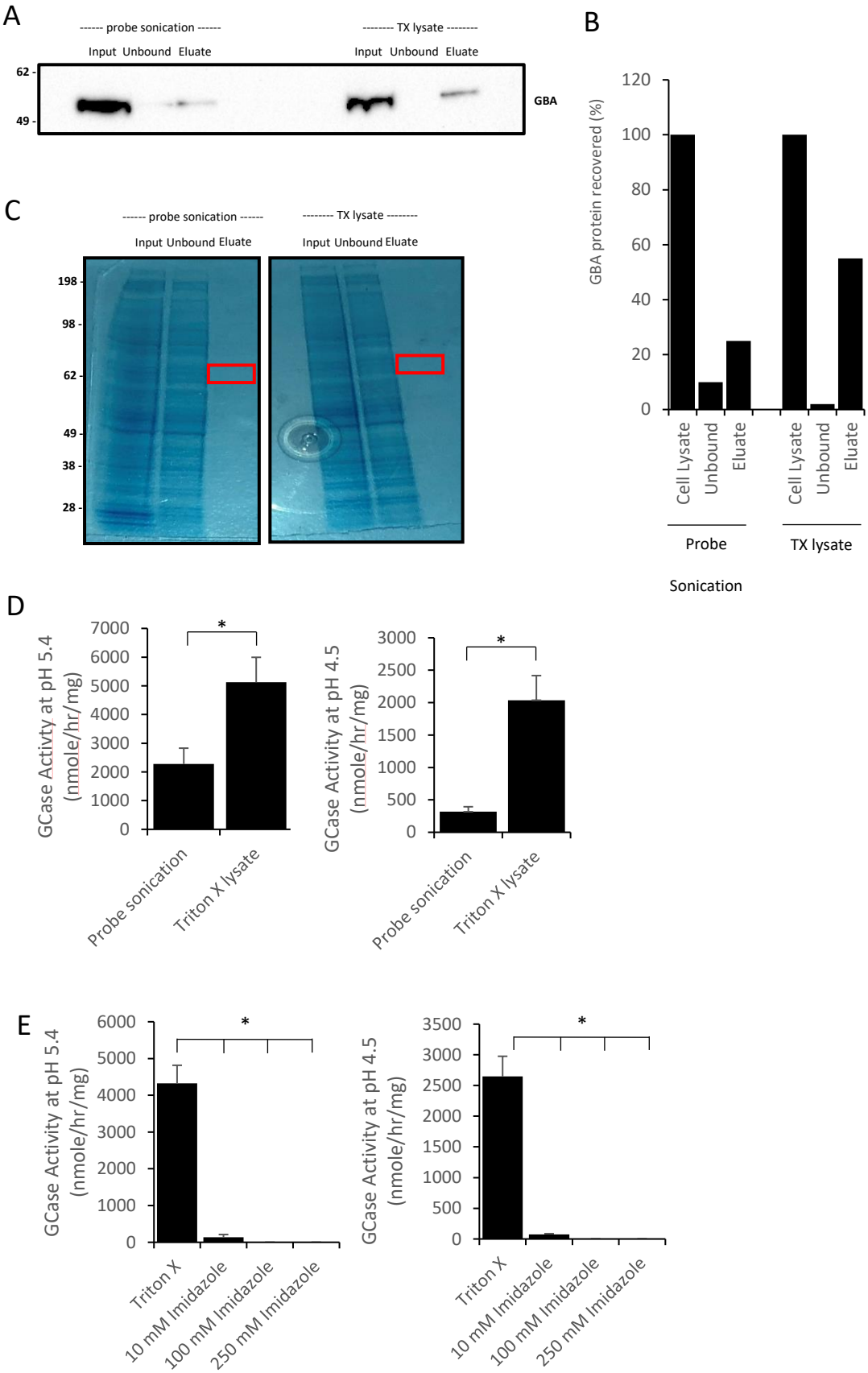
A
------ probe sonication ------
Input Unbound Eluate
-------- TX lysate --------
Input Unbound Eluate
62
49
GBA
B
GBA protein recovered (%)
120
100
80
60
40
20
0
Cell Lysate
Unbound
Eluate
Cell Lysate
Unbound
Eluate
Probe
TX lysate
Sonication
C
------ probe sonication ------
Input Unbound Eluate
-------- TX lysate --------
Input Unbound Eluate
198
98
62
49
38
28
D
GCase Activty at pH 5.4 (nmole/hr/mg)
7000
6000
5000
4000
3000
2000
1000
0
*
Probe sonication
Triton X lysate
GCase Activity at pH 4.5 (nmole/hr/mg)
3000
2500
2000
1500
1000
500
0
*
Probe sonication
Triton X lysate
E
GCase Activity at pH 5.4 (nmole/hr/mg)
6000
5000
4000
3000
2000
1000
0
*
Triton X
10 mM Imidazole
100 mM Imidazole
250 mM Imidazole
GCase Activity at pH 4.5 (nmole/hr/mg)
3500
3000
2500
2000
1500
1000
500
0
*
Triton X
10 mM Imidazole
100 mM Imidazole
250 mM Imidazole

Figure 24. Optimisation of conditions for purification of wild-type GCase protein from HEK293 cells stably transfected with 6xHis-tagged GCase constructs using Ni-NTA resin affinity chromatography.

HEK293 cells over-expressing wild-type GCase were lysed in 0.01% Triton X 100 or by probe sonication. One cell line used (WT-GBA-293).; two separate pellets lysed. **A)** Immunoblot for GCase protein level recovered from each step of affinity chromatography, including cell lysate input from probe sonication and Triton X conditions, unbound fraction and eluate. **B)** Quantification of band density expressed as a percentage of total GCase protein in cell lysate (100%) inputted in to the system. Two technical repeats. C**)** SDS-Page stained with Coomassie Brilliant Blue stain to visualise proteins in each sample. Red box depicts where GCase is expected on the gel (59kDa). **D)** GCase activity assay in nmole/hr/mg in cell lysate from probe sonication and Triton X lysis at pH 5.4 with NaT and at pH 4.5. One cell line used (WT-GBA-293).; two separate pellets lysed. Two biological replicates with three technical repeats. Error bars show SEM. Statistical test used was one way ANOVA with Tukey post-hoc analysis (*$p<0.05$). **E)** GCase activity assay in nmole/hr/mg in cell lysate from Triton X lysis incubated with increasing concentrations of Imidazole. at pH 5.4 with NaT and at pH 4.5. Imidazole significantly inhibited GCase activity compared to Triton X lysate alone. One cell line used (WT-GBA-293).; two separate pellets lysed. Two biological replicates with three technical repeats. Graphs shows mean and error bars show SEM. Statistical test used was one way ANOVA with Tukey post-hoc analysis (*$p<0.05$).

4.3.4 Purification of recombinant GCase protein by affinity chromatography

Following optimisation, affinity chromatography was performed using cell lysate of HEK293 cells over-expressing c-terminal 6xHis-tagged recombinant GCase protein (Figure. 25.). Each fraction was collected and analysed. Input refers to the total protein from total cell lysate. The unbound fraction represents all proteins which do not bind to the Ni-NTA resin. Protein lost during the three wash stages was also collected and is referred to as wash 1, wash 2 and wash 3. The eluate is the final fraction, which was collected for analysis. Immunoblot and quantification of wild-type GCase protein in each fraction (Figure. 25A. and 25B.) demonstrates GCase protein recovery. Data is presented as a percentage of the input (100%). In the unbound fraction 7% ± 1.46% of GCase protein is lost. During the wash steps, there was 1.7% ± 2.02% GCase protein lost. The eluted fraction contains 71.9% ± 1.35% of GCase protein. To assess the purity of each fraction gel electrophoresis was performed and stained using Coomassie Brilliant Blue stain (Figure. 25C.). Cerezyme® was used as a positive control. The data demonstrates that while the majority of GCase protein was eluted following imidazole addition and many contaminating proteins removed, the eluted fraction is not pure, and contains other contaminants.

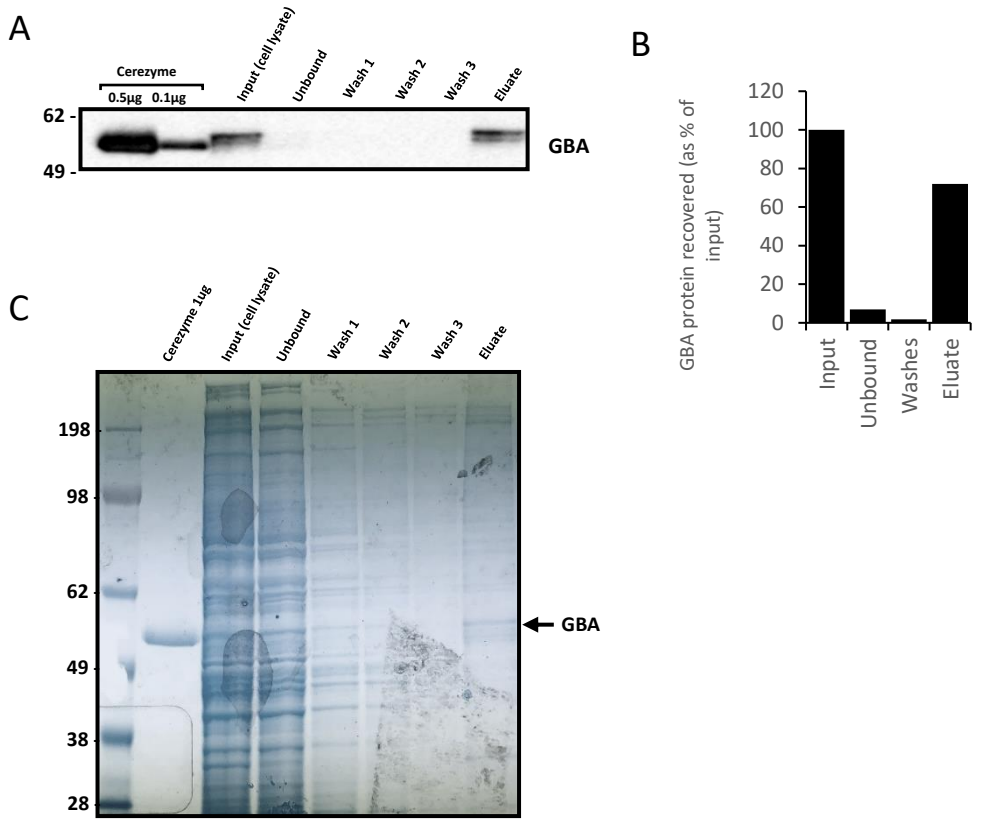

Figure 25. Purification of wild-type GCase protein from HEK293 cells stably transfected with 6xHis-tagged GCase constructs using Ni-NTA resin affinity chromatography.

A) Immunoblot and quantification for GCase protein level recovered from each step of the affinity chromatography including unbound, washes and eluted fraction. Three Cerezyme® bands were used to produce a standard curve of band density for quantification of protein recovered and **B)** data expressed as a percentage of input (100%). One cell line used (WT-GBA-293). Two technical repeats. **C)** SDS-Page stained with Coomassie Brilliant Blue stain to visualise proteins in each sample. Cerezyme® used as a GCase positive control. Arrow points to where GCase is expected on the gel (59kDa).

4.3.5 Fractionation of GCase protein by size-exclusion chromatography and purification by affinity chromatography

To improve the purity of the eluted fraction, cell lysates were subjected to fractionation by size-exclusion chromatography. This technique is a fundamental tool in protein biochemistry, and works as a fractionation step to separate macromolecules in a sample on the basis of size (Burgess, 2018). This technique was employed to obtain the fraction containing the recombinant wild-type and mutant GCase protein expressed in our HEK293 cells. Data for wild-type GCase protein is shown as a representative figure as all mutants behaved the same way (Figure. 26.). The chromatogram for size-exclusion chromatography displays all fractions A1 – E7 (Figure. 26A.) and peaks correspond to proteins being eluted around 60 kDa. The main peak is between fractions A15 – C3. All fractions were collected and subjected to a GCase activity assay at pH 5.4 (Figure. 26B.). Fractions A15 – C3 exhibited detectable GCase activity. As both size-exclusion chromatography and GCase activity assay suggest that GCase is filtered into fractions A15 – C3, these fractions were pooled and proceeded to affinity chromatography.

Affinity chromatography was performed on the filtered fractions of wild-type (Figure. 27A-C), E326K (Figure. 27D-F.), L444P (Figure. 27G-I.) and N370S (Figure. 27J-L.) GCase over-expressing HEK293 cell lysate. Cerezyme® was utilised as a positive control, acting as a reference to recombinant GCase protein. Each fraction was collected and analysed by western blot with anti-*GBA* antibody and also by Coomassie Brilliant Blue stain. The immunoblot was quantified for each cell line and data presented as a percentage of total GCase protein recovered with cell lysate being 100%. Input refers to the GCase protein in the fractions following size-exclusion chromatography. The unbound fraction

represents all proteins which do not bind to the Ni-NTA resin. Protein lost in three wash steps was pooled and is referred to as wash. The eluate is the final fraction, which was collected for analysis.

For the wild-type variant, GCase immunoblot and quantification (Figure. 27A and 27B.) revealed that 65.23% GCase protein is recovered after size-exclusion chromatography, with 34.32% lost in the unbound fraction and a total of 31.39% recovered in the eluate. The yield was between 1-2 µg per 200-250 million cells. Analysis by Coomassie Brilliant Blue stain demonstrated that the eluate is much purer than both cell lysate and input, but too dilute to visualise the GCase band (Figure. 27C.). The mutant variants behaved differently to wild-type GCase. In E326K GCase fractions, immunoblot and quantification (Figure. 27D and 27E.) revealed that 45.25% GCase protein is recovered after size-exclusion chromatography, with 30.35% lost in the unbound fraction and a total of 3.36% recovered in the eluate. Analysis by Coomassie Brilliant Blue stain again demonstrated that the eluate was too dilute to visualise the GCase protein band (Figure. 27F.). For L444P GCase recombinant protein, 23.21% of GCase protein was recovered from size-exclusion chromatography, with 13.32% lost in the unbound fraction and only 2% recovered in the eluted fraction (Figure. 27G and 27H.). Coomassie Brilliant Blue analysis also revealed the eluate is too dilute to visualise the GCase mutant band (Figure. 27I.). Similarly to L444P, N370S GCase protein recovery was also low. Following size-exclusion chromatography 15.23% is recovered, with 3.23% lost in the unbound fraction and 1.21% remaining in the eluate (Figure. 27J. and 27K.). The eluate was too dilute to visualise the band (Figure. 27L.).

Total GCase activity was analysed at pH 5.4 in total cell lysate, input and eluate fractions from wild-type, E326K, L444P and N370S GCase over-expressing

HEK293 cells (Figure. 28.). In wild-type cell lysate activity was 17060 nmole/hr/g, increasing to 171736 nmole/hr/mg after size-exclusion chromatography and 469844 nmole/hr/mg in the eluate, showing an enrichment in GCase protein through each purification stage. Similarly, in the E326K variant activity was 18078 nmole/hr/mg in cell lysate, increasing to 190198 nmole/hr/mg in the input and 553025 nmole/hr/mg in the eluate. The activity in L444P cell lysate was 11763 nmole/hr/mg and the input exhibited 131427 nmole/hr/mg activity. In cells expressing N370S GCase protein the lysate activity was 11963 nmole/hr/mg and increased to 108661 nmole/hr/mg. Unfortunately, the GCase activity was undetectable in the eluate from L444P and N370S GCase HEK293 cells.

A

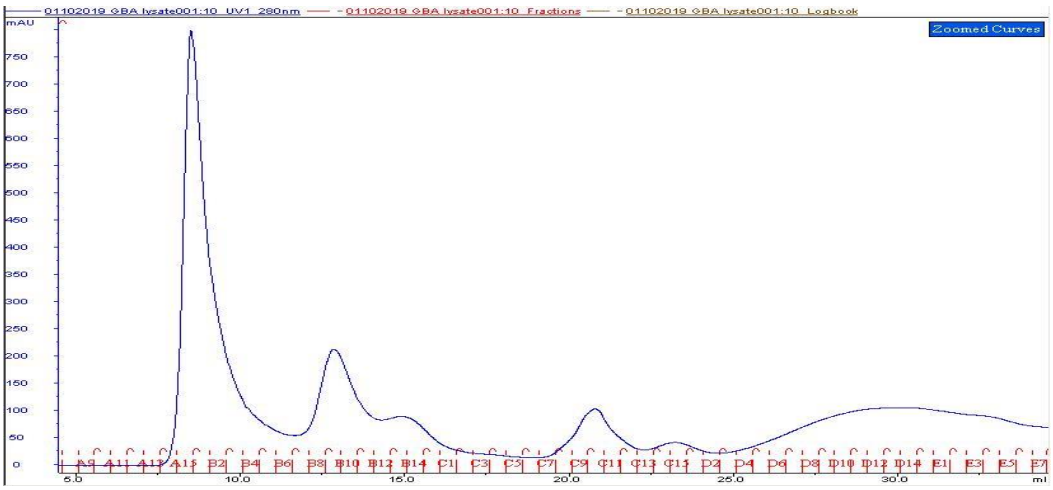

B

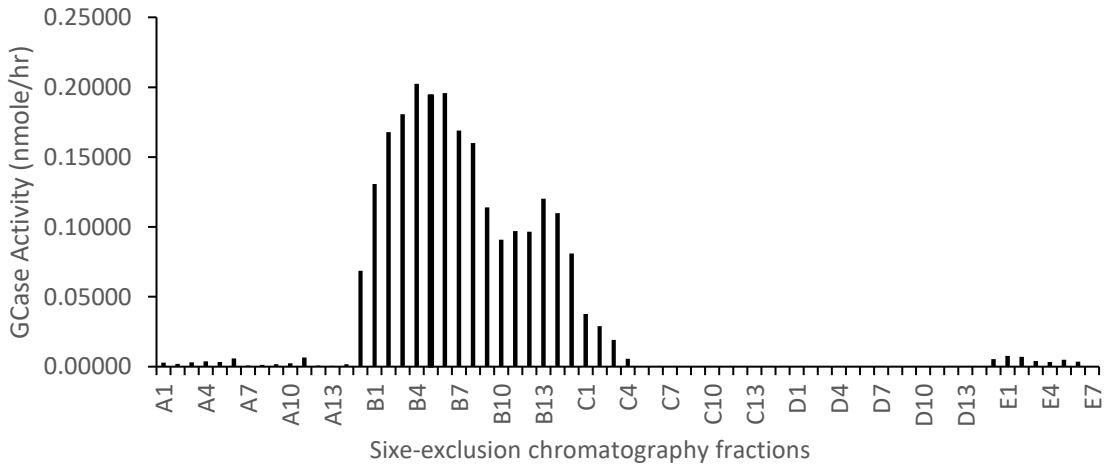

Figure 26. Fractionation of molecules in Triton X lysate of HEK293 cells stably expressing 6xHis-tagged wild-type GCase construct by size-exclusion chromatography.

A) Size-exclusion chromatography chromatogram for fractions A1 to E7. Peaks correspond to fractionation of molecules and complexes around 55 kDa. Largest peaks between fractions A15 and C3. Representative chromatogram shown from WT-GBA-293 cells. **B)** GCase activity assay in nmole/hr in fractions A1 to E7 at pH 5.4 with NaT. GCase activity measurable in fractions A15 to C3. Representative activity graph shown from same technical repeat (WT-GBA-293).

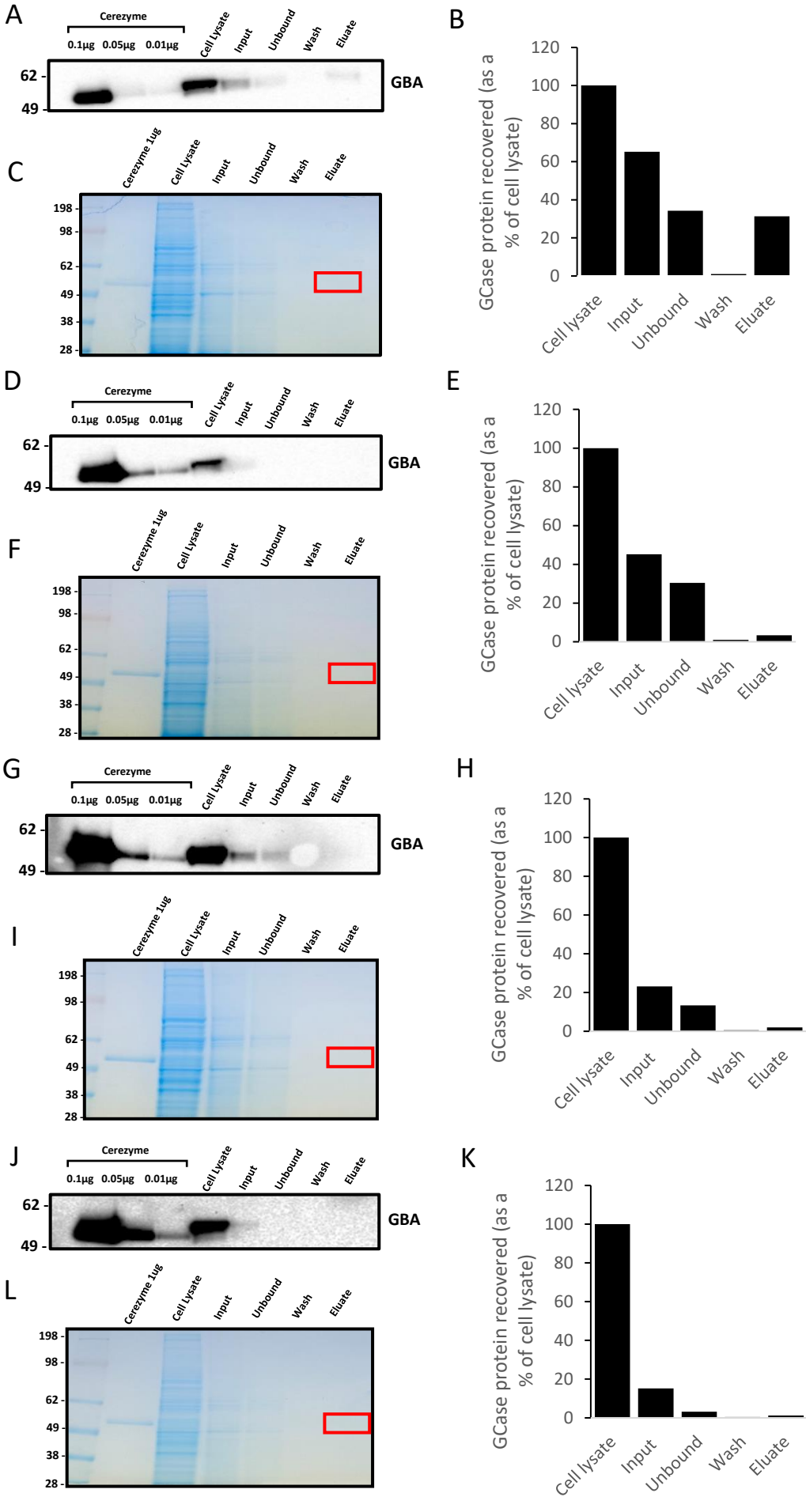
A
Cerezyme
0.1µg 0.05µg 0.01µg
Cell Lysate
Input
Unbound
Wash
Eluate
62
49
GBA
B
GCase protein recovered (as a % of cell lysate)
120
100
80
60
40
20
0
Cell lysate
Input
Unbound
Wash
Eluate
C
Cerezyme 1ug
Cell Lysate
Input
Unbound
Wash
Eluate
198
98
62
49
38
28
D
Cerezyme
0.1µg 0.05µg 0.01µg
Cell Lysate
Input
Unbound
Wash
Eluate
62
49
GBA
E
GCase protein recovered (as a % of cell lysate)
120
100
80
60
40
20
0
Cell lysate
Input
Unbound
Wash
Eluate
F
Cerezyme 1ug
Cell Lysate
Input
Unbound
Wash
Eluate
198
98
62
49
38
28
G
Cerezyme
0.1µg 0.05µg 0.01µg
Cell Lysate
Input
Unbound
Wash
Eluate
62
49
GBA
H
GCase protein recovered (as a % of cell lysate)
120
100
80
60
40
20
0
Cell lysate
Input
Unbound
Wash
Eluate
I
Cerezyme 1ug
Cell Lysate
Input
Unbound
Wash
Eluate
198
98
62
49
38
28
J
Cerezyme
0.1µg 0.05µg 0.01µg
Cell Lysate
Input
Unbound
Wash
Eluate
62
49
GBA
K
GCase protein recovered (as a % of cell lysate)
120
100
80
60
40
20
0
Cell lysate
Input
Unbound
Wash
Eluate
L
Cerezyme 1ug
Cell Lysate
Input
Unbound
Wash
Eluate
198
98
62
49
38
28

Figure 27. Purification of wild-type and mutant GCase protein from HEK293 cells stably transfected with 6xHis-tagged GCase constructs using Ni-NTA resin affinity chromatography following size-exclusion chromatography.

A) Immunoblot and **B)** band density quantification for wild-type GCase protein level recovered from each step of the affinity chromatography including total cell lysate, input, unbound, wash and eluate. Input is fractions A15 to C3 following size-exclusion chromatography. Cerezyme® was loaded in increasing concentrations to produce a standard curve for quantification of protein recovered. Due to over-exposure of all blots, 0.05 µg and 0.01 µg Cerezyme bands used for quantification of wild-type and mutant GCase protein. Data expressed as a percentage of total cell lysate (100%). **C)** SDS-Page stained with Coomassie Brilliant Blue stain to visualise proteins in each sample. Cerezyme® used as a *GBA1* positive control. Red box depicts where GCase band is expected on the gel (59kDa). Analysis repeated for mutants. Analysis of E326K protein by **D)** immunoblot, **E)** quantification of immunoblot and **F)** Coomassie Brilliant Blue stain. Analysis of N370S protein by **G)** immunoblot, **H)** quantification of immunoblot and **I)** Coomassie Brilliant Blue stain. Analysis of L444P protein by **J)** immunoblot, **K)** quantification of immunoblot and **L)** Coomassie Brilliant Blue stain. One cell line used for each genotype. Two technical repeats.

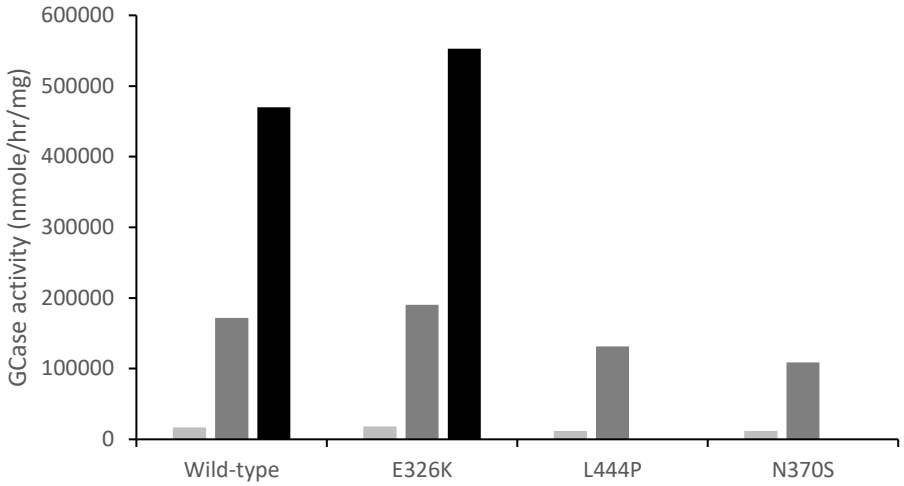

Figure 28. GCase activity in fractions following purification of wild-type and mutant GCase protein from HEK293 cells stably transfected with 6xHis-tagged GCase constructs using Ni-NTA resin affinity chromatography and size-exclusion chromatography.

GCase activity in nmole/hr/mg at pH 5.4 with NaT in total HEK293 cell lysates, input following size-exclusion chromatography and eluate. GCase activity was not detectable in eluate of L444P and N370S GCase protein. Activity measured from two technical repeats of purification from one cell line for each genotype (WT-GBA-293; E326K-GBA-293; L444P-GBA-293; N370S-GBA-293).

4.3.6 Purification of GCase protein from HEK293 cells using size-exclusion chromatography only

As the data demonstrates that GCase activity was undetectable in the final eluted fractions of L444P and N370S cells, the affinity chromatography step was removed and I instead focussed on the size-exclusion chromatography eluates. These were analysed for protein stability. Fractions A15 – C3 from size-exclusion chromatography of HEK293 cells expressing recombinant wild-type, E326K, L444P and N370S GCase constructs were pooled and analysed by western blot with anti-*GBA* protein (Figure. 29A.). The concentration of GCase protein in each was quantified using Cerezyme® band density to generate a standard curve. Proteins in the cell lysate input and size-exclusion chromatography output were separated by gel electrophoresis and stained with Coomassie Brilliant Blue to visualise each individual protein band in the samples (Figure. 29B.). The stain reveals that following size-exclusion chromatography, the sample is more dilute. Next, the percentage of GCase protein recovered by size-exclusion chromatography in each cell line was calculated (Figure. 29C.). In cells expressing recombinant wild-type GCase protein, recovery was 100.85 ± 28.18%. Similarly, in cells expressing E326K recombinant protein, recovery was 94.58 ± 36.9%. The percentage of mutant GCase protein recovered was markedly reduced in L444P and N370S cells, with only 54.46 ± 23.79% and 40.02 ± 3.67% recovered, respectively.

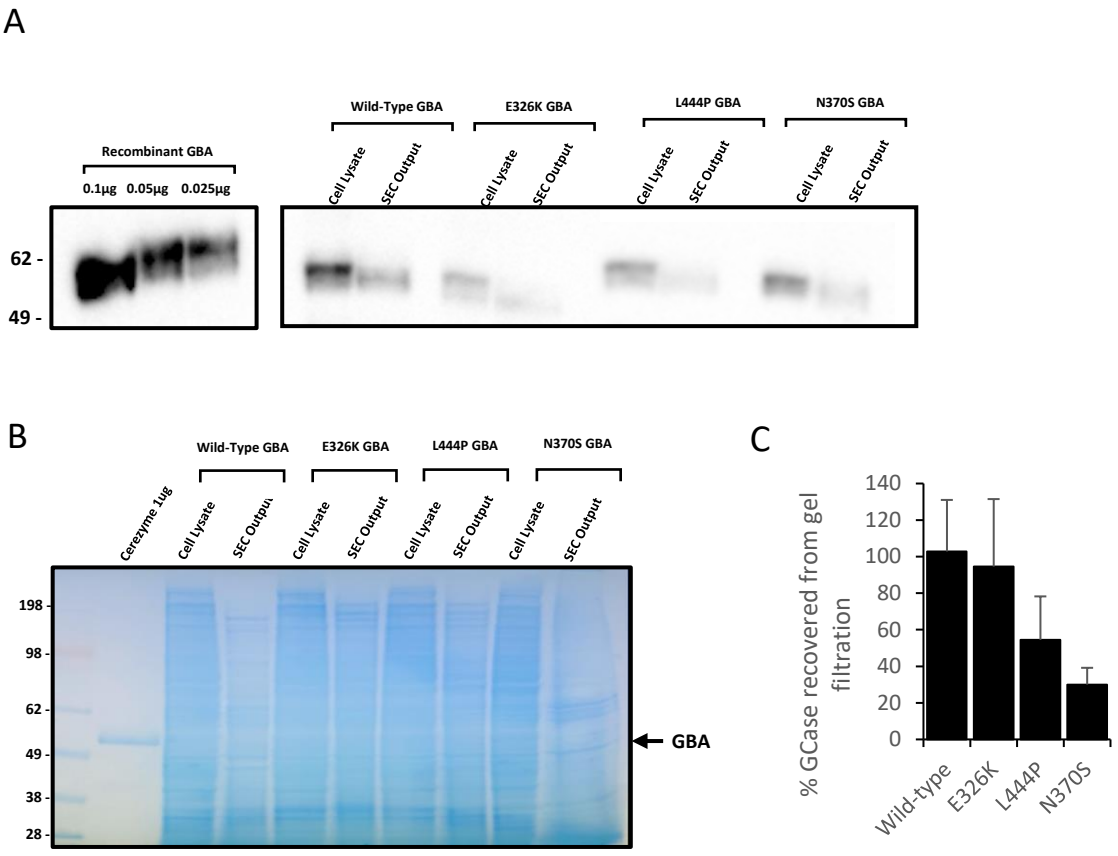

Figure 29. Fractionation of wild-type and mutant GCase protein from HEK293 cells stably transfected with 6xHis-tagged GCase constructs using size-exclusion chromatography.

A) Immunoblot for GCase protein level in total HEK293 cell lysate (WT-GBA-293; E326K-GBA-293; L444P-GBA-293; N370S-GBA-293) and recovered from size-exclusion chromatography (SEC) fractions A15 – C3. Recombinant *GBA1* was used to produce a standard curve for quantification of protein recovered. **B)** SDS-Page stained with Coomassie Brilliant Blue stain to visualise proteins in each sample. Cerezyme® used as a GCase positive control. Arrow points to where GCase is expected on the gel (59kDa). **C)** Quantification of *GBA1* protein recovered from size-exclusion chromatography (SEC), using recombinant *GBA1* band density to calculate sample band density. Data expressed as a percentage from the total cell lysate corresponding to each mutant. One cell line used for each genotype. Three technical repeats. Graph shows mean and error bars show SEM.

4.3.7 Minimal effect of *GBA1* mutations on pH and thermal stability of GCase activity

To assess the effect of *GBA1* mutations on structural stability, the impact of temperature and pH on GCase activity was investigated. As size-exclusion chromatography coupled with affinity chromatography produced N370S and L444P elute with undetectable GCase activity, eluate from size-exclusion chromatography only was used, as demonstrated in chapter 4.3.6. First, pooled size-exclusion chromatography fractions from each cell line were subjected to an increase in temperature at both pH 5.4 (Figure. 30A.) and pH 7.4 (Figure. 30B.).

Data for each cell line is normalised to the activity in nmole/hr/mg at 37°C, with this being set at 100%. Starting activity for each protein at pH 5.4 was as follows: wildtype 223664 nmole/hr/mg; E326K 227601 nmole/hr/mg; L444P 153265 nmole/hr/mg and N370S 50340 nmole/hr/mg. Starting activity for each protein at pH 7.4 was as follows: wildtype 112703 nmole/hr/mg; E326K 94060 nmole/hr/mg; L444P 33103 nmole/hr/mg and N370S 25791 nmole/hr/mg.

For analysis, the melting temperature ™ was calculated, which is defined as the temperature at which a protein retains 50% of its activity (Zhang et al., 2016). Compared to wild-type GCase protein, both E326K and L444P mutants behaved similarly at pH 5.4, with all three variants having a Tm of 50°C in acidic conditions. On the other hand, N370S GCase protein exhibited an increase in activity, reaching a maximum of 244% at 40°C. The Tm of the N370S variant was 54°C. At pH 7.4 wild-type GCase protein exhibited a steady decline in activity as temperature increased, with a Tm of 44°C. The E326K variant exhibited a similar decline to wild-type, with a Tm of 43°C. Similarly, L444P had a Tm of 45°C, however the activity declined at a slower rate to wild-type. The same pattern was seen in the N370S protein, where a slower decline led to a Tm of 46°C.

Next, the impact of pH alone on activity was analysed. Pooled fractions from size-exclusion chromatography were incubated at 37°C for 1 hour at either pH 5.4 (Figure. 30C.) or pH 7.4 (Figure. 30D.), and GCase activity measured at intervals. Data for each cell line is normalised to the activity in nmole/hr/mg at time 1 minute, with this being set at 100%. Starting activity for each protein at pH 5.4 was as follows: wildtype 19540 nmole/hr/mg; E326K 16691 nmole/hr/mg; L444P 15932 nmole/hr/mg and N370S 13879 nmole/hr/mg. Starting activity for each protein at pH 7.4 was as follows: wildtype 14561 nmole/hr/mg; E326K 12698 nmole/hr/mg; L444P 13136 nmole/hr/mg and N370S 11609 nmole/hr/mg.

At pH 5.4, the activity of wild-type recombinant GCase protein changed minimally over the one hour incubation. The activity of E326K protein dropped steadily for 40 minutes, reaching 64% and plateauing. The L444P GCase protein behaved similarly to wild-type until 30-40 minutes, where there was a slight increase to 103% followed by a steady decrease over the remainder of the incubation to 76%. The N370S variant exhibited minimal change in activity until 50-60 minutes, where a marked increase to 170% occurred. At pH 7.4, the wild-type GCase protein exhibited a steady decline in activity over the hour period to 22%. All mutants exhibited a similar steady decline in GCase activity during the incubation time. E326K mutant activity declined slower to 26% and L444P dropped to 42%. The N370S mutant retained more activity, declining more slowly over the one hour period until reaching 51%.

A

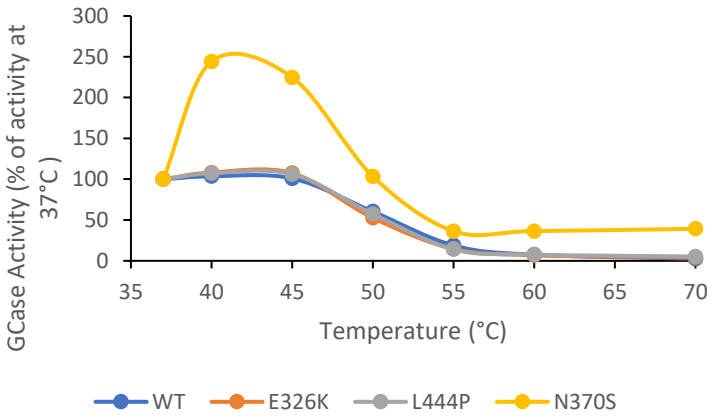
GCase Activity (% of activity at 37°C)
300
250
200
150
100
50
0
35
40
45
50
55
60
65
70
Temperature (°C)
WT
E326K
L444P
N370S

B

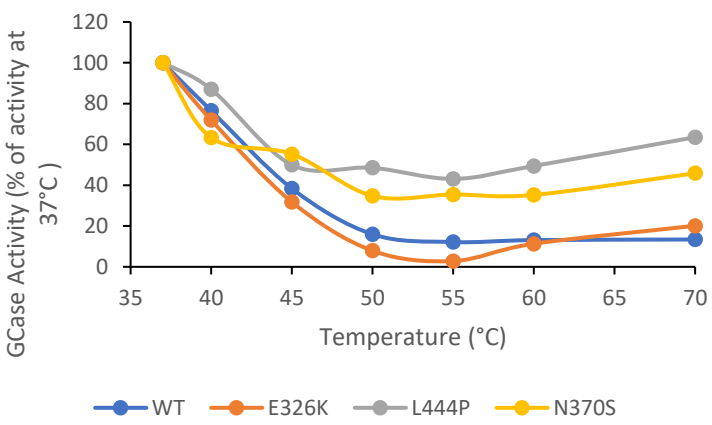
GCase Activity (% of activity at 37°C)
120
100
80
60
40
20
0
35
40
45
50
55
60
65
70
Temperature (°C)
WT
E326K
L444P
N370S

C

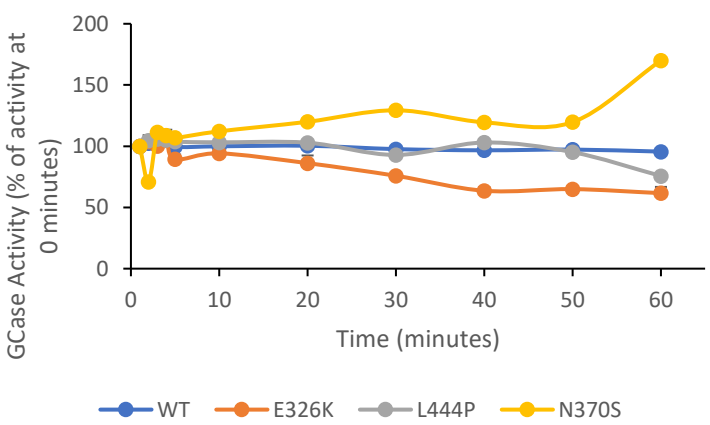
GCase Activity (% of activity at 0 minutes)
200
150
100
50
0
0
10
20
30
40
50
60
Time (minutes)
WT
E326K
L444P
N370S

D

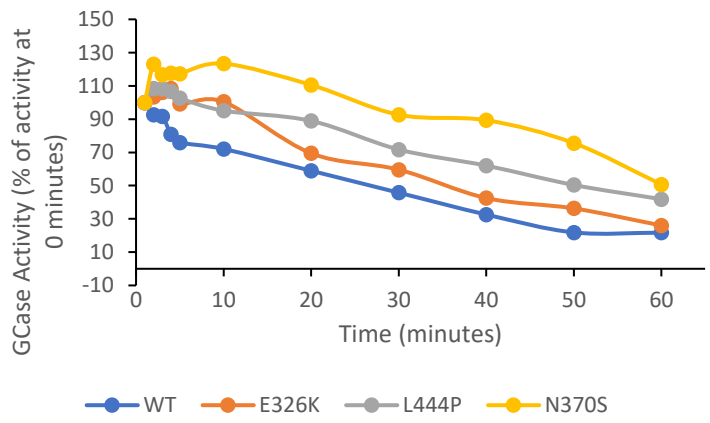
GCase Activity (% of activity at 0 minutes)
150
130
110
90
70
50
30
10
-10
0
10
20
30
40
50
60
Time (minutes)
WT
E326K
L444P
N370S

Figure 30. Thermal and pH dependant stability of wild-type and mutant GCase protein in HEK293 cell lysate following size-exclusion chromatography.

GCase protein activity in nmole/hr/mg **A)** at pH 5.4 with NaT and **B)** at pH 7.4 with NaT at increasing temperatures. All data points normalised to GCase activity at 37°C and expressed as a percentage with GCase activity at 37°C being 100%. GCase protein activity in nmole/hr/mg **C)** at pH 5.4 with NaT and **D)** at pH 7.4 with NaT at 37°C at timepoints up to 1 hour. All data points normalised to GCase activity at time 0 minutes and expressed as a percentage with GCase activity at time 0 minutes being 100%. One cell line used for each genotype (WT-GBA-293; E326K-GBA-293; L444P-GBA-293; N370S-GBA-293). Two biological replicates and three technical repeats. Statistical test used was one way ANOVA with Tukey post-hoc analysis.

4.3.8 Minimal effect of *GBA1* mutation on proteolytic digestion pattern

For an indirect measurement of the effect of *GBA1* mutations on structural stability, pooled size-exclusion chromatography fractions from each cell line were incubated with trypsin at a ratio of 1:20 (Trypsin:*GBA1*) for 2 hours. Trypsin is a proteolytic enzyme that cleaves the c-terminal side of lysine and arginine residues, digesting proteins into smaller peptides (Vandell and Limbach, 2010). The more stable a protein, the longer it can resist proteolytic digestion. Aliquots were collected at frequent timepoints and western blotting was performed with anti-*GBA* antibody (Figure. 31A.). Immunoblot band density was calculated as a percentage of untreated (UT) GCase protein, and averages from repeats shown graphically (Figure. 31B.). The percentage of protein resistant to digestion at 30 minutes and 120 minutes was compared between cell lines. Wild-type protein resisted digestion for 5 minutes. After 30 minutes of incubation, wild-type GCase protein level had reduced to 67.8%, continuing to decline to 32.04% after 120 minutes. The E326K variant was digested to 54.8% after 30 minutes, continuing to decline until 25.6% of protein remained after 120 minutes. L444P behaved similarly to E326K, with 53.9% of protein remaining after 30 minutes and 19.5% of protein remaining at 120 minutes. In fractions containing the N370S variant, GCase protein level after 30 minutes was calculated at 57.6% however by 120 minutes of incubation this had reduced to 15.05%.

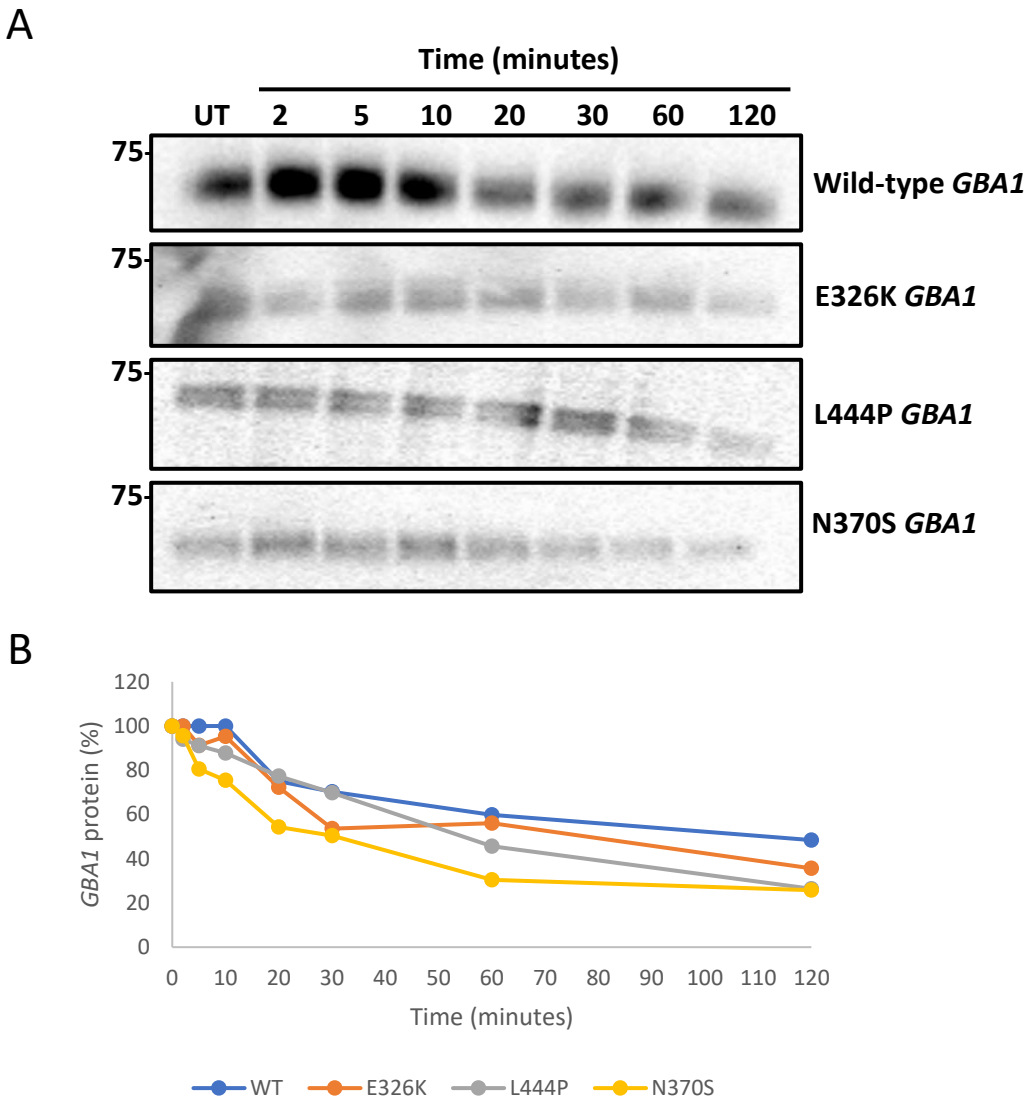

Figure 31. Proteolytic trypsin digestion pattern of wild-type and mutant GCase protein in HEK293 cell lysate following size-exclusion chromatography.

A) Immunoblot of wild-type and mutant GCase protein treated with trypsin proteolytic enzyme for 2 hours. UT refers to untreated protein at time 0. Representative blot shown. One cell line used for each genotype (WT-GBA-293; E326K-GBA-293; L444P-GBA-293; N370S-GBA-293). **B)** Quantification of wild-type and mutant GCase band density from the immunoblot. Band density was calculated and normalised to UT protein band density. Each data point is presented as a percentage of UT protein, with UT protein being 100% and the average of two technical repeats being displayed.

4.4 Discussion

In this chapter, I aimed to investigate the effect of the E326K, L444P and N370S *GBA1* mutations on structural stability and protein folding. The purpose of this was to understand how the individual mutations affect the protein at the structural level, potentially influencing the behaviour of each mutant GCase variant within the cell. Unfortunately, I was unable to obtain pure GCase protein, and thus I was unable to use spectrometry and spectroscopy techniques, such as NMR, circular dichroism and mass spectrometry, to analyse structural dynamics and protein folding in solution. Despite this I was able to indirectly assess protein stability by assessing the impact of temperature and pH on GCase activity, as well as the ability of mutant GCase to resist proteolytic digestion. The starting activity of each mutant was as expected with E326K protein exhibiting similar activity to wild-type and L444P and N370S mutants having generally lower activity. The results demonstrate a minimal change in structural stability induced by mutations; however, this is likely due to the mutant proteins already being highly unstable and as the techniques employed were not specific or sensitive in measuring structural dynamics and folding, it is likely further instability was not detected. A summary of the methodology used to purify GCase protein can be found in Figure. 32.

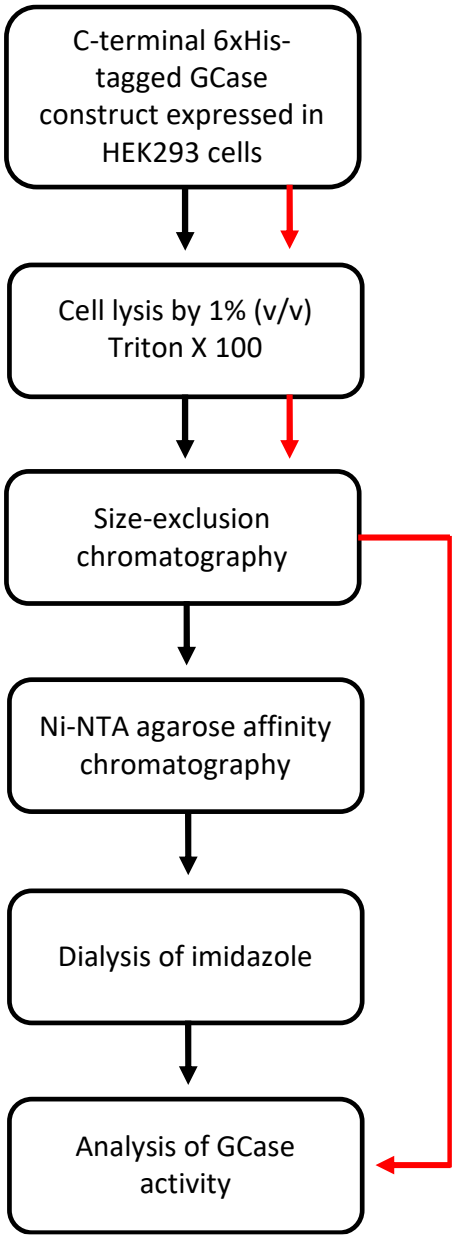

Figure 32. Illustrative diagram of the process used to purify recombinant GCase protein in this study.

Black arrows refer to the originally planned process to obtain pure GCase for activity analysis. Red arrows refer to the revised process that was followed for activity analysis.

4.4.1 Successful expression of c-terminal 6xHis-tagged *GBA1* protein in HEK293 cells

Recombinant GCase constructs were generated for expression of wild-type, E326K, L444P and N370S protein. It was first confirmed that a c-terminal 6xHis-tag did not affect GCase activity (Figure. 22A.). It has been shown previously that a c-terminal tag may hinder catalytic function of an enzyme (Sabaty et al., 2013). An n-terminal tag did not work as the 39 amino acid leader peptide is cleaved off during processing and thus a tag would be lost (Koch et al., 2003, Dalbey and Wickner, 1985). As activity was higher in the transfected cells, and other lysosomal hydrolase activity unaltered (Figure. 22B.), this confirms successful over-expression of GCase.

HEK293 cells were chosen as the expression system, as done previously (Gramlich et al., 2016, Cullen et al., 2011, Ron et al., 2010, Malini et al., 2014, Jebbink et al., 2015). This system was chosen as a human host cell was required to ensure recombinant GCase was fully processed and glycosylated in the same way as native human GCase, making it easier to relate to patient-derived fibroblast cells (Chapter. 3.) and human disease. In addition, these cells are fast-growing, easily transfectable and have low levels of endogenous GCase protein to interfere with abundance calculations. One downfall I encountered with HEK293 cells was the vast number of cells (~200 million) required to purify an appropriate amount of GCase protein. This was difficult to continuously obtain with adherent HEK293 cells grown in 10 cm dishes. To overcome this, I could have grown the cells in suspension in vented, non-baffled shake flasks as done in a previous study (Gramlich et al., 2016).

Expression of recombinant GCase was successful for each variant, with GCase protein (Figure. 23A.) and transcript (Figure. 23C.) levels significantly higher than

untransfected cells. The level of His protein was also markedly increased (Figure. 23B.), providing further evidence of successful expression of 6x-His tagged protein. This was also confirmed by immunofluorescence (Figure. 23D.). A noticeable reduction in GCase expression was observed in E326K cells compared to other variants. As E326K protein levels are reflected in transcript levels, this reduction is likely due to poor quality of E326K plasmid following site-directed mutagenesis. In L444P and N370S cells, protein levels were lower than transcript levels, suggesting that these mutants are misfolded in the ER and targeted for degradation by ERAD. This is similar to previous findings in human cells and *Drosophila* models harbouring the L444P and N370S mutations, where ERAD was activated (Bendikov-Bar et al., 2011, Ron and Horowitz, 2005, Wang et al., 2011, Babajani et al., 2012).

4.4.2 Purification of c-terminal 6xHis-tagged GCase protein by affinity chromatography

As the protein constructs contain a 6xHis-tag, I was able to purify exogenous protein only. Affinity chromatography was the chosen method of purification, with the aim to obtain ≥5g of ≥95% pure GCase protein. This has been performed previously to purify wild-type GCase protein from HEK293 cells (Gramlich et al., 2016) and human placenta (Strasberg et al., 1982, Grabowski and Dagan, 1984). Using an Ni-NTA resin column is the preferred method to purify proteins containing a 6xHis-tag. This specific agarose acts as a matrix to bind histidine residues in His-tags to the vacant positions in the coordination sphere of the immobilised nickel ions, with high specificity and affinity (Spriestersbach et al., 2015).

The protocol was adapted from Gramlich et al. An equilibrium buffer containing 10 mM imidazole, was used to prevent untagged proteins from binding to the

column; a wash buffer containing 20 mM imidazole was used to remove non-specifically bound proteins; and an elution buffer containing 250 mM imidazole was used to collect the His-tagged bound protein (Gramlich et al., 2016, Spriestersbach et al., 2015). Imidazole competes with histidine residues to competitively displace them from the column; however, our results demonstrated a concentration-dependant inhibitory effect on GCase activity (Figure. 24E.), and thus a dialysis step was introduced following affinity chromatography to remove imidazole from the buffer.

Recovery was around 70% for wild-type GCase protein (Figure. 25A. and 25B.), however this was impure and as elution required 10-12 mL of buffer this was also dilute (Figure. 25C.). These results differ from previous, where the same protocol was used to yield pure recombinant protein, with >10 µg/mL protein recovered in some eluates (Gramlich et al., 2016). It is important to note that these constructs were ligated to membrane binding peptides, Tat and the rabies glycoprotein derived peptide (RDP), as this study was assessing which construct was most efficiently purified for enhanced delivery to GD patient cells as a replacement for ERT. This study also employed an Ig K-chain leader sequence, which allows for efficient secretion of recombinant protein out of the cell. This is useful as the accumulation of recombinant proteins in the cytoplasm may lead to the formation of inclusion bodies or trigger proteasomal protein degradation. Furthermore, protein folding may be disturbed by endogenous protein in the ER. If recombinant protein is secreted out of the cell, the above is avoided and this can contribute to high yield of recombinant protein in both the cell-free media and soluble lysate (Peng et al., 2019).

In addition to this, a transient transfection may be more beneficial for rapid and high yield production of recombinant protein in mammalian cells (Gramlich et al.,

2016, Metz et al., 2016). Transient transfections have also been used in combination with an inducible expression system. In one study a specific system designed for high yield in HEK293 cells was utilised (Metz et al., 2016). This could be a future prospective for improving initial yield rather than transfecting stably for a long-term lower yield (Kaufman, 2000)

Size-exclusion chromatography was introduced prior to affinity chromatography, in an attempt to improve the purify of the eluate. This method separates proteins solely on the basis of their molecular weight (Burgess, 2018), and has been performed previously to fractionate GCase protein (Grabowski and Dagan, 1984, Pentchev et al., 1973). Elution of GCase protein in fractions was confirmed by activity analysis (Figure. 26.). These were too dilute to be detected by western blot or an ELISA assay. A more sensitive and accurate approach would be to further characterise the fractions through mass spectrometry, as done previously with other recombinant proteins (Nunes et al., 2017). Proteins in a sample are separated by gel electrophoresis and digested into fragments by trypsin. These fragments are analysed against a protein reference, and fragments matching the reference sequence yield a high percentage of sequence coverage.

All mutant lines were subjected to size-exclusion chromatography, followed by affinity chromatography (Figure. 27.). Although recovery from size-exclusion chromatography was 65.23% for wild-type protein and 45.25% for E326K protein, the recovery of L444P and N370S protein was markedly reduced. It is unknown why this happened, and suggests that the mutations cause the protein to stick to the filter. Another possibility is that the mutations cause GCase to aggregate, and thus the molecular weight is larger than the filter setting, however as lysing in Triton X 100 removes insoluble aggregates it is likely that this is not the case. This could be overcome by the use of denaturing agents, such as urea, as done

previously with other proteins (Schlager et al., 2012), however as natively folded protein is required to monitor folding it is not a preferred technique to denature and refold the protein. It is known that *in vivo* GCase protein may exist in a monomeric structure as well as dimeric and tetrameric (Liedtke and Legler, 1988, Pentchev et al., 1973), which may explain the differences as some higher molecular weight species may be more evident in these cell lines.

Following affinity chromatography, recovery of mutant protein was less than 10%. There is no previous literature purifying mutant GCase protein through affinity chromatography to compare these results, but low yield may arise due to the mutations preventing the 6xHis-tag binding efficiently to the nickel ions. Mutations may also alter the hydrophobicity of the protein, reducing its affinity for the agarose. It has been reported previously that in the L444P mutant, the substitution of leucine to proline causes rigidity in the protein backbone, disrupting the hydrophobicity of domain II (Lieberman, 2011). Furthermore, the percentage of GCase lost in the unbound fraction was larger than expected from optimisation studies, in all cell lines. This suggests that the mutations may make the 6xHis-tag less accessible or that during size-exclusion chromatography there may be some damage to the 6xHis-tag, impeding its binding to the Ni-NTA agarose.

To improve purification in future studies, immunoaffinity chromatography using antibodies against GCase could be used instead. This method has been performed previously to purify endogenous wild-type, L444P and N370S protein from patient fibroblasts (Salvioli et al., 2005, Tan et al., 2014), and has been shown to not lead to any loss of GCase activity (Aerts et al., 1986b). Purification of endogenous protein may lead to a low yield, and thus immunoaffinity can be applied to tagged recombinant protein harbouring epitopes for His, HA, FLAG

and cMyc tags (Choi et al., 2017). These can be used to perform tandem immunoaffinity, which may yield a purer eluate (DeCaprio and Kohl, 2019).

Affinity chromatography was removed from the purification process as the activity in L444P and N370S eluates was undetectable (Figure. 28). The revised process can be found in Figure. 32. Activity was measurable in size-exclusion chromatography eluate for all GCase variants. It is interesting to note that in the wild-type and E326K eluted fractions, GCase activity was much higher than in cell lysate and affinity chromatography input. This is likely due to the sample being purer and thus there is a higher GCase to synthetic substrate ratio, leading to more binding and thus more fluorescence measured. A similar pattern was observed in a study purifying wild-type GCase protein from root culture, where the enzymatic activity of purified GCase was increased compared to the crude protein (Naphatsamon et al., 2018).

4.4.3 Impact of pH and temperature on functional stability of wild-type and mutant GCase protein

Mutant variants of a protein that are less stable than the wild-type are likely to be subjected to ERAD. As there is a plethora of evidence associating L444P and N370S *GBA1* mutations with ERAD (Bendikov-Bar et al., 2011, Ron and Horowitz, 2005, Sanchez-Martinez et al., 2016), I hypothesised that a reduction in protein stability may underlie the differences in cytotoxic mechanisms activated by different *GBA1* mutations. Ideally, structural dynamics, folding kinetics and structural stability would be directly assessed through techniques such as circular dichroism and differential scanning calorimetry, as done previously (Lieberman et al., 2009, Ben Bdira et al., 2017). However, due to the recombinant GCase proteins being crude, focus was instead turned to determining the effect of

mutations on the functional stability of GCase, through manipulating the temperature and pH of solution.

Analysis of the Tm of wild-type GCase protein revealed a melting temperature of 50°C at acidic pH, shifting to 44°C at neutral pH (Figure 30A. and 30B.), suggesting wild-type GCase is more stable in acidic conditions. This is corroborated by previous findings where wild-type GCase had a Tm between 48°C-55°C at acidic pH (Ben Bdira et al., 2017, Abian et al., 2011, He et al., 2011, Pentchev et al., 1973), and exhibited a 4-5°C shift in Tm from acidic to neutral pH (Ben Bdira et al., 2017, Abian et al., 2011). Further analysis supported this, as wild-type GCase protein retained activity in acidic conditions for 60 minutes, whereas at neutral pH there was a decline in activity in a time-dependant manner (Figure. 30C. and 30D.).

A similar pattern was shown in two previous studies (Sawkar et al., 2006, Ben Bdira et al., 2017). The E326K protein behaved similarly to wild-type, with minimal change in Tm at both acidic and neutral conditions (Figure 30A. and 30B.), as expected due to reports that this mutation does not have a marked effect on GCase function (Malini et al., 2014, Alcalay et al., 2015, Grace et al., 1999). Interestingly, although E326K exhibited a similar decline in activity to wild-type at pH 7.4, in acidic conditions there was some destabilisation (Figure. 30C. and 30D.). It is difficult to corroborate these findings as no structural analysis of E326K has been performed previously.

Unexpectedly, stability of L444P protein was similar to wild-type. As L444P generally causes a severe disease (Sidransky and Lopez, 2012), and is associated with significant ER retention and ERAD (Bendikov-Bar et al., 2011), it was expected that this protein would be the least stable. Other studies also report

that this mutation results in an unstable enzyme (Grace et al., 1994). Our findings suggest that this variant is able to retain its stability in both acidic and neutral conditions, with Tm similar to wild-type (Figure 30A. and 30B.). Furthermore, L444P was thermostable under both conditions for 60 minutes (Figure. 30C. and 30D.), and this is supported by another study where stability was measured using L444P fibroblast lysates (Sawkar et al., 2006).

The N370S protein was found to have a higher Tm than wild-type in both acidic and neutral conditions (Figure. 30A. and 30B.), retained stability when incubated at acidic pH and exhibited a slower time-dependant decline in activity at neutral pH (Figure. 30C. and 30D.). This is not supported by previous findings suggesting that the N370S variant is less stable at neutral pH compared to wild-type, with a 4.2°C reduction in melting temperature and significant destabilisation when incubated at the same temperature in neutral conditions (Sawkar et al., 2006). Our data is, however, supported by analysis of the X-ray structure and molecular dynamic simulations of N370S, which revealed that the structure of this variant is virtually indistinguishable to wild-type GCase, aside from increased rigidity in loop 3 off (Offman et al., 2011). These studies also report an increase in thermostability, with another reporting a shift in pH optima towards a more neutral pH (Steet et al., 2006). This may explain why N370S had a slower time-dependant decline in activity compared to wild-type at neutral pH.

A prospective study would be to analyse the effect of the E326K, L444P and N370S mutations on the pH optima of our recombinant GCase protein. Previous analysis of the pH profile of wild-type GCase reveals the optimal pH for the enzyme is approximately pH 5.1 (Karataş et al., 2020, Pentchev et al., 1973), however other studies suggest there is peak activity across a range of pH

conditions between 4.7 – 5.9 (Lieberman et al., 2007, Liou et al., 2006, Tan et al., 2014).

Minimal changes to functional stability may have been demonstrated in this study because the mutants were already highly unstable, and as these techniques are not specific and sensitive to assess structural stability, further destabilisation was not seen through functional assays. Investigating the effect of small molecular chaperones or inhibitors on GCase mutant thermal denaturing may shed more light on the functional stability of our recombinant proteins. Chemical chaperones can bind to proteins, stabilising the native fold of the protein in the ER, shifting folding equilibrium away from the misfolded state (Bernier et al., 2004, Ulloa-Aguirre et al., 2004). Isofagomine and other GCase inhibitors have been shown to increase the thermal stability of wild-type GCase at acidic and neutral pH (Ben Bdira et al., 2017, Sawkar et al., 2006, Lieberman et al., 2007) and mutant N370S in neutral conditions (Sawkar et al., 2006). This may lead to more N370S being correctly folded and exiting the ER to perform its catalysis at the lysosome. It would be interesting to assess whether such chaperones had a more significant effect on E326K, L444P or N370S mutants compared to wild-type.

4.4.4 Impact mutations on proteolytic stability of recombinant *GBA1* protein

Another way crude recombinant protein was used to indirectly analyse structural stability and protein unfolding was to analyse each mutant's ability to resist proteolytic digestion. Proteolytic digestion of a protein is dependent on the stability of the protein and found to increase with an increase in stability, suggesting that protein structures that are partially or completely unfolded are more susceptible to proteolytic digestion (Ahmad et al., 2012).

A proteolysis reaction was performed using trypsin (Figure. 31.) in acidic pH, as done previously with pure recombinant wild-type GCase protein (Ben Bdira et al., 2017). Compared to wild-type GCase protein, all mutant proteins were more sensitive to trypsin digestion within the first 30 minutes. After 120 minutes, E326K, L444P and N370S proteins were digested to a similar level. This doesn't support our functional analysis studies that demonstrate that E326K and L444P proteins have similar stability to wild-type in acidic conditions (Figure. 30.). Furthermore, as the N370S protein exhibited a higher Tm in acidic conditions and was thermostable for an hour incubation, it was expected that this mutant would resist digestion. However, proteolytic digestions studies are not examining functional stability so may be a more accurate method of analysing mutation-induced misfolding of a protein. Further studies should include performing proteolysis reactions in neutral pH, to compare the stability of the variants in different conditions. From the findings in this study, it is expected that the N370S variant would be more stable in a neutral environment however it is important to note that time allowed for only two technical repeats so firm conclusions cannot be drawn.

Although crude protein does not allow accurate analysis of protein unfolding through techniques such as circular dichroism, differential scanning chromatography or NMR spectroscopy, future studies may involve incubating the proteins with denaturing agents to assess stability in a similar way to proteolytic digestion, or through functional analysis of activity. This has been done previously for other proteins (Kleppe et al., 1999, Senthilkumar and Sharma, 2002). Pulse-chase analysis is another technique to measure protein degradation which involves labelling proteins for a short time (Simon and Kornitzer, 2014). This technique has previously demonstrated that N370S and L444P mutants have a

shorter half-life compared to wild-type in HeLa cells (Lu et al., 2011). It would be interesting to compare these two mutations to E326K.

4.4.5 Prospective studies with pure GCase protein

The original aim of this chapter was to investigate the effect of *GBA1* mutations on the structural stability of pure recombinant GCase protein. I initially planned to first determine the glycosylation patterns of each GCase variant using mass spectrometry. This has been done previously, using commercially-available GCase protein as a reference (Tekoah et al., 2013). *N*-linked glycosylation is thought to be a key factor for enzyme functionality (Tekoah et al., 2013, Grace and Grabowski, 1990, Bergmann and Grabowski, 1989). It has also been reported that the unglycosylated GCase protein has a more disordered X-ray structure around the active site (Liou et al., 2006). Molecular dynamic simulations also revealed that the presence of Asn 19 glycosylation stabilises regions around the L444P mutation site, whilst simultaneously improving stability of the active site in wild-type GCase (Pol-Fachin et al., 2016). Mass spectrometry may reveal the post-translational modifications behind the functional stability results in this study. The same molecular dynamics study also revealed the importance of occupancy of other glycosylation sites for structural stability. Investigating the *N*-linked glycosylation patterns in E326K, L444P and N370S mutations may shed more light on why these mutations occur or why the proteins lack stability, which leads to downstream mechanisms in the cell and cytotoxicity.

As mentioned above, obtaining pure recombinant protein would also allow for accurate and sensitive analysis of the effect of *GBA1* mutations on folding dynamics and structural stability through methods including circular dichroism and differential scanning colometry (Ben Bdira et al., 2017, Lieberman et al.,

2009). This would add further understanding to how individual mutations affect the secondary structure.

Another avenue I would have liked to have explored would be to assess the effect of the mutations on the direct interaction between recombinant GCase protein and recombinant alpha-synuclein protein. The molecular interaction between the two is yet to be fully elucidated, but it is proposed to occur in acidic conditions at the lipid membrane, with residues between domains II and III of GCase protein interacting with the c-terminal of alpha-synuclein (Yap et al., 2013b, Yap et al., 2015, Yap et al., 2011). This interaction is thought to be inhibitory (Yap et al., 2013b), so it would be interesting to analyse whether the degree of inhibition is altered across mutations. Analysis of the effect of the E326K, L444P and N370S mutations on this interaction may shed invaluable light on why different mutations are associated with different downstream alpha-synuclein pathologies. I expect E326K may influence protein interactions of GCase, potentially alpha-synuclein, as this mutation occurs on the protein surface (Malini et al., 2014). A 2011 study revealed that the N370S variant has reduced affinity for alpha-synuclein (Yap et al., 2011), further supporting our hypothesis that *GBA1* mutations influence this interaction.

4.5 Conclusion

In this chapter I have demonstrated the successful over-expression of recombinant wild-type, E326K, L444P and N370S GCase protein, containing a 6xHis-tag, in HEK293 cells. size-exclusion chromatography followed by affinity chromatography with Ni-NTA agarose was performed. Unfortunately, this did not yield ≥95% pure GCase protein, as previously described (Gramlich et al., 2016), and therefore I proceeded to analyse the thermostability, pH stability and resistance to proteolytic digestion of crude recombinant GCase protein. These

findings suggest that wild-type recombinant GCase protein is more thermostable in acidic conditions than neutral conditions; the Tm and thermal denaturing was supported by previous studies (Ben Bdira et al., 2017, Abian et al., 2011). E326K and L444P exhibited similar thermostability to wild-type, with both mutations being more sensitive to proteolytic digestion, suggesting they may be slightly less stable than wild-type. Our L444P data was unexpected, as our results suggests this mutation markedly reduces GCase function (Chapter. 3.), however our stability data are corroborated by a previous L444P fibroblast study (Sawkar et al., 2006). The N370S variant has previously been found to be structurally indistinguishable from native GCase protein (Offman et al., 2011), and thus minimal changes in functional stability were expected. In this study it was found that N370S was more thermostable than wild-type in both acidic and neutral conditions, however it was more sensitive to proteolytic digestion.

It is likely that our indirect measurements of functional and structural stability in crude protein lack sensitivity and accuracy for detecting folding dynamics, and thus as the mutants were already unstable further decreases were not detected. Analysis of the effect of *GBA1* mutations on pure recombinant protein folding dynamics via circular dichroism and mass spectrometry analysis of *N*-linked glycosylation patterns may shed light on how different mutations affect the secondary structure of GCase to understand why different mutations activate different pathological mechanisms in the cell. Furthermore, understanding how these mutations affect the direct interaction of recombinant GCase and alpha-synuclein would further our understanding of mutation-specific alpha-synuclein pathology.

5 The influence of *GBA1* mutations on alpha-synuclein

5.1 Introduction

A major hallmark of PD is the loss of dopaminergic neurons in the SNpc, accompanied by an accumulation of alpha-synuclein in Lewy bodies in neurons and neurites (Balestrino and Schapira, 2018). This alpha-synuclein pathology is also evident in *GBA1*-PD brains (Nishioka et al., 2011, Parkkinen et al., 2011). Alpha-synuclein has long been identified to exist physiologically in a dynamic equilibrium between a natively unfolded monomer and an alpha-helical membrane-bound monomer (Davidson et al., 1998). Under pathological conditions, these monomers readily assemble into toxic HMW insoluble oligomers, which adopt a distinctive anti-parallel β-sheet structure (Celej et al., 2012).

It has also been proposed that under physiological conditions, alpha-synuclein exists not only as monomers, but occurs largely as a alpha-helically folded tetrameric and multimeric species (Bartels et al., 2011). Compared to monomers, these physiological, soluble HMW species have a greater affinity for lipid binding. In addition, unlike monomeric alpha-synuclein species which readily aggregated into amyloid-like fibrils *in vitro*, native HMW alpha-synuclein species underwent little to no aggregation. It has therefore been proposed that under pathogenic conditions, there may be a shift in the ratio between physiological monomers and tetramers/multimers toward monomers, due to the destabilisation of native HMW species, preceding alpha-synuclein misfolding and aggregation in cells.

The most widely accepted hypothesis regarding the formation of Lewy bodies is that alpha-synuclein first accumulates in the neuron, where it can aggregate and assemble into abnormal oligomers, possibly through the uptake of extracellular

alpha-synuclein aggregates, which are then transformed into β-sheet rich amyloid fibrils (Lashuel et al., 2013, Spillantini et al., 1998). Accumulated and aberrant alpha-synuclein can be degraded by the ALP (Martinez-Vicente and Cuervo, 2007), released into the extracellular space (Reyes et al., 2015), or be deposited in to inclusions such as Lewy bodies (Spillantini et al., 1997).

To model alpha-synuclein pathology and nigral degeneration it is common to use exogenously applied alpha-synuclein PFFs. The administration of such fibrils has provided a new platform to study the pathogenic cascade associated with the accumulation and aggregation of alpha-synuclein. The alpha-synuclein PFF model has been shown to successfully recapitulate many features of PD including alpha-synuclein inclusion formation and widespread Lewy body-like pathology; neuroinflammation and degeneration of specific neuronal populations (Chung et al., 2019, Duffy et al., 2018).

Intrastriatal injections of alpha-synuclein PFF in mice brains leads to the formation of alpha-synuclein pathology and dopamine neuron loss (Izco et al., 2019, Luk et al., 2012). It has been reported that alpha-synuclein PFFs induce neuronal cell death by inducing the formation of intraneuronal aggregations that compromise synaptic activity, decrease synaptic formation and disrupt dendritic spine dynamics (Wu et al., 2019). The degree of synaptic dysfunction correlated with the alpha-synuclein pathology, suggesting that alpha-synuclein inclusions act as a pathogenic trigger. Alpha-synuclein PFFs are internalised into neurons in culture, and lead to the recruitment of endogenous alpha-synuclein into insoluble aggregates (Grassi et al., 2018, Mahul-Mellier et al., 2020, Mahul-Mellier et al., 2015, Luk et al., 2009). In one study this was accompanied by mitochondrial damage including membrane depolarisation, fragmentation and

cytochrome C release (Grassi et al., 2018), with another demonstrating activation of the intrinsic and extrinsic apoptotic pathway (Mahul-Mellier et al., 2015).

Recently in our lab, it was shown that alpha-synuclein PFFs, but not monomeric alpha-synuclein species, inhibited lysosomal GCase activity and induced the UPR, suggestive of impaired lysosomal trafficking, in mouse cortical neurons and differentiated SH-SY5Y cells. The same study also demonstrated that administration of alpha-synuclein PFFs promoted the spread of alpha-synuclein pathology (Gegg et al., 2020). PFF-induced spread of Lewy body-like pathology has also been demonstrated in a transgenic model of PD (Desplats et al., 2009).

The inflammatory response has also been implicated in the pathology of alpha-synuclein PFFs. When taken up by microglia and astrocytes, alpha-synuclein PFFs can trigger this response which can further affect neuronal protein aggregation and cell viability (Lee et al., 2014).

There are several hypotheses proposed to explain the link between *GBA1* mutations and alpha-synuclein pathology and neurotoxicity. Both loss of function and gain of function mechanisms have been proposed (Clark et al., 2007, Nichols et al., 2009). One hypothesis involves lysosomal dysfunction induced by a loss of GCase activity. This has been associated with increased alpha-synuclein accumulation in mutant models (Osellame and Duchen, 2013), with insoluble β-sheet rich alpha-synuclein aggregates and Lewy body inclusions present (Jo et al., 2021). Furthermore, analysis of post-mortem brain tissue from *GBA1*-PD patients revealed reduced GCase activity correlated with alpha-synuclein accumulation (Bae et al., 2015, Murphy et al., 2014). A bidirectional feedback loop has also been suggested to occur between GCase and alpha-synuclein, as *GBA1* mutation-induced lysosomal dysfunction can lead to the accumulation of

alpha-synuclein, which may impede the transport of newly synthesised GCase protein from the ER to the lysosome; further exacerbating lysosomal dysfunction and impaired degradation of alpha-synuclein (Mazzulli et al., 2011). Mutations in the *GBA1* gene may also lead to the accumulation of misfolded, mutant GCase protein in the ER which can initiate ER stress and the UPR (Fernandes et al., 2016, Maor et al., 2013, Ron and Horowitz, 2005). There has also been an association demonstrated between ER stress and alpha-synuclein, with its accumulation able to elicit an ER stress response in alpha-synuclein over-expressing neurons and in animal models of PD (Heman-Ackah et al., 2017, Cooper et al., 2006). Furthermore, in N370S iPSC-derived dopaminergic neurons, mutant protein induced ER stress and dysfunction which led to elevated extracellular alpha-synuclein release (Fernandes et al., 2016).

If alpha-synuclein is not properly degraded or deposited into Lewy bodies, the neuron may secrete alpha-synuclein via an exosome-mediated pathway (Emmanouilidou et al., 2010). It has been proposed that the secretion of alpha-synuclein is dependent on the efficacy of protein degradation systems and proper mitochondrial function, and it may act as a protective pathway to reduce the intracellular alpha-synuclein burden (Fussi et al., 2018, Lee et al., 2005). This secretion has been demonstrated in models of *GBA1*-PD, with fibroblasts harbouring L444P and N370S mutations exhibiting increased alpha-synuclein release (Cerri et al., 2021, Fernandes et al., 2016). Evidence suggests that pathogenic alpha-synuclein may act as a toxic template when it is taken up by neighbouring cells to propagate pathology (Brundin et al., 2008). Models using PFFs also demonstrate that these fibrils can accelerate alpha-synuclein pathology, inducing endogenous alpha-synuclein to take on a more toxic form (Gegg et al., 2020).

The final hypothesis to be discussed in this chapter involves alterations in lipid metabolism. Mutations in *GBA1* can lead to the accumulation of GSLs (Sardi et al., 2011, Taguchi et al., 2017), altering lipid membrane fluidity and composition (Fabelo et al., 2011, Varela et al., 2016). This may affect the binding of alpha-synuclein, propagating pathology (Bendor et al., 2013). Alterations in lipid metabolism have been demonstrated in several models of *GBA1*-PD, including models of L444P mutations (Galvagnion et al., 2020). It has also been suggested that changes in lipid metabolism may induce a shift in equilibrium from physiological HMW alpha-synuclein species to toxic aggregate-prone monomeric species (Fanning et al., 2019, Kim et al., 2018b). In an effort to overcome lipid overload, cells initially induce a pathway to store excess lipids in lipid droplets, which are spherical organelles that store intracellular lipids including TAGs and cholesteryl esters (Farmer et al., 2020). Alpha-synuclein has been demonstrated to bind to the lipid monolayer of lipid droplets, which may act as a site to enhance oligomerisation of alpha-synuclein (Cole et al., 2002). Furthermore, in human neural crest cells and yeast cells, an increase in the number of lipid droplets has been shown to correlate with an increase in alpha-synuclein accumulation (Fanning et al., 2019, Outeiro and Lindquist, 2003).

The aim of this chapter was to characterise alpha-synuclein pathology induced by different *GBA1* variants. I hoped that this knowledge would improve the understanding as to why different *GBA1* mutations are associated with different ages of onset, disease severity and progression and different odds ratios. To model *GBA1*-PD E326K, L444P and N370S GCase protein was over-expressed in undifferentiated and differentiated SH-SY5Y cells, which express detectable levels of endogenous alpha-synuclein. As previous research suggests the *GBA1*-PD pathogenesis is distinct from that of GD, understanding the mechanisms

involved in the E326K mutation may be invaluable to PD research. These studies shed light on the different pathogenic mechanisms occurring in carriers of different mutations and leading to alpha-synuclein toxicity.

5.2 Materials and Methods

5.2.1 Chemicals and reagents

Unless otherwise stated, all chemicals and reagents were purchased from ThermoFisher, Merck Millipore or Abcam.

5.2.2 Antibodies

Table 15. Antibodies used in Chapter 5.

Antibody Name	Immunogen and epitope	Species	Western Blot or Dot Blot Dilution	Immunofluorescence Dilution
Anti-GBA clone 2e2, AP1140 (Millipore)	Recombinant human GBA protein, AA 146-236 (outside of mutation sites)	Mouse, mAb	1/1000	n/a
Anti-GRP78 BiP, ab21685 (Abcam)	Mouse GRP78 BiP, epitope AA 600 to the C-terminus	Rabbit, pAb	1/1000	n/a
MJFR1, ab138501 (Abcam)	Recombinant full-length human alpha-synuclein, epitope AA 118-123	Rabbit, mAb	1/1000	n/a
LAMP-1/CD107a, NB120-19294 (Novus)	Synthetic peptide corresponding to AA 407-416 of human LAMP1	Rabbit, mAb	1/1000	n/a
Recombinant Anti-ALIX [EPR23653-32], ab275377 (Abcam)	Recombinant ALIX fragment	Rabbit, mAb	1/1000	n/a
Anti-Flotillin 1 antibody, ab41927 (Abcam)	Synthetic peptide corresponding to Human Flotillin 1, AA 1-100	Rabbit, pAb	1/1000	n/a
Beta III Tubulin (TU-2) ab7751 (Abcam)	Class III beta-tubulin specific for neurons epitope AA 441-448	Mouse, mAb	1/4000	1/500
PSD95 (D27E11) XP (Cell Signaling)	Human PSD95	Rabbit, mAb	1/1000	n/a
Recombinant Anti-Alpha-synuclein aggregate antibody [MJFR-14-6-4-2] – Conformation-Specific ab209538 (Abcam)	Recombinant full length alpha-synuclein aggregate	Rabbit, mAb	1/1000	n/a

Tyrosine Hydroxylase ab112 (Abcam)	Full length SDS denatured tyrosine hydroxylase	Rabbit, pAb	n/a	1/100
Beta-actin, ab8227 (Abcam)	Human beta-actin, epitope AA 1-100	Rabbit, pAb	1/4000-1/500	n/a
Anti-Rabbit HRP (Dako)	n/a	n/a	1/3000	n/a
Anti-Mouse HRP (Dako)	n/a	n/a	1/3000	n/a
Anti-Mouse Alex-Fluor 488 (Invitrogen)	n/a	n/a	n/a	1/300 – 1/500
Anti-Rabbit Alex-Fluor 568 (Invitrogen)	n/a	n/a	n/a	1/300 – 1/500

5.2.3 SH-SY5Y cell culture

Culturing of SH-SY5Y cells was carried out as described in Chapter 2.8. A list of SH-SY5Y lines generated in this study can be found in Table. 7.

5.2.4 SH-SY5Y stable transfection

SH-SY5Y cells were stably transfected to express wild-type, E326K, L444P and N370S *GBA1* as described in Chapter 2.10. A green fluorescent protein (GFP) over-expressing SH-SY5Y neuroblastoma cell line was employed as a protein over-expression control with a similar molecular weight as GCase.

5.2.5 Differentiation of SH-SY5Y in to dopaminergic neurons

SH-SY5Y cells were differentiated in to dopaminergic neurons as described in Chapter 2.12.

5.2.6 Induced pluripotent stem cell derived midbrain dopamine neurons

Generation of midbrain dopamine neurons from iPSC was performed as described in Chapter 2.13. A list of midbrain dopamine neurons generated in this study can be found in Table. 9.

5.2.7 Synthesis of alpha-synuclein pre-formed fibrils

Alpha-synuclein PFFs were synthesised by Dr Guglielmo Verona. Briefly, recombinant wild-type alpha-synuclein was expressed in bacteria and purified with ion exchange chromatography. It was dissolved in sterile PBS and filter

sterilised with a 0.22 µm filter, and concentration adjusted to 2 mg/ml. Recombinant alpha-synuclein was incubated for 1 week at 37°C under agitation at 250 RPM. Fibrils were isolated by centrifugation at 10,600 x *g* for 15 minutes and quantified by the amount of monomer left in the supernatant. The pellet was resuspended in sterile PBS at a concentration of 1 mg/ml and amyloid fibrils were confirmed by Congo red staining. These were confirmed to have fibril structure with EM and to induce alpha-synuclein aggregation in primary cortical neurons (Gegg et al., 2020). The same source of PFFs have been shown previously to successfully induce alpha-synuclein pathology in mice 90 days after injection in to the dorsal striatum, with no endotoxin-associated toxicity forming (Izco et al., 2019).

5.2.8 Treatment of cells with alpha-synuclein

Cells were treated with 1 µg/µL alpha-synuclein PFFs on day 3 or 4 *in vitro.* PFFs were sonicated for 5 seconds prior to dilution in culture media to give fibrils of uniform size. Cells were incubated in culture media containing PFFs for 72 hours. Fresh culture media without PFFs was added and changed as necessary. For CBE treatment, 10 µM CBE was added at the same time as PFF treatment and was also present in subsequent media changes. Cells were harvested with trypsin 10 days after addition off PFFs. Culture media was removed and collected from SH-SY5Y cells, centrifuged at 1000 RPM for 5 minutes to remove floating cells and stored at 80°C, as described in Chapter 2.8 and 2.12.

5.2.9 Western blotting

For analysis of proteins in SH-SY5Y cells and midbrain dopamine neurons, cell lysates were generated as described in Chapter 2.14. Western blotting was performed as described in Chapter 2.15, using the NuPAGE™ instruments. For immunoblotting of alpha-synuclein, the membrane was fixed prior to blocking for

1 hour with 10% milk diluted in PBS. For fixing, the membrane was incubated in 0.4% PFA for 30 minutes, followed by three 5 minute washes with 0.4% PBS-T. Antibodies used for western blot analysis in this chapter can be found in Table. 15.

5.2.10 mRNA analysis

Analysis of mRNA levels of *GBA1, SNCA, TH, CHOP* and *GAPDH* was performed as described in Chapter 2.17. A list of primers used in Table. 10.

5.2.11 GCase activity assay

Cell lysates for GCase activity analysis were generated as described in Chapter 2.14. *In vitro* GCase protein activity assay was performed at pH 5.4 with NaT as described in Chapter 2.20.

5.2.12 Lysosomal hydrolase activity assay (β-galactosidase and β-hexosaminidase activity assay)

Cell lysates for analysis of β-Galactosidase and β-Hexosaminidase activity analysis were generated as described in Chapter 2.14. *In vitro* β-Galactosidase and β-Hexosaminidase enzyme activity assay was performed at pH 4.1 as described in Chapter 2.21.

5.2.13 Alpha-synuclein enzyme-linked immunosorbent assay (ELISA)

To investigate the effect of *GBA1* mutations on monomeric alpha-synuclein secretion, we performed an alpha-synuclein ELISA using the Novus Biologicals human alpha-synuclein ELISA kit (colorimetric) (NBP2-62748). This kit uses the sandwich-ELISA methodology. The principle of a sandwich-ELISA is to quantify antigens, in this case alpha-synuclein, between two layers of antibody. The ELISA was performed as per the manufacturer's instructions. Culture media was collected from undifferentiated and differentiated SH-SY5Y cells, centrifuged at

1000 RPM for 5 minutes to remove floating cells and stored at 80°C, as described in Chapter 2.8 and 2.12. 100 µL culture media was added, alongside standard working solution, to the ELISA microplate coated with an antibody specific to alpha-synuclein and incubated at 37°C for 90 minutes. Sample was removed and 100 µL of biotinylated detection antibody was added and the plate incubated at 37°C for 1 hour. Following aspiration and washes, to remove free components, 100 µL of Advin HRP conjugate was added to each well and incubated at 37°C for 30 minutes. Sample was again aspirated and wells washed three times. Next, 90 µL of Substrate Reagent was added to each well and those that contain human alpha-synuclein, biotinylated detection antibody and Advin HRP conjugate will appear blue in colour. Following a 15 minute incubation period at 37°C, 50 µL of Stop Solution was added to each well, causing a colour change from blue to yellow. The optical density (OD) was then measured with spectrophotometry at a wavelength of 450 nm. The OD value is proportional to the concentration of human alpha-synuclein in each well, and the concentration of human alpha-synuclein in each sample was calculated by comparing the OD of the samples with the standard curve. The data were normalised to the cellular protein content of the well from which the conditioned media was taken from, calculated by a BCA assay (Chapter 2.14.4).

5.2.14 Immunofluorescence microscopy

To confirm the differentiation of SH-SY5Y cells into mature dopamine neurons, cells were stained for neuron-specific microtubule protein, β-Tubulin III, and the dopaminergic neuron marker, Tyrosine Hydroxylase (TH). SH-SY5Y cells were differentiated for 10 days (as described in Chapter 2.12) on coverslips and incubated at 37°C at 5% CO_2. Immunofluorescence was performed as described in Chapter 2.19. Cells were stained with either anti-β-Tubulin III antibody (Abcam)

or anti-TH antibody (Abcam) and nuclei stained with DAPI. More information on the antibodies can be found in Table. 15. Coverslips were analysed by fluorescence microscopy as described in Chapter 2.18.

For quantification of neurite length of differentiated SH-SY5Y cells, the NeuronJ plugin was used with the Fiji package for ImageJ, as described previously (Pemberton et al., 2018). Cells were counted using the cell counter plugin and total neurite length/total number of cells calculated.

5.2.15 Analysis of insoluble fraction of alpha-synuclein protein

To analyse the levels of insoluble alpha-synuclein in cells, dry cell pellets of SH-SY5Y were obtained, as described in Chapter 2.15.1, and lysed in 250 µL Triton X 100 buffer mix consisting of 225 µL Triton X 100 buffer (50 mM Tris, pH 7.5; 750 mM NaCl; 5 mM EDTA and 1% v/v TX-100); 25 µL RQ1 RNase-free DNase buffer (Promega); 5 units RQ1 RNase-free DNase and 1X protease and phosphatase inhibitor mix (Halt). Samples were lysed on ice for 5 minutes, followed by 10 minutes at room temperature, with vortexing every 5 minutes. The lysate was then passed through a 23G needle and centrifuged at 17,000 x *g* for 30 minutes at 4°C. The supernatant was transferred to a fresh polypropylene tube, labelled as soluble fraction and stored at -20°C. To obtain the insoluble fraction of alpha-synuclein, the pellets were resuspended in 25 µL 2% (w/v) SDS-8M urea buffer (21.5 µL SDS-urea; 2.5 µL RQ1 RNase-free DNase buffer and 1 µL RQ1 RNase-free DNase) and incubated for 15 minutes at room temperature. Tubes were centrifuged at 17,000 x *g* for 30 minutes at 4°C and stored at -20°C.

Protein concentrations of soluble fractions were determined using a BCA assay, as described in Chapter 2.14.4. As 8M urea is not compatible with protein quantification assays, protein concentrations for insoluble fractions were

estimated by normalising against the protein concentration of the soluble fractions. A western blot was ran using 10 – 30 µg protein, as described in Chapter 2.15 using antibodies listed in Table. 15.

5.2.16 Analysis of alpha-synuclein tetramer and multimer species

To investigate the ratio of monomeric and tetrameric/multimeric alpha-synuclein species, we performed a cross-linking reaction on SH-SY5Y cell lysate, as described previously (Dettmer et al., 2013) . Dry cell pellets of SH-SY5Y were obtained as described in Chapter 2.14.1. 1 mM Di(N-succinimidyl) glutarate (DSG) was made up in DMSO. Cell pellets were resuspended in PBS and supplemented with 1x protease and phosphatase inhibitors (Halt). Intact cell cross-linking occurred by adding 1 mM DSG to each tube and incubating at 37°C for 30 minutes while rotating. The reaction was quenched by adding 50 mM (final concentration) Tris-HCL, pH 7.4 and incubating for 5 minutes at room temperature. Cells were lysed by adding 1% (v/v) Triton X 100 to each sample. Samples were incubated on ice for 20 minutes and sonicated for 15 seconds in a water sonnicator. Following this, cells were centrifuged at 17,000 x *g* for 30 minutes at 4°C, and supernatant transferred to fresh 1.5 mL polypropylene tubes. Protein concentration was determined using a BCA assay, as described in Chapter 2.14.4, and a western blot was ran using 100 µg protein, as described in Chapter 2.15, to analyse alpha-synuclein tetramers and multimers using antibodies listed in Table. 15.

5.2.17 Dot blotting

To analyse the levels of exosomes secreted by undifferentiated and differentiated SH-SY5Y cells, we performed a dot blot to measure the levels of two endogenous exosome marker proteins, ALIX and Flotillin in culture media. A dot blot was also performed to measure alpha-synuclein fibrils secreted by iPSC-derived human

midbrain dopamine neurons. Culture media was collected from cells, centrifuged at 1000 RPM for 5 minutes to remove floating cells and stored at 80°C, as described in Chapter 2.8 and 2.12. Samples were loaded at 200 µL in either duplicates or triplicates. Dot blotting was performed as described in Chapter 2.17., and membranes probed with either anti-ALIX or anti-Flotillin antibodies (Abcam) for exosome analysis, or with anti-alpha-synuclein aggregate antibody (Abcam).

5.2.18 Thioflavin T fluorescence assay

To analyse the characteristics of alpha-synuclein aggregation in SH-SY5Y cell lines, we measured the formation of aggregates by using fluorescence spectroscopy with thioflavin T (ThT) dye. ThT is a specific dye commonly used to monitor *in vitro* amyloid fibril formation. Upon binding to amyloid fibrils, ThT exerts a fluorescence signal at 482 nm (Naiki et al., 1989). We first measured alpha-synuclein aggregation occurring with increasing concentrations of recombinant human alpha-synuclein monomers incubated with 0.18 µM PFF. Next, we analysed aggregation in SH-SY5Y samples at two different volumes: 10 µL (approximately 90 µg) and 50 µL (approximately 450 µg). Cells were either untreated or treated with 1 µg/µL alpha-synuclein PFF and 10 µM CBE, as described in Chapter 5.2.8. Cells were lysed via nitrogen bomb, the principle of which is to lyse cells using nitrogen, without the need for a detergent. Briefly, large quantities of nitrogen are dissolved in the cell under high pressure within a pressure vessel. When the pressure is released suddenly, nitrogen comes out of the solution as expanding bubbles that stretch the membrane of the cells causing them to rupture and release the contents of the cell. This method was chosen to eliminate any potential interactions between detergents and ThT.

Stock solutions of 1 mM ThT in dH2O and 10% (w/v) sodium azide in dH2O were made. The reaction was set up in a 96 well plate, with each sample in triplicate. For analysis of aggregation in alpha-synuclein monomers, each well contained: 20 µM ThT; 0.05% sodium azide; 0.18 µM PFF; appropriate volume of alpha-synuclein monomers and was made up to a final volume of 120 µL with SEC buffer (20 mM K_2HPO_4; 5 mM KH_2PO_4; 100 mM KCl).

For analysis of alpha-synuclein aggregation in SH-SY5Y cells, each well contained: 20 µM ThT; 0.05% sodium azide; 0.18 µM PFF; either 10 µL or 50 µL of cell lysate and was made up to a final volume of 120 µL with SEC buffer (20 mM K_2HPO_4; 5 mM KH_2PO_4; 100 mM KCl). The plate was sealed and incubated for 50 hours at 37°C, shaking at 300 rpm. Fluorescence intensity was monitored at regular intervals at an excitation wavelength of 450 nm and an excitation wavelength of 482 nm.

5.2.19 Alpha-synuclein Cisbio HTRF® aggregation assay

Alpha-synuclein aggregation was quantified in cells using the Cisbio homogenous time resolved fluorescence (HTRF®) assay (Cisbio #6FASYPEG). The principle of this assay is to detect human alpha-synuclein aggregation using one specific monoclonal antibody, labelled with either Tb-Cryptate (donor) or with d2 (acceptor) dyes. When the dyes are in close proximity, the excitation of the donor with a light source triggers a fluorescence resonance energy transfer (FRET) towards the acceptor, which then fluoresces at a specific wavelength of 665 nm. This allows the measurement of aggregation as the antibody labelled with Tb-Cryptate or d2 dyes will bind to human alpha-synuclein and thus when alpha-synuclein aggregates the two labelled antibodies come into a close proximity generating FRET. The signal intensity is proportional to the number of aggregates formed.

The kit was used following the manufacturers recommendations. Briefly, dry cell pellets were generated (Chapter 2.14.1) and lysed in 25 – 50 µL lysis buffer provided in the Cisbio kit. Samples included in analysis were untreated undifferentiated SH-SY5Y cells; differentiated SH-SY5Y cells (untreated and PFF treated); iPSC-derived dopamine neurons (untreated and PFF treated); SH-SY5Y cells incubated with 25 ng monomeric alpha-synuclein and SH-SY5Y cells incubated with 25 ng PFF. 10 µL of cell samples were loaded into a HTRF® 96-well low volume plate (Cisbio #66PL96100) at dilutions between 1 – 1/1024 and mixed with 10 µL of the FRET donor and acceptor labelled antibodies. The plate was sealed and incubated for 20 hours at 20°C without shaking. After incubation, the fluorescence emission was read at both 665 nm and 620 nm on a HTRF® compatible reader. The amount of aggregated alpha-synuclein was derived from the 665/620 HTRF® fluorescence ratio and normalised to protein concentration in each sample calculated from a BCA assay (Chapter 2.14.4).

5.2.20 Analysis of lipid profiles using high-liquid performance chromatography

Dry cell pellets were generated for undifferentiated SH-SY5Y cells, as described in Chapter 2.14.1, and sent to the Fran Platt Lab, Department of Pharmacology, University of Oxford. Analysis of GSL composition was performed by Dr David Priestman using high-liquid performance chromatography (HPLC).

5.2.21 Staining for lipid droplets

Lipid droplets are organelles involved in intracellular lipid homeostasis, as well as playing key roles in a variety of cellular functions including cellular signalling, metabolic disease and inflammation (Farmer et al., 2020). To investigate the effect of *GBA1* mutations on the accumulation of lipid droplets, cells were grown on coverslips in 6 well plates until 50-80% confluent. Analysis was performed on

SH-SY5Y cells cultured in normal media, as well as SH-SY5Y cells treated for 5 hours with 100 µM oleic acid (OA) following over-night starvation in Opti-MEM. OA is a potent inducer of lipid droplet formation (Nakajima et al., 2019). Cells were treated with 250 µL BODIPY™ 493/503 (4,4-Difluoro-1,3,5,7,8-Pentamethyl-4-Bora-3a,4a-Diaza-*s*-Indacene) diluted in PBS at a final concentration of 1 mg/ml for 15 minutes in the dark at room temperature. BODIPY™ 493/503 is a fatty acid-conjugated fluorescent probe that has been shown to successfully visualise the localisation and dynamics of lipid droplets in cells (Wang et al., 2010). Following incubation, coverslips were washed three times in PBS and mounted onto glass slides with 1 µg/mL DAPI CitiFluor and sealed with nail polish for later analysis by fluorescence microscopy, as described in Chapter 2.18.

5.2.22 Counting lipid droplets

To count lipid droplets, the ImageJ software was used. The local intensity maxima of each lipid droplet was determined and counted in pre-processed images. The image was first converted into a grayscale 8-bit image. To ease localisation and separation of lipid droplets, the background of each image was subtracted. Next, the find maxima tool was utilised to count each lipid droplet in the picture. Noise tolerance was adjusted as appropriate to ensure accurate counting. Cell bodies were counted manually and lipid droplets per 100 cells calculated.

5.3 Results

5.3.1 Undifferentiated SH-SY5Y cells over-expressing mutant GCase protein

5.3.1.1 Characterisation of GCase protein level, expression and activity in undifferentiated SH-SY5Y cell lines expressing GCase mutants

SH-SY5Y stable cell lines expressing wild-type, E326K, L444P and N370S *GBA1* constructs were generated. For each genotype, two clones expressing untagged GCase protein, and one clone expressing a c-terminal 6xHis-tagged GCase protein were generated. To characterise and confirm over-expression of recombinant GCase, the expression levels of the GCase mRNA transcript relative to untransfected SH-SY5Y cell lines were measured (Figure. 33A.). Untransfected cells was set at 1. Compared to untransfected cells, all cell lines had significantly higher levels of GCase mRNA transcript, except N370S-3 cell line which was still increased by 16-fold compared to untransfected cells. Next, the levels of intracellular GCase protein were measured by western blot and quantified, normalising to untransfected cells which was set at 1 (Figure. 33B.). Compared to untransfected cells all stable clones had significantly higher levels of GCase protein level (*$p<0.05$; ***$p<0.001$), including the N370S-3 clone, which did not have significantly higher GCase mRNA levels. As the majority of analysis was carried out the on untagged clones, data from each genotype of untagged clones was pooled and GCase transcript and protein levels compared. There were no obvious changes between genotypes when comparing GCase mRNA levels. Compared to wild-type cells, L444P cells had significantly lower protein level (*$p<0.05$), and N370S cells exhibited a 1.2-fold decrease although this was not significant. There were minimal changes in GCase protein levels between wild-type and E326K cell lines.

To finalise the characterisation of over-expressed GCase protein in the undifferentiated SH-SY5Y cell lines, a GCase activity assay at pH 5.4 was performed. The data was presented relative to untransfected cells, which was set at 1 (Figure. 33C.). All clones exhibited a significant increase in GCase activity compared to untransfected SH-SY5Y cells, except the N370S-3 line which was still increased by 3.1-fold compared to untransfected cells (***$p<0.001$; *$p<0.05$). When mutation groups were compared, it revealed no significant difference between wild-type and E326K clones. GCase activity was significantly reduced in L444P and N370S clones, compared to wild-type (L444P *$p<0.05$; N370S ***$p<0.001$), with N370S clones also exhibiting a significant reduction compared to E326K (*$p<0.05$).

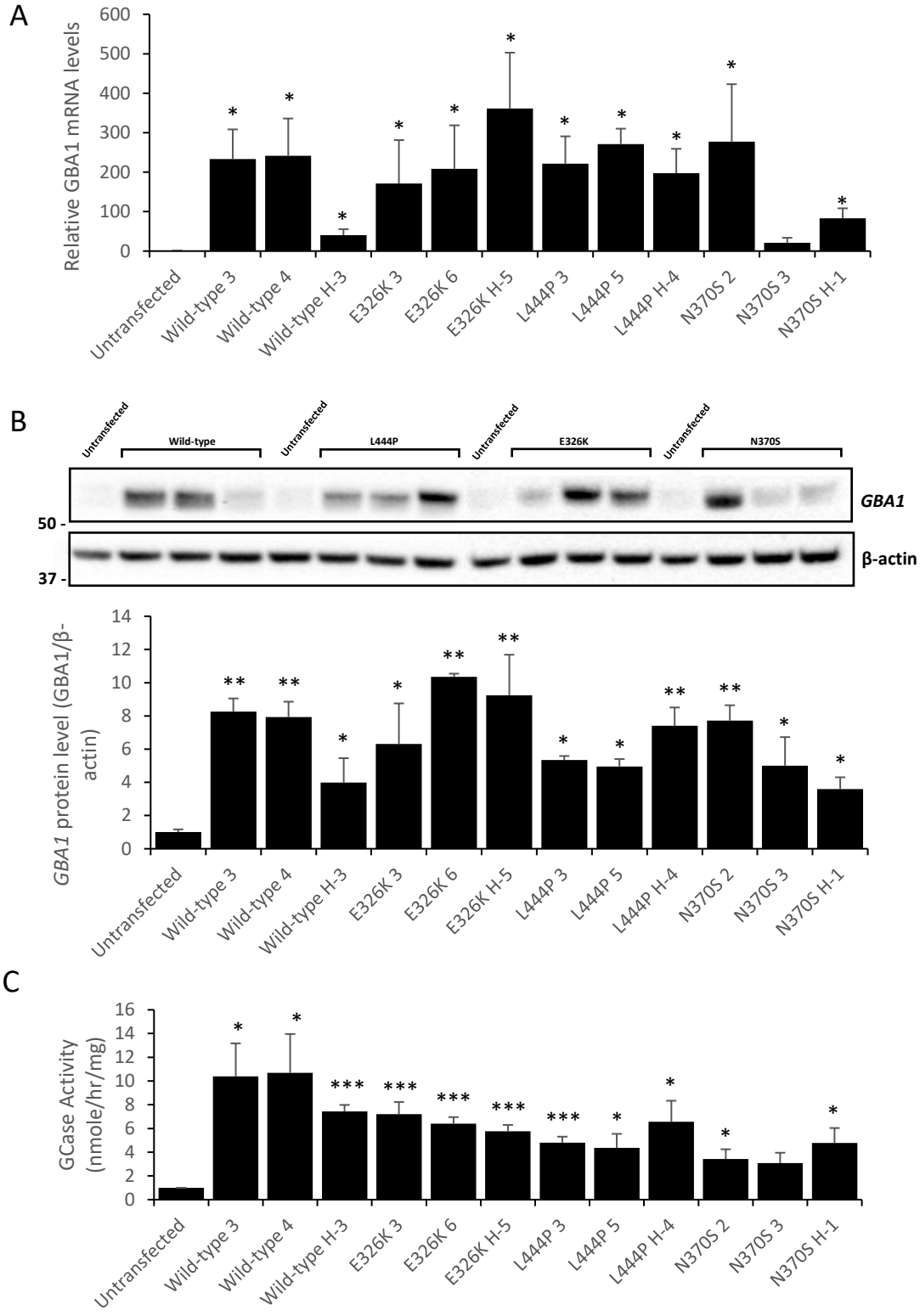

Figure 33. GCase protein, mRNA and activity level in undifferentiated SH-SY5Y cells over-expressing mutant GCase.

A) Quantification of *GBA1* mRNA levels in stable SH-SY5Y cell lines, normalised to untransfected SH-SY5Y cells, which is set at 1. For each cell line, two biological replicates were used and three technical repeats. Graph shows mean and error bars show SEM. Statistical test used was one way ANOVA with Tukey post-hoc analysis

(*p<0.05). **B)** Immunoblot and quantification for *GBA1* protein levels in stable SH-SY5Y cell lines. For each experiment, the band density of untransfected SH-SY5Y cells was quantified and averaged. The band density of each mutant line was quantified and normalised to untransfected SH-SY5Y cells, which was set at 1. Three technical repeats. Graph shows mean and error bars show SEM. Statistical test used was one way ANOVA with Tukey post-hoc analysis (*p<0.05, **p<0.01). **C)** GCase activity in nmole/hr/mg relative to untransfected cells, in stable SH-SY5Y cell lines measured at pH 5.4 with NaT and normalised to untransfected SH-SY5Y cells, which is set at 1. For each cell line, three biological replicates were used and three technical repeats. Graph shows mean and error bars show SEM. Statistical test used was one way ANOVA with Tukey post-hoc analysis (*p<0.05, ***p<0.001).

5.3.1.2 Overall lysosomal content and function unaltered by GCase mutations in undifferentiated SH-SY5Y cells

To assess the effect of the E326K, L444P and N370S *GBA1* mutations on overall lysosomal content and function, the lysosomal machinery of each SH-SY5Y cell line was analysed. First, the activities of the lysosomal hydrolases, β-galactosidase and β-Hexosaminidase were measured. Activities were normalised to untransfected cells, which was set at 1 (Figure. 34A. and 34B.). The effect of *GBA1* mutations on the overall lysosomal content of the SH-SY5Y clones was also investigated by immunoblotting for the endogenous endolysosomal marker LAMP1 (Figure. 34C.). The LAMP1 band density was normalised to that of β-actin and displayed relative to wild-type, which was set at 1. There were only minimal changes in LAMP1 level across the different mutations, as well as the GFP over-expressing control cell line. This data suggests that in SH-SY5Y cells, over-expressing mutant GCase protein does not affect overall lysosomal content.

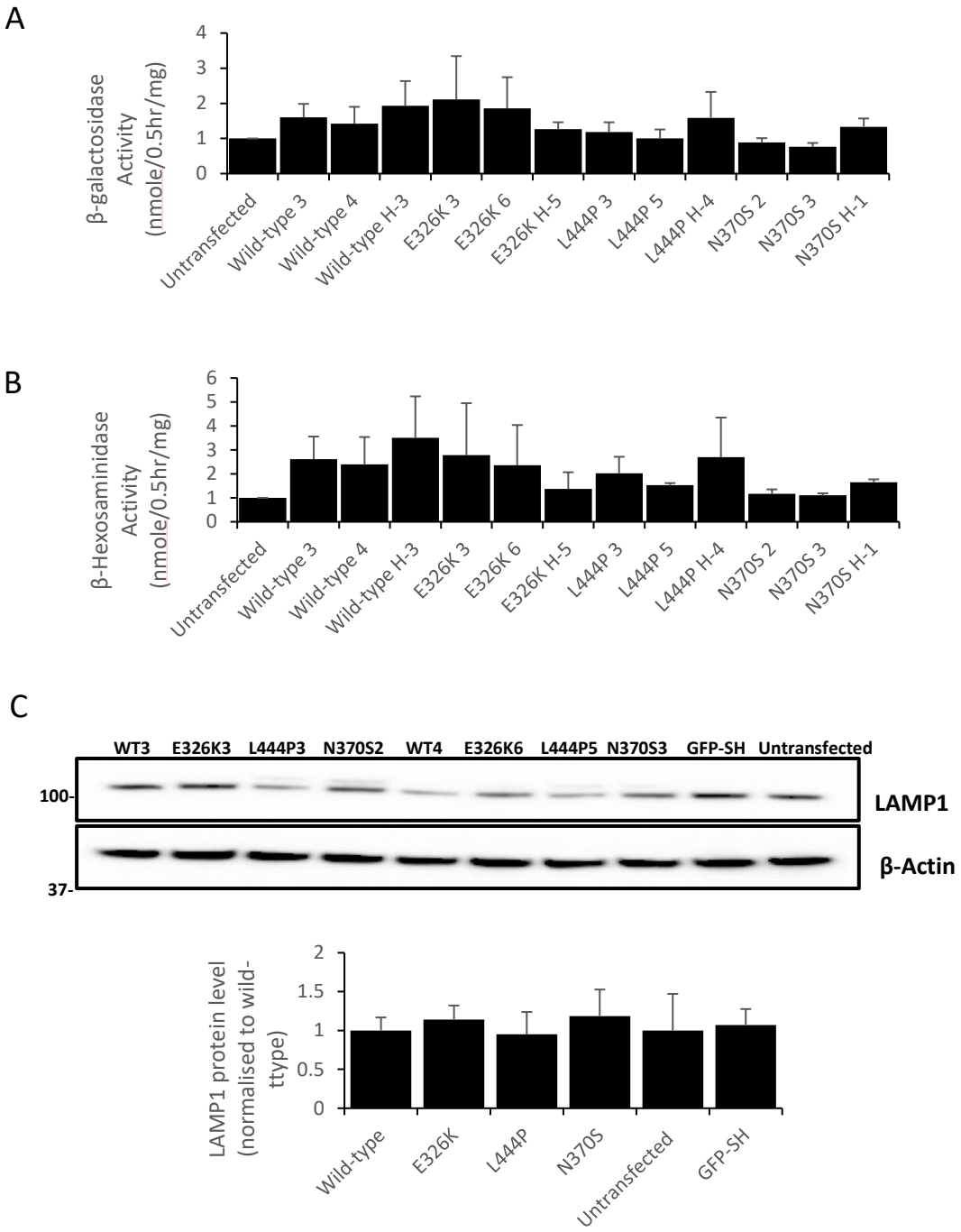

Figure 34. Overall lysosomal content and function in undifferentiated SH-SY5Y cells over-expressing mutant GCase.

The activities of lysosomal hydrolases, β-galactosidase and β-Hexosaminidase were measured at pH 5.1 in SH-SY5Y stable cell lines. For each cell line, three biological replicates were used and four technical repeats. Graph shows mean and error bars show SEM. Statistical test used was one way ANOVA with Tukey post-hoc analysis. **A)** β-galactosidase activity in nmole/0.5hr/mg in undifferentiated SH-SY5Y clones normalised to untransfected SH-SY5Y cells, which was set at 1. **B)** β-Hexosaminidase activity in nmole/0.5hr/mg measured in undifferentiated SH-SY5Y clones normalised to untransfected SH-SY5Y cells, which was set at 1. **C)** LAMP1 levels were measured via

western blot to assess the overall endo-lysosomal content of the SH-SY5Y cell lines. Immunoblot and quantification for LAMP1 protein level in SH-SY5Y stable cell lines. For quantification, band density of each cell line was calculated, pooled and averaged for each genotype. Data normalised to wild-type SH-SY5Y cells band density, which was set at 1. Three technical repeats. Graph shows mean and error bars show SEM. Statistical test used was one way ANOVA with Tukey post-hoc analysis.

5.3.1.3 ER stress is increased in undifferentiated SH-SY5Y cells over-expressing L444P mutant GCase

To characterise the effect of over-expressing mutant GCase in undifferentiated SH-SY5Y cells on UPR and ER stress, the levels of intracellular markers of UPR/ER stress were measured and compared to wild-type. GRP78, also known as BiP, is a central regulator for ER stress (Lee, 2005). BiP levels were measured using western blot and quantified the data, normalising to wild-type cells which was set at 1 (Figure. 35A.). Compared to wild-type cells, cells expressing L444P mutant protein had significantly higher levels of BiP protein (****$p<0.0001$), increasing to 2.38 ± 0.9. The levels of BiP protein in E326K and N370S mutants was altered minimally compared to wild-type. Among the mutants, BiP protein levels in L444P cells was significantly elevated compared to E326K cells (****$p<0.0001$) and N370S cells (****$p<0.0001$). Importantly, BiP protein expression in L444P cells was significantly higher than GFP expressing control cells (****$p<0.0001$), suggesting this activation of UPR/ER stress is specific to L444P and not due to over-expression of protein.

The effect of GCase mutations on the level of the *CHOP* transcription factor was assessed. *CHOP* plays an important role in ER stress-induced apoptosis and may be up-regulated in response to prolonged activation of the UPR (Hu et al., 2018). Quantitative PCR was performed and results normalised to wild-type cells, which was set at 1 ± 0.57 (Figure. 35B.). No significant difference was found between any of the mutant cell lines. The cycle number for *CHOP* was high (e.g.31.02) suggesting low transcript levels and resulted in high variation between samples. Indeed, *CHOP* protein levels were undetectable in SH-SY5Y cells (result not shown).

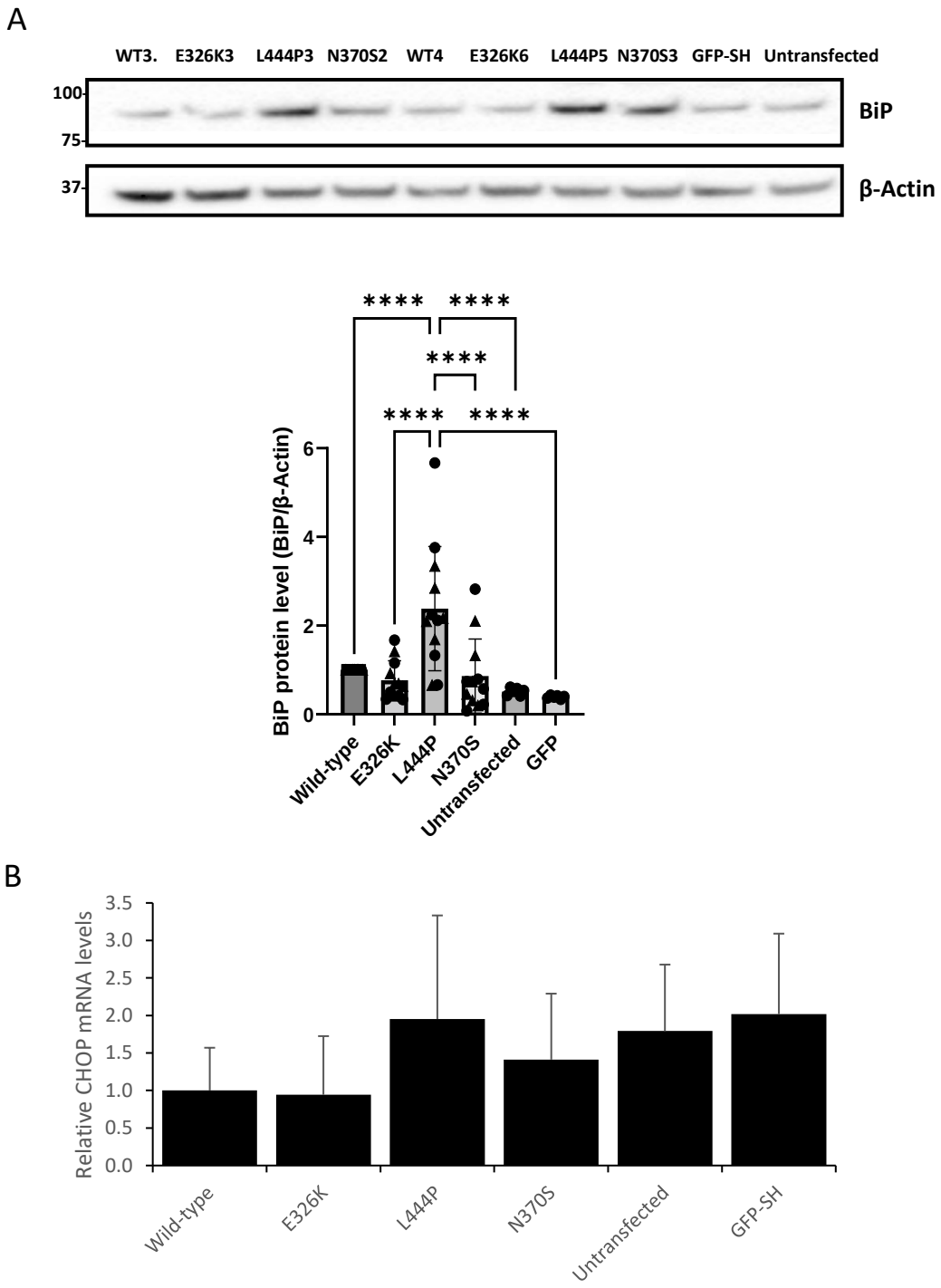

Figure 35. ER stress in undifferentiated SH-SY5Y stable cell lines expressing mutant GCase protein.

A) Immunoblot and quantification of BiP protein level in SH-SY5Y clones. For quantification, band density of each cell line was calculated, pooled and averaged for each genotype Data was normalised to wild-type SH-SY5Y cells band density, which was set at 1. Six technical repeats. Graph made using GraphPad Prism and shows mean and error bars show SEM. Each cell line for each genotype depicted as a different symbol. Statistical test used was one way ANOVA with Tukey post-hoc analysis (****p<0.0001). **B)** Quantification of *CHOP* mRNA levels in SH-SY5Y clones. For each

experiment, two biological repeats used for each cell line. For quantification, *CHOP* expression for each cell line was calculated, pooled and averaged for each genotype. Data normalised to wild-type SH-SY5Y cells, which was set at 1. Three technical repeats. Graph shows mean and error bars show SEM. Statistical test used was one way ANOVA with Tukey post-hoc analysis.

5.3.1.4 Increased soluble intracellular alpha-synuclein protein level in undifferentiated SH-SY5Y cells over-expressing L444P mutant GCase

To investigate the effect of *GBA1* mutations on intracellular soluble alpha-synuclein in undifferentiated SH-SY5Y cells, protein levels were measured by western blot (Figure. 36A.). A single band at the expected molecular weight of 15 kDa was detected in all SH-SY5Y clones. The human HAP1 parental cell line and a HAP1 alpha-synuclein knock-out cell line (as a negative control) were used to confirm specificity of the alpha-synuclein antibody. Quantification of the immunoblot was normalised to wild-type cells at 1 (Figure. 36B.). In SH-SY5Y cells expressing the L444P variant, alpha-synuclein protein level was 2.18 ± 1.5. This was significantly higher than wild-type (**$p<0.01$) and E326K (0.49 ± 0.53) (***$p<0.001$), N370S (*$p<0.05$), untransfected (*$p<0.05$) and GFP over-expressing cells (*$p<0.05$). In N370S cells soluble alpha-synuclein levels were similar to control at 1.16 ± 0.84, which was comparable GFP over-expressing SH-SY5Y cells (0.72 ± 0.5). In untransfected SH-SY5Y cells, alpha-synuclein soluble monomers were increased slightly to 1.44 ± 0.86).

To further the analysis of alpha-synuclein levels, quantitative PCR was used to measure *SNCA* mRNA transcript levels (Figure. 36C.). Data was normalised to *SNCA* transcript levels in wild-type cells. No significant changes in the expression level of alpha-synuclein were found across the mutations. Therefore, the increase in alpha-synuclein protein levels in L444P cells was not due to increased transcription of the *SNCA* gene.

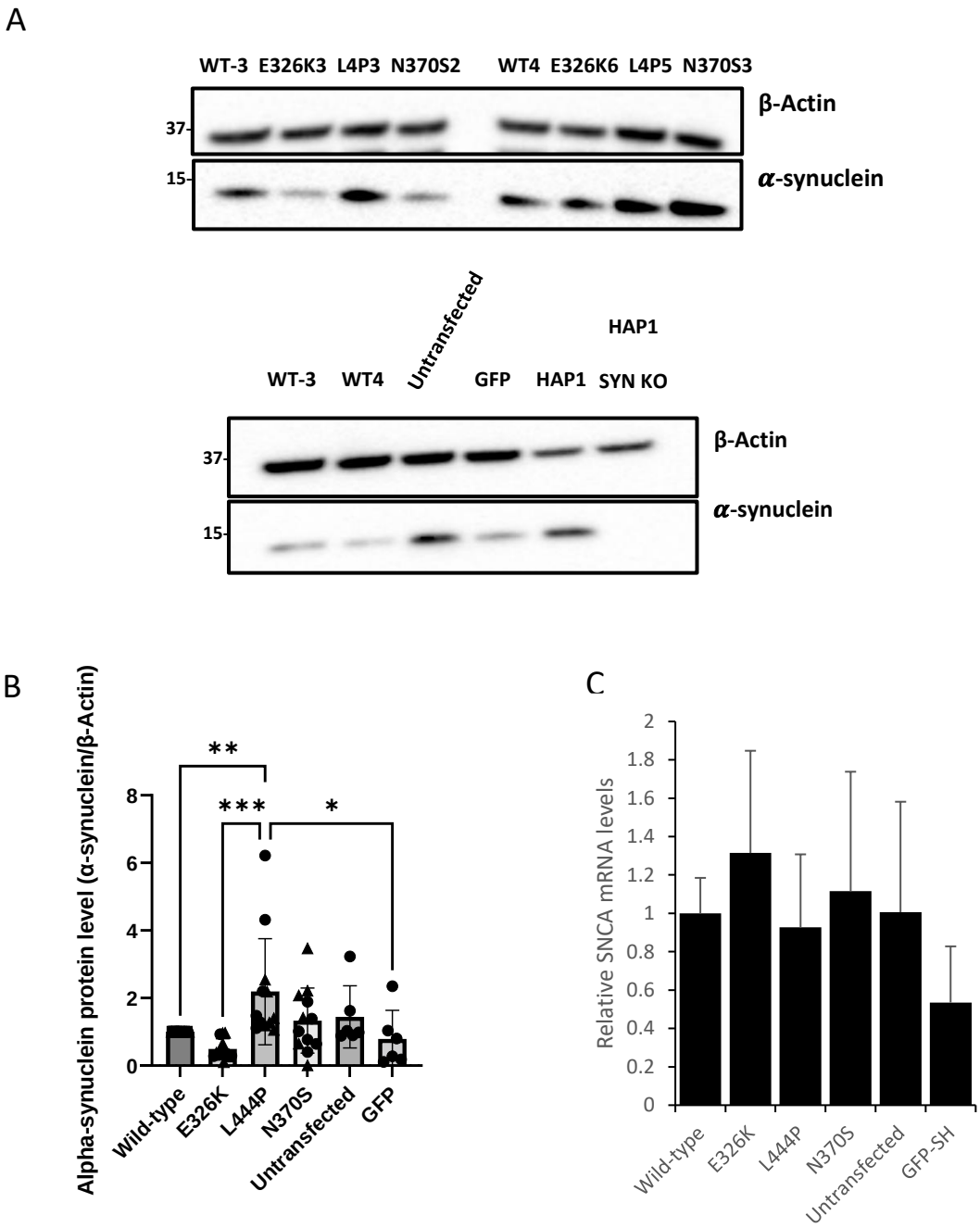

Figure 36. Soluble alpha-synuclein levels in SH-SY5Y stable cell lines expressing mutant GCase.

A) Immunoblot of monomeric, soluble alpha-synuclein protein level in SH-SY5Y clones. For analysis of *GBA1* over-expressing SH-SY5Y cell lines, each line was run together on a blot. For analysis of control lines including untransfected SH-SY5Y cells, GFP over-expressing cells, HAP1 cells and HAP1 *SNCA* knock-out cells, these were tan together with both wild-type *GBA1* SH-SY5Y cell lines. **B)** Quantification of alpha-synuclein immunoblotting in SH-SY5Y clones. For quantification, band density of each cell line was calculated and pooled for each genotype. Data was normalised to wild-type SH-SY5Y cells band density, which was set at 1. Six technical repeats. Graph made using

GraphPad Prism and error bars show SEM. Each cell line for each genotype depicted as a different symbol. Statistical test used was one way ANOVA with Tukey post-hoc analysis (*p<0.05, **p<0.01, ***p<0.001, ****p<0.0001). **C)** Quantification of *SNCA* mRNA levels in SH-SY5Y stable clones. For each experiment, two biological repeats used for each cell line. For quantification, *SNCA* expression for each cell line was calculated, pooled and averaged for each genotype. Data normalised to wild-type SH-SY5Y cells, which was set at 1. Three technical repeats. Graphs show mean and error bars show SEM. Statistical test used was one way ANOVA with Tukey post-hoc analysis.

5.3.1.5 Increased insoluble alpha-synuclein protein level in undifferentiated SH-SY5Y cells over-expressing mutant GCase protein

As alpha-synuclein can form insoluble, phosphorylated aggregates (Iwatsubo, 2003), the effect of *GBA1* mutations on alpha-synuclein aggregates in the Triton X 100 insoluble fraction was investigated. Soluble and insoluble Triton X 100 fractions were run on same western blot and immunoblotted for alpha-synuclein (Figure. 37.). The majority of alpha-synuclein remained in the soluble fraction. Monomeric, soluble alpha-synuclein was a single band at the expected molecular weight of 15 kDa. Quantification revealed minimal changes in the level of soluble, alpha-synuclein monomers across the cell lines, with cells expressing L444P GCase having the highest level (1.4-fold higher than wild-type) (Figure 37E.). Insoluble, monomeric alpha-synuclein was 2.03-fold higher than wild-type in cells expressing L444P protein. Compared to wild-type, all other cell lines had lower levels of insoluble alpha-synuclein monomers, with E326K 1.6-fold lower; N370S 1.9-fold lower and untransfected cells 2.9-fold lower.

There was evidence of a HMW alpha-synuclein species in the insoluble fraction (75 kDa). To confirm this band was alpha-synuclein a variety of controls were employed. HAP1 alpha-synuclein knock-out cells were utilised to confirm this band was alpha-synuclein and not non-specific binding (Figure. 37B.). As the band was missing in these cell lines, this suggests this band corresponds to a HMW alpha-synuclein aggregate, although to be certain an SH-SY5Y alpha-synuclein knock-out line should be used in future studies. This HMW band was also detected in untransfected cells and cells over expressing GFP (Figure. 37C. and 37D.). Note that in the insoluble fraction, β-actin band density was much lower than the soluble fraction. This might be as β-actin associated with Triton X

insoluble membranes (e.g. lipid rafts) or a small amount of contamination from the soluble fraction. Insoluble alpha synuclein band density was expressed as a ratio against soluble β-actin.

Western blots were quantified and normalised to wild-type cells (Figure. 37E.). There were no significant differences in the level of soluble and insoluble monomeric alpha-synuclein across all mutant cell lines. Analysis of the insoluble HMW alpha-synuclein fraction revealed a significant increase in L444P and E326K cells, compared to wild-type cells. In cells expressing the E326K variant, insoluble HMW alpha-synuclein increased from 1 ± 0.45 to 2.86 ± 0.77. In cells expressing the L444P variant, insoluble HMW alpha-synuclein increased from 1 ± 0.45 to 2.86 ± 0.58. Although N370S cells exhibited an increase in insoluble alpha-synuclein (1.87 ± 0.38), this was not significantly different to wild-type and was similar to that of untransfected SH-SY5Y cells (1.71 ± 0.73). Similarly, the levels of insoluble HMW alpha-synuclein in GFP over-expressing cells was similar to wild-type at 0.88 ± 0.46.

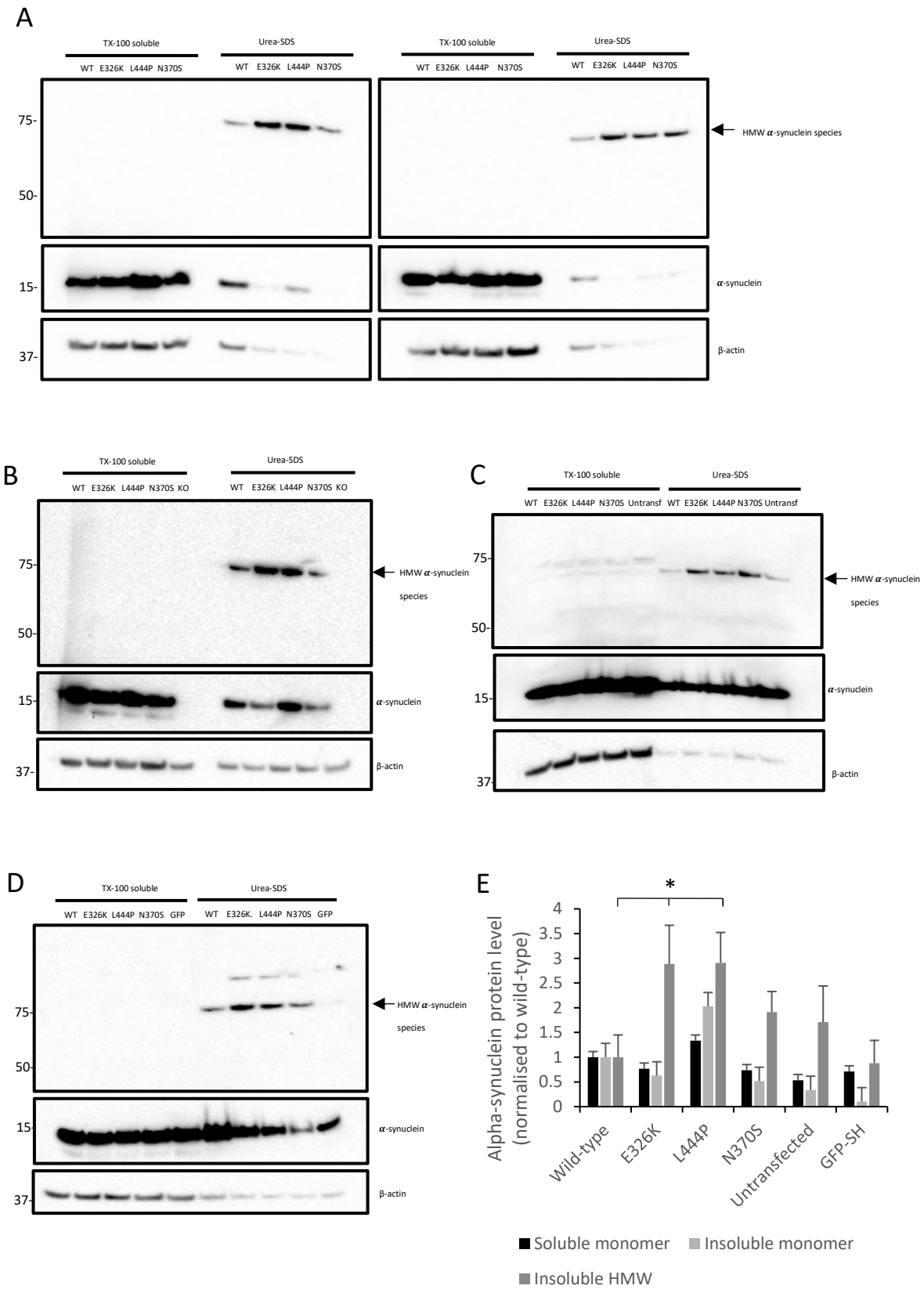

Figure 37. Insoluble alpha-synuclein levels in undifferentiated SH-SY5Y stable cell lines expressing mutant GCase.

TX-100 soluble and insoluble fractions (urea-SDS) were made from cells and analysed for alpha-synuclein by western blotting. For each experiment, cell lines WT3, E326K 3, L4P3, N370S 2 were grouped and ran together and cell lines WT4, E326K 6, L4P5 and

N370S 3 were grouped and ran together. Controls were used including HAP1 *SNCA* knockout cells, untransfected SH-SY5Y cells and GFP over-expressing SH-SY5Y cells were also employed. For each control there were three technical repeats performed. Overall, ten technical repeats were performed for *GBA1* over-expressing cells. HMW alpha-synuclein species (arrow) were detected in urea-SDS fractions. Monomeric alpha-synuclein was present in the TX-100 soluble fraction and some urea-SDS fractions. **A)** Immunoblots for all SH-SY5Y cell lines over-expressing mutant *GBA1* protein. **B)** Representative blot for HAP1 *SNCA* knock-out cell line control. **C)** Representative blot for untransfected SH-SY5Y cell line control. **D)** Representative blot for GFP over-expressing SH-SY5Y cell line control. **E)** Quantification of soluble and insoluble monomers and insoluble HMW alpha-synuclein immunoblots. For quantification, band density of each cell line was quantified, pooled and averaged for each genotype. For soluble monomers, insoluble monomers and insoluble HMW species, data was normalised to corresponding wild-type SH-SY5Y cells band density, which was set at 1. Graph show mean and error bars show SEM. For statistical analysis, a linear mixed-effects model fit by REML using R version 3.6.2 was used (*$p<0.05$).

5.3.1.6 Qualitative analysis of physiological alpha-synuclein monomeric, tetrameric and multimeric species in undifferentiated SH-SY5Y cells

In addition to insoluble alpha-synuclein aggregates being associated with PD, the ratio of physiological soluble alpha-synuclein tetramers/multimers to monomers has been implicated in PD (Kim et al., 2018b, Glajch et al., 2021). A reduction in the ratio of soluble tetramer:monomer has been linked with increased pathogenesis, increasing the intracellular pool of monomeric alpha-synuclein that can aggregate and become insoluble. To explore whether *GBA1* mutations could influence the formation of alpha-synuclein tetramers and other multimeric species, an intact cell cross-linking method (1mM DSG) was required to allow the detection of the alpha-synuclein detergent-sensitive tetramers/multimers (Dettmer et al., 2013). Each cell line was run in duplicate, with one untreated sample and one cross-linked sample and alpha-synuclein bands detected by western blot (Figure. 38.).

In order to visualise the HMW alpha-synuclein bands, 100 µg protein was loaded which resulted in rapid over-exposure of the alpha-synuclein monomeric species (aS14). Untransfected SH-SY5Y cells (Figure. 38A.) and GFP over-expressing SH-SY5Y cells (Figure. 38B.) were included as control lines. In all cell lines incubated with DSG cross-linker, there was the presence of cross-linked alpha-synuclein tetramers (aS60) and related multimers (aS80 and aS30).

Qualitative analysis of the blots suggests that the amount of alpha-synuclein monomer is similar across the mutant lines, however due to band over-exposure at 1 second, it cannot be accurately quantified. The blots also suggest that there is increased alpha-synuclein tetramer and related multimers in the mutant cell lines compared to wild-type, untransfected and GFP SH-SY5Y cells. Unlike previous studies where band densities of aS80 + aS60 were divided by the

density of as14, I was unable to accurately quantify the ratio due to rapid over-exposure of monomeric alpha-synuclein species (Kim et al., 2018b). I instead calculated the ratio of aS80 + aS60 to β-actin (Figure. 38C.). Compared to wild-type, the ratio in cells expressing L444P protein was 3.2-fold higher, although not significant. This was similar to untransfected cells which were 2.3-fold higher than wild-type, but also not significant. Other cell lines were similar to wild-type. This ratio suggested that in L444P and untransfected cells, there is a shift in the ratio toward aggregate-resistant tetramers and multimers.

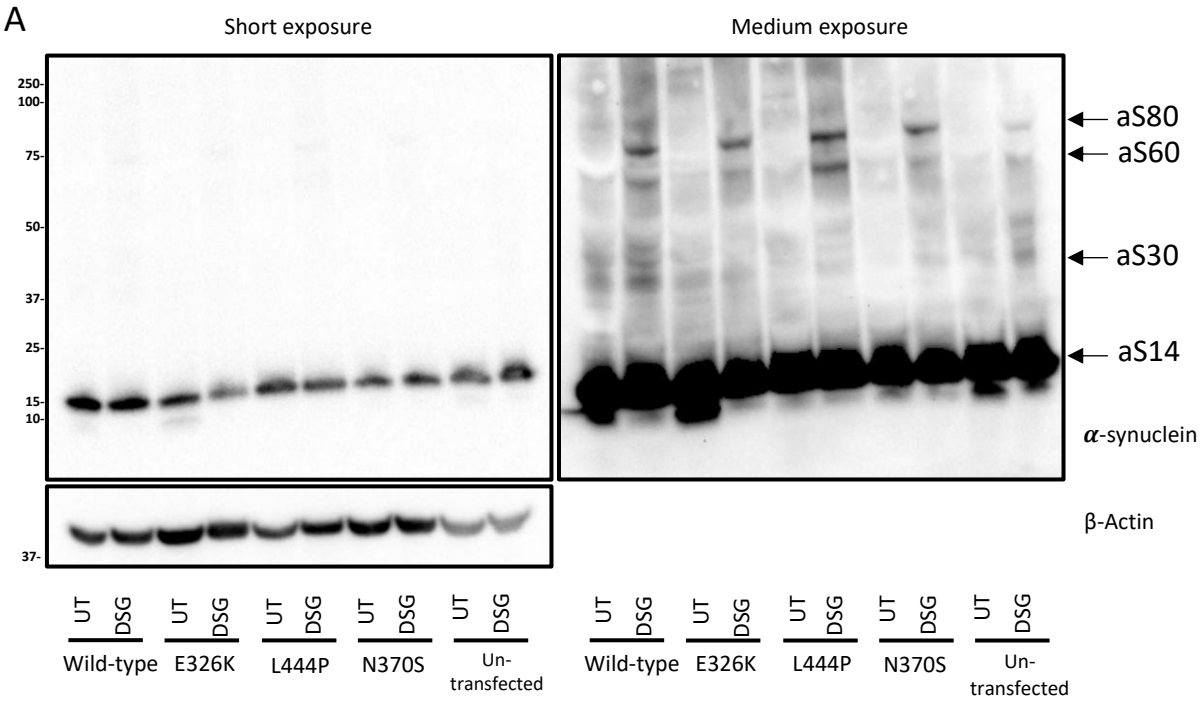
A
Short exposure
Medium exposure
250-
100-
75-
50-
37-
25-
15-
10-
37-
aS80
aS60
aS30
aS14
α-synuclein
β-Actin
UT
DSG
Wild-type
E326K
L444P
N370S
Un-transfected

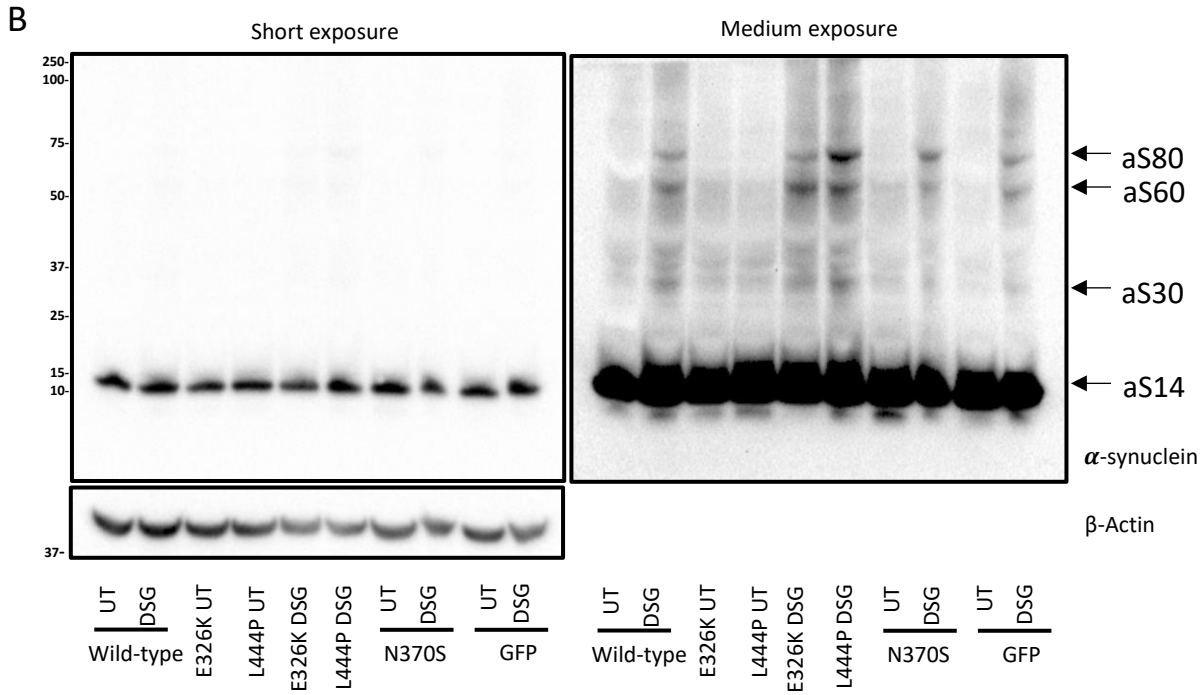
B
Short exposure
Medium exposure
250-
100-
75-
50-
37-
25-
15-
10-
37-
aS80
aS60
aS30
aS14
α-synuclein
β-Actin
UT
DSG
Wild-type
E326K UT
L444P UT
E326K DSG
L444P DSG
N370S
GFP

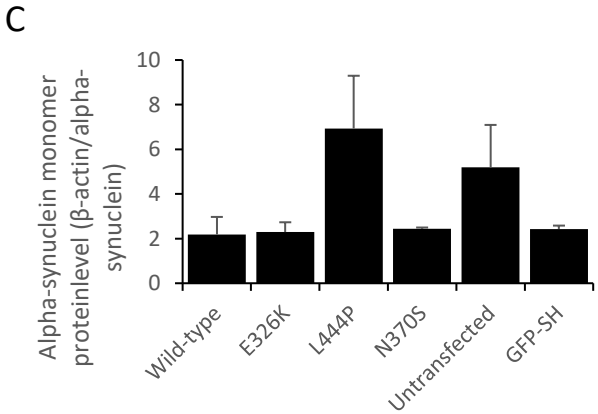
C
Alpha-synuclein monomer proteinlevel (β-actin/alpha-synuclein)
10
8
6
4
2
0
Wild-type
E326K
L444P
N370S
Untransfected
GFP-SH

Figure 38. Analysis of monomeric and HMW species of alpha-synuclein undifferentiated SH-SY5Y lines over-expressing mutant GCase protein.

Cells were lysed in TX 100 and 100 µg total cell lysate was either untreated (UT) or incubated with DSG cross-linker. For each experiment, each cell line was untreated (UT) or cross-linked (DSG) and ran on two western blots with untransfected SH-SY5Y cells and GFP over-expressing SH-SY5Y cells. Representative blots shown at short and long exposure with **A)** untransfected SH-SY5Y control and **B)** GFP over-expressing SH-SY5Y control. HMW alpha-synuclein species are present in the DSG-treated cells. Arrow marks show HMW species as80, possible tetrameric species at as60 possible dimeric species at as30. These bands were absent in untreated lysates. Monomeric alpha-synuclein present at 15 kDa (aS14). **C)** Quantification of ratio of monomeric alpha-synuclein species to β-actin. For quantification, monomeric alpha-synuclein band density of each cell line was calculated at low exposure, pooled and averaged for each genotype. Graphs show mean and error bars show SEM. Three technical repeats. Statistical test used was one way ANOVA with Tukey post-hoc analysis.

5.3.1.7 Analysis of alpha-synuclein aggregation in undifferentiated SH-SY5Y cells by Thioflavin T binding assay

In an attempt to monitor how *GBA1* mutations influence the characteristics of alpha-synuclein aggregation in SH-SY5Y cell lines, the ThT binding assay was employed. ThT is a specific dye commonly used to monitor *in vitro* amyloid fibril formation. Upon binding to amyloid fibrils, ThT exerts a fluorescence signal at 482 nm (Naiki et al., 1989), which is proportional to aggregate formation. In order to first optimise the ThT assay, the aggregation of recombinant monomeric alpha-synuclein was measured when incubated with PFFs, which act as a template to induce the monomeric alpha-synuclein to misfold and form fibrils (Figure. 39A.) (Wu et al., 2019, Volpicelli-Daley et al., 2014). No aggregation was observed with 6.25 or 12 µM, with ThT fluorescence similar to the water blank. Incubation of 25 µM alpha-synuclein monomers with PFFs exhibited a steady increase in ThT fluorescence that reached a maximum within 23 minutes and then remained constant. Both 50 µM and 75 µM of alpha-synuclein monomers demonstrated a steep increase in aggregation for 45 minutes before plateauing and showing the characteristic sigmoid curve for ThT assays (Xue et al., 2017).

Having shown that the ThT assay could detect aggregation of recombinant alpha-synuclein, the ThT binding assay was performed on differentiated SH-SY5Y cells to determine if the aggregation of cellular alpha-synuclein could be measured (Figure. 39B.). These cells were either untreated or treated with both PFF and CBE for 10 days prior to harvest, and have been previously shown to contain aggregated alpha-synuclein (Gegg et al., 2020). When these lysates (50 µL) were incubated with PFF to initiate aggregation and then mixed with ThT, the initial fluorescence (0 minutes) was higher than the blank in both samples. However, there was an initial drop in fluorescence within 5 minutes of incubation, which was

sustained for the remainder of the assay. This occurred in both untreated cells, and the cells that were known to already have aggregated alpha-synuclein in them. In case the amount of starting material was too high and interfered with the assay or quenched fluorescence the amount of lysate was lowered to 10 µL. The initial fluorescence for the test samples were close to the blank. However, addition of PFF to initiate aggregation still did not result in an increase in ThT fluorescence. As the assay was unable to detect aggregation in cell lysates already known to have aggregating species (SH-SY5Y+PFF+CBE), the GCase mutant over-expressing SH-SY5Y cell lines were not analysed.

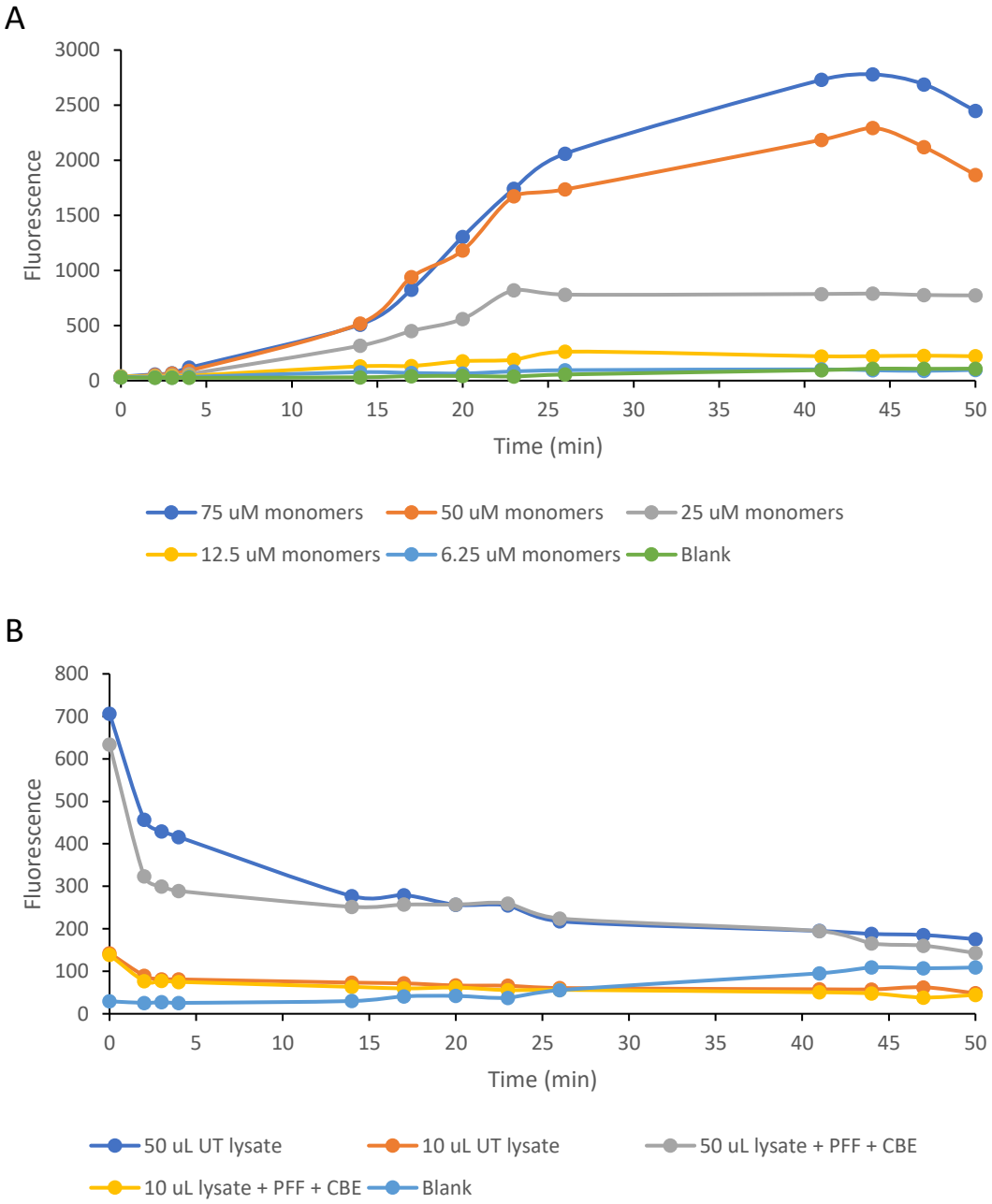

Figure 39. Thioflavin T analysis in differentiated SH-SY5Y cell lysate.

A) Increasing concentrations of alpha-synuclein monomers were incubated with Thioflavin T reagent for 50 hours. Fluorescence measurements were taken at regular intervals. Data suggests a minimum of 25 µM alpha-synuclein monomers required for a fluorescence signal. **B)** Lysates from untreated differentiated SH-SY5Y cells pre-treated with PFF and 10 µM CBE. For the assay, 10 µL and 50 µL of cell lysate per well was used and mixed with PFF to initiate aggregation of alpha-synuclein species in cell lysates. Cells were incubated with Thioflavin T reagent for 50 hours and fluorescence measurements were taken at regular intervals. Three technical repeats.

5.3.1.8 Analysis of alpha-synuclein aggregation in undifferentiated SH-SY5Y cells by Cisbio HTRF® alpha-synuclein assay

To further investigate the effect of *GBA1* mutations on alpha-synuclein aggregation, the Cisbio HTRF® alpha-synuclein kit was employed to detect human alpha-synuclein aggregation though FRET. The luminescence signal intensity is proportional to the number of alpha-synuclein aggregates formed. The linear range was calculated by measuring aggregation in SH-SY5Y cell lysate; SH-SY5Y cell lysate spiked with 25 ng alpha-synuclein monomers; and SH-SY5Y cells spiked with 25 ng alpha-synuclein PFFs (Figure. 41A). Serial dilutions were then mixed with the detection antibodies and FRET measured. As expected, no change in luminescence was observed in untreated SH-SY5Y cells or in SH-SY5Y cells incubated with 25 ng alpha-synuclein monomers. Analysis of SH-SY5Y cells spiked with 25 ng PFF demonstrated a hook effect, with a signal increase until a maximum followed be a decrease, as expected. The linear range was calculated to be between 1:4 and 1:16 dilutions.

Having established the assay could detect alpha-synuclein aggregates and that the presence of cell lysates (0.3 -13 µg/µL) didn't interfere with this, the HTRF® assay was run on undifferentiated SH-SY5Y cells over-expressing GCase mutants (Figure. 41B.). Data was normalised to protein concentration. Alongside this, SH-SY5Y cells spiked with 25 ng PFFs was used as a positive control. The positive control produced a marked increase in luminescence. However, the SH-SY5Y mutant cell lines failed to exhibit a measurable increase in luminescence at any lysate dilution.

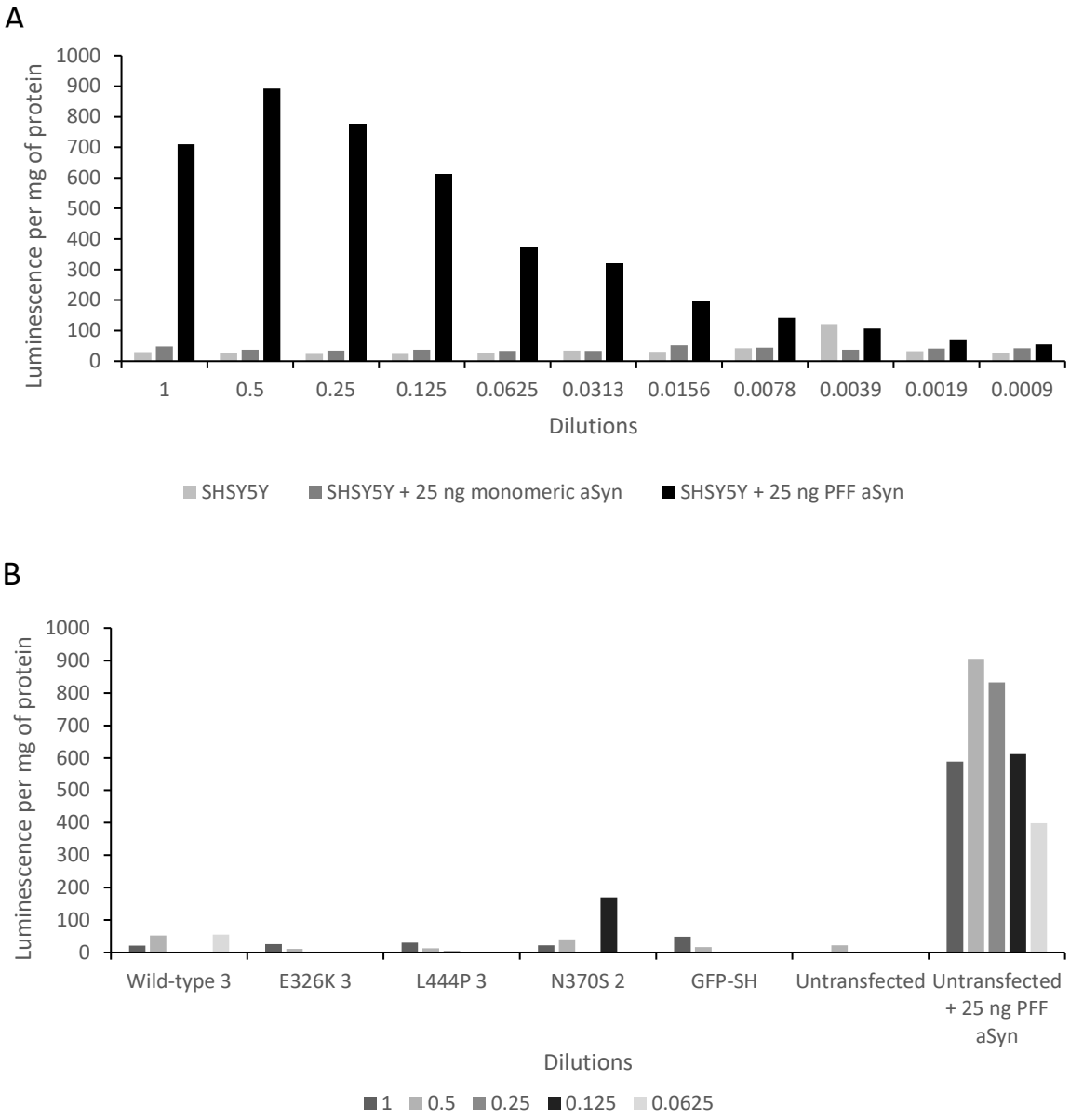

Figure 40. HTRF fluorescence analysis of alpha-synuclein aggregation in undifferentiated SH-SY5Y cells over-expressing GCase protein.

A) Undifferentiated SH-SY5Y cells were incubated alone, with 25 ng alpha-synuclein monomers or 25 ng PFF, serially diluted and mixed with the Cisbio HTRF alpha-synuclein aggregation kit. PFF acts as a positive control with the linear range between 0.25x and 0.0625x dilutions. Untreated cells and cells incubated with 25 ng monomeric alpha-synuclein below limit of detection. **B)** Undifferentiated SH-SY5Y cells over-expressing *GBA1* protein were loaded on to Cisbio HTRF alpha-synuclein aggregation kit at dilutions within the linear range. Untransfected SH-SY5Y cell lysate spiked with PFFs were used as a positive control. Undifferentiated SH-SY5Y cells alpha-synuclein aggregation was below limit of detection. One cell line from each genotype shown in representative graph. Two technical repeats.

5.3.1.9 Exosomal release of alpha-synuclein from undifferentiated SH-SY5Y cells over-expressing mutant GCase protein

To investigate whether the E326K, L444P or N370S *GBA1* mutations influence alpha-synuclein secretion from cells, the levels of alpha-synuclein monomers in culture media were analysed using an alpha-synuclein ELISA (Figure. 41A.). Data was normalised against wild-type SH-SY5Y cells, which was set at 1 ± 0.02. There were no significant differences between wild-type and mutant cells, nor was there a marked difference between mutations. However, all cell lines over-expressing GCase protein, and GFP, had increased levels of alpha-synuclein protein in culture media compared to untransfected SH-SY5Y cells. For untransfected cells, alpha-synuclein protein concentration was 0.08 ± 0.15. In wild-type GCase cells alpha-synuclein secretion was increased 12.5-fold; in E326K GCase cells there was an 8.75-fold increase; in L444P mutants there was a 13.75-fold increase; in N370S GCase cells secretion was increased 9.38-fold and in GFP over-expressing cells there was a 17.9-fold increase in alpha-synuclein compared to untransfected cells.

As literature suggests that alpha-synuclein can be released from cells via an exosome-mediated pathway (Emmanouilidou et al., 2010), the level of exosomes in culture media was measured. A dot blot was performed and probed for the endogenous exosome marker, Flotillin (Figure. 41B.). Results were normalised against wild-type SH-SY5Y cells which was set at 1 ± 0.03 (Figure. 41C.). Compared to wild-type GCase, the level of flotillin in media was similar in L444P GCase cells (1.31 ± 0.62) and GFP cells (1.22 ± 0.59). There was an increase in E326K GCase cells to 1.81 ± 0.32 and N370S GCase cells to 2.48 ± 0.62 however, these weren't significantly elevated compared to wild-type cells. Similarly to alpha-synuclein ELISA data, all cell lines over-expressing GCase

protein or GFP protein were markedly higher than untransfected cells, with E326K and N370S being significantly higher (*$p<0.05$).

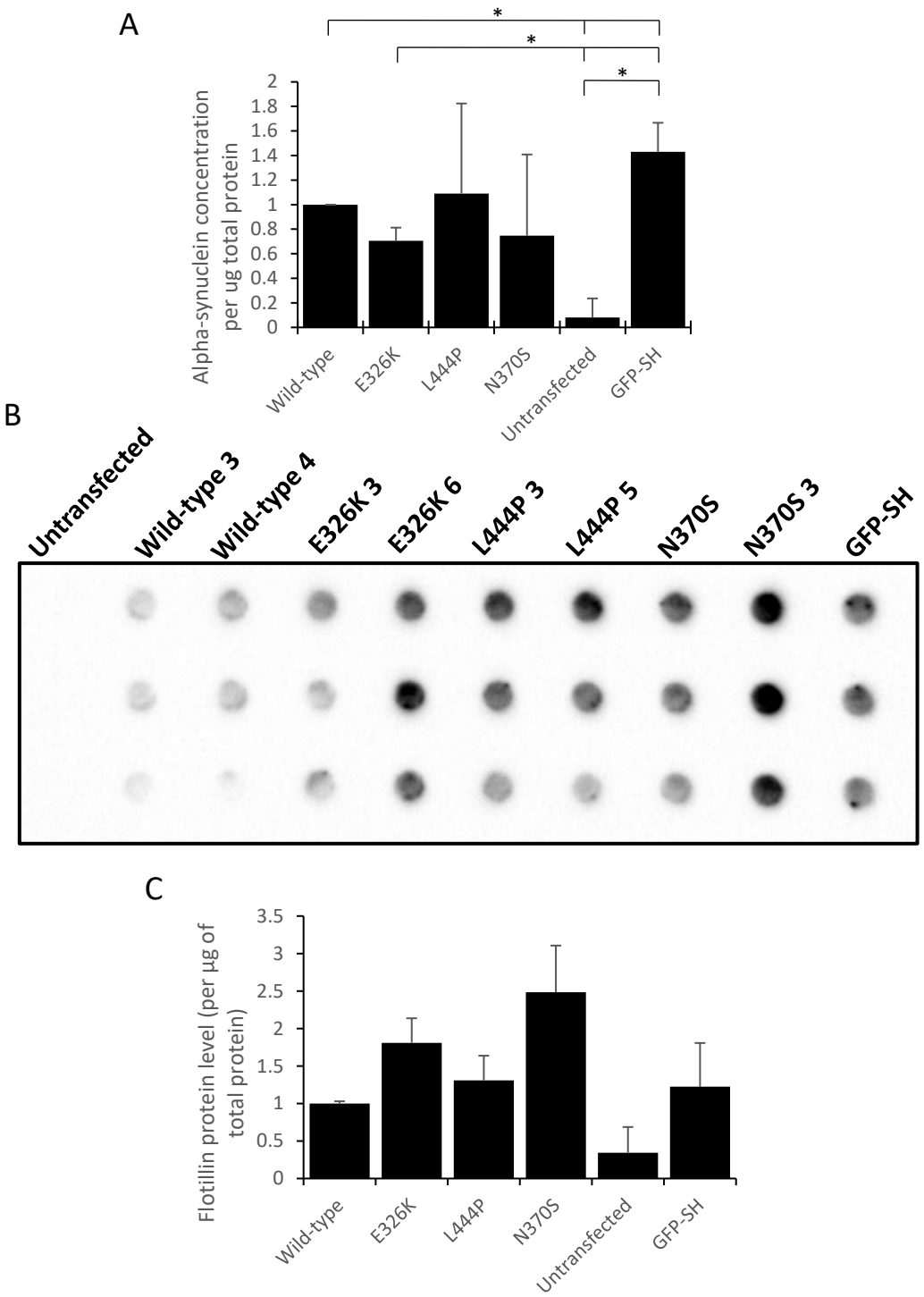

Figure 41. Secretion of monomeric alpha-synuclein from undifferentiated SH-SY5Y cell lines over-expressing mutant GCase protein.

Undifferentiated SH-SY5Y cells were grown for 3 days and culture media collected. **A)** Culture media was analysed by an alpha-synuclein ELISA in duplicates, specific against monomeric alpha-synuclein. For each experiment, two biological replicates were used. Three technical repeats. For quantification, data from each cell line was pooled and averaged for each genotype. Data normalised to wild-type SH-SY5Y cells, which was set at 1. Graphs show mean and error bars show SEM. Statistical test used was one way ANOVA with Tukey post-hoc analysis (*$p<0.05$). Culture media was blotted as triplicates

onto **B)** a dot blot, immunoblotted with anti-Flotillin antibody and **C)** quantified by taking the mean average of triplicates. For quantification, dot density from each cell line was pooled and averaged for each genotype. Data normalised to wild-type SH-SY5Y cells, which was set at 1. Graphs show mean and error bars show SEM. Three technical repeats. Statistical test used was one way ANOVA with Tukey post-hoc analysis.

5.3.1.10 No difference in GSL expression in undifferentiated SH-SY5Y cells over-expressing GCase mutants

To understand how *GBA1* mutations influence the lipid composition of cells, wild-type and mutant GCase SH-SY5Y cells were sent for analysis by HPLC. A representative HPLC trace figure for wild-type GCase cells showing the pattern of GSL expression is shown in Figure. 42A. The GSL expression pattern was the same across wild-type and mutant GCase lines. Each peak represents a different species of GSL, with peak height corresponding to fluorescence. Analysis reveals there are 12 major GSL species expressed in the SH-SY5Y clones. The concentration of each species was quantified and displayed graphically to compare the relative GSL areas in undifferentiated SH-SY5Y cells over-expressing wild-type, E326K, L444P and N370S GCase protein (Figure. 42B.). Analysis demonstrates the most abundant GSL species is GM2, followed by GD1b. There was no difference in GSL pattern or expression in SH-SY5Y cells expressing mutant GCase compared to wild-type cells, nor was there a difference between the different mutations. Further HPLC analysis was performed to measure the concentration of GlcCer in wild-type, E326K, L444P and N370S SH-SY5Y cells (Figure. 42C.). There were no differences demonstrated between the different cell lines.

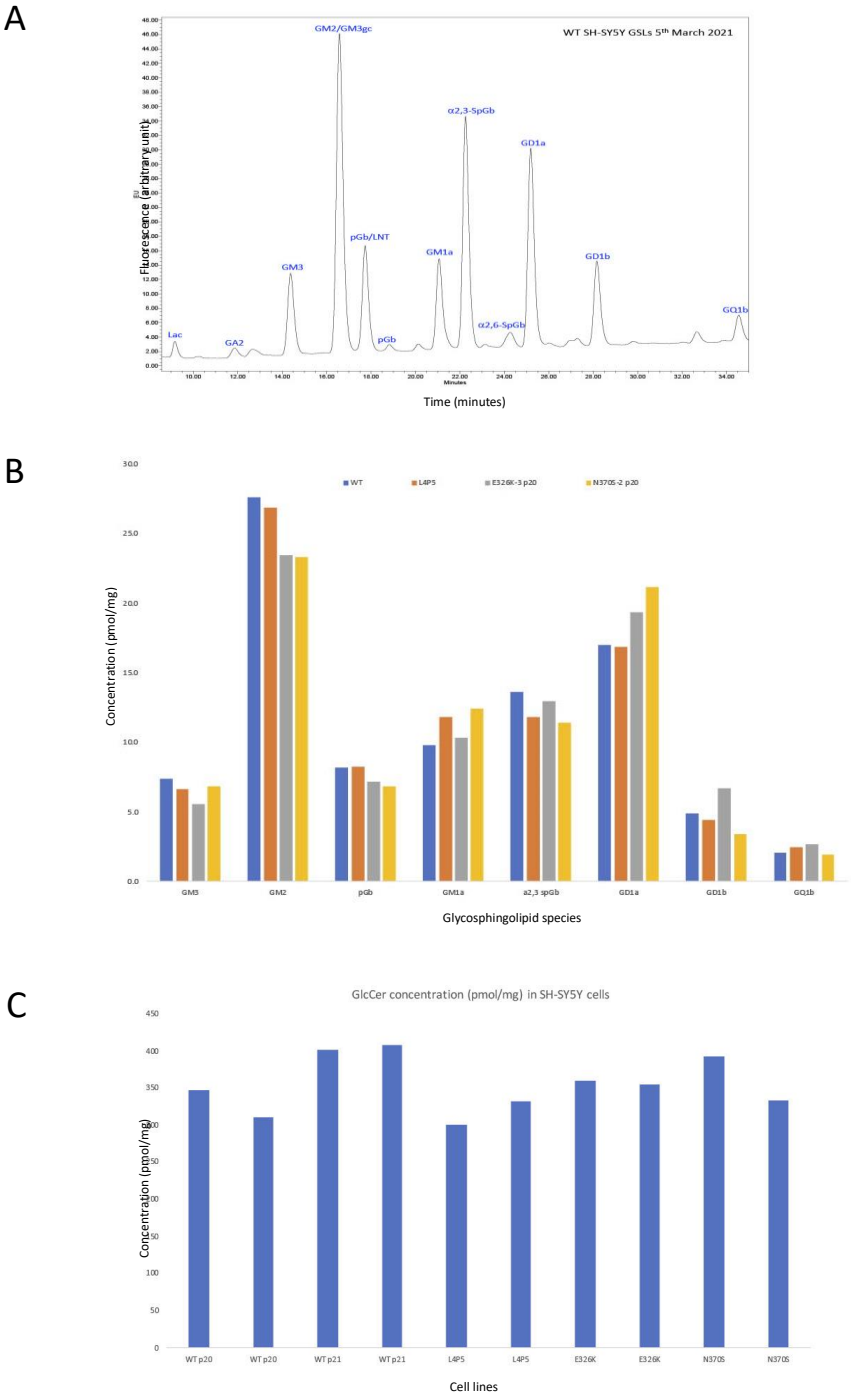

Figure 42. HPLC lipid analysis in undifferentiated SH-SY5Y cells.

A) HPLC trace figure showing the pattern of glycosphingolipid expression in wild-type *GBA1* SH-SY5Y cells. Peaks annotated with corresponding glycosphingolipid species. No difference between the pattern of glycosphingolipid expression in wild-type and mutant cell lines. **B)** Comparison of the relative glycosphingolipid areas in two pellets from each undifferentiated SH-SY5Y cell lines over-expressing wild-type, E326K, L444P and N370S *GBA1* protein. Wild-type (WT) is blue. E326K (E326K-3 p20) is grey. L444P (L4P5) is orange. N370S (N370S-2 p20) is yellow. **C)** HPLC analysis of pattern of

glucosylceramide in SH-SY5Y cells. Graph shows the comparison of glucosylceramide across wild-type and mutant cells.

5.3.1.11 Increased number of lipid droplets in E326K GCase SH-SY5Y cells

To further investigate whether *GBA1* mutations influence lipid metabolism in undifferentiated SH-SY5Y cells, the number of lipid droplets in each cell line was measured. Lipid droplets are organelles involved in intracellular lipid homeostasis (Farmer et al., 2020). Staining was first performed on SH-SY5Y cells under basal conditions, imaged and quantified (Figure. 43A.). BODIPY 493/503 stains neutral lipids and lipid droplets are visualised as green punctate structures, examples of which are shown by arrows. All lipid droplets and cells were counted and data displayed as the number of lipid droplets per 100 cells. Quantification revealed that in E326K cells, the number of lipid droplets was 562 ± 57.7 per 100 cells. This was significantly higher than wild-type cells (194 ± 91.5) (**$p<0.01$), as well as L444P (375 ± 33.3); N370S (389 ± 86.5); untransfected cells (252 ± 100.7) and GFP over-expressing cells (278 ± 151.9) (*$p<0.05$). The number of lipid droplets calculated in L444P mutant cells was also significantly higher than wild-type (*$p<0.05$).

To analyse the ability of cells to form lipid droplets, cells were starved overnight and then treated with OA, which is a potent inducer of lipid droplet formation (Nakajima et al., 2019) (Figure. 43B.). Again, white arrows point to lipid droplets visusalised by immunofluorescence microscopy. Quantification of lipid droplets per 100 cells revealed that there was minimal changes across cell lines in untreated starved cells. However, in E326K cells, treatment with OA resulted in a marked increase to 1400 ± 531.42 lipid droplets per 100 cells. This was significantly elevated compared to treated wild-type cells (142 ± 24.27 lipid droplets per 100 cells) and treated N370S cells (203 ± 72.49 lipid droplets per

100 cells) (*$p<0.05$). The number of lipid droplets was similar in L444P cells (254 ± 60.73 per 100 cells) to that of N370S cells.

A

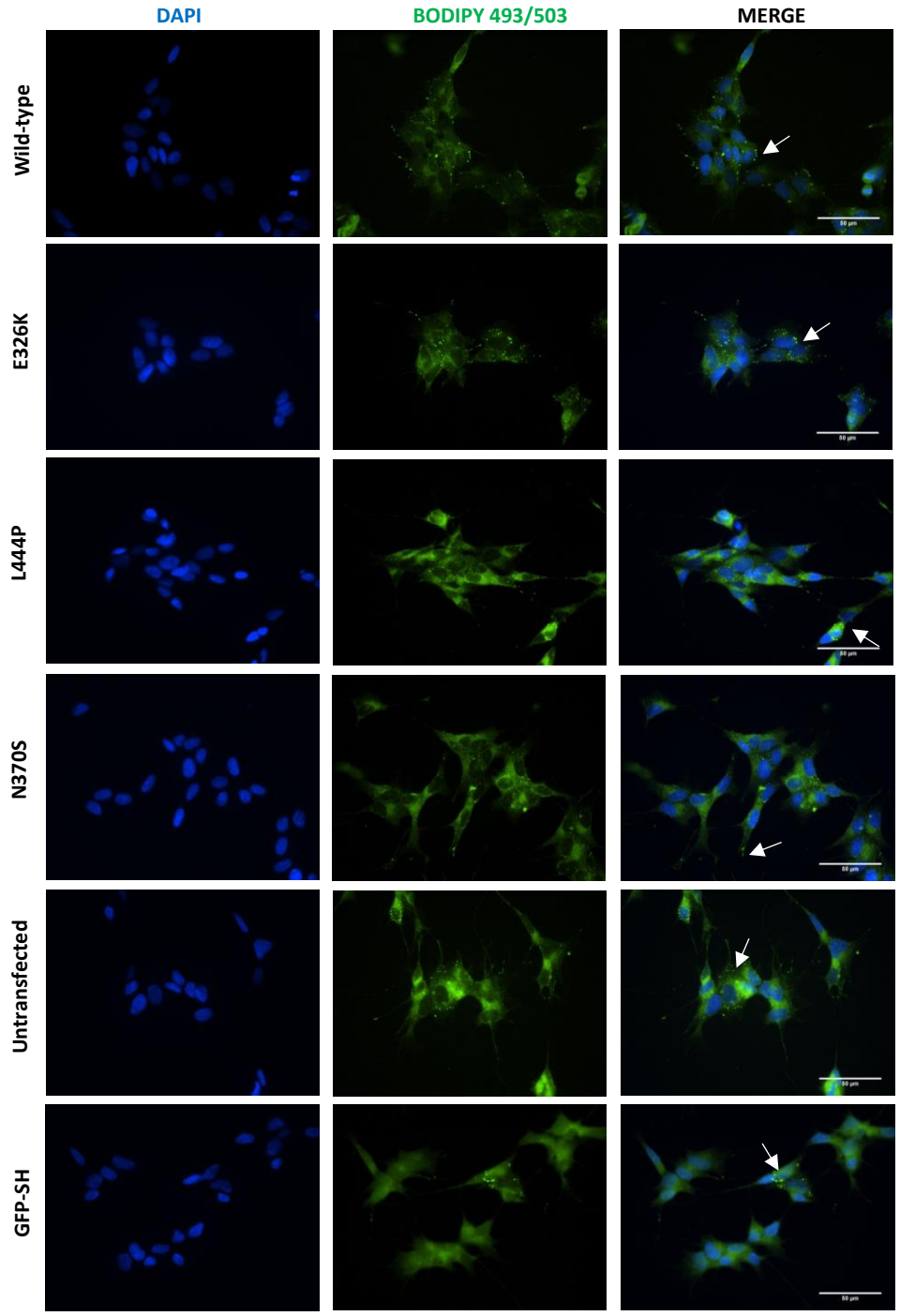
DAPI
BODIPY 493/503
MERGE
Wild-type
E326K
L444P
N370S
Untransfected
GFP-SH

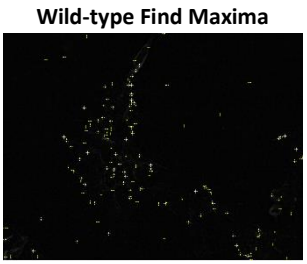
Wild-type Find Maxima

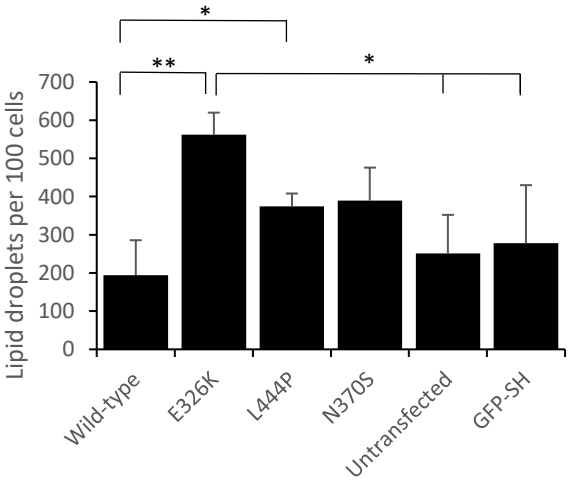
*
**
*
Lipid droplets per 100 cells
700
600
500
400
300
200
100
0
Wild-type
E326K
L444P
N370S
Untransfected
GFP-SH

B

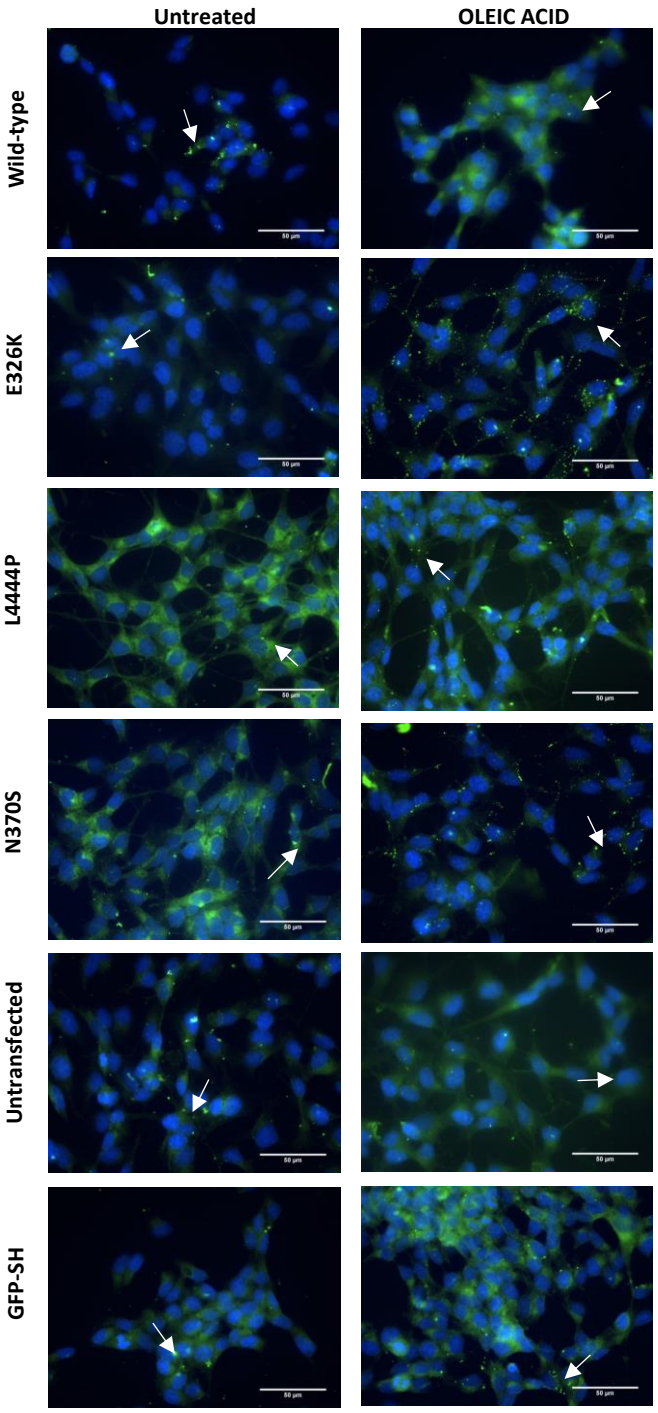
Untreated
OLEIC ACID
Wild-type
E326K
L444P
N370S
Untransfected
GFP-SH

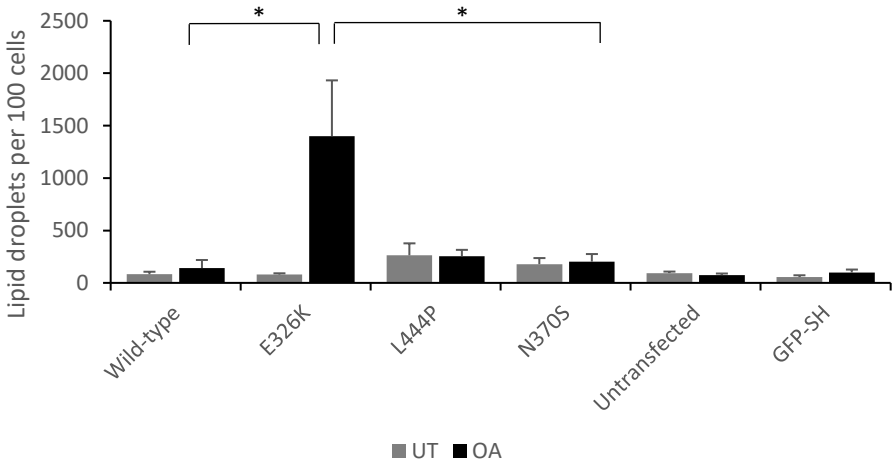
Lipid droplets per 100 cells
2500
2000
1500
1000
500
0
*
*
Wild-type
E326K
L444P
N370S
Untransfected
GFP-SH
UT
OA

Figure 43. Lipid droplet analysis in undifferentiated SH-SY5Y cells.

A) Cells were grown on coverslips and stained with lipophilic fluorescent probe BODIPY 493/503. Lipid droplets present as concentrated green dots (arrows). Representative images from each genotype shown. For each experiment, six images from each cell line were taken. All cells were counted in the images and the number of lipid droplets were quantified using the find maxima tool in Image J (below left) and shown graphically as lipid droplets per 100 cells (below right). Three technical repeats. For quantification, lipid droplets per 100 cells of each cell line was calculated, pooled and averaged for each genotype. Graphs show mean and error bars show SEM. Statistical test used was one way ANOVA with Tukey post-hoc analysis (*$p<0.05$, **$p<0.01$). **B)** Cells were starved in Opti-MEM overnight and incubated with and without 100 µM oleic acid for 5 hours. Cells were stained with lipophilic fluorescent probe BODIPY 493/503. Lipid droplets present as concentrated green dots (arrows). Representative images from each genotype shown (UT is untreated and OA is oleic acid). For each experiment, six images from each cell line were taken. All cells were counted in the images and the number of lipid droplets were quantified using the find maxima tool in Image J (below left) and shown graphically as lipid droplets per 100 cells (below right). Three technical repeats. For quantification, lipid droplets per 100 cells of each cell line was calculated, pooled and averaged for each genotype. Graphs show mean and error bars show SEM. Statistical test used was one way ANOVA with Tukey post-hoc analysis (*$p<0.05$).

5.3.2 Differentiated SH-SY5Y neurons over-expressing mutant GCase protein

5.3.2.1 Characterisation of differentiated SH-SY5Y dopamine neurons

The proliferating mutant *GBA1* SH-SY5Y cells might not accumulate alpha-synuclein as they can divide and pass on alpha-synuclein to daughter cells. Therefore, the cell lines were differentiated with retinoic acid and BDNF. To ensure the SH-SY5Y differentiation protocol used yielded highly viable, homogenous, differentiated neuronal cultures within 10 days, we performed biochemical and imaging analyses.

Undifferentiated SH-SY5Y neuroblastoma cells exhibit a large, flat, epithelial-like phenotype with short projections (Figure. 44A.), whereas differentiated SH-SY5Y neurons demonstrate smaller cell bodies with extensive and elongated neurite projections that connect to neighbouring cells (Figure. 44B.). The neuronal characteristics of fully differentiated SH-SY5Y cells were investigated using both immunofluorescence and western blotting techniques. Differentiated cells were harvested on day 10 and immunostained for mature neuron marker, β-Tubulin III (Figure. 45A-45B.), and for dopaminergic neuron marker, TH (Figure. 45C.), and imaged by fluorescence microscopy. Cells were counterstained with DAPI to visualise DNA in the nucleus. Immunostaining for β-Tubulin III allowed visualisation of neurons, demonstrating extensive projections connecting to surrounding cells, confirming the SH-SY5Y neuroblastoma cells were successfully differentiated. Total neurite length was quantified and normalised to the total number of cells analysed (Figure. 45B.) Compared to wild-type cells (54.9 ± 7.2), differentiated SH-SY5Y cells expressing L444P (23.1 ± 5.4) and N370S (10.7 ± 1.3) GCase protein had significantly reduced neurite length (L444P *$p<0.05$ and N370S ***$p<0.001$). Similarly, there was a significant

reduction in neurite length compared to E326K cells (47.1 ± 3.6) in those expressing L444P (*p<0.05) and N370S (***p<0.01) protein. Immunostaining for TH demonstrated the presence of dopamine neurons in the culture. Following harvesting, differentiated cells were also subjected to western blot analysis and stained for classical neuronal markers, β-Tubulin III (Figure. 46A.) and the synaptic marker PSD95 (Figure. 46B.). There were minimal changes in β-Tubulin III protein level across all cell lines, and PSD95 across cell lines.

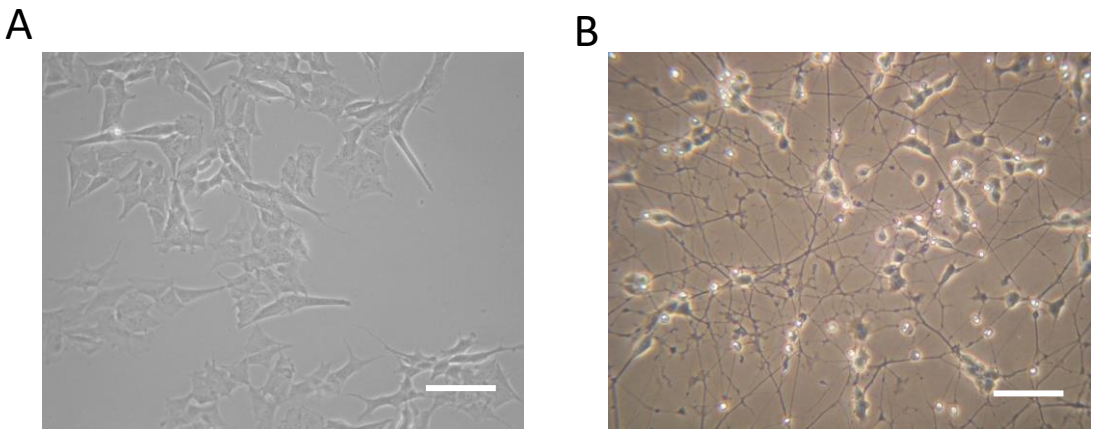

Figure 44. Morphological appearance of undifferentiated and differentiated SH-SY5Y cells.

A) Undifferentiated SH-SY5Y cells have a flat phenotype with few projections **B)** whereas differentiated SH-SY5Y neurons demonstrate extensive and elongated neurite projections. Representative images of untransfected SH-SY5Y cell line. Images were obtained in phase at 20X magnification using an inverted epifluorescence microscope. Scale bar is 25 μm.

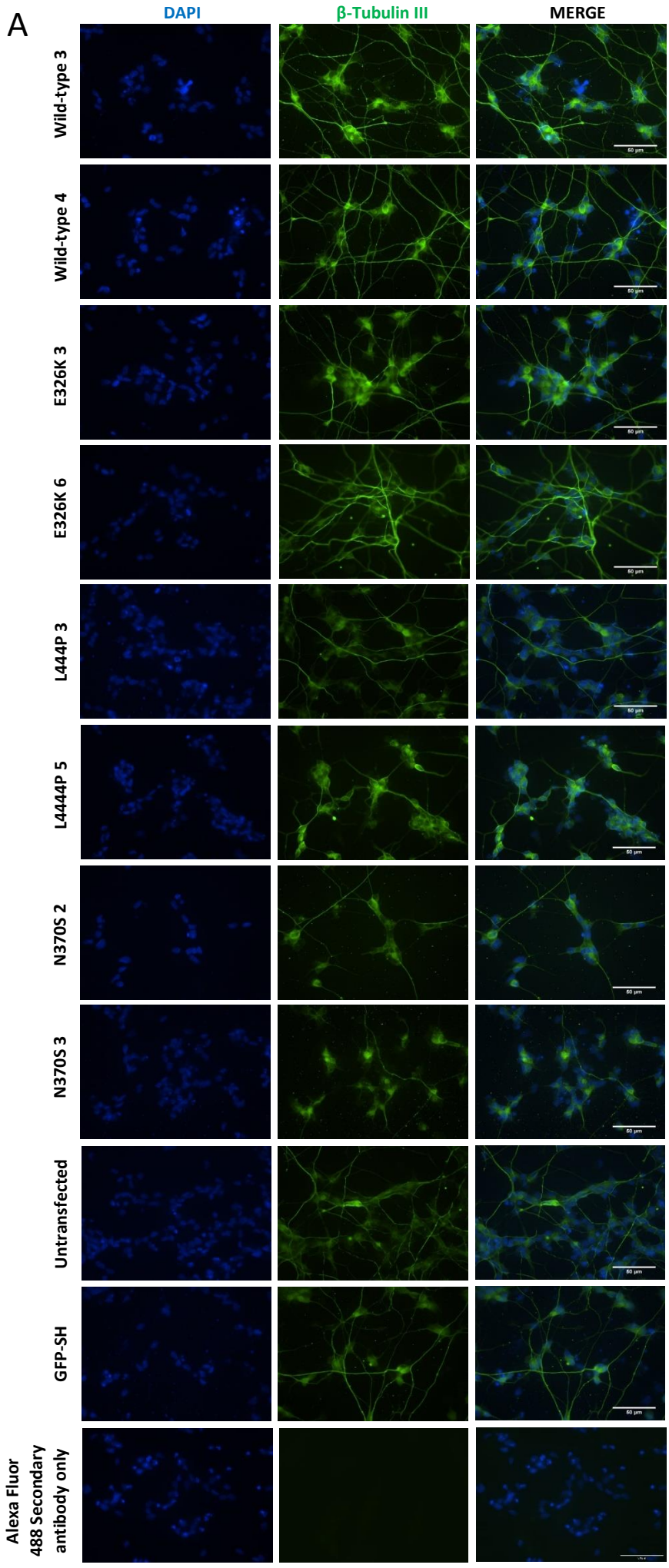
A
DAPI
β-Tubulin III
MERGE
Wild-type 3
Wild-type 4
E326K 3
E326K 6
L444P 3
L4444P 5
N370S 2
N370S 3
Untransfected
GFP-SH
Alexa Fluor 488 Secondary antibody only

B

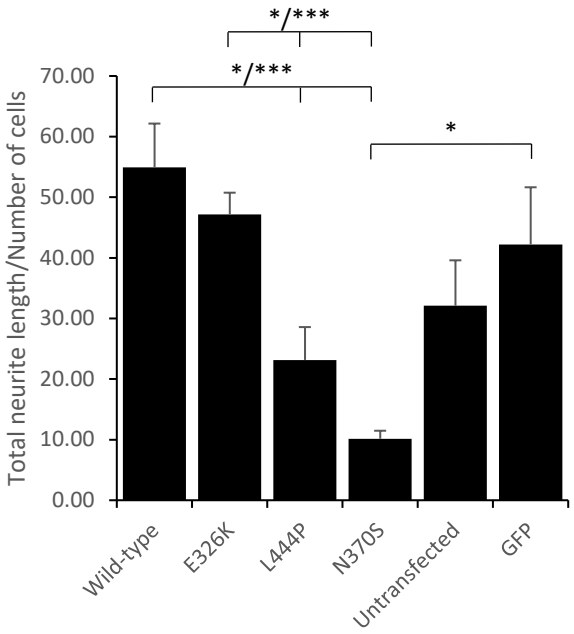
*/***
*/***
*
70.00
60.00
50.00
40.00
30.00
20.00
10.00
0.00
Total neurite length/Number of cells
Wild-type
E326K
L444P
N370S
Untransfected
GFP

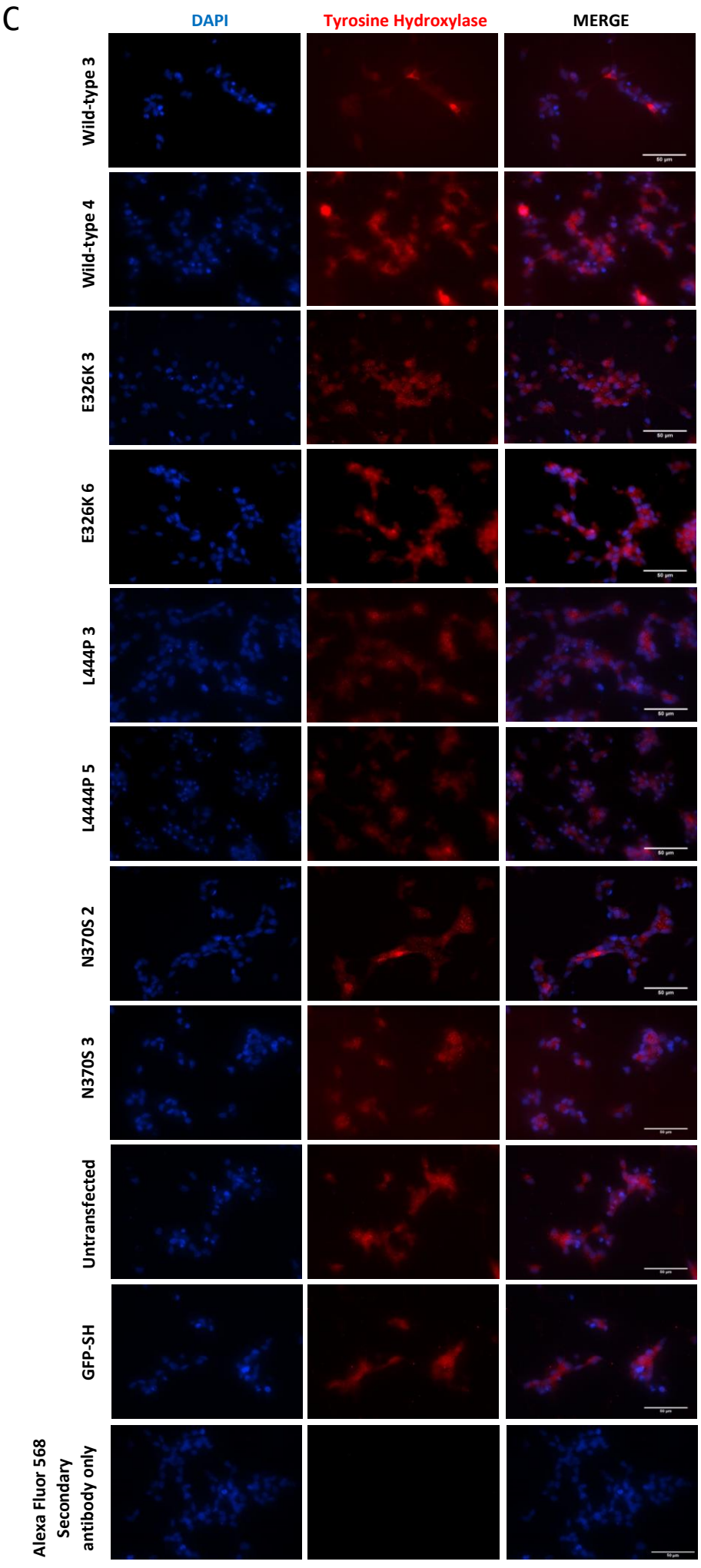
C
DAPI
Tyrosine Hydroxylase
MERGE
Wild-type 3
Wild-type 4
E326K 3
E326K 6
L444P 3
L4444P 5
N370S 2
N370S 3
Untransfected
GFP-SH
Alexa Fluor 568 Secondary antibody only

Figure 45. Immunofluorescence analysis of neuronal markers in differentiated SH-SY5Y cells.

Cells were differentiated for 10 days on coverslips and stained for neuronal markers. One image from each cell line shown. For each experiment, two coverslips were stained for each cell line and three pictures taken per coverslip. **A)** Differentiated SH-SY5Y cells were stained for neuron-specific microtubule protein, β-Tubulin III (green) and DAPI for nuclei staining (blue). Scale bar is 50 μm. **B)** Quantification of neurite length of each differentiated SH-SY5Y cell line. Total neurite length was calculated using the NeuronJ plugin with Fiji for ImageJ and divided by total number of cells for each cell line. Data was pooled and presented per genotype. For each genotype, 250-300 cells were quantified. Two biological replicates and two technical repeats. Error bars show SEM. Statistical test used was one way ANOVA with Tukey post-hoc analysis (*p<0.05; **p<0.01; ***p<0.001). Wild-type vs L444P *p<0.05; Wild-type vs N370S ***p<0.001; E326K vs L444P *p<0.05; E326K vs. N370S ***p<0.001; GFP vs N370S *p<0.05. **C)** Differentiated SH-SY5Y cells were stained for Tyrosine Hydroxylase, a dopaminergic neuron marker (red), and DAPI for nuclei staining (blue). Scale bar is 50 μm.

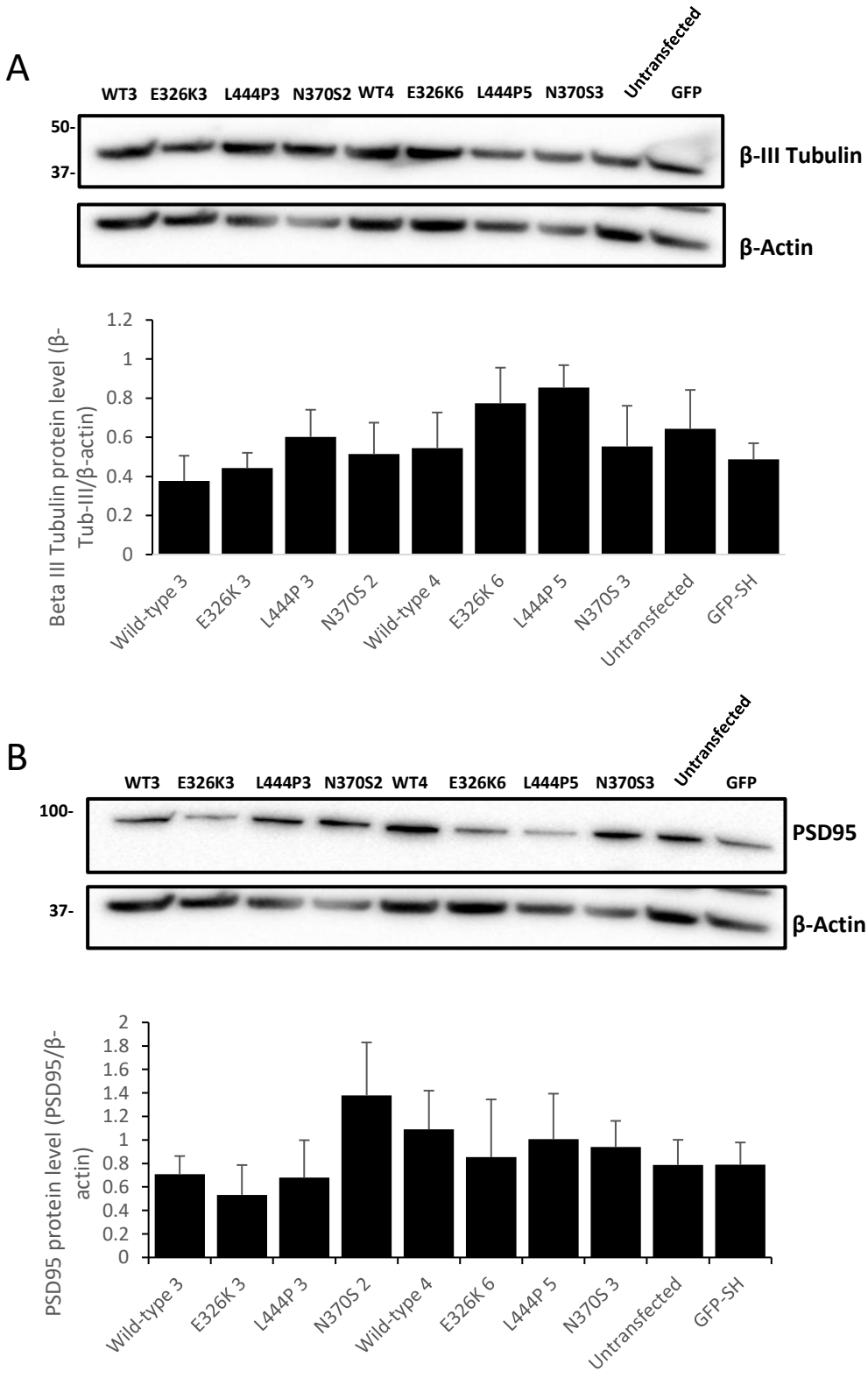

Figure 46. Western blot analysis of neuronal markers in differentiated SH-SY5Y cells.

A) Immunoblot and quantification of post-synaptic protein, PSD95, in differentiated SH-SY5Y neurons. For quantification, band density of each cell line was calculated. Four technical repeats. Error bars show SEM. Statistical test used was one way ANOVA with Tukey post-hoc analysis. **B)** Immunoblot and quantification of neuron-specific microtubule protein, β-Tubulin III, in differentiated SH-SY5Y neurons. For quantification,

band density of each cell line was calculated. Four technical repeats. Graphs show mean and error bars show SEM. Statistical test used was one way ANOVA with Tukey post-hoc analysis.

5.3.2.2 Assessment of GCase protein and transcript level, and activity in differentiated SH-SY5Y cell lines expressing GCase mutants

Levels of GCase protein (Figure. 47A.), mRNA transcript (Figure. 47B.) and activity (Figure. 47C.) in differentiated cells were normalised to untransfected cells. There were minimal changes across all cell lines. Although all cell lines exhibited increased levels compared to untransfected cells, this was not significant in all lines except GCase mRNA transcript of clone N370S 2.

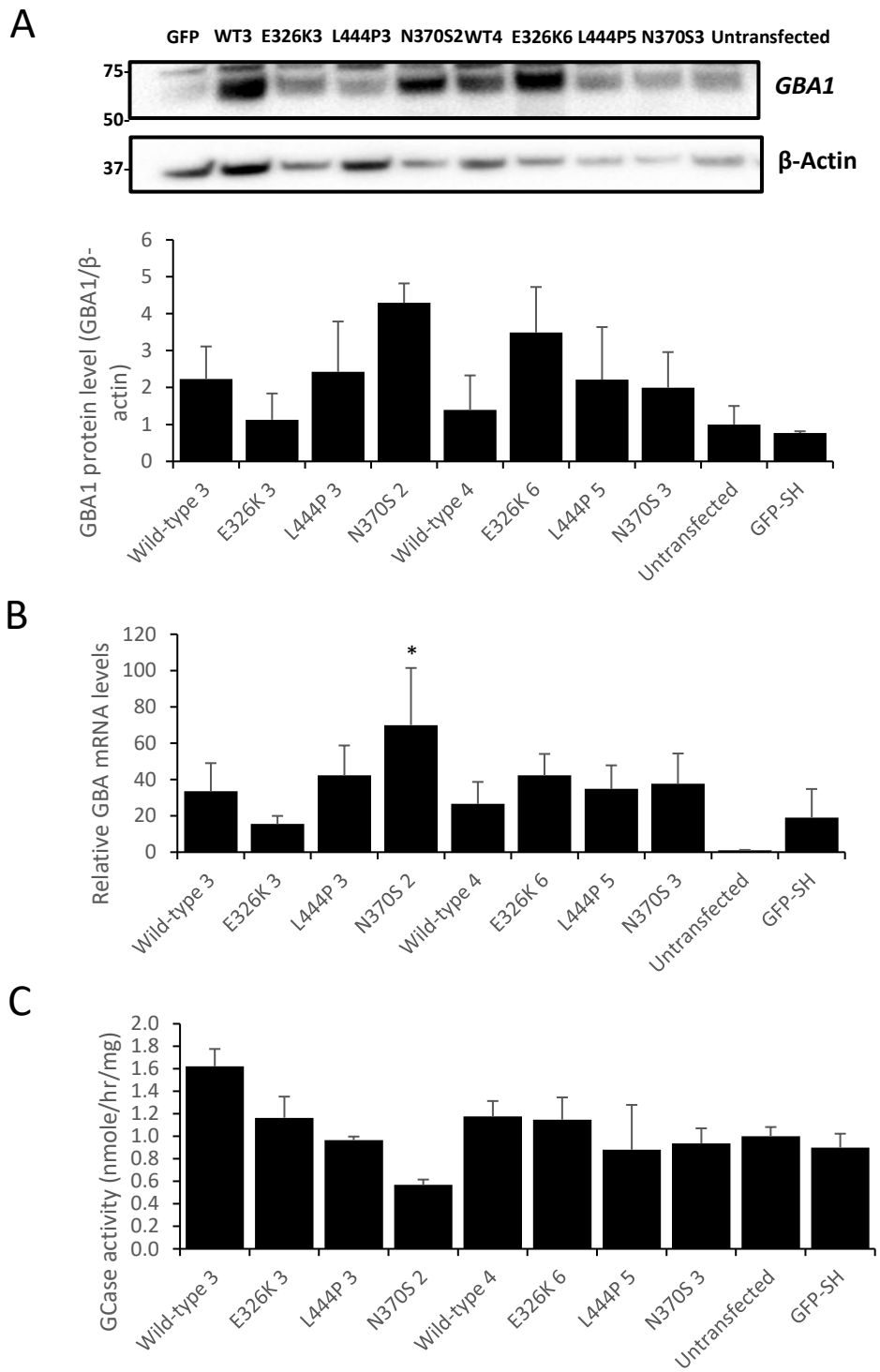

Figure 47. GCase protein, mRNA and activity level in differentiated SH-SY5Y neurons over-expressing mutant GCase.

A) Immunoblot and quantification for *GBA1* protein levels in differentiated SH-SY5Y cell lines. For quantification, band density of each cell line was calculated, pooled and averaged for each genotype. Data normalised to untransfected SH-SY5Y cells band density, which was set at 1. Three technical repeats. Graphs show mean and error bars show SEM. Statistical test used was one way ANOVA with Tukey post-hoc analysis. **B)** Quantification of *GBA1* mRNA levels in differentiated SH-SY5Y cell lines. Two biological repeats were used per cell line and data averaged. Three technical repeats. Data

normalised to untransfected SH-SY5Y cells band density, which was set at 1. Graphs show mean and error bars show SEM. Statistical test used was one way ANOVA with Tukey post-hoc analysis. **C)** GCase activity in nmole/hr/mg in differentiated SH-SY5Y cell lines measured at pH 5.4 with NaT. Two biological repeats were used per cell line and data averaged. Three technical repeats. Data normalised to untransfected SH-SY5Y cells band density, which was set at 1. Graphs show mean and error bars show SEM. Statistical test used was one way ANOVA with Tukey post-hoc analysis.

5.3.2.3 Assessment of overall lysosomal content in differentiated SH-SY5Y cells

To confirm that differentiation did not lead to a change in lysosomal mass, total cellular β-galactosidase and β-hexosaminidase activities were measured (Figure. 48A. and 48B.). Data was normalised to untransfected cells, which was set at 1. Similar to results seen in undifferentiated cells, there was minimal changes to lysosomal hydrolase activities across the cell lines. Western blot analysis of endogenous endolysosomal marker, LAMP1, revealed no marked differences in protein level across all mutant lines (Figure. 48C.). Together, these results suggest that lysosomal content remains unaltered in differentiated SH-SY5Y cells expressing mutant GCase protein.

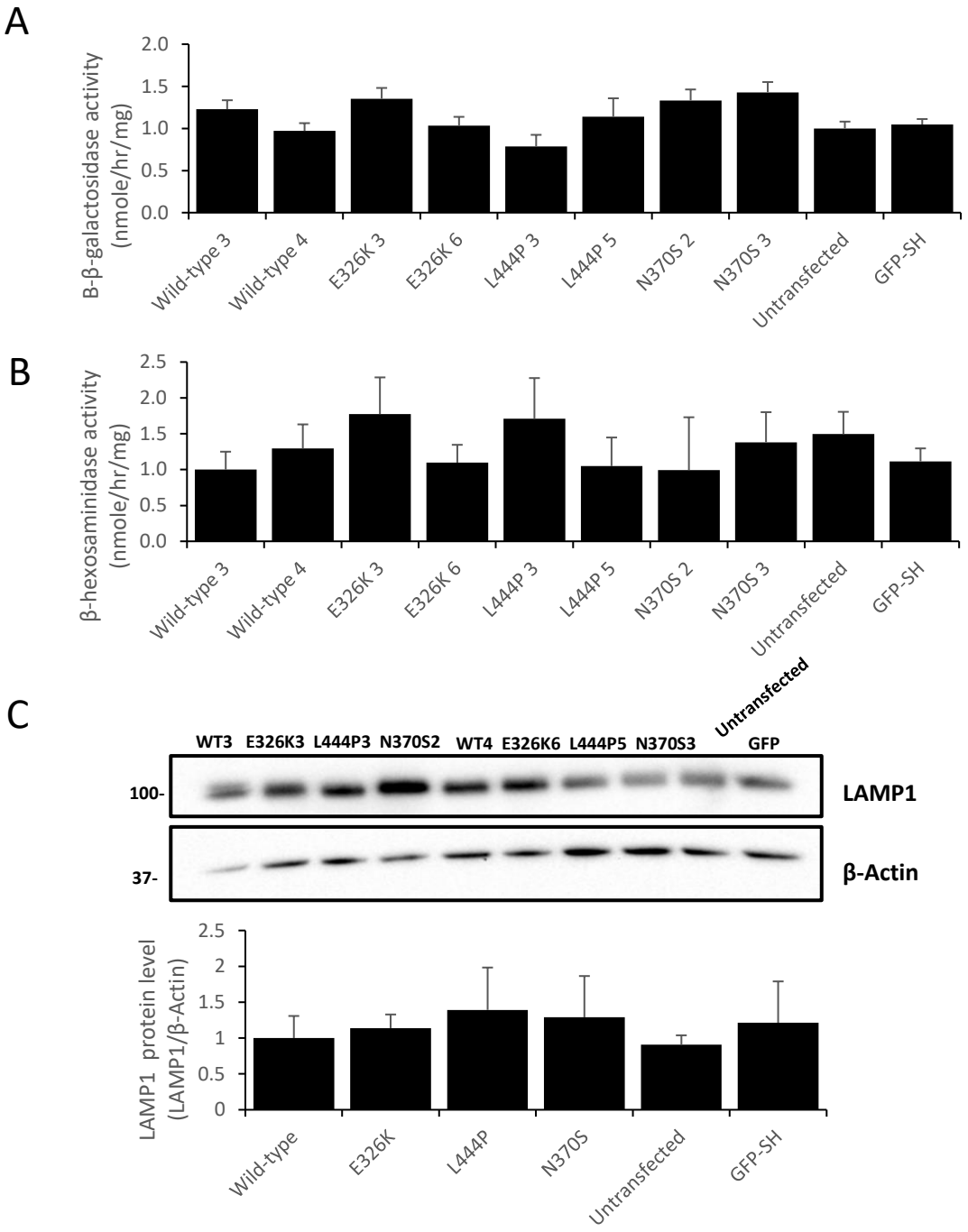

Figure 48. Overall lysosomal content and function in differentiated SH-SY5Y neuronal cells over-expressing mutant GCase.

The activities of lysosomal hydrolases, β-galactosidase and β-Hexosaminidase were measured at pH 5.1 in differentiated SH-SY5Y stable cell lines. For each experiment, two biological repeats were used per cell line. Four technical repeats. Graphs show mean and error bars show SEM. Statistical test used was one way ANOVA with Tukey post-hoc analysis. **A)** β-galactosidase activity in nmole/0.5hr/mg in differentiated SH-SY5Y clones normalised to wild-type cells. **B)** β-Hexosaminidase activity in nmole/0.5hr/mg measured in differentiated SH-SY5Y clones normalised to wild-type cells. (n=3). **C)** LAMP1 levels were measured via western blot to assess the overall endo-lysosomal

content of the differentiated SH-SY5Y cell lines. Immunoblot and quantification for LAMP1 protein level in SH-SY5Y stable cell lines. For quantification, band density of each cell line was calculated, pooled and averaged for each genotype. Data normalised to wild-type SH-SY5Y cells band density, which was set at 1. Four technical repeats. Graphs show mean and error bars show SEM. Statistical test used was one way ANOVA with Tukey post-hoc analysis.

5.3.2.4 ER stress in differentiated SH-SY5Y cells over-expressing GCase mutants

To investigate the effect of *GBA1* mutations on ER stress in differentiated SH-SY5Y neurons, we measured the levels of intracellular ER stress markers and compared these to wild-type cells. Analysis of BiP protein level and *CHOP* transcript level, as was done in undifferentiated SH-SY5Y cells, was repeated. BiP protein levels were measured by western blot and quantified, normalising to wild-type cells, which was set at 1 (Figure. 49A.). There were minimal changes in E326K and N370S mutant lines. In differentiated cells expressing L444P protein, BiP protein level was increased to 2.9 ± 1.98 (***$p<0.001$). This was significantly elevated compared to E326K (**$p<0.01$) and N370S (***$p<0.001$) lines. The level of BiP protein in the GFP control cells was minimally increased compared to wild-type to 1.67 ± 0.29. Analysis of *CHOP* transcript levels revealed a similar pattern to that seen in BiP protein analysis (Figure. 49B.). Data was normalised to wild-type cells which was set at 1 ± 0.36. There was an increase in *CHOP* expression in L444P mutant cells to 9.32 ± 4.45, which was significantly elevated compared to wild-type cells (***$p<0.001$). There was also a 2.65-fold increase in E326K cells; a 3.6-fold increase in N370S cells and a 2.1-fold increase in GFP cells.

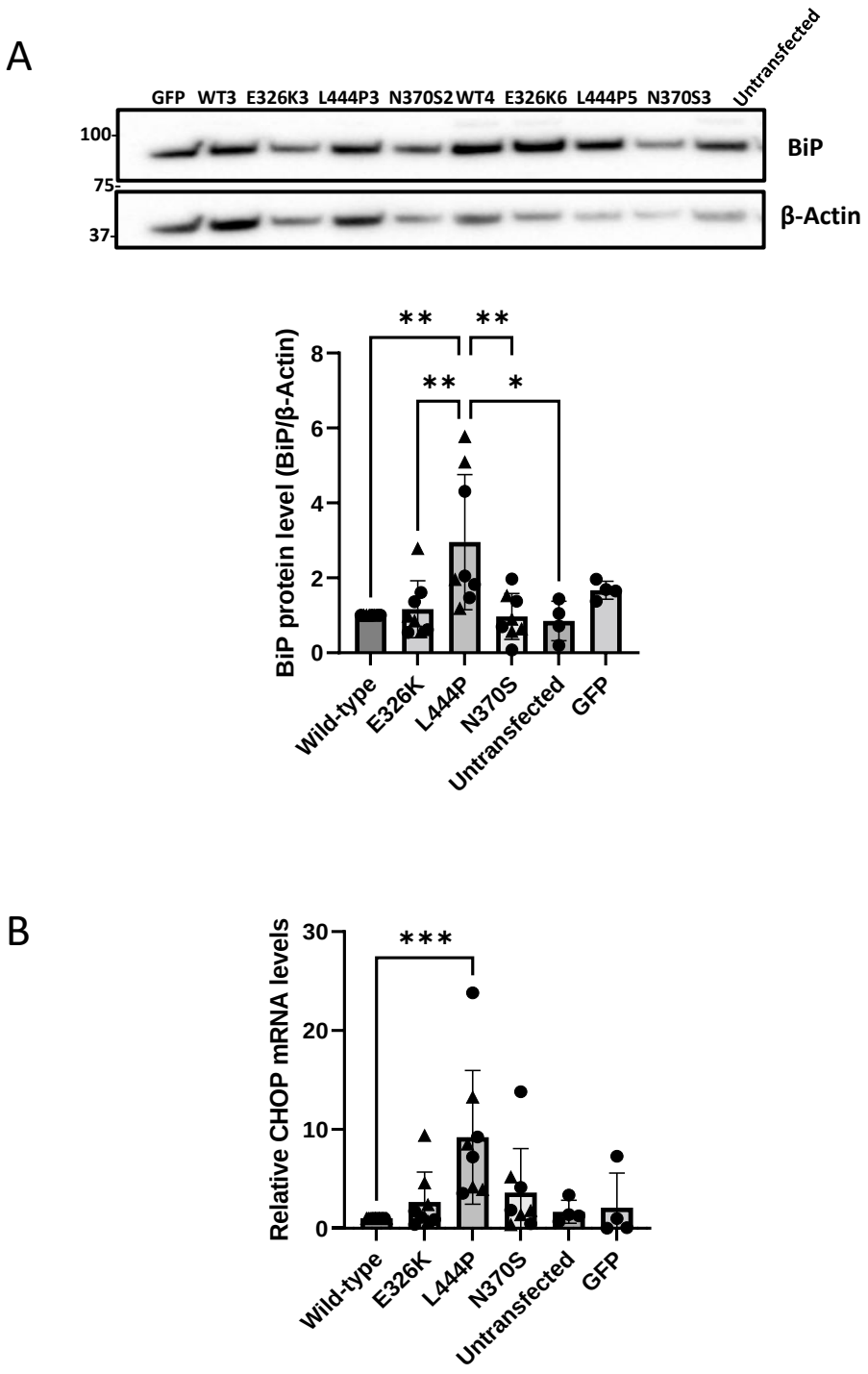

Figure 49. ER stress in differentiated SH-SY5Y neuronal cell lines expressing mutant GCase.

A) Immunoblot and quantification of BiP protein level in SH-SY5Y clones. For quantification, band density of each cell line was calculated, pooled and averaged for each genotype. Data normalised to wild-type SH-SY5Y cells band density, which was set at 1. Three technical repeats. Graph made with GraphPad Prism showing mean and error bars show SEM. Statistical test used was one way ANOVA with Tukey post-hoc analysis. **B)** For each experiment, two biological repeats used for each cell line. For quantification, *CHOP* expression for each cell line was calculated, pooled and averaged

for each genotype. Data normalised to wild-type SH-SY5Y cells, which was set at 1. Three technical repeats. Graph made with GraphPad Prism showing mean and error bars show SEM. Statistical test used was one way ANOVA with Tukey post-hoc analysis.

5.3.2.5 Soluble intracellular alpha-synuclein protein levels in differentiated SH-SY5Y cells over-expressing mutant GCase

To understand how *GBA1* mutations influence the metabolism of intracellular, soluble alpha-synuclein in differentiated SH-SY5Y neuronal cells, level of soluble, monomeric alpha-synuclein was measured by western blot (Figure. 50A.). Immunostaining of alpha-synuclein revealed a double band at 15 kDa in all differentiated SH-SY5Y cells. We included HAP1 parental cells and HAP1 alpha-synuclein knock-out cells as a negative control. The lower second band was not detected in parental or alpha-synuclein knock-out HAPI cells. This extra band might be an alternative alpha-synuclein transcript following differentiation. Differentiating SH-SY5Y alpha-synuclein knock-out cell lines would aid to confirm this. Due to this uncertainty, for quantitative analysis only the density of the top band was normalised to that of wild-type cells (Figure. 50B.). In differentiated cells expressing the L444P variant, soluble alpha-synuclein levels increased from 1 in wild-type cells to 3.86 ± 3.21 (**$p<0.01$). This was also significantly higher than E326K (*$p<0.05$) and untransfected cells (*$p<0.05$). In cells expressing the N370S variant, alpha-synuclein levels were 2.20 ± 0.86. The levels in E326K cells (1.19 ± 0.32) and GFP over-expressing cells (1.49 ± 0.73) were similar to wild-type. Analysis of *SNCA* mRNA transcript levels in differentiated SH-SY5Y cells by qualitative PCR revealed no significant changes in across all cell lines (Figure. 50C.).

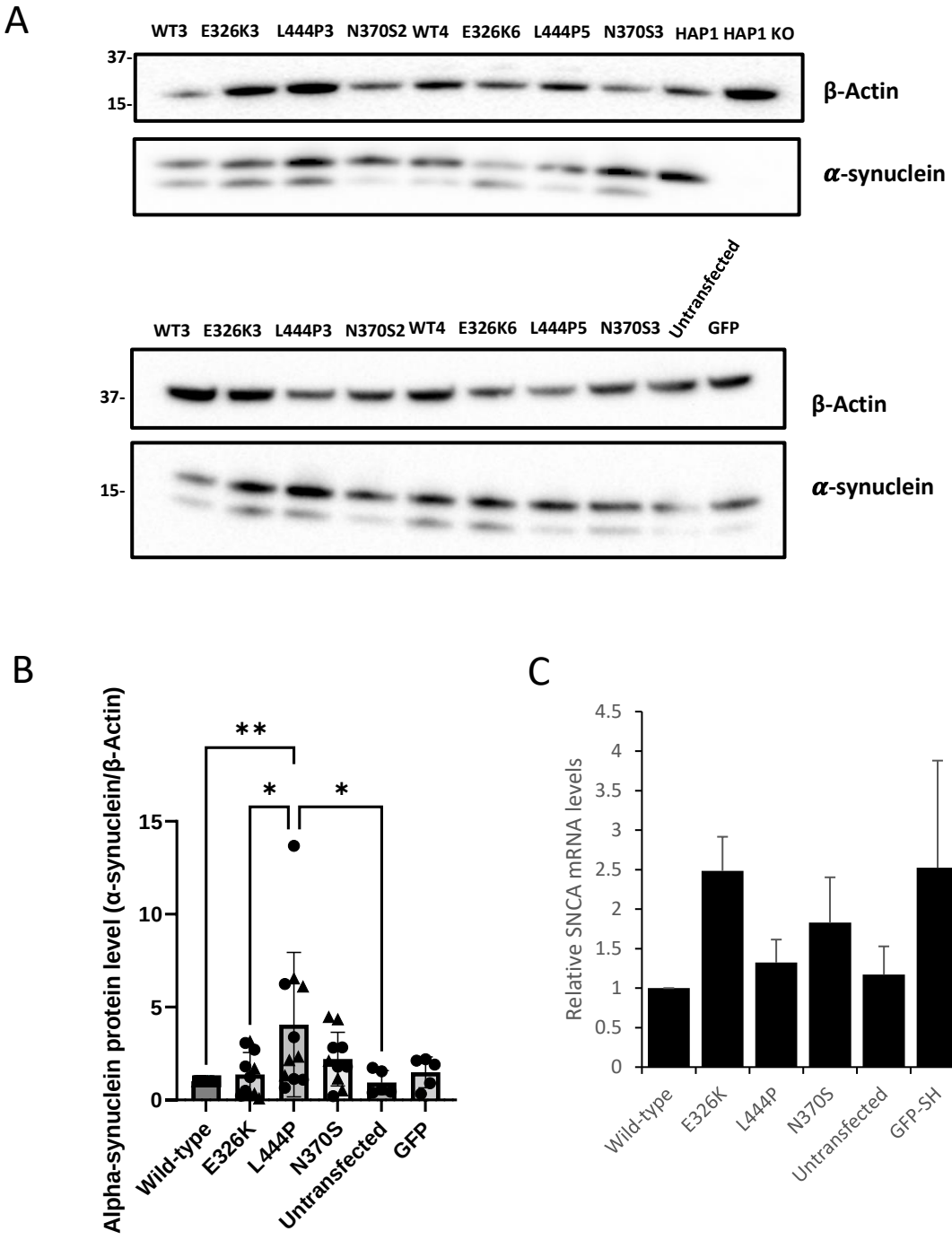

Figure 50. Soluble alpha-synuclein levels in differentiated SH-SY5Y neuronal cell lines expressing mutant GCase.

A) Immunoblot of alpha-synuclein protein level in differentiated SH-SY5Y neuronal cells. **B)** Quantification of alpha-synuclein immunoblotting in differentiated SH-SY5Y. For quantification, band density of each cell line was calculated, pooled and averaged for each genotype. Data normalised to wild-type SH-SY5Y cells band density, which was set at 1. Three technical repeats. Graph was made using GraphPad Prism and shows mean and error bars show SEM. Statistical test used was one way ANOVA with Tukey post-hoc analysis (*p<0.05,

p<0.01). **C) *SNCA* mRNA levels in differentiated SH-SY5Y neuronal cells. For each experiment, two biological repeats used for each cell line. For quantification, *SNCA* expression for each cell line was calculated, pooled and averaged for each genotype. Data normalised to wild-type SH-SY5Y cells, which was set at 1. Three technical repeats. Error bars show SEM. Statistical test used was one way ANOVA with Tukey post-hoc analysis.

5.3.2.6 Analysis of alpha-synuclein aggregation in differentiated SH-SY5Y cells by Cisbio HTRF® alpha-synuclein assay

The Cisbio HTRF® alpha-synuclein kit was employed to investigate the effect of the E326K, L444P and N370S *GBA1* mutations on alpha-synuclein aggregation in differentiated SH-SY5Y cells. Differentiated SH-SY5Y cells were treated on day 3 or 4 with 1 µg/ml PFF for 4 days, and harvested on day 10, where they were subjected to the Cisbio HTRF® aggregation assay. Dilutions were used within the linear range, calculated from undifferentiated SH-SY5Y + PFF analysis. Data was normalised to protein concentration and expressed as the percentage increase of luminescence per mg of protein in PFF-treated cells compared to untreated cells (Figure. 51.). There was no increase in alpha-synuclein aggregation in mutant GCase cell lines compared to wild-type cells. Note that the FRET signal in untreated differentiated cells was at the limit of detection, and in some cases, undetectable. While PFF treatment increased FRET signal above blank it was still relatively low (compared to recombinant PFF alone; Figure. 40.) leading to high variability in data. The cell density needs to be increased in future for more robust detection.

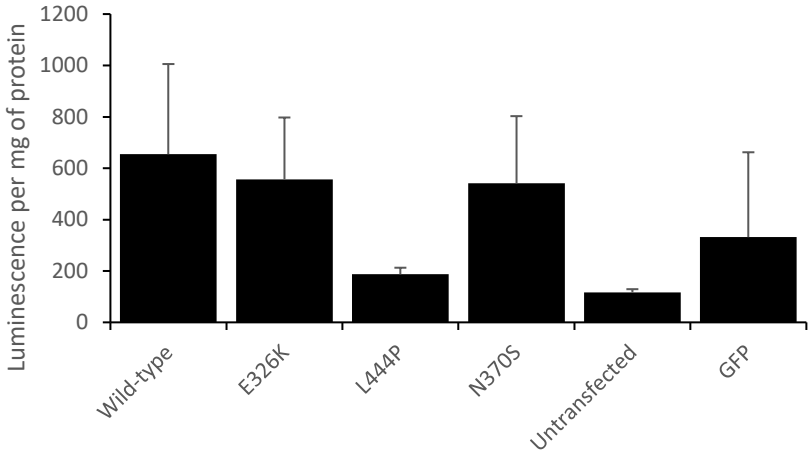

Figure 51. HTRF fluorescence analysis of alpha-synuclein aggregation in differentiated SH-SY5Y neuronal cells over-expressing GCase protein.

Differentiated SH-SY5Y cells were treated for 4 days with 1 µg/µl PFF. Culture media was replaced and cells were grown for another 7 days and harvested. For each experiment, one cell pellet per cell line was lysed and loaded onto the Cisbio HTRF alpha-synuclein aggregation kit. Samples were loaded at dilutions within the linear range (Figure. 39) with one biological repeat per dilution. Luminescence was calculate by the HTRF ratio, which is the ratio between the emission at 665 nm and the emission at 620 nm and normalised to mg of total protein. Data is presented as the percentage increase of luminescence per mg of total protein from untreated to PFF treated cell lines. For each genotype, the percentage increase in luminescence per mg of total protein was pooled and averaged. Three technical repeats. Graph shows mean and error bars show SEM. Statistical test used was one way ANOVA with Tukey post-hoc analysis.

5.3.2.7 Analysis of secretion of alpha-synuclein in differentiated SH-SY5Y cells

Conditioned media from differentiated cells treated with PFFs described above was collected from each. The levels of alpha-synuclein monomers in culture media were analysed using an alpha-synuclein ELISA and the OD was normalised to protein content of the cells in the well (Figure. 52A.). Data was normalised to wild-type GCase cells. The level of alpha-synuclein monomers detected was close to the limit of detection, and in some samples was undetectable. This resulted in large variability between experiments causing large standard errors. Thus, we were unable to conclude whether GCase mutations influence alpha-synuclein secretion in differentiated SH-SY5Y neurons by ELISA. Dot blot analysis of the exosomal marker, ALIX, in conditioned media was also unsuccessful (Figure. 52B.). The level of exosomes in media was below the limit of detection in most differentiated cell lines and I was unable to use this method to conclude how GCase mutations affect exosome release from differentiated SH-SY5Y cells.

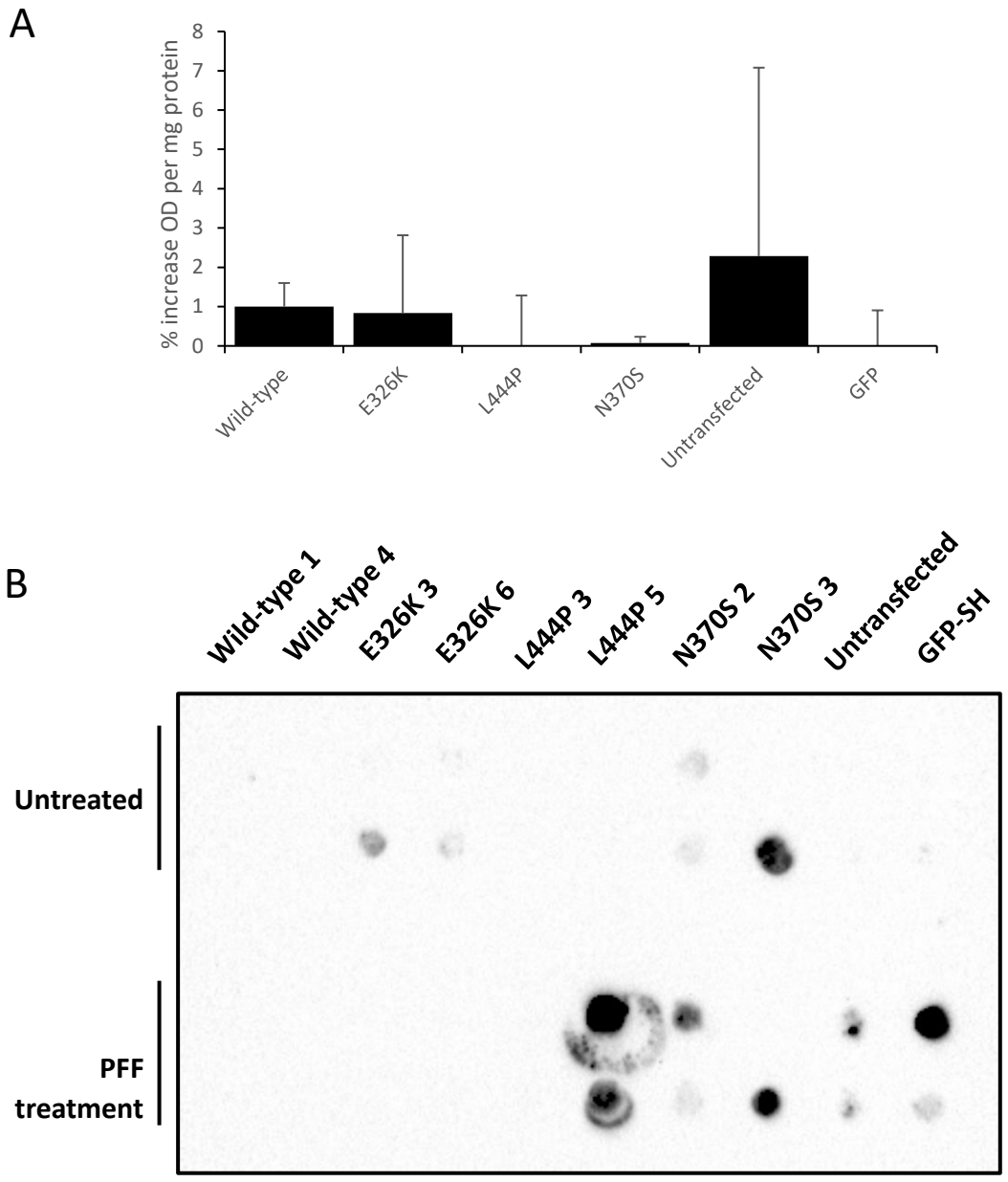

Figure 52. Secretion of monomeric alpha-synuclein from differentiated SH-SY5Y neurons over-expressing mutant GCase protein.

Differentiated SH-SY5Y cells were treated for 4 days with 1 µg/µl PFF. Culture media was replaced and cells were grown for another 7 days where culture media was collected. **A)** Culture media was analysed by an alpha-synuclein ELISA in duplicates, specific against monomeric alpha-synuclein. For each experiment, culture media was collected from one 10 cm plate for each cell line and two biological repeats used. For quantification, an average of the OD per mg protein two repeats was calculated. For each genotype, data from corresponding cell lines were pooled and averaged. Data shown as percentage increase in alpha-synuclein OD per mg protein between untreated and PFF treated cells. Data normalised to wild-type SH-SY5Y cells, which was set at 1. Three technical repeats. Graph shows mean and error bars show SEM. **B)** Culture

media was blotted as duplicates on to a dot blot, vacuum applied and the membrane was immunoblotted with anti-ALIX antibody. For each experiment, culture media was collected from one 10 cm plate for each cell line and three biological repeats used. Three technical repeats. For all repeats, flotillin concentration was below limit of detection.

5.3.3 Induced pluripotent stem cell-derived midbrain dopamine neurons with wild-type, heterozygous E326K and heterozygous N370S genotype

To complete the investigation of how the E326K mutation affects GCase protein and alpha-synuclein, midbrain neuronal cultures differentiated from iPSCs were generated from wild-type fibroblasts and the WT/E326K fibroblast line used in Chapter 3. A heterozygous N370S mutant line was also generated to act as an example of a common pathogenic *GBA1* mutation.

Similar to other studies using the floor plate differentiation model developed by Kriks et al, 30-40% of neurons were TH positive (Kriks et al., 2011). Markers of neurons (β-III tubulin, PSD95) dopaminergic neurons (TH, Nurr1) and substantia nigra A9 DA neurons (GIRK2) were all increased in midbrain cultures versus iPSC (Data from Dr Matt Gegg).

5.3.3.1 Assessment of GCase protein and activity level in iPSC-derived midbrain dopamine neurons

The effect of heterozygous E326K and N370S mutations on GCase function in midbrain dopamine neurons was assessed. First, GCase protein was analysed by western blot (Figure. 53). Quantification of band density revealed that in neurons harbouring the E326K mutation, GCase protein levels were 2.33-fold lower than those in wild-type cells. There was not enough lysate to detect GCase in N370S cells by western blot. The activity of GCase protein in the cells was also analysed at pH 5.4 (Figure. 54A.). As lysosomal content was higher in WT/E326K, when compared to control (Figure. 54B. and 54C.), GCase activity was normalised to the lysosomal hydrolase β-Galactosidase. In MNO (WT/WT) neurons GCase activity was 0.48 ± 0.11 nmole/hr/mg. Although not significant, neurons harbouring the E326K mutation exhibited 1.5-fold decrease in GCase

activity to 0.32 ± 0.09 nmole/hr/mg. A similar reduction was demonstrated in neurons harbouring the N370S variant, which dropped to 0.35 ± 0.01.

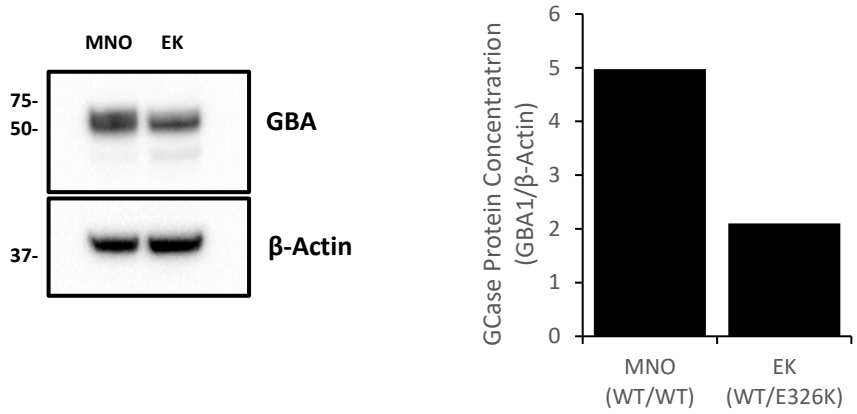

Figure 53. GCase protein level in induced pluripotent stem cell-derived midbrain dopamine neurons.

Immunoblot and quantification of GCase protein level in induced pluripotent stem cell-derived midbrain dopamine neurons harbouring the wild-type genotype and E326K heterozygote genotype. For each experiment, cells were differentiated, pelleted and analysed by western blot and band density quantified. Data shown is from two differentiations.

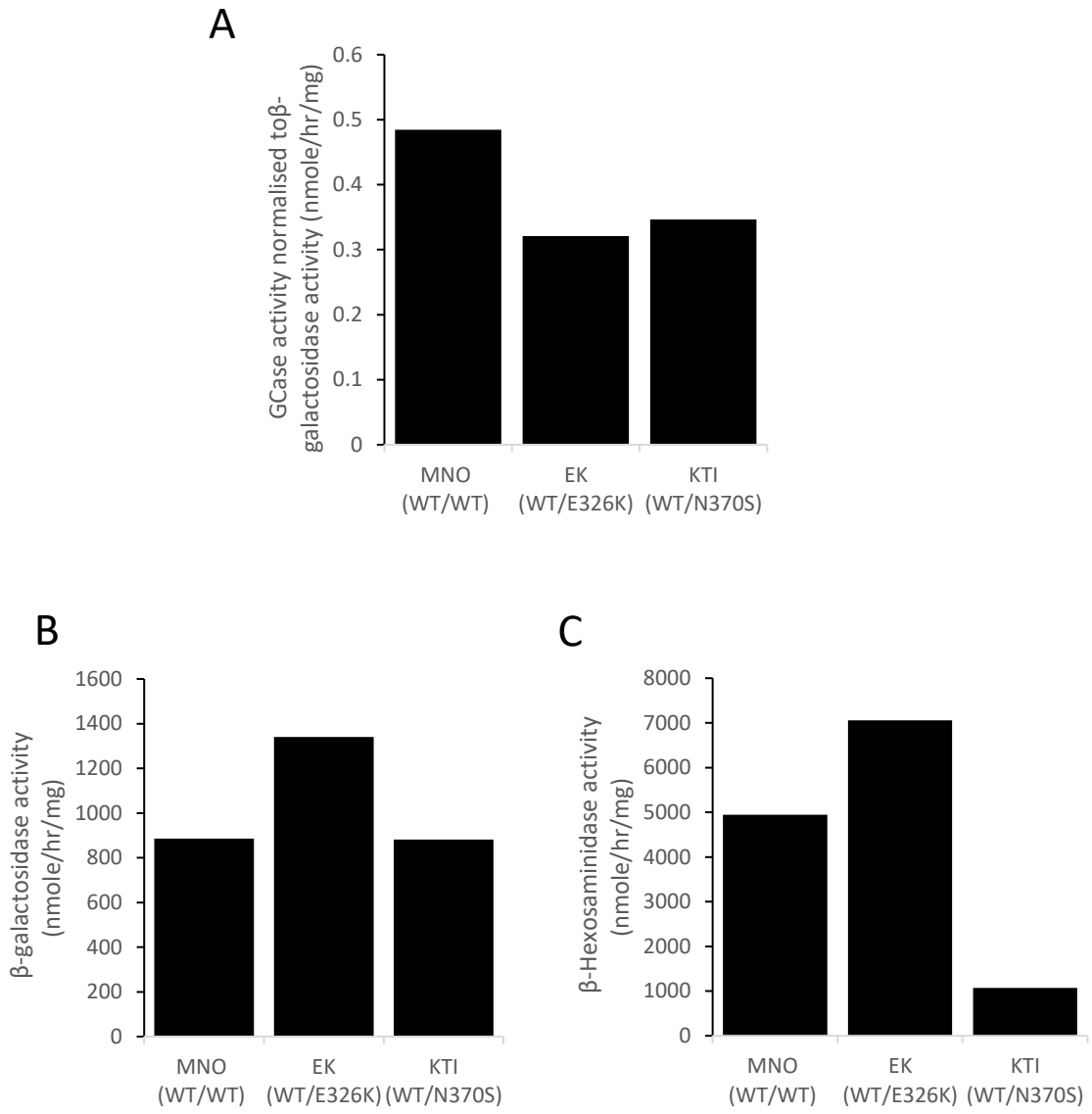

Figure 54. GCase activity in induced pluripotent stem cell-derived midbrain dopamine neurons heterozygous for E326K and N370S GCase mutations.

A) GCase activity was measured at pH 5.4 with NaT and normalised to β-galactosidase activity. For each differentiation, cells were pelleted and loaded as three biological repeats. Activity of repeats were averaged. The data shown is for three differentiations of MNO and EK and one differentiation of KTI. **B)** β-galactosidase activity in mole/hr/mg. For each differentiation, cells were pelleted and loaded as three biological repeats. Activity of repeats were averaged. The data shown is for three differentiations of MNO and EK and one differentiation of KTI. **C)** β-Hexosaminidase activity (nmole/h/mg). For each differentiation, cells were pelleted and loaded as three biological repeats. Activity of repeats were averaged. The data shown is for three differentiations of MNO and EK and one differentiation of KTI.

5.3.3.2 Assessment of soluble intracellular alpha-synuclein protein level in iPSC-derived midbrain dopamine neurons

To further our understanding of how the E326K *GBA1* mutation influences the intracellular accumulation of soluble alpha-synuclein in midbrain dopaminergic neurons, the level of soluble, monomeric alpha-synuclein was assessed by western blot (Figure. 55.). In wild-type neurons, soluble alpha-synuclein levels were 1.52 ± 0.25. In neurons harbouring the E326K mutation, there was an increase to 1.85 ± 0.05. This increase was not significant.

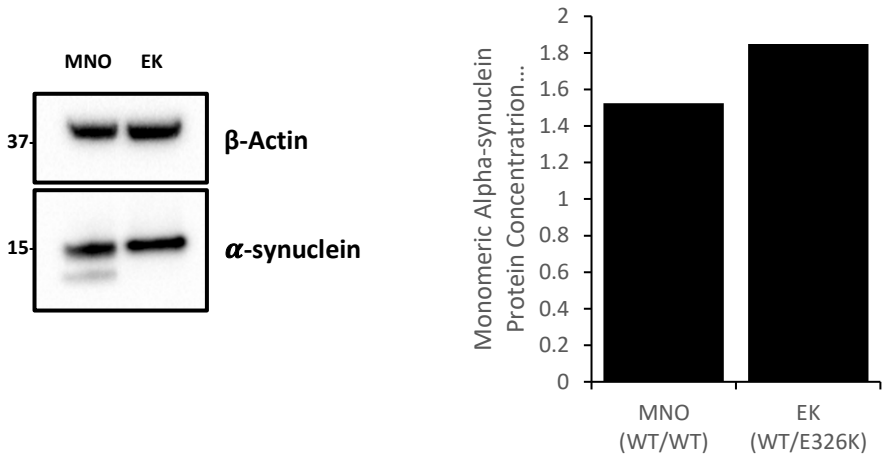

Figure 55. Soluble alpha-synuclein level in induced pluripotent stem cell-derived midbrain dopamine neurons

Immunoblot and quantification of alpha-synuclein protein level in induced pluripotent stem cell-derived midbrain dopamine neurons harbouring the wild-type genotype and E326K heterozygote genotype. For each experiment, cells were differentiated, pelleted and analysed by western blot and band density quantified. Data shown is from two differentiations.

5.3.3.3 Analysis of alpha-synuclein aggregation in iPSC-derived midbrain dopamine neurons by Cisbio HTRF® alpha-synuclein assay

I wanted to investigate whether *GBA1* mutations could induce alpha-synuclein aggregation in midbrain dopamine neurons. Cells were treated with 1 µg/ml PFF for 4 days, media changed and incubated for a further 6 days, with media changes every two days. Harvested cells were lysed and analysed using the Cisbio HTRF® alpha-synuclein kit to detect human alpha-synuclein aggregation though FRET. This was normalised to protein concentration (Figure. 56.). In all cell lines, treatment with PFF caused an increase in alpha-synuclein aggregation. In E326K neurons, this was a significant increase (*$p<0.05$). There was no significant difference between the mutations. Treatment with PFF resulted in similar level of aggregates in wild-type (55778 ± 33674) and E326K (61672 ± 3298) neurons, however the standard error of wild-type data was large. N370S homozygotes exhibited fewer aggregates after PFF treatment (36402 ± 11260) compared to wild-type and E326K neurons.

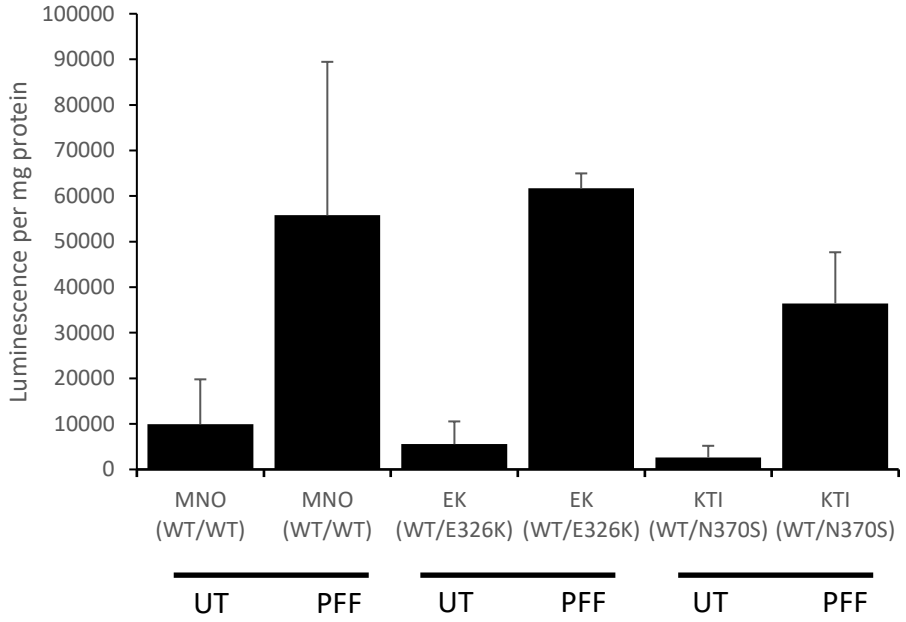

Figure 56. HTRF® fluorescence analysis of alpha-synuclein aggregation in in induced pluripotent stem cell-derived midbrain dopamine neurons

Cells were treated for 4 days with 1 µg/ml PFF. Culture media was replaced and cells were grown for another 6 days and harvested. For each experiment, cells were differentiated and one pellet was lysed and loaded onto the Cisbio HTRF alpha-synuclein aggregation kit. Samples were loaded at dilutions within the linear range (Figure. 39) with one biological repeat per dilution. Three technical repeats were performed. Luminescence was calculated by the HTRF ratio, which is the ratio between the emission at 665 nm and the emission at 620 nm and normalised to mg of total protein.

5.3.3.4 Analysis of release of alpha-synuclein monomers and fibrils from iPSC-derived midbrain dopamine neurons

To investigate whether the E326K mutation influences alpha-synuclein release, the level of alpha-synuclein monomers and aggregates were measured in culture media of iPSC-derived midbrain neurons from control, N370S heterozygous and E326K heterozygous patients. Media was conditioned for 48 hours (day 8-10). Levels of monomeric alpha-synuclein in culture media was measured using an alpha-synuclein ELISA kit (Figure. 57A.). For untreated cells, the level of alpha-synuclein in the media was 13.1 $\pm$ 12.1 ng alpha-synuclein/mg protein for wild-type; 11.6 $\pm$ 6.6 ng alpha-synuclein/mg protein for WT/E326K and 5.5 $\pm$ 9.9 ng alpha-synuclein/mg protein for WT/N370S. Data for each cell line was expressed as a percentage of untreated cells, which were set at 100%. There were no significant increases upon PFF treatment in any cell line, however PFF did induced an increase in monomeric alpha-synuclein release from neurons, although not significantly. Compared to wild-type, which exhibited a 742 ± 461% increase, N370S cells demonstrated a 1117 ± 963% increase in monomeric alpha-synuclein release upon treatment with PFF. In E326K cells, secretion was increased 326 ± 80. Mutant GCase does not increase alpha-synuclein release in midbrain dopamine neurons. More differentiations are needed to repeat analysis and reduce variability between repeats.

To examine the release of alpha-synuclein fibrils from iPSC-derived dopamine neurons, culture media was loaded on to a membrane for analysis by dot blot and immunostained with an antibody specific to alpha-synuclein aggregates (Figure. 57B.), as previous (Gegg et al., 2020). Data was quantified and each cell line expressed as a percentage of untreated cells (100%). Treatment with PFF led to increased release of alpha-synuclein fibrils from control, N370S and E326K cell

lines, with wild-type cells exhibited the highest levels of fibrils in culture media. Similar to monomeric alpha-synuclein levels, E326K released fewer aggregates compared to WT.

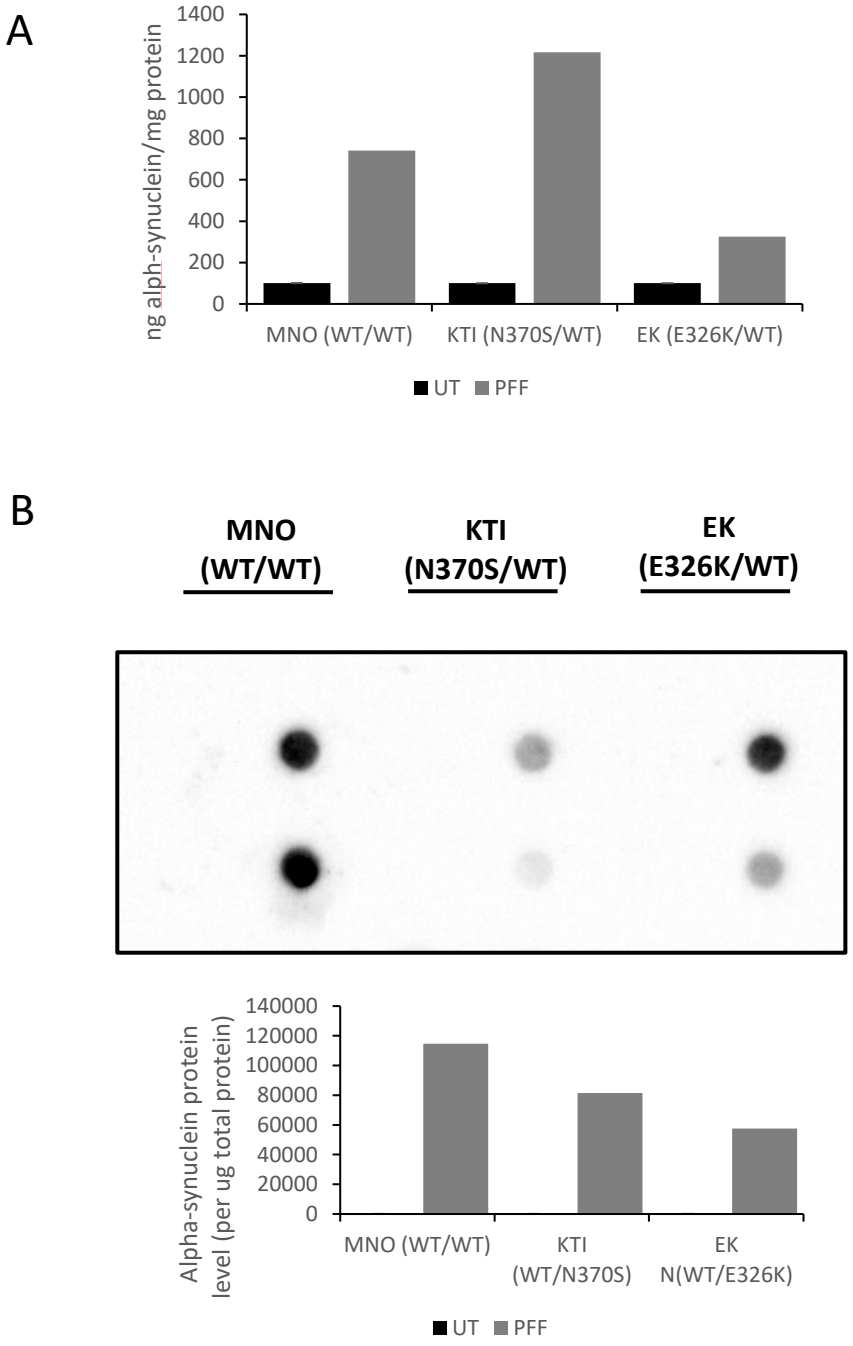

Figure 57. Secretion of monomeric alpha-synuclein from induced pluripotent stem cell-derived midbrain dopamine neurons.

Cells were treated for 4 days with 1 µg/µl PFF. Culture media was replaced and cells were grown for another 7 days where culture media was collected. **A)** Culture media was analysed by an alpha-synuclein ELISA in duplicates, specific against monomeric alpha-synuclein. For each experiment, culture media was collected one plate from one differentiation of each cell line and loaded in two biological repeats. For quantification, an average of the OD per mg protein two repeats was calculated. Data shown as a percentage of untreated (UT) cells, expressed as 100. Data shown from two differentiations. **B)** Culture media was blotted as duplicates on to a dot blot, vacuum

applied and the membrane was immunoblotted with antibody specific against alpha-synuclein fibrils and quantification. For each experiment, culture media was collected one plate from one differentiation of each cell line and loaded in two biological repeats. For quantification, the density for each dot was averaged per cell line and expressed per µg of total protein. Data shown from two differentiations.

5.4 Discussion

The main aim of this chapter was to understand how the E326K, L444P and N370S *GBA1* mutations influence the metabolism and turnover of alpha-synuclein to induce pathology. This was evaluated by investigating pathways involved with lysosomal dysfunction, ER stress and lipid metabolism. A summary of the findings in this chapter can be found in Table. 16. The results demonstrate that the E326K mutation does not significantly induce lysosomal dysfunction or ER stress, but is associated with altered lipid metabolism which may underlie the increase of insoluble alpha-synuclein aggregates in proliferating SH-SY5Y cells. The L444P mutation leads to ER stress and accumulation of soluble and insoluble alpha-synuclein. On the other hand, N370S mutations do not significantly influence the ER stress response or assembly of insoluble alpha-synuclein aggregates. These results support the hypothesis that the pathology of different *GBA1* mutations may be multifaceted, with different pathways associated with each mutation, leading varying degrees of alpha-synuclein pathology.

Table 16. Summary of main findings in Chapter 5.

Arrows indicate either an increase (↑) or decrease (↓) compared to wild-type. (-) denotes unchanged. (n.d) indicates no data. Undiff refers to undifferentiated; Diff refers to differentiated. (*p<0.05; **p<0.001; ***p<0.001, ****p<0.001).

Mutation		GCase			Lysosomal content	Alpha-synuclein			ER stress	Lipid droplets	
		mRNA	Protein level	Activity		Soluble monomer	Insoluble oligomer	Secretion		Basal condition	+ OA
E326K	Undiff SH-SY5Y cells	-	-	-	-	-	↑ *	-	-	↑ **	↑ *
	Diff SH-SY5Y cells	-	-	-	-	-	n.d	n.d	-	n.d	n.d
	Midbrain dopamine neurons	n.d	-	-	-	-	n.d	-	n.d	n.d	n.d
L444P	Undiff SH-SY5Y cells	-	↓ *	↓ *	-	↑ **	↑ *	-	↑ ****	↑ *	-
	Diff SH-SY5Y cells	-	-	-	-	↑ **	n.d	n.d	↑ **	n.d	n.d
	Midbrain dopamine neurons	n.d	n.d	n.d	n.d	n.d	n.d	n.d	n.d	n.d	n.d
N370S	Undiff SH-SY5Y cells	-	-	↓ **	-	-	-	-	-	-	-
	Diff SH-SY5Y cells	-	-	-	-	-	n.d	n.d	-	n.d	n.d
	Midbrain dopamine neurons	n.d	n.d	-	n.d	n.d	n.d	-	n.d	n.d	n.d

5.4.1 Characterisation of SH-SY5Y cells over-expressing mutant GCase

As *GBA1*-PD is characterised by the selective degeneration of dopamine neurons in the SNpc and the presence of widespread alpha-synuclein pathology (Neumann et al., 2009), it was crucial to generate a reliable and well-established neuronal model capable of recapitulating these aspects of *GBA1*-PD pathology. Although patient-derived fibroblast cultures from GD and *GBA1*-PD patients represent a model of primary human cells, which comprise the chronological and biological aging of patients according to their genetic predisposition and environmental etiopathology, these cells do not store lysosomal substrate and GSLs, or express detectable levels of alpha-synuclein, nor do they exhibit the highly sophisticated vesicle/receptor/ion channel control that is seen in neurons (Auburger et al., 2012).

The well-established neuronal cell model, the neuroblastoma SH-SY5Y cell line, was therefore utilised. This line is a thrice cloned subline of SK-N-SH cells, which was originally established in 1970 from a bone marrow biopsy of a neuroblastoma patient (Biedler et al., 1978). This cell line is used frequently to model disease as it is of human origin, catecholaminergic and has neuronal properties such as neuronal marker enzyme activity (tyrosine and dopamine-β-hydroxylases), specific uptake of noradrenaline and exhibits neurofilament proteins and nerve growth factor receptors (Xie et al., 2010, Xicoy et al., 2017). Previous published work supports the usefulness of SH-SY5Y neuroblastoma cell lines as a powerful and non-invasive way to investigate PD. These cells have been used to model *GBA1*-PD and investigate the link between *GBA1* mutations and alpha-synuclein (Bae et al., 2015, Maor et al., 2019). Additionally, other mutations associated with familial PD have been successfully modelled in SH-SY5Y cells including *SNCA* (Melo et al., 2017), *PINK1* (Michiorri et al., 2010) and *LRRK2 (*Wang et al., 2012).

An over-expression model should be appropriate as my fibroblast data suggests that E326K is likely a gain of function mutation (Chapter 3.), and previous literature demonstrates that both L444P and N370S have gain of function mechanisms, through activation of the UPR (Bendikov-Bar et al., 2011, Sanchez-Martinez et al., 2016, Fernandes et al., 2016).

It was expected that the L444P and N370S mutations would express lower levels of GCase, as the fibroblast studies demonstrated a significant loss in protein and transcript level. In this model, both L444P and N370S clones expressed lower levels of GCase protein compared to wild-type, but to a lesser extent than anticipated likely due to this being an over-expression model. The SH-SYSY clones also retain endogenous GCase activity (Figure 33.).

Although undifferentiated SH-SY5Y neuroblastoma cells provide a good model to study *GBA1*-PD, using immortalised cells makes it difficult to reproduce the same morphology and physiology of a neuronal cell phenotype, as the cells as continuously dividing (Falkenburger and Schulz, 2006). Furthermore, it has been suggested that cell cycle arrest may make cells more sensitive to aggregation of proteins, such as alpha-synuclein (Hasegawa et al., 2004), which may make it easier to investigate the relationship between GCase and alpha-synuclein. I therefore differentiated SH-SY5Y neuroblastoma cells into neurons as described previously (Gegg et al., 2020). Upon differentiation, cell proliferation is halted and cells become morphologically and biochemically similar to living neurons in the human brain. Many papers also state that differentiation of SH-SY5Y cells leads to a dopaminergic phenotype, which is important as dopamine neurons in the SNpc are the vulnerable neurons in PD (Xicoy et al., 2017).

Following differentiation, SH-SY5Y cells became morphologically similar to mature neurons (Figure. 44.), as previously described (Gegg et al., 2020, Shipley et al., 2016, Kovalevich and Langford, 2013), in addition to abundantly expressing markers specific to mature dopamine neurons (Figure. 45. And 46.) (Murillo et al., 2017). Staining the cells with β-III-Tubulin allowed visualisation of neurites and enabled the quantification of neurite length to assess whether *GBA1* mutations affect neuritogenesis of differentiated SH-SY5Y cells. Quantification of neurite length revealed significant reductions in differentiated cells expressing L444P and N370S GCase protein, suggesting that these mutations may lead to neurite outgrowth deficits. This observation is supported by a recent study demonstrating a 31% reduction in neurite outgrowth of N370S *GBA1*-PD dopamine neurons (Bogetofte et al., 2021). Administration of a GCase-specific small molecular chaperone was able to rescue the neuritogenesis deficits in the previous study, suggesting a potential role for GCase in neurogenesis. However, impaired neurite growth has also been observed in neurons harbouring other PD mutations including *SNCA* triplication (Oliveira et al., 2015) and LRRK2 (Borgs et al., 2016), indicating that this phenotype could be a characteristic for PD in general. Impaired neurite growth has previously been associated with autophagic defects which may explain these observations (Chen et al., 2013, Ban et al., 2013). Furthermore, as E326K neurite growth is minimally altered compared to wild-type, this supports the hypothesis that the E326K mutation behaves differently to the common *GBA1* loss of function mutations

This differentiation protocol induces the expression of TH (Gegg et al., 2020). However, we were unable to detect strong TH expression via both western blot and quantitative PCR to compare to undifferentiated cells. Further characterisation of dopamine neuron markers could include analysing increases

in dopamine transporter (DAT) and dopamine receptor 2 and 3 subtypes (D2R and D3R) expression (Presgraves et al., 2004). Future confirmation of a neuronal phenotype should also include electrophysiology of undifferentiated and differentiated SH-SY5Y cells. There is evidence that differentiated SH-SY5Y cells are more excitable, with increased membrane potential compared to untransfected cells (Brown et al., 2005, Tosetti et al., 1998, Akerman et al., 1984). Patch-clamp electrophysiology should be employed to investigate the electrical properties of the cells. A previous study has demonstrated that compared to undifferentiated SH-SY5Y cells, differentiated cells exhibited prominent inward Na^+ currents (Şahin et al., 2021). Furthermore, atomic force microscopy (AFM) allows measurements to compare biochemical properties, giving information surrounding the elasticity of cells. Neurons are expected to be stiffer as neuroblastoma cells are cancer cells and therefore have disorganised actin fibrils and microtubules (Lekka, 2016). In undifferentiated SH-SY5Y cells, a larger outward K+ current would also be expected, as this is characteristic of cancer cells (Şahin et al., 2021).

Correct lysosomal function is critical for effective degradation by the ALP. There are several lysosome-resident hydrolases that aid with degradation (Westbroek et al., 2011). We therefore assessed how *GBA1* mutations influence lysosomal function in neuronal cells.

First, GCase function was analysed, revealing minimal changes in mRNA transcript level across undifferentiated and differentiated cells (Figure. 33A. and 47B). Although GCase protein level was lower in undifferentiated cells expressing L444P and N370S GCase (Figure. 33B.), there were minimal changes in differentiated cells (Figure. 47A). Compared to wild-type, undifferentiated cells expressing E326K mutant exhibited similar activity, with L444P and N370S

activities significantly lower than both wild-type and E326K (Figure. 33A.). These findings were expected as in a previous study over-expressing N370S and L444P GCase in transgenic flies, no significant alteration in transcript and protein level was found however there was a significant reduction in activity (Sanchez-Martinez et al., 2016). Furthermore, over-expression of wild-type and L444P GCase in SH-SY5Y neuroblastoma cells also demonstrated minimal changes in L444P protein compared to wild-type, with activity reduced but not significantly (Li et al., 2019). As a future prospective, an improved model would be to perform genome editing to model PD in SH-SY5Y neurons. Gene editing techniques such as the clustered regularly interspaced short palindromic repeats (CRISPR)/CRISPR-associated protein (Cas) system have been used to model PD (Cota-Coronado et al., 2020). This technique relies on accurately targeting a specific nucleotide sequence in the gene of interest. The CRISPR/Cas9 system employs the Cas9 nuclease guided by small RNAs, for a highly specific and efficient gene editing technique with high throughput (Ran et al., 2013). This system has been shown to be capable of introducing point mutations into the *GBA1* gene in human embryonic stem cells (Hanss et al., 2020) and LRRK2 mutations in marmoset embryonic and induced pluripotent stem cells to model PD (Vermilyea et al., 2020).

These data support the hypothesis that both loss of function and gain of function mechanisms may underlie the pathology of individual mutations, and that the E326K mutation does not behave in the same way as common loss of function mutations, L444P and N370S. There were no significant changes in lysosomal content or activity of lysosomal hydrolases, β-galactosidase and β-hexosaminidase, in both undifferentiated and differentiated SH-SY5Y cells (Figure. 34. And 48.). These data suggest that any lysosomal dysfunction is

induced by defective GCase and not through overall dysfunction of the lysosomal pool.

I further investigated the mechanisms underlying the E326K mutation in midbrain dopamine neurons derived from iPSCs. These cells were utilised to corroborate findings in the SH-SY5Y models. This will allow understanding of how the endogenous mutant protein behaves in a model of the specific cells vulnerable to degeneration in PD. Interestingly, the findings suggest that the E326K mutation may be more deleterious to GCase expression and activity in midbrain dopamine neurons, exhibiting a 1.7-fold reduction in protein level (Figure. 53.) and a 1.5-fold reduction in GCase activity (Figure. 54.), although not significant. No previous studies have investigated E326K activity in these neurons to corroborate findings. Hence, we employed the heterozygous N370S line as an example of a well-known, pathogenic *GBA1* mutation. It is known that the N370S mutation is associated with a reduction in GCase activity and lysosomal dysfunction in iPSC-derived neurons (Fernandes et al., 2016), and our findings corroborated this. To confirm the E326K findings, more differentiated E326K clones are required to repeat analysis. These should include both heterozygous and homozygous lines to allow comparison of how the zygosity of E326K mutations affect GCase protein in a cellular environment of midbrain dopamine neurons.

A more detailed investigation in to how *GBA1* mutations, specifically E326K, affect lysosomal dysfunction would be to assess markers of defective ALP. A previous study in fibroblasts, harbouring heterozygous mutations for L444P and N37S0S, demonstrated a reduction in GCase activity was accompanied by increased β-galactosidase activity and increased lysosomal content, suggesting an accumulation of dysfunctional lysosomes due to impaired lysosomal recycling (Magalhaes et al., 2016). Similarly, in dopamine neurons with L444P and N370S

mutations, reduced activity is accompanied by increased lysosomal number and size and impaired autophagy (Schöndorf et al., 2014). A fully functioning, healthy pool of lysosomes is required for adequate clearance of proteins by autophagy, including alpha-synuclein. Macroautophagy and CMA play a key role in the regulation of alpha-synuclein turnover (Cuervo et al., 2004, Martinez-Vicente and Cuervo, 2007). Defective ALP may also lead to the accumulation of lipids, through inadequate degradation (Parzych and Klionsky, 2014). In dopamine neurons derived from iPSCs harbouring L444P and N370S mutations, impaired lysosomal and autophagic mechanisms were accompanied by alpha-synuclein pathology (Schöndorf et al., 2014, Fernandes et al., 2016). Understanding how the E326K mutation influences the ALP, in comparison to L444P and N370S, would shed light on the underlying pathways specific to *GBA1*-PD.

5.4.2 *GBA1* mutations and alpha-synuclein metabolism

Impairment of ALP function can lead to alpha-synuclein accumulation in PD (Alvarez-Erviti et al., 2010). There have been several models of *GBA1*-PD that have demonstrated ALP dysfunction accompanied by alpha-synuclein accumulation (Bae et al., 2015, Fernandes et al., 2016, Schöndorf et al., 2014). The assembly of accumulated alpha-synuclein monomers into toxic oligomers and fibrils, which are eventually deposited into Lewy body inclusions, is a major hallmark of *GBA1*-PD and sporadic PD (Neumann et al., 2009). I therefore set out to assess how the E326K, L444P and N370S mutations influence alpha-synuclein pathology in human cells, whilst correlating the loss of function and gain of function mechanisms associated with the individual mutations.

Although the E326K mutation was not associated with an accumulation of monomeric, soluble alpha-synuclein in undifferentiated (Figure. 36.) and differentiated cells (Figure. 50.), it did induce a 2.86-fold increase in insoluble,

HMW alpha-synuclein species in proliferating cells (Figure. 37.). In iPSC-derived midbrain dopamine neurons, alpha-synuclein monomers were minimally increased however, time did not allow for the analysis of insoluble alpha-synuclein in these cells (Figure 55.). As E326K function is reduced more in midbrain neurons compared to the SH-SY5Y models, it could be hypothesised that alpha-synuclein pathology may be greater in midbrain neurons, possibly leading to higher levels of insoluble alpha-synuclein. The increase in insoluble alpha-synuclein in E326K cells was similar to that observed in L444P cells (2.86-fold).

The L444P mutation was expected to induce an increase in alpha-synuclein accumulation, as previous studies in SH-SY5Y neuroblastoma cells and dopamine neurons expressing this mutant exhibit increased alpha-synuclein levels (Maor et al., 2019, Zunke et al., 2018, Schöndorf et al., 2014). Evidence of increased insoluble aggregates was also anticipated as the L444P mutation has been shown to accelerate alpha-synuclein pathology and spread in mouse brains (Migdalska-Richards et al., 2020, Yun et al., 2018). This propagation of pathology was accompanied by a decrease in GCase activity, however as alpha-synuclein pathology has been shown to not correlate with GCase activity in PD primary neurons and transgenic mice (Henderson et al., 2020), and increased aggregates in E326K cells are observed, a loss of GCase function may not be solely responsible. Furthermore, the observation that the level of insoluble alpha-synuclein aggregates is similar in the E326K risk variant and the L444P pathogenic variant may underlie the disease severity and fast progression demonstrated in PD patients with these mutations (Stoker et al., 2020b, Davis et al., 2016, Sidransky et al., 2009). Surprisingly, there was no significant elevation in either soluble or insoluble alpha-synuclein in N370S mutants. This was

unexpected as in SH-SY5Y neuroblastoma cells and human dopamine neurons this mutation has been shown to induce alpha-synuclein accumulation, although to a lesser extent to L444P (Zunke et al., 2018, Maor et al., 2019). However, in another study although an increase in alpha-synuclein was demonstrated in L444P heterozygous dopamine neurons, the same was not observed in N370S heterozygotes (Schöndorf et al., 2014) even though they exhibited a similar decline in activity, like the SH-SY5Y cells.

As there is very little literature surrounding the pathogenesis of the E326K mutation and the involvement of alpha-synuclein, I sought to further characterise alpha-synuclein pathology in cells harbouring this mutation. The ThT assay was utilised in an attempt to characterise aggregation (Figure. 39.). It was expected that the E326K and L444P mutations would accelerate the formation of aggregates in cells, due to the presence of insoluble aggregates. This assay has been performed previously on recombinant alpha-synuclein protein incubated with fibroblast-derived lipids (Galvagnion et al., 2020). Unfortunately, the findings suggests that a minimum of 25 μM alpha-synuclein monomers are required for a robust response, which is far more than can be obtained from cell lysate. Further, analysis of SH-SY5Y cell lysate suggests that a component of cells may interfere with ThT binding, preventing a fluorescence response. This points toward ThT being more beneficial for detection of *in vitro* amyloid formation of recombinant protein. Similarly to ThT, thioflavin S (ThS) is another dye that binds to β-sheet rich amyloid fibrils and gives a distinct increase in fluorescence emission. However unlike ThT, ThS does not produce a characteristic shift in the excitation or emission spectra (LeVine, 1999), and is instead used mainly to stain amyloids in tissue and cell culture for imaging alpha-synuclein aggregates by fluorescence microscopy (Melnikova et al., 2020, Stojkovska and Mazzulli, 2021, Creed and

Goldberg, 2019). It has also been previously suggested that coupling of ThS fluorescence with flow cytometry provides a quantitative method to detect the aggregation of amyloid-like conformations *in vivo* (Espargaró et al., 2012). ThS analysis is a potential avenue to explore in future studies.

The Cisbio HTFR® kit failed to measure an aggregation response in undifferentiated SH-SY5Y cells (Figure. 40.). As the presence of alpha-synuclein PFFs seemed to be required for a robust response, differentiated cells and midbrain dopamine neurons were treated with PFFs (Figure. 51. and 56). Alpha-synuclein PFFs have been shown to induce the self-assembly of endogenous alpha-synuclein when applied exogenously to SH-SY5Y cells, enhancing pathology (Sang et al., 2021), and thus it was hypothesised that this would enable easier analysis of alpha-synuclein pathology. Surprisingly, data from differentiated SH-SY5Y neurons did not exhibit an increase in aggregation in E326K mutants, however analysis of aggregation in midbrain dopamine neurons demonstrated a significant elevation in aggregation following PFF treatment in E326K mutants. This suggests that the E326K mutation may make neurons more vulnerable to alpha-synuclein pathology induced by extracellular fibrils. As treatment with PFFs has been shown to increase the levels of insoluble alpha-synuclein in differentiated SH-SY5Y cells (Gegg et al., 2020), this would be an invaluable avenue to follow in E326K neurons.

To further characterise the influence of E326K GCase on alpha-synuclein pathology, the levels of insoluble, p-S129-alpha-synuclein, should be measured. P-S129-alpha-synuclein has been reported to enhance alpha-synuclein toxicity both *in vivo* and *in vitro* (Fujiwara et al., 2002), possibly though accelerating the formation of alpha-synuclein aggregates, as it has been shown previously to increase upon administration of PFFs in mouse cortical neurons and

differentiated SH-SY5Y cells (Gegg et al., 2020). Levels of phosphorylated alpha-synuclein can be measured via western blotting (Gegg et al., 2020) and immunofluorescence analysis (Smith et al., 2005). In addition to analysing p-S129-alpha-synuclein, confocal scanning microscopy has also demonstrated usefulness when detected oligomeric alpha-synuclein species in SH-SY5Y cells (Maor et al., 2019). Using confocal microscopy to generate 3-dimentional Z-stack images of alpha-synuclein pathology may allow for more detailed analysis of intracellular alpha-synuclein fibrillar structures (Weish et al., 2021). Further to this, immunoelectron microscopy can be utilised to visualise fibrillar inclusions in cell models. This has been previously employed to image p-S129-alpha-synuclein positive aggregates in SH-SY5Y cells (Smith et al., 2005). Understanding the ratio of p-S129-alpha-synuclein/oligomeric alpha-synuclein to total alpha-synuclein may shed light on alpha-synuclein pathology induced by *GBA1* mutations. This ratio has been shown to be shifted toward phosphorylated alpha-synuclein in plasma exosomes isolated from PD patients (Zheng et al., 2021).

Misfolded, proteinase-K (PK) resistant alpha-synuclein is also thought to be a pathogenic form of alpha-synuclein present in models of PD and alpha-synucleinopathies (Conway et al., 2000, Miake et al., 2002, Neumann et al., 2002, Tanji et al., 2010). In these studies, immunoreactivity of abnormal alpha-synuclein is enhanced by pre-treating with PK, suggesting that fibrilisation and proteinase resistance of alpha-synuclein may be implicated in synucleinopathies. A future prospective should be to analyse the PK resistance of alpha-synuclein in the *GBA1* mutant models, to assess whether E326K mutations influence this.

In addition to increased resistance to proteinase enzymes, the stability of alpha-synuclein has also been proposed to increase in synucleinopathies. Pulse-chase

analysis is a technique involving labelling proteins for a short time and has been used previously to measure the half-life of wild-type and mutant alpha-synuclein in mouse cortical neurons (Li et al., 2004). Another method used to analyse protein stability is the cycloheximide chase assay. This involves incubating cells with cycloheximide and calculating protein abundance at frequent time points by western blot. This method has been previously employed in *GBA1* mutant SH-SY5Y cells to assess both alpha-synuclein and GCase protein stability (Maor et al., 2019). Interestingly, expressing L444P protein increased alpha-synuclein half-life by 30 hours and expressing N370S protein increased alpha-synuclein half-life by 6 hours. It would be interesting to compare these two mutations to E326K. Furthermore, in this study the half-life of L444P and N370S GCase was significantly increased. As our findings do not point toward a loss of function, but perhaps a gain of function, mechanism for E326K, the observation that mutant GCase is around for longer in the cell to exert its function may play a role in accelerating pathology.

Evidence also suggests that a GCase deficiency may influence the ratio between physiological helically-folded alpha-synuclein tetramers and multimers, and natively unfolded monomeric species, by shifting the ratio towards free monomers. These native HMW species have been shown to resist aggregation, whereas unfolded monomers readily aggregate into amyloid-like structures. They also differ from pathological HMW oligomers as they are soluble and are alpha-helical rich unlike β-sheet rich insoluble amyloid-like aggregates (Bartels et al., 2011). As my data indicates increased insoluble aggregates in E326K and L444P cells, a reduced ratio of alpha-synuclein multimers to free monomers was anticipated. This has been observed in primary cortical neurons from L444P heterozygous transgenic mice (Kim et al., 2018b) and in L444P and N370S

heterozygous human dopamine neurons (Kim et al., 2018b, Zunke et al., 2018). I was unable to quantify monomeric alpha-synuclein, due to rapid over-exposure, and thus could not analyse the effect of *GBA1* mutations on the shift towards free monomers (Figure. 38.).

Previous studies have been performed using post-mitotic iPSC-derived neurons and endogenous alpha-synuclein levels may be higher so future analysis of alpha-synuclein tetramer to monomer ratio in these cells may shed light on E326K-induced aggregation. It has been shown in a synucleinopathy mouse model that over-expression of wild-type GCase reduced the number of toxic free monomeric alpha-synuclein, accompanied by an increase in lipid turnover and decreased lipid droplet number (Glajch et al., 2021). Moreover, previous studies have demonstrated the ability of GSLs to destabilise physiological alpha-synuclein tetramers and multimers (Kim et al., 2018b), and to induce the conversion of alpha-synuclein monomers into a unique toxic HMW species (Zunke et al., 2018) in *GBA1*-PD dopamine neurons. For future, more accurate, analysis alpha-synuclein could be purified from cross-linked lysate of cells expressing *GBA1* mutants by immunoaffinity with anti-alpha-synuclein antibodies (Anderson et al., 2006). Circular dichroism spectroscopy analysis of purified alpha-synuclein could be utilised to identify natively unfolded and folded alpha-synuclein, as previously performed (Bartels et al., 2011).

As E326K had minimal changes in soluble, monomeric alpha-synuclein I assessed whether this mutation may influence the release of alpha-synuclein. Neuronal cells secrete both monomeric and oligomeric alpha-synuclein (Lee et al., 2005), and changes to alpha-synuclein turnover may affect this. GCase deficient cells have also been shown to demonstrate increased spread of alpha-synuclein pathology in a co-culture model with differentiated SH-SY5Y cells

(Gegg et al., 2020). In SH-SY5Y neuroblastoma cells, over-expression of GCase or GFP protein led to the release of alpha-synuclein monomers (Figure. 41A.), suggesting protein over-expression affects this pathway in neuroblastoma cells. To accelerate release, differentiated SH-SY5Y and dopamine neurons were treated with alpha-synuclein PFFs. As expected, from previous literature where PFF treatment promoted the release of alpha-synuclein fibrils from mouse cortical neurons (Gegg et al., 2020), treatment with PFFs induced the release of alpha-synuclein monomers and fibrils from dopamine neurons (Figure. 57.). The E326K mutation did not increase alpha-synuclein release, compared to controls. As PFF treatment significantly increased the number of aggregates in E326K neurons (Figure. 56.), it may be that alpha-synuclein monomers are being recruited into toxic alpha-synuclein oligomers instead of being released by the cell. On the other hand, the N370S mutation did lead to an increase in monomeric alpha-synuclein release from human midbrain neurons compared to wild-type (Figure 57A.) and increased exosome release from SH-SY5Y cells (Figure. 41B.), although not significant. This was expected as N370S/WT human midbrain neurons have been shown to increase release of monomeric alpha-synuclein into media (Fernandes et al., 2016) and virus-mediated expression of N370S GCase in mouse striatum promoted release (Papadopoulos et al., 2018).

The L444P SH-SY5Y cells did not exhibit a marked increase in exosome release. This is not supported by previous literature where both L444P and N370S fibroblasts have increased release of extracellular vesicles (Cerri et al., 2021). Furthermore, incubation with extracellular vesicles isolated from these L444P cells, but not N370S, promoted alpha-synuclein pathology in SH-SY5Y cells, and as plasma extracellular vesicles isolated from PD patients exhibit more pathogenic alpha-synuclein species compared to controls (Zheng et al., 2021),

this suggests that the L444P mutation induces release of alpha-synuclein to propagate pathology in a prion-like manner. It may be that as the cell model used in this study was an L444P over-expression system, the residual activity was higher than in patient-derived cells and thus this prevented toxic release of alpha-synuclein.

Data regarding alpha-synuclein secretion was inconclusive from differentiated SH-SY5Y cells (Figure. 52.), likely as these were grown in 6 well plates and thus the concentration of alpha-synuclein and exosomes in the culture media was below the limit of detection. Improved methods to isolate exosomes include commercial exosome isolation kids and centrifugations. The standard method to isolate exosomes involves several centrifugation steps, mainly differential centrifugations followed by ultracentrifugations. This separates organelles and sub-cellular particles first on the basis of sedimentation rate, then on the basis of mass by high speed centrifugation (Lobb et al., 2015). Both the centrifugation protocol and specific exosomal isolation kits have demonstrated the capability to isolate exosomes from conditioned culture media (Lobb et al., 2015, Tang et al., 2017), SH-SY5Y cells (Park et al., 2015, Alvarez-Erviti et al., 2011b) and plasma from *GBA1*-PD patients (Cerri et al., 2021). It has been proposed that a combination of commercial exosome isolation kit, followed by size-exclusion chromatography, differential centrifugation and ultracentrifugation is the optimal methodology for isolating pure exosomes (Patel et al., 2019). In addition to transmission electron microscopy to characterise isolated exosomes, specific exosome markers, such as CD9, should be analysed to confirm the presence of exosomes in fractions. The presence of alpha-synuclein species in exosomes could be analysed by western blotting or ELISA with antibodies against alpha-synuclein monomers, fibrils and p-S129-alpha-synuclein species. It has

previously been reported that p-S129-alpha-synuclein levels were greater in exosomes isolated from fibroblasts harbouring the L444P and N370S mutation (Cerri et al., 2021). In plasma exosomes isolated from PD patients, the levels of pathological alpha-synuclein were higher than those compared to controls (Zheng et al., 2021). Furthermore, it has been proposed that the concentration of alpha-synuclein in exosomes may be used as a diagnostic marker for PD (Sang et al., 2021). Analysis of these alpha-synuclein species in exosomes isolated from cells expressing the E326K GCase protein would be a future study.

5.4.3 *GBA1* mutations and ER stress

Emerging evidence demonstrates the involvement of ER stress in the pathogenesis of PD (Ryu et al., 2002). ER stress was increased in L444P SH-SY5Y cells (Figure. 35. and 49). As these levels were also increased compared to GFP over-expressing cells, we can conclude the increase in ER stress markers is specific to the L444P mutation and not due to over-expression of a protein with a similar molecular weight. These results were as expected, as previous studies in human fibroblast cells, dopamine neurons and *Drosophila* models harbouring the L444P mutation report significant elevations in markers of ER stress (Lu et al., 2010, Maor et al., 2016, Bendikov-Bar et al., 2011, Schöndorf et al., 2014, Mu et al., 2008, Maor et al., 2013).

These results revealed that the E326K mutation did not elicit an ER stress response, suggesting that the presence of the mutant enzyme in the ER does not have a toxic gain of function. Considering my analysis of fibroblasts (Chapter 3.) and undifferentiated SH-SY5Y cells (Figure. 33.) suggest that the E326K mutation does not induce a loss of mutant protein and activity, and thus is likely not heavily misfolded in the ER, these results were anticipated.

Interestingly, neither undifferentiated nor differentiated cells expressing N370S GCase protein demonstrated ER stress. This does not fit with previous findings in *Drosophila* models, where both L444P and N370S GCase induced ER stress accompanied by locomotor deficits, which were reversed when ER stress was alleviated (Sanchez-Martinez et al., 2016). Furthermore, in iPSC-derived neurons heterozygous for N370S there was an upregulation of ER stress associated with autophagic disturbances (Fernandes et al., 2016). This may be because the level of ER stress is variable in cells with the same genotype, as a previous study investigating N370S in the homozygous, heterozygous and compound heterozygous form in fibroblasts, revealed variable levels of ER stress (Ron and Horowitz, 2005). A more sensitive approach to measure ER stress is through measuring ER-associated Ca^{2+}, which has been shown to be impaired in fibroblasts and dopamine neurons with *GBA1* mutations (Kilpatrick et al., 2016, Schöndorf et al., 2014).

In some mutations, ER stress may underlie a key pathway involved in alpha-synuclein pathology, as a link between the two has been demonstrated previously (Colla et al., 2012a, Colla et al., 2012b). It has also been reported that alpha-synuclein has the ability to interact and activate BiP to elicit the UPR (Bellucci et al., 2011), and in N370S dopamine neurons ER stress led to altered alpha-synuclein turnover (Fernandes et al., 2016). However, in a *Drosophila* model study of L444P and N370S mutants, ER stress induced locomotor deficits which were independent of alpha-synuclein pathology (Sanchez-Martinez et al., 2016). These findings suggest that the E326K mutation may exert its pathogenic affect independent of ER stress, however this pathway is key to understanding the pathology of the L444P mutant.

5.4.4 *GBA1* mutations and lipid metabolism

Lipid homeostasis is necessary for maintaining proper function of the neuron and synaptic plasticity (Farmer et al., 2020). Proper regulation of cellular lipids is critical to maintain the composition and fluidity of lipid membranes. Such lipids can bind alpha-synuclein, and accelerate its formation into toxic oligomeric and fibrillar species, propagating PD pathology. In addition, alterations in lipid membrane integrity can influence alpha-synuclein binding, with hydrolysed TAGs, GSLs (particularly GM1 and GM3), acidic phospholipid vesicles and ordered regions of lipid membranes enhancing the conversation of monomeric alpha-synuclein into toxic aggregates (Alecu and Bennett, 2019).

As the main function of GCase is to cleave GSLs, it is not surprising that in cellular and animal models of GCase deficiency there is an accumulation in GlcCer and GlcSph (Kim et al., 2018b, Farfel-Becker et al., 2014, Taguchi et al., 2017, Nagata et al., 2017). I therefore sought to assess whether individual *GBA1* mutations affect the lipid composition of SH-SY5Y neuroblastoma cells, to influence their pathology. Analysis of total cellular GSL level by HPLC did not reveal significant changes between genotypes (Figure. 42.) The chromatogram demonstrating GSL species replicates the trace pattern of GSL species in SH-SY5Y cells previously demonstrated by the same method (Vieira et al., 2015). Although, spleens from GD patients show elevated levels of GSLs (Orvisky et al., 2002), the findings in this study are similar to analysis in GCase deficient mice where GSL levels were unaltered (Farfel-Becker et al., 2014). However, as the mice brains showed an accumulation of GlcCer I next chose to specifically investigate the levels of total GlcCer in SH-SY5Y cells. Again, no noticeable difference in GlcCer levels was induced by any of the three *GBA1* mutations. GlcCer accumulation has been demonstrated in iPSC-derived dopamine neurons

harbouring the L444P mutation in homozygous form (Schöndorf et al., 2014, Zunke et al., 2018). However, in GCase mutant mice residual enzymatic activity was sufficient to prevent the accumulation of GlcCer (Sardi et al., 2011), and as our model was an over-expression system with all lines retaining endogenous GCase activity, this may be why no accumulation was observed.

It has been reported that GlcSph may be more pathogenic, with its accumulation observed in GCase mutant neurons and mice (Sardi et al., 2011, Taguchi et al., 2017). Interestingly, in one of these studies the accumulation of GlcSph, but not GlcCer, triggered the formation of oligomeric alpha-synuclein capable of templating and was co-localised with pathology (Taguchi et al., 2017). Although understanding how mutations influence the levels and distribution of these lipids may shed light on pathogenesis of individual *GBA1* mutations in cell models, it still remains elusive whether GSLs accumulate in human brains as one study of human *GBA1*-PD patient brains demonstrated no evidence of GlcCer and GlcSph accumulation (Gegg et al., 2015), whereas another showed a marked elevation of GlcCer and GlcSph levels in the SNpc of PD brains (Huebecker et al., 2019).

Alterations in L444P fibroblast GSL lipid profile have been previously reported, however in this study lipids were extracted and subjected to liquid chromatography mass spectrometry (LC-MS) (Galvagnion et al., 2020). It may be that a different mass spectrometry method is required rather than HPLC. Furthermore, this analysis revealed that in L444P mutants, there was a shift towards short-chain lipids. Interestingly, these specific lipids have been shown to induce the toxic conversion of alpha-synuclein monomers to aggregates. Understanding whether other mutations such as E326K and N370S also induce this shift would aid in our understanding of specific mutation pathogenesis. Furthermore, in N370S heterozygous dopamine neurons, Fernandes et al.,

analysed the distribution of GlcCer species and found alterations in species C16:0, C20:0 and C24:0. They suggested that these changes were due to impaired GCase trafficking; with increased species occurring as GCase is

reduced so unable to perform hydrolysis and reduced species occurring due to GCase accessing a species that is normally not degraded (Fernandes et al., 2016).

In an effort to overcome lipid overload, cells initially induce a pathway to store excess lipids in lipid droplets. Lipid droplets are spherical organelles with a pivotal role in controlling cell metabolism and maintain a healthy cellular environment. They offer a protective mechanism for many cells in response to stressors including oxidative stress. During fatty acid surplus, lipid droplets store fatty acids in the form of neutral lipid such as TAGs and cholesteryl esters (Farmer et al., 2020). This storage is essential to control the release of fatty acids when needed for lipid synthesis, cell signalling and energy production (Ralhan et al., 2021). Lipid droplets protect cells from excess fatty acids which can be targeted for lipid peroxidation. During oxidative stress, ROS can attack free fatty acids and generate toxic lipid peroxides and reactive aldehydes which can exert lipotoxicity including damage to lipid membranes, ER stress, mitochondrial damage and subsequent neurodegeneration (Yang et al., 2020a, Fanning et al., 2019, Unger and Orci, 2002, Fu et al., 2011, Velázquez et al., 2016, Nguyen et al., 2017). Excessive lipid droplet formation has however been demonstrated to trigger neurotoxicity (Han et al., 2018). It may be this that contributes to neurodegeneration in E326K mutants.

In E326K cells, there was a 2.9-fold increase in lipid droplet number compared to wild-type cells (Figure. 43A.). This was also markedly higher than the other

mutants: 1.5-fold higher than L444P and 1.4-fold higher than N370S cells. As there was a 2-fold increase compared to GFP expressing cells, we can conclude the formation of excess lipid droplets was specific to the presence of the E326K mutant protein and not from over-expression alone. Both L444P and N370S cells exhibited an increase in lipid droplet number compared to control cells, suggesting all three mutations induce lipid alterations, but E326K to a greater extent.

To further investigate lipid metabolism, cells were loaded with the unsaturated fatty acid, OA. Lipid loading has been done previously with OA to induce lipid droplet formation (Cole et al., 2002, Alza et al., 2021). Cells were starved over-night in culture medium in the absence of FBS, in order to deplete cells of lipid droplets before treatment, as previously described (Gubern et al., 2009, Cabodevilla et al., 2013). Again, E326K cells exhibited the greatest number of lipid droplets, with a 9.9-fold increase after OA treatment, compared to wild-type (Figure. 43B.). Interestingly, the same increase was not observed in L444P and N370S mutants, suggesting that cells harbouring the E326K mutation are more susceptible to changes in lipid metabolism. This may be as the E326K mutation may remodel cell metabolism, making them more reliant on fatty acid metabolism for energy supply. Reprogramming of cellular metabolism is a well-established hallmark of cancer cells; with fatty acid metabolism included as one of the most widely altered lipid metabolism pathways in pan-cancer analysis (Hao et al., 2019, Koundouros and Poulogiannis, 2020). Such cancer cells have been shown to accumulate lipid droplets to maintain lipid homeostasis and prevent lipotoxicity, as well as to provide a source of ATP and nicotinamide adenine dinucleotide phosphate (NADPH) (Koundouros and Poulogiannis, 2020). It could be that the

E326K mutant protein exerts a gain of function mechanism that involves the formation of lipid droplets.

These findings reinforce the previously reported link between a GCase deficiency and lipid droplet formation; with over-expression of wild-type GCase reducing lipid droplet number, whilst increasing lipid turnover and alleviating alpha-synuclein pathology and PD phenotype in a synucleinopathy mouse model (Glajch et al., 2021). Lipid loading with excess OA, which is a fatty acid, demonstrated an increase in alpha-synuclein inclusions in human neural crest cells (Fanning et al., 2019), and a correlation between lipid droplet accumulation and alpha-synuclein was observed in yeast cells (Outeiro and Lindquist, 2003). Further links between lipid droplets and alpha-synuclein have been demonstrated in human cells, with excess fatty acids inducing the re-organisation of wild-type alpha-synuclein onto intracellular lipid droplets (Cole et al., 2002), which is proposed to protect the stored TAGs from hydrolysis. Hydrolysed TAGs have been shown to accelerate the toxic conversion of alpha-synuclein monomers into oligomers (Alecu and Bennett, 2019). However, under pathological conditions excess lipid droplet accumulation may lead to regions of highly concentrated lipid-bound alpha-synuclein to induce aggregation. This strengthens the hypothesis that the E326K mutation may alter lipid metabolism to lead to alpha-synuclein pathology.

Furthermore, saturated fatty acids are thought to stabilise physiological alpha-synuclein tetramers, whereas unsaturated fatty acids shift the equilibrium toward monomeric alpha-synuclein (Fanning et al., 2019), so it may be that the E326K mutation alters metabolism toward unsaturated fatty acids, leading to increased lipid droplet formation and presence of alpha-synuclein amyloid-like aggregates. In addition, excess lipid droplet formation has been associated with inflammation

(Bozza and Viola, 2010, Khatchadourian et al., 2012), and oxidative stress (Lee et al., 2015, Lee et al., 2013) which can also induce toxicity.

From lipid droplet analysis in SH-SY5Y cells under basal conditions, a similar increase in lipid droplet formation was expected to occur following lipid loading in cells expressing L444P and N370S protein. It was surprising this was not the case as these cells also exhibit reduced GCase function and proper function of the ALP is required for lipid droplets to be broken down by lipophagy (Cingolani and Czaja, 2016). However, impaired function of the ALP or ER stress may underlie the accumulation of soluble monomers, insoluble alpha-synuclein aggregates and increased lipid droplets under basal conditions in L444P cells. As these mechanisms were not evident in cells expressing E326K protein, the exact mechanism underlying E326K-induced lipid dysfunction remains elusive.

To further characterise the effect of the E326K mutation on lipid metabolism in human cells, methods for quantitative lipid analysis should be employed to assess changes in the composition or concentration of lipid pools. Most methods involve the use of mass spectrometry. To analyse intracellular lipids, they must first be extracted. This has been done previously using a two-step chloroform/methanol procedure (Galvagnion et al., 2020). LC-MS has been utilised previously to analyse lipidomic changes in breast cancer cells (Eiriksson et al., 2020). This method was able to identify changes in several fatty acids including TAGs, phosphatidylcholines, sphingomyelins, diacylglycerols, whilst also giving information on whether these were saturated or unsaturated. Other methods of mass spectrometry could be utilised for future experiments analysing the effect of *GBA1* mutations on the intracellular composition of fatty acids. TAG species have previously been isolated and separated by reverse-phase (RP)-HPLC and identified by atmospheric pressure chemical ionization mass

spectrometry. The composition of TAGs was then quantified by RP-HPLC with evaporate light scanning detection (Mu and Høy, 2001). Improving the understanding of how E326K mutations influence fatty acid metabolism may aid in strengthening the hypothesis that E326K mutations shift cellular metabolism toward fatty acids. In addition, Q Exactive™ mass spectrometry has been performed previously on lipids extracted from L444P fibroblasts and revealed that lipids from these cells were capable of accelerating alpha-synuclein aggregation (Galvagnion et al., 2020). Repeating this with lipid extracts from cells expressing E326K protein would be useful.

More detailed analysis of lipid droplets in *GBA1* mutant cells should be performed in future studies. In addition to an increase in lipid droplet number, treating leukocytes with pro-inflammatory stimuli also led to an increase in lipid droplet size (Khatchadourian et al., 2012). This suggests that size and density may play a role in their lipotoxicity. Quantification of lipid droplet diameters could be accomplished by imaging cells through EM or confocal scanning microscopy, following staining of intracellular neutral lipids with Oil Red O (Schott et al., 2019) or BODIPY 493/503 (Khatchadourian et al., 2012). For more detailed analysis, confocal Z-stack images of fluorescently labelled lipid droplets can be analysed to determine number and size (Khatchadourian et al., 2012). Biochemical separation of lipid droplets, based on their size, could be carried out by a two-stage centrifugation protocol described previously (Schott et al., 2019). This may allow quantification of lipid droplet density. Isolated lipid droplets could then be subjected to mass spectrometry for lipidomic analysis.

In mouse brains, the accumulation of lipid droplets was accompanied by lipid-rich aggregates of alpha-synuclein (Glajch et al., 2021). Confocal scanning microscopy could be employed to analyse these inclusions in *GBA1* mutant cells.

Co-staining with a lipid stain and antibodies against alpha-synuclein oligomers, p-S129-alpha-synuclein or fibrils would allow visualisation of the co-aggregation of lipids and alpha-synuclein across cell lines. Lipid droplets have also been shown to promote the resistance of alpha-synuclein to PK in *Drosophila* models (Girard et al., 2021). PK resistance could be assessed by western blot analysis in *GBA1* mutant cells to understand more how E326K-induced lipid droplet formation influences alpha-synuclein pathology.

These findings fit in with data from the wider PD cohort, where lipid homeostasis is reported to be dysregulated and may have a role in alpha-synuclein pathology (Alecu and Bennett, 2019). In the brains of sporadic PD patients, significant changes in the chain length of ceramides and sphingomyelins have been demonstrated, shifting toward short chain lipids (Abbott et al., 2014). Another study demonstrated increases in diglyceride and unsaturated fatty acids in the frontal cortex of sporadic PD patients (Wood et al., 2018). This suggests that altered diglyceride synthesis and metabolism may be a key feature in PD and supports the findings of altered lipid homeostasis and lipid droplet formation in E326K *GBA1*-PD.

In addition to *GBA1*, another genetic link between aberrant lipid metabolism and PD has been identified through *SMPD1* mutations. *SMPD1* encodes for lysosomal acid sphingomyelinase which hydrolyses sphingomyelins to ceramides and phosphocholine (Alecu and Bennett, 2019). Mutations in *SMPD1* have been linked to an increased risk for PD (Gan-Or et al., 2009). Interestingly, in a study of 1200 Ashkenazi Jews, it was found that a high percentage of patients with E326K mutations also caried another mutation, *SMPD1* or *LRRK2*, which significantly increased the frequency of PD, potentially further highlighting a role for lipids in the pathogenesis of E326K (Goldstein et al., 2019).

5.5 Conclusion

In SH-SY5Y neuroblastoma cells, differentiated SH-SY5Y cells and human midbrain dopamine neurons harbouring the E326K mutation, there was no significant loss of GCase function. There was, however, a significant elevation of insoluble alpha-synuclein aggregates, which was not associated with an accumulation of alpha-synuclein monomers or increased secretion of alpha-synuclein. This was coincident with an accumulation of lipid droplets. The level of insoluble alpha-synuclein oligomers in E326K cells was similar in cells harbouring the L444P mutation, which is a common *GBA1* mutation that has been shown to be associated with accelerating alpha-synuclein pathology (Migdalska-Richards et al., 2020, Migdalska-Richards et al., 2017b) to lead to a severe, fast progressing type of PD (Sidransky et al., 2009). As the E326K mutation exerts pathogenesis in neurons via different pathways to L444P and N370S mutations, it can be hypothesised that the aetiology of *GBA1*-PD is separate to that of GD and primarily involves the relationship between mutant GCase and alpha-synuclein. In cells expressing N370S GCase there was no evidence of significant alpha-synuclein toxicity.

I attempted to further characterise the aggregation of alpha-synuclein in E326K cells using specific aggregation assays, however these data did not exhibit a marked increase induced by E326K. Unlike L444P cells, where alpha-synuclein pathology may be explained by a loss of GCase function and thus lysosomal dysfunction or ER stress, E326K cells did not exhibit an increase in ER stress markers. This data point toward a dysfunction of lipid homeostasis playing a key role in the onset of alpha-synuclein pathology in E326K mutants. Undifferentiated SH-SY5Y cells exhibited an elevation of lipid droplets compared to wild-type, L444P and N370S cells which was further increased upon treatment with excess

fatty acids. As lipid droplets and alpha-synuclein have been reported to be linked in many different cell models, with lipid droplet accumulation associated with defective alpha-synuclein turnover (Girard et al., 2020, Glajch et al., 2021), I hypothesise that the E326K mutation induces dysregulation of lipid homeostasis, leading to increased lipid droplets and alpha-synuclein aggregation. However, as the E326K mutation did not induce lysosomal dysfunction or ER stress in these cells, it remains elusive how the variant causes irregular lipid metabolism. It may be that the E326K mutation induces lipid abnormalities via different mechanisms in different cell types; a more robust investigation into E326K across various human cell types would be an exciting avenue to explore.

6 General Discussion and Conclusion

The main findings from studying E326K *GBA1* mutations in four cell models were:

1. The E326K mutation does not behave in a similar fashion to common pathogenic *GBA1* mutations L444P and N370S and does not undergo ER-trapping.
2. Despite no loss of GCase activity, E326K mutant SH-SY5Y neuroblastoma cell lines accumulate insoluble alpha-synuclein aggregates.
3. Lipid homeostasis is likely be altered by the E326K mutation, as there is enhanced formation and accumulation of lipid droplets.

The degree of PD pathogenicity associated with individual *GBA1* mutations is variable. Pathogenic *GBA1* mutations are stratified into mild or severe mutations, based on the effect on GCase enzyme activity and the category of GD they cause. As *GBA1* mutation carriers are just as likely to develop PD as homozygotes, and not every GD patient develops PD, a deficiency in GCase activity alone cannot underlie the pathogenesis of *GBA1*-PD (Alcalay et al., 2015, Rosenbloom et al., 2011). The E326K mutation is known as a risk variant, as it does not cause clinical features of GD when homozygous, but does increase the risk of PD (Duran et al., 2013). The most common pathogenic mutations are L444P and N370S, which are categorised as severe and mild, respectively (Beutler et al., 2005). Both of these mutants have been studied intensely in a variety of cell models, and have shown both loss and gain of function mechanisms, associated with extensive alpha-synuclein pathology (Maor et al., 2019, Sanchez-Martinez et al., 2016, Schöndorf et al., 2014). We hypothesised that the E326K mutation exerts its toxic function through influencing the relationship between GCase and alpha-synuclein.

In order to recapitulate all aspects of PD pathogenesis, the mechanisms involved in the E326K mutants would ideally be studied in SNpc dopamine neurons from PD patients. Furthermore, initially the protocol for generating iPSC-derived midbrain dopamine neurons was not yet optimised in our lab. Once optimised the cell population remains heterogenous, yielding 30-40% dopamine neurons, similar to other reports (Hu et al., 2010, Fernandes et al., 2016, Kriks et al., 2011, Schöndorf et al., 2014). To overcome this, I first set out to characterise the loss and gain of function mechanisms associated with E326K mutations in patient-derived fibroblasts, and translated these findings to neuronal SH-SY5Y cell models and finally iPSC-derived midbrain dopamine neurons to investigate alpha-synuclein pathology.

In homozygous and heterozygous form, E326K mutations are not associated with a significant loss of GCase expression and activity in fibroblasts (Chapter 3.3.1 and 3.3.2). This was also the case in proliferating and differentiated SH-SY5Y cells (Chapter 5.3.11 and 5.3.2.2). Unlike the L444P GCase protein, the localisation of E326K protein appears to be mainly lysosomal (Chapter 3.3.5), suggesting proper trafficking due to the absence of a misfolded secondary structure. This was corroborated by analysis of ER-trapping in fibroblasts (Chapter 3.3.4) and functional stability assays in recombinant GCase protein (Chapter 4.3.7 and 4.3.8). Further to this, cells expressing E326K GCase protein did not activate the ER stress response, unlike those expressing L444P mutant protein (Chapter 3.3.6, 5.3.1.3 and 5.3.2.4). It may be that the mutant E326K protein exerts a gain of function mechanism through an alternative pathway. It has been proposed GCase may have a moonlighting function, playing a role in the glucosylation of cholesterol at the lysosome (Marques et al., 2016). Lysosomal GCase can hydrolyse glucosylated cholesterol (GlcChol) and has also

been shown to catalyse the transfer of glucosyl-moieties from GlcCer to cholesterol, likely in response to cholesterol accumulation at the lysosome. The glucosylation of cholesterol alters its physiochemical properties. The E326K mutation may increase glucosylation of cholesterol or other lipids. On the other hand, E326K mutations may impair the hydrolysis of GlcChol resulting in its accumulation. The altered properties of GlcChol may increase its storage in lipid droplets or influence lipid membrane fluidity, which may promote the aggregation of alpha-synuclein (Galvagnion et al., 2016). Alterations to the composition of lipid rafts, which are central regulators of CMA (Kaushik et al., 2006), may impair CMA-mediated degradation of alpha-synuclein.

Interestingly, the E326K mutation was associated with 2.5-fold reduction in GCase levels and 1.7-fold reduction in activity when in the environment of midbrain dopamine neurons (Chapter 5.3.3.1 and 5.3.3.2). Although this was not significant, this was reduced to a similar level to the pathogenic WT/N370S neuronal line. This suggests that the local environment of midbrain dopamine neurons are the most susceptible to neurodegeneration, potentially exacerbating a loss of E326K activity. One possible explanation is the presence of oxidised dopamine, which has been shown to be increased in dopamine neurons from PD patients and correlates with a decrease in GCase enzyme activity, lysosomal dysfunction and alpha-synuclein accumulation (Burbulla et al., 2017). Additionally, SNpc dopamine neurons exhibit activation of L-type Ca^{2+} channels during autonomous pacemaker activity; this can create oxidative stress and mitochondrial dysfunction (Guzman et al., 2010), which may promote a loss of function in E326K GCase. Finally, it may be the specific expression of proteins in midbrain dopamine neurons that increase the deleterious effect of the E326K mutation on GCase expression and function. Such proteins include G-protein-

regulated inward-rectifier potassium channel 2 (GIRK2) and adenine nucleotide translocator 2 (ANT-2), which have been shown to be involved in the vulnerability of these neurons to toxicity (Chung et al., 2005). This may also explain why the E326K mutation does not cause GD, as macrophages are absent of these characteristics, but can lead to the development of PD through degeneration of SNpc dopamine neurons. To further investigate this GCase activity should be measured in entire midbrain neuronal cultures harbouring the E326K mutation. It would be interesting to see whether a reduction in GCase activity is specific to the 30-40% of neurons that have successfully differentiated into dopamine neurons.

Another avenue to explore is to understand the effect of the E326K mutation on GCase in astrocytes and microglia. These cells play a key role in the uptake and autophagic-mediated degradation of alpha-synuclein (Fellner and Stefanova, 2013) and a GCase deficiency may prevent this. Transcriptome analysis has demonstrated that *GBA1* mRNA is higher in mouse microglia compared to neurons in the hippocampus, striatum and cortex (www.bainrnaseq.org; www.astrocyternaseq.org; www.holt-sc-glialab.org), while GCase activity is twice as high in mouse cortical astrocytes than in neurons (Unpublished data, Dr Matt Gegg). These findings point toward an important, yet unidentified, role for GCase in microglia. The same analysis of human *GBA1* mRNA revealed mixed results; with both higher (www.brainrnaseq.org) and lower (www.brain-map.org) expression reported in mature astrocytes, relative to neurons.

Despite no loss of GCase function, or evidence of an accumulation of soluble alpha-synuclein monomers (Chapter 5.3.1.4 and 5.3.2.5), proliferating SH-SY5Y cells expressing E326K GCase protein exhibit an increase in insoluble alpha-synuclein aggregates (Chapter 5.3.1.5). This was increased to a similar level as

L444P mutant cells. As the L444P variant has been shown to accelerate alpha-synuclein pathology and spread in mice (Migdalska-Richards et al., 2020, Yun et al., 2018), this points toward a potentially similar propagation of pathology in E326K mutation carriers. The observation that the E326K mutation occurs on the GCase protein surface (Smith et al., 2017) suggests protein interactions may be influenced. It's possible that the E326K mutant GCase protein has a reduced affinity for binding alpha-synuclein, as suggested in the N370S protein (Yap et al., 2011) which could induce alpha-synuclein lipid binding and aggregation.

Accumulation of insoluble alpha-synuclein aggregates may be explained by the accumulation of lipid droplets observed in proliferating SH-SY5Y cells expressing E326K GCase protein (Chapter 5.3.1.11). Unlike cells expressing L444P and N370S protein, which had increases in lipid droplet number under basal conditions, loading of cells with excess fatty acids significantly exacerbated the formation of lipid droplets in E326K cells.

Neurons can normally form only a minimal number of lipid droplets compared to other cells, and have limited capacity for fatty acid catabolism (Schönfeld and Reiser, 2013). Instead, they transfer fatty acids between neighbouring microglia to be stored in microglial lipid droplets (Liu et al., 2017). This is thought to occur through the glia-lactate shuttle. Studies in *Drosophila* have shown that glucose is taken up from the blood by microglia where it is broken down into lactate. Monocarboxylate transporters allow microglia to secrete lactate and neurons to absorb lactate. Inside the neuron, lactate is converted to pyruvate and acetyl coenzyme A in mitochondria which leads to a subsequent increase in ROS production. Elevated levels of ROS can trigger Jun N-terminal Kinase (JNK) and sterol regulatory-element binding proteins (SREBPs) activity in neurons, which leads to increased lipid synthesis, with lactate acting as a substrate for the

synthesis of fatty acids. Fatty acids can then be processed and transferred to microglia by apolipoprotein E (ApoE) and fatty acid transporter proteins, ultimately leading to an increase in lipid droplet formation in microglia (Liu et al., 2017, Liu et al., 2015). In *Drosophila*, reducing ROS levels, lipid peroxidation or lactate and fatty acid transfer led to a reduction in lipid droplet accumulation in microglia. In Ndusf4 mutant mice with mitochondrial defects, a similar pattern was observed suggesting that lipid droplet accumulation following mitochondrial dysfunction is a promoter of neurodegeneration (Liu et al., 2015). It may be that the E326K mutation leads to defects in the glia-lactate shuttle, perhaps preventing the neuron from efficiently transferring lipids to the microglia and thus promoting the formation of lipid droplets in the neuron as a protective mechanism against free fatty acids. Additionally, E326K mutant microglia may have an impaired phagocytotic mechanisms impeding the uptake of neuron-derived fatty acids and thus increasing the build-up of fatty acids in the neuron. This also points to a role for mitochondrial dysfunction in E326K cells, leading to an elevation of ROS and an increase in lipid droplet formation.

Supporting this, analysis of PD patient brain revealed that although there was no overall change in total lipid content in the SNpc, there was significant accumulation of lipid droplets in dopamine neurons and microglia, with a reduction observed in adjacent astrocytes, compared to age-matched controls (Brekk et al., 2020). This highlights the importance of neuron-glia-astrocyte lipid exchange pathways in PD. This was recapitulated in mice treated with CBE to inhibit GCase activity, suggesting a potential role for GCase in controlling fatty acid metabolism in the brain, which an E326K mutation may affect. This accumulation of lipid droplets may be in response to increased lipid phagocytosis by microglia or activation of inflammatory signalling cascades. In addition to

microglia, astrocytes have been demonstrated to internalise and store fatty acids released from neurons in lipid droplets (Ioannou et al., 2019). Therefore, it may be possible that the E326K mutation influences the endocytosis of neuron-released lipids by astrocytes, leading to an increase in lipids in neurons.

The E326K mutation may induce an overall dysfunction of cellular lipid homeostasis by influencing lipolysis of sphingomyelins, cholesterols and glycerophospholipids, potentially through interacting with enzymes involved in their hydrolysis. Alterations in such pathways have been reported in PD; increasing levels of TAGs, cholesterol and ceramides (Alecu and Bennett, 2019), which may require storage in lipid droplets. Another possibility is that the E326K GCase protein induces cell metabolism remodelling, shifting lipid metabolism towards oxidation of fatty acids as a source of energy. This has been demonstrated in amyotrophic lateral sclerosis (ALS) (Steyn et al., 2020) and cancer cells (Koundouros and Poulogiannis, 2020). This shift may prime neurons to more efficiently synthesise fatty acids. De novo synthesis of fatty acids may also be a potential target, with the E326K mutation increasing expression of ER-bound SREBPS transcription factors which regulate lipogenesis (Koundouros and Poulogiannis, 2020), potentially increasing the uptake of fatty acids through the upregulation of membrane transporters. This has been shown in prostate cancer cells (Watt et al., 2019). This shift may lead to an increase in the synthesis of total fatty acids such as TAGs, increasing lipid droplets, or a shift toward more unsaturated fatty acids which have been shown to destabilise physiological HMW alpha-synuclein species and accelerate aggregation (Fanning et al., 2019). Furthermore, hydrolysed TAGs have been shown to accelerate alpha-synuclein aggregation (Alecu and Bennett, 2019).

Fatty acid oxidation occurs in mitochondria, to provide ATP for the cell (Wajner and Amaral, 2015). Dysfunction in the mitochondrial network can contribute to alterations in fatty acid metabolism. Mitochondrial dysfunction has long been implicated in the pathogenesis of PD (Schapira and Gegg, 2011). Mitochondria have been reported to associate with lipid droplets, forming mitochondria with a unique structure and function less prone to fatty acid oxidation (Benador et al., 2018). An increase in lipid droplet formation in E326K cells may increase the formation of these mitochondria, preventing the breakdown of fatty acids and further exacerbating storage of lipids in droplets. A defective mitochondrial network may lead to an increase in fatty acid content and more lipid droplets. Furthermore, increased oxidative stress and mitochondrial dysfunction can lead to a subsequent increase in lipid droplets (Lee et al., 2015). Mitochondrial defects have also been associated with *GBA1* mutations. In neurons from *GBA1*-PD patients defects in mitochondrial function, increased oxidative stress, defective dynamics and impaired mitophagy have been reported (Kim et al., 2021, Schöndorf et al., 2018). Alpha-synuclein can directly induce mitochondrial damage and cell death (Ganjam et al., 2019), as well as defective mitochondrial demonstrating the capability of inducing alpha-synuclein pathology (Yun et al., 2018). Understanding the role of mitochondria in E326K dopamine neurons is an exciting avenue to explore.

In addition to mitochondria, E326K may exert its toxic function through neuroinflammation and activation of the microglia. This has been demonstrated in models of GCase deficiency (Rocha et al., 2015c, Keatinge et al., 2015). Microglia play a key role in the uptake of lipids and alpha-synuclein (Loving and Bruce, 2020). During inflammation cell metabolism may be remodelled to increase fatty acid oxidation (McFadden et al., 2014). The activation of microglia

and astrocytes in inflammation is associated with the formation of large lipid droplets (Khatchadourian et al., 2012). Aged microglia also demonstrate defective autophagy, mitochondrial dysfunction and increased pro-inflammatory cytokines (Marschallinger et al., 2020). These characteristics may be exacerbated by E326K mutations, leading to further accumulation of lipids and alpha-synuclein. Furthermore, alpha-synuclein can bind and activate the microglia directly, which may lead to their dysfunction (Kim et al., 2013, Thome et al., 2016).

Excess lipid droplets may exacerbate alpha-synuclein pathology. Under physiological conditions, alpha-synuclein has been shown to bind to lipid droplets (Cole et al., 2002). It may be that under pathological conditions, this local increase of lipid droplet-bound alpha-synuclein is more prone to aggregation. To further characterise alpha-synuclein fibrilisation in E326K cells, aggregation was induced using alpha-synuclein PFFs. Exogenously applied alpha-synuclein PFFs have been shown to induce the self-assembly of endogenous alpha-synuclein in SH-SY5Y cells previously (Sang et al., 2021). No obvious change in alpha-synuclein aggregation was demonstrated in differentiated cells expressing E326K, L444P or N370S GCase protein (Chapter 5.3.2.6) or in heterozygous E326K and N370S midbrain dopamine neurons (Chapter 5.3.3.3), nor was any obvious increase in the release of alpha-synuclein monomers or fibrils upon treatment with PFFs demonstrated (Chapter 5.3.1.9 and 5.3.3.4). Difficulty arises when analysing the misfolding and aggregation of alpha-synuclein in cell models as this is often absent or weak. A similar difficulty was met when measuring the levels of insoluble alpha-synuclein aggregates in E326K SH-SY5Y neuroblastoma cells, as levels were often on the limit of detection. The lack of aggregates may be explained by the inability to recapitulate the ageing brain over days and weeks in

cell culture, and it has been suggested that age may be a crucial factor required to observe well defined alpha-synuclein pathology and propagation (Van Den Berge et al., 2021). Another explanation to the lack of increased aggregates in E326K mutations could be that instead of an increase in alpha-synuclein aggregation, the mutation may induce the formation of a distinct strain of alpha-synuclein. Such strains have been described in synucleinopathies and exhibit specific characteristics including increased seeding capabilities, different conformation and higher resistance to PK digestion (Peng et al., 2018).

A final hypothesis arises from the observation that PD patients carrying the E326K mutation demonstrate an alteration in the abundance of several metabolites including anhydroglucitol, ornithine and glutamine (Greuel et al., 2020). The E326K mutation may influence pathways involved in these metabolites such as the polyol pathway, which has been shown to contribute to oxidative stress (Chung et al., 2003), and may lead to an increase in lipid droplets. Further metabolomic studies of the E326K mutation would increase understanding.

7 References

ABBOTT, S. K., LI, H., MUÑOZ, S. S., KNOCH, B., BATTERHAM, M., MURPHY, K. E., HALLIDAY, G. M. & GARNER, B. 2014. Altered ceramide acyl chain length and ceramide synthase gene expression in Parkinson's disease. *Movement Disorders,* 29**,** 518-526.

ABIAN, O., ALFONSO, P., VELAZQUEZ-CAMPOY, A., GIRALDO, P., POCOVI, M. & SANCHO, J. 2011. Therapeutic Strategies for Gaucher Disease: Miglustat (NB-DNJ) as a Pharmacological Chaperone for Glucocerebrosidase and the Different Thermostability of Velaglucerase Alfa and Imiglucerase. *Molecular Pharmaceutics,* 8**,** 2390-2397.

ABUL KHAIR, S. B., DHANUSHKODI, N. R., ARDAH, M. T., CHEN, W., YANG, Y. & HAQUE, M. E. 2018. Silencing of Glucocerebrosidase Gene in Drosophila Enhances the Aggregation of Parkinson's Disease Associated alpha-Synuclein Mutant A53T and Affects Locomotor Activity. *Front Neurosci,* 12**,** 81.

AERTS, J. M., BRUL, S., DONKER-KOOPMAN, W. E., VAN WEELY, S., MURRAY, G. J., BARRANGER, J. A., TAGER, J. M. & SCHRAM, A. W. 1986a. Efficient routing of glucocerebrosidase to lysosomes requires complex oligosaccharide chain formation. *Biochem Biophys Res Commun,* 141**,** 452-8.

AERTS, J. M., DONKER-KOOPMAN, W. E., MURRAY, G. J., BARRANGER, J. A., TAGER, J. M. & SCHRAM, A. W. 1986b. A procedure for the rapid purification in high yield of human glucocerebrosidase using immunoaffinity chromatography with monoclonal antibodies. *Anal Biochem,* 154**,** 655-63.

AFLAKI, E., BORGER, D. K., MOAVEN, N., STUBBLEFIELD, B. K., ROGERS, S. A., PATNAIK, S., SCHOENEN, F. J., WESTBROEK, W., ZHENG, W., SULLIVAN, P., FUJIWARA, H., SIDHU, R., KHALIQ, Z. M., LOPEZ, G. J., GOLDSTEIN, D. S., ORY, D. S., MARUGAN, J. & SIDRANSKY, E. 2016. A New Glucocerebrosidase Chaperone Reduces alpha-Synuclein and Glycolipid Levels in iPSC-Derived Dopaminergic Neurons from Patients with Gaucher Disease and Parkinsonism. *J Neurosci,* 36**,** 7441-52.

AHARON-PERETZ, J., BADARNY, S., ROSENBAUM, H. & GERSHONI-BARUCH, R. 2005. Mutations in the glucocerebrosidase gene and Parkinson disease: phenotype-genotype correlation. *Neurology,* 65**,** 1460-1.

AHARON-PERETZ, J., ROSENBAUM, H. & GERSHONI-BARUCH, R. 2004. Mutations in the glucocerebrosidase gene and Parkinson's disease in Ashkenazi Jews. *N Engl J Med,* 351**,** 1972-7.

AHMAD, S., KUMAR, V., RAMANAND, K. B. & RAO, N. M. 2012. Probing protein stability and proteolytic resistance by loop scanning: a comprehensive mutational analysis. *Protein science : a publication of the Protein Society,* 21**,** 433-446.

AKERMAN, K. E., SCOTT, I. G. & ANDERSSON, L. C. 1984. Functional differentiation of a human ganglion cell derived neuroblastoma cell line SH-SY5Y induced by a phorbol ester (TPA). *Neurochem Int,* 6**,** 77-80.

ALAM, P., BOUSSET, L., MELKI, R. & OTZEN, D. E. 2019. alpha-synuclein oligomers and fibrils: a spectrum of species, a spectrum of toxicities. *J Neurochem,* 150**,** 522-534.

ALBRECHT, L. V., TEJEDA-MUÑOZ, N. & DE ROBERTIS, E. M. 2020. Protocol for Probing Regulated Lysosomal Activity and Function in Living Cells. *STAR Protocols,* 1**,** 100132.

ALCALAY, R. N., CACCAPPOLO, E., MEJIA-SANTANA, H., TANG, M., ROSADO, L., ORBE REILLY, M., RUIZ, D., ROSS, B., VERBITSKY, M., KISSELEV, S., LOUIS, E., COMELLA, C., COLCHER, A., JENNINGS, D., NANCE, M., BRESSMAN, S., SCOTT, W. K., TANNER, C., MICKEL, S., ANDREWS, H., WATERS, C., FAHN, S., COTE, L., FRUCHT, S., FORD, B., REZAK, M., NOVAK, K., FRIEDMAN, J. H., PFEIFFER, R., MARSH, L., HINER, B., SIDEROWF, A., PAYAMI, H., MOLHO, E., FACTOR, S., OTTMAN, R., CLARK, L. N. & MARDER, K. 2012. Cognitive performance of GBA mutation carriers with early-onset PD: the CORE-PD study. *Neurology,* 78**,** 1434-40.

ALCALAY, R. N., DINUR, T., QUINN, T., SAKANAKA, K., LEVY, O., WATERS, C., FAHN, S., DOROVSKI, T., CHUNG, W. K., PAUCIULO, M., NICHOLS, W., RANA, H. Q., BALWANI, M., BIER, L., ELSTEIN, D. & ZIMRAN, A. 2014. Comparison of Parkinson risk in Ashkenazi Jewish patients with Gaucher disease and GBA heterozygotes. *JAMA Neurol,* 71**,** 752-7.

ALCALAY, R. N., LEVY, O. A., WATERS, C. C., FAHN, S., FORD, B., KUO, S. H., MAZZONI, P., PAUCIULO, M. W., NICHOLS, W. C., GAN-OR, Z., ROULEAU, G. A., CHUNG, W. K., WOLF, P., OLIVA, P., KEUTZER, J., MARDER, K. & ZHANG, X. K. 2015. Glucocerebrosidase activity in Parkinson's disease with and without GBA mutations. *Brain,* 138**,** 2648-2658.

ALCALAY, R. N., WOLF, P., CHIANG, M. S. R., HELESICOVA, K., ZHANG, X. K., MERCHANT, K., HUTTEN, S. J., SCHERZER, C., CASPELL-GARCIA,

C., BLAUWENDRAAT, C., FOROUD, T., NUDELMAN, K., GAN-OR, Z., SIMUNI, T., CHAHINE, L. M., LEVY, O., ZHENG, D., LI, G., SARDI, S. P. & THE PARKINSON'S PROGRESSION MARKERS, I. 2020. Longitudinal Measurements of Glucocerebrosidase activity in Parkinson's patients. *Annals of Clinical and Translational Neurology,* 7**,** 1816-1830.

ALECU, I. & BENNETT, S. A. L. 2019. Dysregulated Lipid Metabolism and Its Role in α-Synucleinopathy in Parkinson's Disease. *Frontiers in neuroscience,* 13**,** 328-328.

ALFONSO, P., RODRIGUEZ-REY, J. C., GANAN, A., PEREZ-CALVO, J. I., GIRALT, M., GIRALDO, P. & POCOVI, M. 2004. Expression and functional characterization of mutated glucocerebrosidase alleles causing Gaucher disease in Spanish patients. *Blood Cells Mol Dis,* 32**,** 218-25.

ALLEN, M. J., MYER, B. J., KHOKHER, A. M., RUSHTON, N. & COX, T. M. 1997. Pro-inflammatory cytokines and the pathogenesis of Gaucher's disease: increased release of interleukin-6 and interleukin-10. *QJM,* 90**,** 19-25.

ALVAREZ-ERVITI, L., COUCH, Y., RICHARDSON, J., COOPER, J. M. & WOOD, M. J. 2011a. Alpha-synuclein release by neurons activates the inflammatory response in a microglial cell line. *Neurosci Res,* 69**,** 337-42.

ALVAREZ-ERVITI, L., RODRIGUEZ-OROZ, M. C., COOPER, J. M., CABALLERO, C., FERRER, I., OBESO, J. A. & SCHAPIRA, A. H. 2010. Chaperone-mediated autophagy markers in Parkinson disease brains. *Arch Neurol,* 67**,** 1464-72.

ALVAREZ-ERVITI, L., SEOW, Y., SCHAPIRA, A. H., GARDINER, C., SARGENT, I. L., WOOD, M. J. A. & COOPER, J. M. 2011b. Lysosomal dysfunction increases exosome-mediated alpha-synuclein release and transmission. *Neurobiology of Disease,* 42**,** 360-367.

ALVAREZ-ERVITI, L., SEOW, Y., SCHAPIRA, A. H., RODRIGUEZ-OROZ, M. C., OBESO, J. A. & COOPER, J. M. 2013. Influence of microRNA deregulation on chaperone-mediated autophagy and alpha-synuclein pathology in Parkinson's disease. *Cell Death Dis,* 4**,** e545.

ALZA, N. P., CONDE, M. A., SCODELARO-BILBAO, P. G. & SALVADOR, G. A. 2021. Neutral lipids as early biomarkers of cellular fate: the case of α-synuclein overexpression. *Cell Death & Disease,* 12**,** 52.

AMBROSI, G., GHEZZI, C., SEPE, S., MILANESE, C., PAYAN-GOMEZ, C., BOMBARDIERI, C. R., ARMENTERO, M. T., ZANGAGLIA, R., PACCHETTI, C., MASTROBERARDINO, P. G. & BLANDINI, F. 2014. Bioenergetic and proteolytic defects in fibroblasts from patients with sporadic Parkinson's disease. *Biochim Biophys Acta,* 1842**,** 1385-94.

ANDERSON, J. P., WALKER, D. E., GOLDSTEIN, J. M., DE LAAT, R., BANDUCCI, K., CACCAVELLO, R. J., BARBOUR, R., HUANG, J., KLING, K., LEE, M., DIEP, L., KEIM, P. S., SHEN, X., CHATAWAY, T., SCHLOSSMACHER, M. G., SEUBERT, P., SCHENK, D., SINHA, S., GAI, W. P. & CHILCOTE, T. J. 2006. Phosphorylation of Ser-129 is the dominant pathological modification of alpha-synuclein in familial and sporadic Lewy body disease. *J Biol Chem,* 281**,** 29739-52.

ANGELI, A., MENCACCI, N. E., DURAN, R., AVILES-OLMOS, I., KEFALOPOULOU, Z., CANDELARIO, J., RUSBRIDGE, S., FOLEY, J., PRADHAN, P., JAHANSHAHI, M., ZRINZO, L., HARIZ, M., WOOD, N. W., HARDY, J., LIMOUSIN, P. & FOLTYNIE, T. 2013. Genotype and phenotype in Parkinson's disease: lessons in heterogeneity from deep brain stimulation. *Mov Disord,* 28**,** 1370-5.

ANHEIM, M., ELBAZ, A., LESAGE, S., DURR, A., CONDROYER, C., VIALLET, F., POLLAK, P., BONAITI, B., BONAITI-PELLIE, C., BRICE, A. & FRENCH PARKINSON DISEASE GENETIC, G. 2012. Penetrance of Parkinson disease in glucocerebrosidase gene mutation carriers. *Neurology,* 78**,** 417-20.

ARRANT, A. E., ROTH, J. R., BOYLE, N. R., KASHYAP, S. N., HOFFMANN, M. Q., MURCHISON, C. F., RAMOS, E. M., NANA, A. L., SPINA, S., GRINBERG, L. T., MILLER, B. L., SEELEY, W. W. & ROBERSON, E. D. 2019. Impaired β-glucocerebrosidase activity and processing in frontotemporal dementia due to progranulin mutations. *Acta Neuropathologica Communications,* 7**,** 218.

ATASHRAZM, F., HAMMOND, D., PERERA, G., DOBSON-STONE, C., MUELLER, N., PICKFORD, R., KIM, W. S., KWOK, J. B., LEWIS, S. J. G., HALLIDAY, G. M. & DZAMKO, N. 2018. Reduced glucocerebrosidase activity in monocytes from patients with Parkinson's disease. *Sci Rep,* 8**,** 15446.

ATRIAN, S., LOPEZ-VINAS, E., GOMEZ-PUERTAS, P., CHABAS, A., VILAGELIU, L. & GRINBERG, D. 2008. An evolutionary and structure-based docking model for glucocerebrosidase-saposin C and glucocerebrosidase-substrate interactions - relevance for Gaucher disease. *Proteins,* 70**,** 882-91.

AUBURGER, G., KLINKENBERG, M., DROST, J., MARCUS, K., MORALES-GORDO, B., KUNZ, W. S., BRANDT, U., BROCCOLI, V., REICHMANN, H., GISPERT, S. & JENDRACH, M. 2012. Primary skin fibroblasts as a model of Parkinson's disease. *Molecular neurobiology,* 46**,** 20-27.

BABAJANI, G., TROPAK, M. B., MAHURAN, D. J. & KERMODE, A. R. 2012. Pharmacological chaperones facilitate the post-ER transport of recombinant N370S mutant β-glucocerebrosidase in plant cells: evidence that N370S is a folding mutant. *Molecular genetics and metabolism,* 106**,** 323-329.

BAE, E. J., YANG, N. Y., LEE, C., LEE, H. J., KIM, S., SARDI, S. P. & LEE, S. J. 2015. Loss of glucocerebrosidase 1 activity causes lysosomal dysfunction and alpha-synuclein aggregation. *Exp Mol Med,* 47**,** e153.

BAE, E. J., YANG, N. Y., SONG, M., LEE, C. S., LEE, J. S., JUNG, B. C., LEE, H. J., KIM, S., MASLIAH, E., SARDI, S. P. & LEE, S. J. 2014. Glucocerebrosidase depletion enhances cell-to-cell transmission of alpha-synuclein. *Nat Commun,* 5**,** 4755.

BAEK, J.-H., WHITFIELD, D., HOWLETT, D., FRANCIS, P., BERECZKI, E., BALLARD, C., HORTOBÁGYI, T., ATTEMS, J. & AARSLAND, D. 2016. Unfolded protein response is activated in Lewy body dementias. *Neuropathology and Applied Neurobiology,* 42**,** 352-365.

BALESTRINO, R. & SCHAPIRA, A. H. V. 2018. Glucocerebrosidase and Parkinson Disease: Molecular, Clinical, and Therapeutic Implications. *Neuroscientist,* 24**,** 540-559.

BALESTRINO, R. & SCHAPIRA, A. H. V. 2020. Parkinson disease. *European Journal of Neurology,* 27**,** 27-42.

BAN, B. K., JUN, M. H., RYU, H. H., JANG, D. J., AHMAD, S. T. & LEE, J. A. 2013. Autophagy negatively regulates early axon growth in cortical neurons. *Mol Cell Biol,* 33**,** 3907-19.

BARBER, M., BALDWIN, A., GILBERT, R. & MULLER, H. 2018. Glucocerebrosidase rescues alpha-synuclein from amyloid formation. *bioRxiv*.

BARTELS, T., CHOI, J. G. & SELKOE, D. J. 2011. α-Synuclein occurs physiologically as a helically folded tetramer that resists aggregation. *Nature,* 477**,** 107-110.

BEAVAN, M., MCNEILL, A., PROUKAKIS, C., HUGHES, D. A., MEHTA, A. & SCHAPIRA, A. H. 2015. Evolution of prodromal clinical markers of Parkinson disease in a GBA mutation-positive cohort. *JAMA Neurol,* 72**,** 201-8.

BELLUCCI, A., NAVARRIA, L., ZALTIERI, M., FALARTI, E., BODEI, S., SIGALA, S., BATTISTIN, L., SPILLANTINI, M., MISSALE, C. & SPANO, P. 2011. Induction of the unfolded protein response by α-synuclein in experimental models of Parkinson's disease. *J Neurochem,* 116**,** 588-605.

BEN BDIRA, F., KALLEMEIJN, W. W., OUSSOREN, S. V., SCHEIJ, S., BLEIJLEVENS, B., FLOREA, B. I., VAN ROOMEN, C. P. A. A., OTTENHOFF, R., VAN KOOTEN, M. J. F. M., WALVOORT, M. T. C., WITTE, M. D., BOOT, R. G., UBBINK, M., OVERKLEEFT, H. S. & AERTS, J. M. F. G. 2017. Stabilization of Glucocerebrosidase by Active Site Occupancy. *ACS Chemical Biology,* 12**,** 1830-1841.

BENADOR, I. Y., VELIOVA, M., MAHDAVIANI, K., PETCHERSKI, A., WIKSTROM, J. D., ASSALI, E. A., ACÍN-PÉREZ, R., SHUM, M., OLIVEIRA, M. F., CINTI, S., SZTALRYD, C., BARSHOP, W. D., WOHLSCHLEGEL, J. A., CORKEY, B. E., LIESA, M. & SHIRIHAI, O. S. 2018. Mitochondria Bound to Lipid Droplets Have Unique Bioenergetics,

Composition, and Dynamics that Support Lipid Droplet Expansion. *Cell metabolism,* 27**,** 869-885.e6.

BENDIKOV-BAR, I., MAOR, G. & HOROWITZ, M. 2013. Processing and maturation of human glucocerebrosidase. *Advances in Gaucher Disease: Basic and Clinical Perspectives.* Future Medicine Ltd.

BENDIKOV-BAR, I., RON, I., FILOCAMO, M. & HOROWITZ, M. 2011. Characterization of the ERAD process of the L444P mutant glucocerebrosidase variant. *Blood Cells, Molecules, and Diseases,* 46**,** 4-10.

BENDOR, J. T., LOGAN, T. P. & EDWARDS, R. H. 2013. The function of alpha-synuclein. *Neuron,* 79**,** 1044-66.

BENYAIR, R., RON, E. & LEDERKREMER, G. Z. 2011. Protein quality control, retention, and degradation at the endoplasmic reticulum. *Int Rev Cell Mol Biol,* 292**,** 197-280.

BERG-FUSSMAN, A., GRACE, M. E., IOANNOU, Y. & GRABOWSKI, G. A. 1993. Human acid beta-glucosidase. N-glycosylation site occupancy and the effect of glycosylation on enzymatic activity. *J Biol Chem,* 268**,** 14861-6.

BERGE-SEIDL, V., PIHLSTRØM, L., MAPLE-GRØDEM, J., FORSGREN, L., LINDER, J., LARSEN, J. P., TYSNES, O.-B. & TOFT, M. 2017. The GBA variant E326K is associated with Parkinson's disease and explains a genome-wide association signal. *Neuroscience Letters,* 658**,** 48-52.

BERGER, Z., PERKINS, S., AMBROISE, C., OBORSKI, C., CALABRESE, M., NOELL, S., RIDDELL, D. & HIRST, W. D. 2015. Tool compounds robustly increase turnover of an artificial substrate by glucocerebrosidase in human brain lysates. *PLoS One,* 10**,** e0119141.

BERGMANN, J. E. & GRABOWSKI, G. A. 1989. Posttranslational processing of human lysosomal acid beta-glucosidase: a continuum of defects in Gaucher disease type 1 and type 2 fibroblasts. *American journal of human genetics,* 44**,** 741-750.

BERNIER, V., BICHET, D. G. & BOUVIER, M. 2004. Pharmacological chaperone action on G-protein-coupled receptors. *Curr Opin Pharmacol,* 4**,** 528-33.

BERRIDGE, M. J., LIPP, P. & BOOTMAN, M. D. 2000. The versatility and universality of calcium signalling. *Nat Rev Mol Cell Biol,* 1**,** 11-21.

BEUTLER, E., BEUTLER, L. & WEST, C. 2004. Mutations in the gene encoding cytosolic beta-glucosidase in Gaucher disease. *J Lab Clin Med,* 144**,** 65-8.

BEUTLER, E., GELBART, T. & SCOTT, C. R. 2005. Hematologically important mutations: Gaucher disease. *Blood Cells Mol Dis,* 35**,** 355-64.

BEUTLER, E. & KUHL, W. 1986. Glucocerebrosidase processing in normal fibroblasts and in fibroblasts from patients with type I, type II, and type III Gaucher disease. *Proc Natl Acad Sci U S A,* 83**,** 7472-4.

BIEDLER, J. L., ROFFLER-TARLOV, S., SCHACHNER, M. & FREEDMAN, L. S. 1978. Multiple neurotransmitter synthesis by human neuroblastoma cell lines and clones. *Cancer Res,* 38**,** 3751-7.

BLANZ, J., GROTH, J., ZACHOS, C., WEHLING, C., SAFTIG, P. & SCHWAKE, M. 2010. Disease-causing mutations within the lysosomal integral membrane protein type 2 (LIMP-2) reveal the nature of binding to its ligand beta-glucocerebrosidase. *Hum Mol Genet,* 19**,** 563-72.

BLANZ, J. & SAFTIG, P. 2016. Parkinson's disease: acid-glucocerebrosidase activity and alpha-synuclein clearance. *Journal of Neurochemistry,* 139**,** 198-215.

BLAUWENDRAAT, C., REED, X., KROHN, L., HEILBRON, K., BANDRES-CIGA, S., TAN, M., GIBBS, J. R., HERNANDEZ, D. G., KUMARAN, R., LANGSTON, R., BONET-PONCE, L., ALCALAY, R. N., HASSIN-BAER, S., GREENBAUM, L., IWAKI, H., LEONARD, H. L., GRENN, F. P., RUSKEY, J. A., SABIR, M., AHMED, S., MAKARIOUS, M. B., PIHLSTRØM, L., TOFT, M., VAN HILTEN, J. J., MARINUS, J., SCHULTE, C., BROCKMANN, K., SHARMA, M., SIITONEN, A., MAJAMAA, K., EEROLA-RAUTIO, J., TIENARI, P. J., PANTELYAT, A., HILLIS, A. E., DAWSON, T. M., ROSENTHAL, L. S., ALBERT, M. S., RESNICK, S. M., FERRUCCI, L., MORRIS, C. M., PLETNIKOVA, O., TRONCOSO, J., GROSSET, D., LESAGE, S., CORVOL, J. C., BRICE, A., NOYCE, A. J., MASLIAH, E., WOOD, N., HARDY, J., SHULMAN, L. M., JANKOVIC, J., SHULMAN, J. M., HEUTINK, P., GASSER, T., CANNON, P., SCHOLZ, S. W., MORRIS, H., COOKSON, M. R., NALLS, M. A., GAN-OR, Z. & SINGLETON, A. B. 2020. Genetic modifiers of risk and age at onset in GBA associated Parkinson's disease and Lewy body dementia. *Brain,* 143**,** 234-248.

BOGETOFTE, H., RYAN, B. J., JENSEN, P., VERGOOSSEN, D. L. E., BARNKOB, M. B., KIANI, L., CHUGHTAI, U., BRANDES, J., VOWLES, J., BUNN, F., KILFEATHER, P., FERNANDES, H. J. R., CAFFREY, T., MEYER, M., COWLEY, S. A., LARSEN, M. R. & WADE-MARTINS, R. 2021. A novel post-translational proteomics platform identifies neurite outgrowth impairments in Parkinson’s disease GBA-N370S dopamine neurons. *bioRxiv***,** 2021.06.30.450333.

BOOT, R. G., VERHOEK, M., DONKER-KOOPMAN, W., STRIJLAND, A., VAN MARLE, J., OVERKLEEFT, H. S., WENNEKES, T. & AERTS, J. M. F. G.

2007. Identification of the non-lysosomal glucosylceramidase as beta-glucosidase 2. *Journal of Biological Chemistry,* 282**,** 1305-1312.

BORGHI, R., MARCHESE, R., NEGRO, A., MARINELLI, L., FORLONI, G., ZACCHEO, D., ABBRUZZESE, G. & TABATON, M. 2000. Full length alpha-synuclein is present in cerebrospinal fluid from Parkinson's disease and normal subjects. *Neurosci Lett,* 287**,** 65-7.

BORGS, L., PEYRE, E., ALIX, P., HANON, K., GROBARCZYK, B., GODIN, J. D., PURNELLE, A., KRUSY, N., MAQUET, P., LEFEBVRE, P., SEUTIN, V., MALGRANGE, B. & NGUYEN, L. 2016. Dopaminergic neurons differentiating from LRRK2 G2019S induced pluripotent stem cells show early neuritic branching defects. *Scientific reports,* 6**,** 33377-33377.

BOUTIN, M., SUN, Y., SHACKA, J. J. & AURAY-BLAIS, C. 2016. Tandem Mass Spectrometry Multiplex Analysis of Glucosylceramide and Galactosylceramide Isoforms in Brain Tissues at Different Stages of Parkinson Disease. *Anal Chem,* 88**,** 1856-63.

BOZZA, P. T. & VIOLA, J. P. 2010. Lipid droplets in inflammation and cancer. *Prostaglandins Leukot Essent Fatty Acids,* 82**,** 243-50.

BRAAK, H. 2017. Neuropathological Staging of Brain Pathology in Sporadic Parkinson’s disease: Separating the Wheat from the Chaff. 7**,** S71-85.

BRAAK, H., TREDICI, K. D., RÜB, U., DE VOS, R. A. I., JANSEN STEUR, E. N. H. & BRAAK, E. 2003. Staging of brain pathology related to sporadic Parkinson’s disease. *Neurobiology of Aging,* 24**,** 197-211.

BRADE, L., VIELHABER, G., HEINZ, E. & BRADE, H. 2000. In vitro characterization of anti-glucosylceramide rabbit antisera. *Glycobiology,* 10**,** 629-636.

BRAULKE, T. & BONIFACINO, J. S. 2009. Sorting of lysosomal proteins. *Biochim Biophys Acta,* 1793**,** 605-14.

BRAUNSTEIN, H., MAOR, G., CHICCO, G., FILOCAMO, M., ZIMRAN, A. & HOROWITZ, M. 2018. UPR activation and CHOP mediated induction of GBA1 transcription in Gaucher disease. *Blood Cells, Molecules, and Diseases,* 68**,** 21-29.

BREKK, O. R., HONEY, J. R., LEE, S., HALLETT, P. J. & ISACSON, O. 2020. Cell type-specific lipid storage changes in Parkinson's disease patient brains are recapitulated by experimental glycolipid disturbance. *Proceedings of the National Academy of Sciences,* 117**,** 27646.

BROCKMANN, K., SRULIJES, K., HAUSER, A. K., SCHULTE, C., CSOTI, I., GASSER, T. & BERG, D. 2011. GBA-associated PD presents with nonmotor characteristics. *Neurology,* 77**,** 276-80.

BROCKMANN, K., SRULIJES, K., PFLEDERER, S., HAUSER, A. K., SCHULTE, C., MAETZLER, W., GASSER, T. & BERG, D. 2015. GBA-associated Parkinson's disease: reduced survival and more rapid progression in a prospective longitudinal study. *Mov Disord,* 30**,** 407-11.

BROWN, A. M., RIDDOCH, F. C., ROBSON, A., REDFERN, C. P. & CHEEK, T. R. 2005. Mechanistic and functional changes in Ca2+ entry after retinoic acid-induced differentiation of neuroblastoma cells. *Biochem J,* 388**,** 941-8.

BRUNDIN, P., LI, J. Y., HOLTON, J. L., LINDVALL, O. & REVESZ, T. 2008. Research in motion: the enigma of Parkinson's disease pathology spread. *Nat Rev Neurosci,* 9**,** 741-5.

BULTRON, G., KACENA, K., PEARSON, D., BOXER, M., YANG, R., SATHE, S., PASTORES, G. & MISTRY, P. K. 2010. The risk of Parkinson's disease in type 1 Gaucher disease. *J Inherit Metab Dis,* 33**,** 167-73.

BURBULLA, L. F., SONG, P., MAZZULLI, J. R., ZAMPESE, E., WONG, Y. C., JEON, S., SANTOS, D. P., BLANZ, J., OBERMAIER, C. D., STROJNY, C., SAVAS, J. N., KISKINIS, E., ZHUANG, X., KRÜGER, R., SURMEIER, D. J. & KRAINC, D. 2017. Dopamine oxidation mediates mitochondrial and lysosomal dysfunction in Parkinson's disease. *Science (New York, N.Y.),* 357**,** 1255-1261.

BURGESS, R. R. 2018. A brief practical review of size exclusion chromatography: Rules of thumb, limitations, and troubleshooting. *Protein Expr Purif,* 150**,** 81-85.

CABODEVILLA, A. G., SANCHEZ-CABALLERO, L., NINTOU, E., BOIADJIEVA, V. G., PICATOSTE, F., GUBERN, A. & CLARO, E. 2013. Cell survival during complete nutrient deprivation depends on lipid droplet-fueled beta-oxidation of fatty acids. *J Biol Chem,* 288**,** 27777-88.

CASCELLA, R., CHEN, S. W., BIGI, A., CAMINO, J. D., XU, C. K., DOBSON, C. M., CHITI, F., CREMADES, N. & CECCHI, C. 2021. The release of toxic oligomers from alpha-synuclein fibrils induces dysfunction in neuronal cells. *Nat Commun,* 12**,** 1814.

CAVALIERE, F., CERF, L., DEHAY, B., RAMOS-GONZALEZ, P., DE GIORGI, F., BOURDENX, M., BESSEDE, A., OBESO, J. A., MATUTE, C., ICHAS, F. & BEZARD, E. 2017. In vitro alpha-synuclein neurotoxicity and spreading among neurons and astrocytes using Lewy body extracts from Parkinson disease brains. *Neurobiol Dis,* 103**,** 101-112.

CELEJ, M. S., SARROUKH, R., GOORMAGHTIGH, E., FIDELIO, G. D., RUYSSCHAERT, J. M. & RAUSSENS, V. 2012. Toxic prefibrillar α-synuclein amyloid oligomers adopt a distinctive antiparallel β-sheet structure. *Biochem J,* 443**,** 719-26.

CERRI, S., GHEZZI, C., ONGARI, G., CROCE, S., AVENALI, M., ZANGAGLIA, R., DI MONTE, D. A., VALENTE, E. M. & BLANDINI, F. 2021. GBA Mutations Influence the Release and Pathological Effects of Small Extracellular Vesicles from Fibroblasts of Patients with Parkinson's Disease. *Int J Mol Sci,* 22.

CHABAS, A., GORT, L., DIAZ-FONT, A., MONTFORT, M., SANTAMARIA, R., CIDRAS, M., GRINBERG, D. & VILAGELIU, L. 2005. Perinatal lethal phenotype with generalized ichthyosis in a type 2 Gaucher disease patient with the [L444P;E326K]/P182L genotype: effect of the E326K change in neonatal and classic forms of the disease. *Blood Cells Mol Dis,* 35**,** 253-8.

CHARROW, J., ANDERSSON, H. C., KAPLAN, P. & ET AL. 2000. The gaucher registry: Demographics and disease characteristics of 1698 patients with gaucher disease. *Archives of Internal Medicine,* 160**,** 2835-2843.

CHEN, J., LI, W., ZHANG, T., WANG, Y. J., JIANG, X. J. & XU, Z. Q. 2014. Glucocerebrosidase gene mutations associated with Parkinson's disease: a meta-analysis in a Chinese population. *PLoS One,* 9**,** e115747.

CHEN, J. X., SUN, Y. J., WANG, P., LONG, D. X., LI, W., LI, L. & WU, Y. J. 2013. Induction of autophagy by TOCP in differentiated human neuroblastoma cells lead to degradation of cytoskeletal components and inhibition of neurite outgrowth. *Toxicology,* 310**,** 92-7.

CHEN, S. W., DRAKULIC, S., DEAS, E., OUBERAI, M., APRILE, F. A., ARRANZ, R., NESS, S., ROODVELDT, C., GUILLIAMS, T., DE-GENST, E. J.,

KLENERMAN, D., WOOD, N. W., KNOWLES, T. P. J., ALFONSO, C., RIVAS, G., ABRAMOV, A. Y., VALPUESTA, J. M., DOBSON, C. M. & CREMADES, N. 2015. Structural characterization of toxic oligomers that are kinetically trapped during α-synuclein fibril formation. *Proceedings of the National Academy of Sciences of the United States of America,* 112**,** E1994-E2003.

CHERIAN, A. & DIVYA, K. P. 2020. Genetics of Parkinson's disease. *Acta Neurologica Belgica,* 120**,** 1297-1305.

CHETRIT, E. B., ALCALAY, R. N., STEINER-BIRMANNS, B., ALTARESCU, G., PHILLIPS, M., ELSTEIN, D. & ZIMRAN, A. 2013. Phenotype in patients with Gaucher disease and Parkinson disease. *Blood Cells Mol Dis,* 50**,** 218-21.

CHI, Y. I., MARTINEZ-CRUZ, L. A., JANCARIK, J., SWANSON, R. V., ROBERTSON, D. E. & KIM, S. H. 1999. Crystal structure of the beta-glycosidase from the hyperthermophile Thermosphaera aggregans: insights into its activity and thermostability. *Febs Letters,* 445**,** 375-383.

CHIASSERINI, D., PACIOTTI, S., EUSEBI, P., PERSICHETTI, E., TASEGIAN, A., KURZAWA-AKANBI, M., CHINNERY, P. F., MORRIS, C. M., CALABRESI, P., PARNETTI, L. & BECCARI, T. 2015. Selective loss of glucocerebrosidase activity in sporadic Parkinson's disease and dementia with Lewy bodies. *Mol Neurodegener,* 10**,** 15.

CHOI, H., KIM, T.-L., CHO, M.-H. & BHOO, S.-H. 2017. Immuno-affinity purification of 2B8-tagged proteins. *Applied Biological Chemistry,* 60**,** 563-568.

CHOI, J. H., STUBBLEFIELD, B., COOKSON, M. R., GOLDIN, E., VELAYATI, A., TAYEBI, N. & SIDRANSKY, E. 2011. Aggregation of α-synuclein in

brain samples from subjects with glucocerebrosidase mutations. *Molecular genetics and metabolism,* 104**,** 185-188.

CHUNG, C. Y., SEO, H., SONNTAG, K. C., BROOKS, A., LIN, L. & ISACSON, O. 2005. Cell type-specific gene expression of midbrain dopaminergic neurons reveals molecules involved in their vulnerability and protection. *Human molecular genetics,* 14**,** 1709-1725.

CHUNG, H. K., HO, H.-A., PÉREZ-ACUÑA, D. & LEE, S.-J. 2019. Modeling α-Synuclein Propagation with Preformed Fibril Injections. *Journal of movement disorders,* 12**,** 139-151.

CHUNG, S. S. M., HO, E. C. M., LAM, K. S. L. & CHUNG, S. K. 2003. Contribution of Polyol Pathway to Diabetes-Induced Oxidative Stress. *Journal of the American Society of Nephrology,* 14**,** S233-S236.

CILIA, R., TUNESI, S., MAROTTA, G., CEREDA, E., SIRI, C., TESEI, S., ZECCHINELLI, A. L., CANESI, M., MARIANI, C. B., MEUCCI, N., SACILOTTO, G., ZINI, M., BARICHELLA, M., MAGNANI, C., DUGA, S., ASSELTA, R., SOLDA, G., SERESINI, A., SEIA, M., PEZZOLI, G. & GOLDWURM, S. 2016. Survival and dementia in GBA-associated Parkinson's disease: The mutation matters. *Ann Neurol,* 80**,** 662-673.

CINGOLANI, F. & CZAJA, M. J. 2016. Regulation and Functions of Autophagic Lipolysis. *Trends Endocrinol Metab,* 27**,** 696-705.

CLARK, L. N., CHAN, R., CHENG, R., LIU, X., PARK, N., PARMALEE, N., KISSELEV, S., CORTES, E., TORRES, P. A., PASTORES, G. M., VONSATTEL, J. P., ALCALAY, R., MARDER, K., HONIG, L. L., FAHN, S., MAYEUX, R., SHELANSKI, M., DI PAOLO, G. & LEE, J. H. 2015. Gene-wise association of variants in four lysosomal storage disorder genes in

neuropathologically confirmed Lewy body disease. *PLoS One,* 10**,** e0125204.

CLARK, L. N., KARTSAKLIS, L. A., WOLF GILBERT, R., DORADO, B., ROSS, B. M., KISSELEV, S., VERBITSKY, M., MEJIA-SANTANA, H., COTE, L. J., ANDREWS, H., VONSATTEL, J. P., FAHN, S., MAYEUX, R., HONIG, L. S. & MARDER, K. 2009. Association of glucocerebrosidase mutations with dementia with lewy bodies. *Arch Neurol,* 66**,** 578-83.

CLARK, L. N., ROSS, B. M., WANG, Y., MEJIA-SANTANA, H., HARRIS, J., LOUIS, E. D., COTE, L. J., ANDREWS, H., FAHN, S., WATERS, C., FORD, B., FRUCHT, S., OTTMAN, R. & MARDER, K. 2007. Mutations in the glucocerebrosidase gene are associated with early-onset Parkinson disease. *Neurology,* 69**,** 1270-1277.

CLEETER, M. W., CHAU, K. Y., GLUCK, C., MEHTA, A., HUGHES, D. A., DUCHEN, M., WOOD, N. W., HARDY, J., MARK COOPER, J. & SCHAPIRA, A. H. 2013. Glucocerebrosidase inhibition causes mitochondrial dysfunction and free radical damage. *Neurochem Int,* 62**,** 1-7.

COLE, N. B., MURPHY, D. D., GRIDER, T., RUETER, S., BRASAEMLE, D. & NUSSBAUM, R. L. 2002. Lipid droplet binding and oligomerization properties of the Parkinson's disease protein alpha-synuclein. *J Biol Chem,* 277**,** 6344-52.

COLLA, E., COUNE, P., LIU, Y., PLETNIKOVA, O., TRONCOSO, J. C., IWATSUBO, T., SCHNEIDER, B. L. & LEE, M. K. 2012a. Endoplasmic Reticulum Stress Is Important for the Manifestations of alpha-Synucleinopathy In Vivo. *Journal of Neuroscience,* 32**,** 3306-3320.

COLLA, E., JENSEN, P. H., PLETNIKOVA, O., TRONCOSO, J. C., GLABE, C. & LEE, M. K. 2012b. Accumulation of Toxic alpha-Synuclein Oligomer within Endoplasmic Reticulum Occurs in alpha-Synucleinopathy In Vivo. *Journal of Neuroscience,* 32**,** 3301-3305.

COLLINS, L. M., DROUIN-OUELLET, J., KUAN, W. L., COX, T. & BARKER, R. A. 2017. Dermal fibroblasts from patients with Parkinson's disease have normal GCase activity and autophagy compared to patients with PD and GBA mutations. *F1000Res,* 6**,** 1751.

CONWAY, K. A., HARPER, J. D. & LANSBURY, P. T., JR. 2000. Fibrils formed in vitro from alpha-synuclein and two mutant forms linked to Parkinson's disease are typical amyloid. *Biochemistry,* 39**,** 2552-63.

COOPER, A. A., GITLER, A. D., CASHIKAR, A., HAYNES, C. M., HILL, K. J., BHULLAR, B., LIU, K., XU, K., STRATHEARN, K. E., LIU, F., CAO, S., CALDWELL, K. A., CALDWELL, G. A., MARSISCHKY, G., KOLODNER, R. D., LABAER, J., ROCHET, J. C., BONINI, N. M. & LINDQUIST, S. 2006. Alpha-synuclein blocks ER-Golgi traffic and Rab1 rescues neuron loss in Parkinson's models. *Science,* 313**,** 324-8.

COTA-CORONADO, J. A., SANDOVAL-ÁVILA, S., GAYTAN-DÁVILA, Y. P., DIAZ, N. F., VEGA-RUIZ, B., PADILLA-CAMBEROS, E. & DÍAZ-MARTÍNEZ, N. E. 2020. New transgenic models of Parkinson's disease using genome editing technology. *Neurología (English Edition),* 35**,** 486-499.

CREED, R. B. & GOLDBERG, M. S. 2019. Analysis of α-Synuclein Pathology in PINK1 Knockout Rat Brains. *Frontiers in Neuroscience,* 12.

CUERVO, A. M., STEFANIS, L., FREDENBURG, R., LANSBURY, P. T. & SULZER, D. 2004. Impaired degradation of mutant alpha-synuclein by chaperone-mediated autophagy. *Science,* 305**,** 1292-5.

CUERVO, A. M. & WONG, E. 2013. Chaperone-mediated autophagy: roles in disease and aging. *Cell Research,* 24**,** 92.

CULLEN, V., SARDI, P., NG, J., XU, Y. H., SUN, Y., TOMLINSON, J. J., KOLODZIEJ, P., KAHN, I., SAFTIG, P., WOULFE, J., ROCHET, J. C., GLICKSMAN, M. A., CHENG, S. H., GRABOWSKI, G. A., SHIHABUDDIN, L. S. & SCHLOSSMACHER, M. G. 2011. Acid beta-Glucosidase Mutants Linked to Gaucher Disease, Parkinson Disease, and Lewy Body Dementia Alter alpha-Synuclein Processing. *Annals of Neurology,* 69**,** 940-953.

DALBEY, R. E. & WICKNER, W. 1985. Leader peptidase catalyzes the release of exported proteins from the outer surface of the Escherichia coli plasma membrane. *J Biol Chem,* 260**,** 15925-31.

DANDANA, A., BEN KHELIFA, S., CHAHED, H., MILED, A. & FERCHICHI, S. 2016. Gaucher Disease: Clinical, Biological and Therapeutic Aspects. *Pathobiology,* 83**,** 13-23.

DASGUPTA, N., XU, Y.-H., LI, R., PENG, Y., PANDEY, M. K., TINCH, S. L., LIOU, B., INSKEEP, V., ZHANG, W., SETCHELL, K. D. R., KEDDACHE, M., GRABOWSKI, G. A. & SUN, Y. 2015. Neuronopathic Gaucher disease: dysregulated mRNAs and miRNAs in brain pathogenesis and effects of pharmacologic chaperone treatment in a mouse model. *Human molecular genetics,* 24**,** 7031-7048.

DAVIDSON, W. S., JONAS, A., CLAYTON, D. F. & GEORGE, J. M. 1998. Stabilization of alpha-synuclein secondary structure upon binding to synthetic membranes. *J Biol Chem,* 273**,** 9443-9.

DAVIS, M. Y., JOHNSON, C. O., LEVERENZ, J. B., WEINTRAUB, D., TROJANOWSKI, J. Q., CHEN-PLOTKIN, A., VAN DEERLIN, V. M., QUINN, J. F., CHUNG, K. A., PETERSON-HILLER, A. L., ROSENTHAL, L. S., DAWSON, T. M., ALBERT, M. S., GOLDMAN, J. G., STEBBINS, G. T., BERNARD, B., WSZOLEK, Z. K., ROSS, O. A., DICKSON, D. W., EIDELBERG, D., MATTIS, P. J., NIETHAMMER, M., YEAROUT, D., HU, S. C., CHOLERTON, B. A., SMITH, M., MATA, I. F., MONTINE, T. J., EDWARDS, K. L. & ZABETIAN, C. P. 2016. Association of GBA Mutations and the E326K Polymorphism With Motor and Cognitive Progression in Parkinson Disease. *JAMA Neurol,* 73**,** 1217-1224.

DE LA MATA, M., COTÁN, D., OROPESA-ÁVILA, M., GARRIDO-MARAVER, J., CORDERO, M. D., VILLANUEVA PAZ, M., DELGADO PAVÓN, A., ALCOCER-GÓMEZ, E., DE LAVERA, I., YBOT-GONZÁLEZ, P., PAULA ZADERENKO, A., ORTIZ MELLET, C., GARCÍA FERNÁNDEZ, J. M. & SÁNCHEZ-ALCÁZAR, J. A. 2015. Pharmacological Chaperones and Coenzyme Q10 Treatment Improves Mutant β-Glucocerebrosidase Activity and Mitochondrial Function in Neuronopathic Forms of Gaucher Disease. *Scientific reports,* 5**,** 10903-10903.

DECAPRIO, J. & KOHL, T. O. 2019. Tandem Immunoaffinity Purification Using Anti-FLAG and Anti-HA Antibodies. *Cold Spring Harb Protoc,* 2019.

DEHAY, B., BOVE, J., RODRIGUEZ-MUELA, N., PERIER, C., RECASENS, A., BOYA, P. & VILA, M. 2010. Pathogenic lysosomal depletion in Parkinson's disease. *J Neurosci,* 30**,** 12535-44.

DEHAY, B., MARTINEZ-VICENTE, M., CALDWELL, G. A., CALDWELL, K. A., YUE, Z., COOKSON, M. R., KLEIN, C., VILA, M. & BEZARD, E. 2013. Lysosomal impairment in Parkinson's disease. *Mov Disord,* 28**,** 725-32.

DEN HEIJER, J. M., CULLEN, V. C., QUADRI, M., SCHMITZ, A., HILT, D. C., LANSBURY, P., BERENDSE, H. W., VAN DE BERG, W. D. J., DE BIE, R. M. A., BOERTIEN, J. M., BOON, A. J. W., CONTARINO, M. F., VAN HILTEN, J. J., HOFF, J. I., VAN MIERLO, T., MUNTS, A. G., VAN DER PLAS, A. A., PONSEN, M. M., BAAS, F., MAJOOR-KRAKAUER, D., BONIFATI, V., VAN LAAR, T. & GROENEVELD, G. J. 2020. A Large-Scale Full GBA1 Gene Screening in Parkinson's Disease in the Netherlands. *Mov Disord,* 35**,** 1667-1674.

DERMENTZAKI, G., DIMITRIOU, E., XILOURI, M., MICHELAKAKIS, H. & STEFANIS, L. 2013. Loss of β-Glucocerebrosidase Activity Does Not Affect Alpha-Synuclein Levels or Lysosomal Function in Neuronal Cells. *PLOS ONE,* 8**,** e60674.

DESPLATS, P., LEE, H.-J., BAE, E.-J., PATRICK, C., ROCKENSTEIN, E., CREWS, L., SPENCER, B., MASLIAH, E. & LEE, S.-J. 2009. Inclusion formation and neuronal cell death through neuron-to-neuron transmission of α-synuclein. *Proceedings of the National Academy of Sciences,* 106**,** 13010.

DETTMER, U., NEWMAN, A. J., LUTH, E. S., BARTELS, T. & SELKOE, D. 2013. In vivo cross-linking reveals principally oligomeric forms of α-synuclein and β-synuclein in neurons and non-neural cells. *J Biol Chem,* 288**,** 6371-85.

DILSIZOGLU SENOL, A., SAMARANI, M., SYAN, S., GUARDIA, C. M., NONAKA, T., LIV, N., LATOUR-LAMBERT, P., HASEGAWA, M., KLUMPERMAN, J., BONIFACINO, J. S. & ZURZOLO, C. 2021. alpha-Synuclein fibrils subvert lysosome structure and function for the propagation of protein misfolding between cells through tunneling nanotubes. *PLoS Biol,* 19**,** e3001287.

DU, T. T., WANG, L., DUAN, C. L., LU, L. L., ZHANG, J. L., GAO, G., QIU, X. B., WANG, X. M. & YANG, H. 2015. GBA deficiency promotes SNCA/alpha-synuclein accumulation through autophagic inhibition by inactivated PPP2A. *Autophagy,* 11**,** 1803-20.

DUFFY, M. F., COLLIER, T. J., PATTERSON, J. R., KEMP, C. J., FISCHER, D. L., STOLL, A. C. & SORTWELL, C. E. 2018. Quality Over Quantity: Advantages of Using Alpha-Synuclein Preformed Fibril Triggered Synucleinopathy to Model Idiopathic Parkinson's Disease. *Frontiers in Neuroscience,* 12.

DUNN, K. W., KAMOCKA, M. M. & MCDONALD, J. H. 2011. A practical guide to evaluating colocalization in biological microscopy. *American journal of physiology. Cell physiology,* 300**,** C723-C742.

DURAN, R., MENCACCI, N. E., ANGELI, A. V., SHOAI, M., DEAS, E., HOULDEN, H., MEHTA, A., HUGHES, D., COX, T. M., DEEGAN, P., SCHAPIRA, A. H., LEES, A. J., LIMOUSIN, P., JARMAN, P. R., BHATIA, K. P., WOOD, N. W., HARDY, J. & FOLTYNIE, T. 2013. The glucocerobrosidase E326K variant predisposes to Parkinson's disease, but does not cause Gaucher's disease. *Mov Disord,* 28**,** 232-236.

DVIR, H., HAREL, M., MCCARTHY, A. A., TOKER, L., SILMAN, I., FUTERMAN, A. H. & SUSSMAN, J. L. 2003. X-ray structure of human acid-beta-glucosidase, the defective enzyme in Gaucher disease. *EMBO Rep,* 4**,** 704-9.

EIRIKSSON, F. F., NØHR, M. K., COSTA, M., BÖDVARSDOTTIR, S. K., ÖGMUNDSDOTTIR, H. M. & THORSTEINSDOTTIR, M. 2020. Lipidomic study of cell lines reveals differences between breast cancer subtypes. *PloS one,* 15**,** e0231289-e0231289.

EL-AGNAF, O. M., JAKES, R., CURRAN, M. D., MIDDLETON, D., INGENITO, R., BIANCHI, E., PESSI, A., NEILL, D. & WALLACE, A. 1998. Aggregates from mutant and wild-type alpha-synuclein proteins and NAC peptide induce apoptotic cell death in human neuroblastoma cells by formation of beta-sheet and amyloid-like filaments. *FEBS Lett,* 440**,** 71-5.

EL-AGNAF, O. M., SALEM, S. A., PALEOLOGOU, K. E., COOPER, L. J., FULLWOOD, N. J., GIBSON, M. J., CURRAN, M. D., COURT, J. A., MANN, D. M., IKEDA, S., COOKSON, M. R., HARDY, J. & ALLSOP, D. 2003. Alpha-synuclein implicated in Parkinson's disease is present in extracellular biological fluids, including human plasma. *FASEB J,* 17**,** 1945-7.

EMMANOUILIDOU, E., MELACHROINOU, K., ROUMELIOTIS, T., GARBIS, S. D., NTZOUNI, M., MARGARITIS, L. H., STEFANIS, L. & VEKRELLIS, K. 2010. Cell-produced alpha-synuclein is secreted in a calcium-dependent manner by exosomes and impacts neuronal survival. *J Neurosci,* 30**,** 6838-51.

ENQUIST, I. B., LO BIANCO, C., OOKA, A., NILSSON, E., MANSSON, J. E., EHINGER, M., RICHTER, J., BRADY, R. O., KIRIK, D. & KARLSSON, S. 2007. Murine models of acute neuronopathic Gaucher disease. *Proc Natl Acad Sci U S A,* 104**,** 17483-8.

ESPARGARÓ, A., SABATE, R. & VENTURA, S. 2012. Thioflavin-S staining coupled to flow cytometry. A screening tool to detect in vivo protein aggregation. *Mol Biosyst,* 8**,** 2839-44.

FABELO, N., MARTIN, V., SANTPERE, G., MARIN, R., TORRENT, L., FERRER, I. & DIAZ, M. 2011. Severe alterations in lipid composition of frontal cortex

lipid rafts from Parkinson's disease and incidental Parkinson's disease. *Mol Med,* 17**,** 1107-18.

FAIRLEY, C., ZIMRAN, A., PHILLIPS, M., CIZMARIK, M., YEE, J., WEINREB, N. & PACKMAN, S. 2008. Phenotypic heterogeneity of N370S homozygotes with type I Gaucher disease: an analysis of 798 patients from the ICGG Gaucher Registry. *J Inherit Metab Dis,* 31**,** 738-44.

FALKENBURGER, B. H. & SCHULZ, J. B. 2006. Limitations of cellular models in Parkinson's disease research. *J Neural Transm Suppl***,** 261-8.

FANNING, S., HAQUE, A., IMBERDIS, T., BARU, V., BARRASA, M. I., NUBER, S., TERMINE, D., RAMALINGAM, N., HO, G. P. H., NOBLE, T., SANDOE, J., LOU, Y., LANDGRAF, D., FREYZON, Y., NEWBY, G., SOLDNER, F., TERRY-KANTOR, E., KIM, T.-E., HOFBAUER, H. F., BECUWE, M., JAENISCH, R., PINCUS, D., CLISH, C. B., WALTHER, T. C., FARESE, R. V., JR., SRINIVASAN, S., WELTE, M. A., KOHLWEIN, S. D., DETTMER, U., LINDQUIST, S. & SELKOE, D. 2019. Lipidomic Analysis of α-Synuclein Neurotoxicity Identifies Stearoyl CoA Desaturase as a Target for Parkinson Treatment. *Molecular cell,* 73**,** 1001-1014.e8.

FARFEL-BECKER, T., VITNER, E. B., KELLY, S. L., BAME, J. R., DUAN, J., SHINDER, V., MERRILL, A. H., JR., DOBRENIS, K. & FUTERMAN, A. H. 2014. Neuronal accumulation of glucosylceramide in a mouse model of neuronopathic Gaucher disease leads to neurodegeneration. *Hum Mol Genet,* 23**,** 843-54.

FARMER, B. C., WALSH, A. E., KLUEMPER, J. C. & JOHNSON, L. A. 2020. Lipid Droplets in Neurodegenerative Disorders. *Front Neurosci,* 14**,** 742.

FELLNER, L. & STEFANOVA, N. 2013. The role of glia in α-synucleinopathies. *Molecular neurobiology,* 47**,** 575-586.

FERNANDES, H. J. R., HARTFIELD, E. M., CHRISTIAN, H. C., EMMANOULIDOU, E., ZHENG, Y., BOOTH, H., BOGETOFTE, H., LANG, C., RYAN, B. J., SARDI, S. P., BADGER, J., VOWLES, J., EVETTS, S., TOFARIS, G. K., VEKRELLIS, K., TALBOT, K., HU, M. T., JAMES, W., COWLEY, S. A. & WADE-MARTINS, R. 2016. ER Stress and Autophagic Perturbations Lead to Elevated Extracellular α-Synuclein in GBA-N370S Parkinson's iPSC-Derived Dopamine Neurons. *Stem cell reports,* 6**,** 342-356.

FISHBEIN, I., KUO, Y. M., GIASSON, B. I. & NUSSBAUM, R. L. 2014. Augmentation of phenotype in a transgenic Parkinson mouse heterozygous for a Gaucher mutation. *Brain,* 137**,** 3235-3247.

FOG, C. K., ZAGO, P., MALINI, E., SOLANKO, L. M., PERUZZO, P., BORNAES, C., MAGNONI, R., MEHMEDBASIC, A., PETERSEN, N. H. T., BEMBI, B., AERTS, J., DARDIS, A. & KIRKEGAARD, T. 2018. The heat shock protein amplifier arimoclomol improves refolding, maturation and lysosomal activity of glucocerebrosidase. *EBioMedicine,* 38**,** 142-153.

FU, S., YANG, L., LI, P., HOFMANN, O., DICKER, L., HIDE, W., LIN, X., WATKINS, S. M., IVANOV, A. R. & HOTAMISLIGIL, G. S. 2011. Aberrant lipid metabolism disrupts calcium homeostasis causing liver endoplasmic reticulum stress in obesity. *Nature,* 473**,** 528-31.

FUJIWARA, H., HASEGAWA, M., DOHMAE, N., KAWASHIMA, A., MASLIAH, E., GOLDBERG, M. S., SHEN, J., TAKIO, K. & IWATSUBO, T. 2002. alpha-Synuclein is phosphorylated in synucleinopathy lesions. *Nat Cell Biol,* 4**,** 160-4.

FULLER, M., ROZAKLIS, T., LOVEJOY, M., ZARRINKALAM, K., HOPWOOD, J. J. & MEIKLE, P. J. 2008. Glucosylceramide accumulation is not confined

to the lysosome in fibroblasts from patients with Gaucher disease. *Molecular Genetics and Metabolism,* 93**,** 437-443.

FUSCO, G., DE SIMONE, A., GOPINATH, T., VOSTRIKOV, V., VENDRUSCOLO, M., DOBSON, C. M. & VEGLIA, G. 2014. Direct observation of the three regions in alpha-synuclein that determine its membrane-bound behaviour. *Nat Commun,* 5**,** 3827.

FUSSI, N., HÖLLERHAGE, M., CHAKROUN, T., NYKÄNEN, N.-P., RÖSLER, T. W., KOEGLSPERGER, T., WURST, W., BEHRENDS, C. & HÖGLINGER, G. U. 2018. Exosomal secretion of α-synuclein as protective mechanism after upstream blockage of macroautophagy. *Cell Death & Disease,* 9**,** 757.

GALVAGNION, C., BROWN, J. W. P., OUBERAI, M. M., FLAGMEIER, P., VENDRUSCOLO, M., BUELL, A. K., SPARR, E. & DOBSON, C. M. 2016. Chemical properties of lipids strongly affect the kinetics of the membrane-induced aggregation of α-synuclein. *Proceedings of the National Academy of Sciences of the United States of America,* 113**,** 7065-7070.

GALVAGNION, C., CERRI, S., SCHAPIRA, A. H. V., BLANDINI, F. & DI MONTE, D. A. 2020. Sphingolipid changes in Parkinson L444P GBA mutation fibroblasts promote α-synuclein aggregation. *bioRxiv***,** 2020.11.09.375048.

GAN-OR, Z., AMSHALOM, I., KILARSKI, L. L., BAR-SHIRA, A., GANA-WEISZ, M., MIRELMAN, A., MARDER, K., BRESSMAN, S., GILADI, N. & ORR-URTREGER, A. 2015. Differential effects of severe vs mild GBA mutations on Parkinson disease. *Neurology,* 84**,** 880-7.

GAN-OR, Z., BAR-SHIRA, A., MIRELMAN, A., GUREVICH, T., KEDMI, M., GILADI, N. & ORR-URTREGER, A. 2010. LRRK2 and GBA mutations

differentially affect the initial presentation of Parkinson disease. *Neurogenetics,* 11**,** 121-5.

GAN-OR, Z., GILADI, N. & ORR-URTREGER, A. 2009. Differential phenotype in Parkinson's disease patients with severe versus mild GBA mutations. *Brain,* 132**,** e125-e125.

GAN-OR, Z., GILADI, N., ROZOVSKI, U., SHIFRIN, C., ROSNER, S., GUREVICH, T., BAR-SHIRA, A. & ORR-URTREGER, A. 2008. Genotype-phenotype correlations between GBA mutations and Parkinson disease risk and onset. *Neurology,* 70**,** 2277-2283.

GANJAM, G. K., BOLTE, K., MATSCHKE, L. A., NEITEMEIER, S., DOLGA, A. M., HÖLLERHAGE, M., HÖGLINGER, G. U., ADAMCZYK, A., DECHER, N., OERTEL, W. H. & CULMSEE, C. 2019. Mitochondrial damage by α-synuclein causes cell death in human dopaminergic neurons. *Cell Death & Disease,* 10**,** 865.

GARCIA-SANZ, P., ORGAZ, L., BUENO-GIL, G., ESPADAS, I., RODRIGUEZ-TRAVER, E., KULISEVSKY, J., GUTIERREZ, A., DAVILA, J. C., GONZALEZ-POLO, R. A., FUENTES, J. M., MIR, P., VICARIO, C. & MORATALLA, R. 2017. N370S-GBA1 mutation causes lysosomal cholesterol accumulation in Parkinson's disease. *Mov Disord,* 32**,** 1409-1422.

GEGG, M. E., BURKE, D., HEALES, S. J., COOPER, J. M., HARDY, J., WOOD, N. W. & SCHAPIRA, A. H. 2012. Glucocerebrosidase deficiency in substantia nigra of parkinson disease brains. *Ann Neurol,* 72**,** 455-63.

GEGG, M. E. & SCHAPIRA, A. H. V. 2018. The role of glucocerebrosidase in Parkinson disease pathogenesis. *FEBS J,* 285**,** 3591-3603.

GEGG, M. E., SWEET, L., WANG, B. H., SHIHABUDDIN, L. S., SARDI, S. P. & SCHAPIRA, A. H. 2015. No evidence for substrate accumulation in Parkinson brains with GBA mutations. *Mov Disord,* 30**,** 1085-9.

GEGG, M. E., VERONA, G. & SCHAPIRA, A. H. V. 2020. Glucocerebrosidase deficiency promotes release of alpha-synuclein fibrils from cultured neurons. *Hum Mol Genet,* 29**,** 1716-1728.

GINNS, E. I., MAK, S. K., KO, N., KARLGREN, J., AKBARIAN, S., CHOU, V. P., GUO, Y., LIM, A., SAMUELSSON, S., LAMARCA, M. L., VAZQUEZ-DEROSE, J. & MANNING-BOG, A. B. 2014. Neuroinflammation and alpha-synuclein accumulation in response to glucocerebrosidase deficiency are accompanied by synaptic dysfunction. *Mol Genet Metab,* 111**,** 152-62.

GIRARD, V., JOLLIVET, F., KNITTELFELDER, O., ARSAC, J.-N., CHATELAIN, G., VAN DEN BRINK, D. M., BARON, T., SHEVCHENKO, A., DAVOUST-NATAF, N. & MOLLEREAU, B. 2020. Alpha-synuclein enhances lipid droplet accumulation in neurons in a Drosophila model of Parkinson’s disease. *bioRxiv***,** 2020.09.16.299354.

GIRARD, V., JOLLIVET, F., KNITTELFELDER, O., ARSAC, J.-N., CHATELAIN, G., VAN DEN BRINK, D. M., BARON, T., SHEVCHENKO, A., DAVOUST, N. & MOLLEREAU, B. 2021. A non-canonical lipid droplet metabolism regulates the conversion of alpha-Synuclein to proteolytic resistant forms in neurons of a Drosophila model of Parkinson disease. *bioRxiv***,** 2020.09.16.299354.

GLAJCH, K. E., MOORS, T. E., CHEN, Y., BECHADE, P. A., NAM, A. Y., RAJSOMBATH, M. M., MCCAFFERY, T. D., DETTMER, U., WEIHOFEN, A., HIRST, W. D., SELKOE, D. J. & NUBER, S. 2021. Wild-type GBA1

increases the alpha-synuclein tetramer-monomer ratio, reduces lipid-rich aggregates, and attenuates motor and cognitive deficits in mice. *Proc Natl Acad Sci U S A,* 118.

GOKER-ALPAN, O., GIASSON, B. I., EBLAN, M. J., NGUYEN, J., HURTIG, H. I., LEE, V. M. Y., TROJANOWSKI, J. Q. & SIDRANSKY, E. 2006. Glucocerebrosidase mutations are an important risk factor for Lewy body disorders. *Neurology,* 67**,** 908-910.

GOKER-ALPAN, O., LOPEZ, G., VITHAYATHIL, J., DAVIS, J., HALLETT, M. & SIDRANSKY, E. 2008. The spectrum of parkinsonian manifestations associated with glucocerebrosidase mutations. *Arch Neurol,* 65**,** 1353-7.

GOKER-ALPAN, O., STUBBLEFIELD, B. K., GIASSON, B. I. & SIDRANSKY, E. 2010. Glucocerebrosidase is present in alpha-synuclein inclusions in Lewy body disorders. *Acta Neuropathologica,* 120**,** 641-649.

GOLDSTEIN, O., GANA-WEISZ, M., COHEN-AVINOAM, D., SHINER, T., THALER, A., CEDARBAUM, J. M., JOHN, S., LALIOTI, M., GUREVICH, T., BAR-SHIRA, A., MIRELMAN, A., GILADI, N. & ORR-URTREGER, A. 2019. Revisiting the non-Gaucher-GBA-E326K carrier state: Is it sufficient to increase Parkinson's disease risk? *Mol Genet Metab,* 128**,** 470-475.

GOMES, A. R. & ROCHA-SANTOS, T. A. P. 2019. Bioassays | Enzyme Assays☆. *In:* WORSFOLD, P., POOLE, C., TOWNSHEND, A. & MIRÓ, M. (eds.) *Encyclopedia of Analytical Science (Third Edition).* Oxford: Academic Press.

GRABOWSKI, G. A. 2008. Phenotype, diagnosis, and treatment of Gaucher's disease. *Lancet,* 372**,** 1263-71.

GRABOWSKI, G. A. & DAGAN, A. 1984. Human lysosomal β-glucosidase: Purification by affinity chromatography. *Analytical Biochemistry,* 141**,** 267-279.

GRABOWSKI, G. A., GATT, S. & HOROWITZ, M. 1990. Acid beta-glucosidase: enzymology and molecular biology of Gaucher disease. *Crit Rev Biochem Mol Biol,* 25**,** 385-414.

GRABOWSKI, G. A., WHITE, W. R. & GRACE, M. E. 1989. Expression of Functional Human Acid Beta-Glucosidase in Cos-1 and Spodoptera-Frugiperda Cells. *Enzyme,* 41**,** 131-142.

GRACE, M. E., ASHTON-PROLLA, P., PASTORES, G. M., SONI, A. & DESNICK, R. J. 1999. Non-pseudogene-derived complex acid beta-glucosidase mutations causing mild type 1 and severe type 2 gaucher disease. *J Clin Invest,* 103**,** 817-23.

GRACE, M. E., BERG, A., HE, G. S., GOLDBERG, L., HOROWITZ, M. & GRABOWSKI, G. A. 1991. Gaucher disease: heterologous expression of two alleles associated with neuronopathic phenotypes. *Am J Hum Genet,* 49**,** 646-55.

GRACE, M. E. & GRABOWSKI, G. A. 1990. Human Acid Beta-Glucosidase - Glycosylation Is Required for Catalytic Activity. *Biochemical and Biophysical Research Communications,* 168**,** 771-777.

GRACE, M. E., NEWMAN, K. M., SCHEINKER, V., BERGFUSSMAN, A. & GRABOWSKI, G. A. 1994. Analysis of Human Acid Beta-Glucosidase by Site-Directed Mutagenesis and Heterologous Expression. *Journal of Biological Chemistry,* 269**,** 2283-2291.

GRAMLICH, P. A., WESTBROEK, W., FELDMAN, R. A., AWAD, O., MELLO, N., REMINGTON, M. P., SUN, Y., ZHANG, W., SIDRANSKY, E.,

BETENBAUGH, M. J. & FISHMAN, P. S. 2016. A peptide-linked recombinant glucocerebrosidase for targeted neuronal delivery: Design, production, and assessment. *Journal of biotechnology,* 221**,** 1-12.

GRASSI, D., HOWARD, S., ZHOU, M., DIAZ-PEREZ, N., URBAN, N. T., GUERRERO-GIVEN, D., KAMASAWA, N., VOLPICELLI-DALEY, L. A., LOGRASSO, P. & LASMÉZAS, C. I. 2018. Identification of a highly neurotoxic α-synuclein species inducing mitochondrial damage and mitophagy in Parkinson's disease. *Proceedings of the National Academy of Sciences of the United States of America,* 115**,** E2634-E2643.

GREUEL, A., TREZZI, J.-P., GLAAB, E., RUPPERT, M. C., MAIER, F., JÄGER, C., HODAK, Z., LOHMANN, K., MA, Y., EIDELBERG, D., TIMMERMANN, L., HILLER, K., TITTGEMEYER, M., DRZEZGA, A., DIEDERICH, N. & EGGERS, C. 2020. GBA Variants in Parkinson's Disease: Clinical, Metabolomic, and Multimodal Neuroimaging Phenotypes. *Movement Disorders,* 35**,** 2201-2210.

GUBERN, A., BARCELÓ-TORNS, M., CASAS, J., BARNEDA, D., MASGRAU, R., PICATOSTE, F., BALSINDE, J., BALBOA, M. A. & CLARO, E. 2009. Lipid droplet biogenesis induced by stress involves triacylglycerol synthesis that depends on group VIA phospholipase A2. *J Biol Chem,* 284**,** 5697-708.

GUEDES, L. C., CHAN, R. B., GOMES, M. A., CONCEICAO, V. A., MACHADO, R. B., SOARES, T., XU, Y., GASPAR, P., CARRICO, J. A., ALCALAY, R. N., FERREIRA, J. J., OUTEIRO, T. F. & MILTENBERGER-MILTENYI, G. 2017. Serum lipid alterations in GBA-associated Parkinson's disease. *Parkinsonism Relat Disord,* 44**,** 58-65.

GUNDNER, A. L., DURAN-PACHECO, G., ZIMMERMANN, S., RUF, I., MOORS, T., BAUMANN, K., JAGASIA, R., VAN DE BERG, W. D. J. & KREMER, T. 2019. Path mediation analysis reveals GBA impacts Lewy body disease status by increasing alpha-synuclein levels. *Neurobiol Dis,* 121**,** 205-213.

GUZMAN, J. N., SANCHEZ-PADILLA, J., WOKOSIN, D., KONDAPALLI, J., ILIJIC, E., SCHUMACKER, P. T. & SURMEIER, D. J. 2010. Oxidant stress evoked by pacemaking in dopaminergic neurons is attenuated by DJ-1. *Nature,* 468**,** 696-700.

HALABAN, R., SVEDINE, S., CHENG, E., SMICUN, Y., ARON, R. & HEBERT, D. N. 2000. Endoplasmic reticulum retention is a common defect associated with tyrosinase-negative albinism. *Proceedings of the National Academy of Sciences,* 97**,** 5889-5894.

HALIC, M. & BECKMANN, R. 2005. The signal recognition particle and its interactions during protein targeting. *Curr Opin Struct Biol,* 15**,** 116-25.

HALLETT, P. J., HUEBECKER, M., BREKK, O. R., MOLONEY, E. B., ROCHA, E. M., PRIESTMAN, D. A., PLATT, F. M. & ISACSON, O. 2018. Glycosphingolipid levels and glucocerebrosidase activity are altered in normal aging of the mouse brain. *Neurobiol Aging,* 67**,** 189-200.

HAN, X., ZHU, J., ZHANG, X., SONG, Q., DING, J., LU, M., SUN, S. & HU, G. 2018. Plin4-Dependent Lipid Droplets Hamper Neuronal Mitophagy in the MPTP/p-Induced Mouse Model of Parkinson's Disease. *Frontiers in Neuroscience,* 12.

HANSEN, C., ANGOT, E., BERGSTROM, A. L., STEINER, J. A., PIERI, L., PAUL, G., OUTEIRO, T. F., MELKI, R., KALLUNKI, P., FOG, K., LI, J. Y. & BRUNDIN, P. 2011. alpha-Synuclein propagates from mouse brain to

grafted dopaminergic neurons and seeds aggregation in cultured human cells. *J Clin Invest,* 121**,** 715-25.

HANSS, Z., BOUSSAAD, I., JARAZO, J., SCHWAMBORN, J. C. & KRÜGER, R. 2020. Quality Control Strategy for CRISPR-Cas9-Based Gene Editing Complicated by a Pseudogene. *Frontiers in Genetics,* 10.

HAO, Y., LI, D., XU, Y., OUYANG, J., WANG, Y., ZHANG, Y., LI, B., XIE, L. & QIN, G. 2019. Investigation of lipid metabolism dysregulation and the effects on immune microenvironments in pan-cancer using multiple omics data. *BMC bioinformatics,* 20**,** 195-195.

HARA, T., HASHIMOTO, Y., AKUZAWA, T., HIRAI, R., KOBAYASHI, H. & SATO, K. 2014. Rer1 and calnexin regulate endoplasmic reticulum retention of a peripheral myelin protein 22 mutant that causes type 1A Charcot-Marie-Tooth disease. *Scientific Reports,* 4**,** 6992.

HARAYAMA, T. & RIEZMAN, H. 2018. Understanding the diversity of membrane lipid composition. *Nature Reviews Molecular Cell Biology,* 19**,** 281-296.

HARRIES, L. W., HATTERSLEY, A. T. & ELLARD, S. 2004. Messenger RNA transcripts of the hepatocyte nuclear factor-1alpha gene containing premature termination codons are subject to nonsense-mediated decay. *Diabetes,* 53**,** 500-4.

HASEGAWA, T., MATSUZAKI, M., TAKEDA, A., KIKUCHI, A., AKITA, H., PERRY, G., SMITH, M. A. & ITOYAMA, Y. 2004. Accelerated alpha-synuclein aggregation after differentiation of SH-SY5Y neuroblastoma cells. *Brain Res,* 1013**,** 51-9.

HE, X., GALPIN, J. D., TROPAK, M. B., MAHURAN, D., HASELHORST, T., VON ITZSTEIN, M., KOLARICH, D., PACKER, N. H., MIAO, Y., JIANG, L., GRABOWSKI, G. A., CLARKE, L. A. & KERMODE, A. R. 2011. Production

of active human glucocerebrosidase in seeds of Arabidopsis thaliana complex-glycan-deficient (cgl) plants. *Glycobiology,* 22**,** 492-503.

HEIN, L. K., DUPLOCK, S., HOPWOOD, J. J. & FULLER, M. 2008. Lipid composition of microdomains is altered in a cell model of Gaucher disease. *Journal of lipid research,* 49**,** 1725-1734.

HEMAN-ACKAH, S. M., MANZANO, R., HOOZEMANS, J. J. M., SCHEPER, W., FLYNN, R., HAERTY, W., COWLEY, S. A., BASSETT, A. R. & WOOD, M. J. A. 2017. Alpha-synuclein induces the unfolded protein response in Parkinson's disease SNCA triplication iPSC-derived neurons. *Human Molecular Genetics,* 26**,** 4441-4450.

HENDERSON, M. X., SEDOR, S., MCGEARY, I., CORNBLATH, E. J., PENG, C., RIDDLE, D. M., LI, H. L., ZHANG, B., BROWN, H. J., OLUFEMI, M. F., BASSETT, D. S., TROJANOWSKI, J. Q. & LEE, V. M. Y. 2020. Glucocerebrosidase Activity Modulates Neuronal Susceptibility to Pathological alpha-Synuclein Insult. *Neuron,* 105**,** 822-+.

HIGGINS, A. L., TOFFOLI, M., MULLIN, S., LEE, C. Y., KOLETSI, S., AVENALI, M., BLANDINI, F. & SCHAPIRA, A. H. 2021. The remote assessment of parkinsonism supporting the ongoing development of interventions in Gaucher disease. *Neurodegener Dis Manag,* 11**,** 451-458.

HOEPKEN, H. H., GISPERT, S., AZIZOV, M., KLINKENBERG, M., RICCIARDI, F., KURZ, A., MORALES-GORDO, B., BONIN, M., RIESS, O., GASSER, T., KOGEL, D., STEINMETZ, H. & AUBURGER, G. 2008. Parkinson patient fibroblasts show increased alpha-synuclein expression. *Experimental Neurology,* 212**,** 307-313.

HOROWITZ, M., PASMANIK-CHOR, M., BOROCHOWITZ, Z., FALIK-ZACCAI, T., HELDMANN, K., CARMI, R., PARVARI, R., BEIT-OR, H., GOLDMAN,

B., PELEG, L., LEVY-LAHAD, E., RENBAUM, P., LEGUM, S., SHOMRAT, R., YEGER, H., BENBENISTI, D., NAVON, R., DROR, V., SHOHAT, M., MAGAL, N., NAVOT, N. & EYAL, N. 1998. Prevalence of glucocerebrosidase mutations in the Israeli Ashkenazi Jewish population. *Hum Mutat,* 12**,** 240-4.

HOROWITZ, M., PASMANIK-CHOR, M., RON, I. & KOLODNY, E. H. 2011. The enigma of the E326K mutation in acid beta-glucocerebrosidase. *Mol Genet Metab,* 104**,** 35-8.

HOROWITZ, M., WILDER, S., HOROWITZ, Z., REINER, O., GELBART, T. & BEUTLER, E. 1989. The human glucocerebrosidase gene and pseudogene: structure and evolution. *Genomics,* 4**,** 87-96.

HRUSKA, K. S., LAMARCA, M. E., SCOTT, C. R. & SIDRANSKY, E. 2008. Gaucher disease: Mutation and polymorphism spectrum in the glucocerebrosidase gene (GBA). *Human Mutation,* 29**,** 567-583.

HU, B. Y., WEICK, J. P., YU, J., MA, L. X., ZHANG, X. Q., THOMSON, J. A. & ZHANG, S. C. 2010. Neural differentiation of human induced pluripotent stem cells follows developmental principles but with variable potency. *Proc Natl Acad Sci U S A,* 107**,** 4335-40.

HU, H., TIAN, M., DING, C. & YU, S. 2018. The C/EBP Homologous Protein (CHOP) Transcription Factor Functions in Endoplasmic Reticulum Stress-Induced Apoptosis and Microbial Infection. *Front Immunol,* 9**,** 3083.

HUANG, Y., DENG, L., ZHONG, Y. & YI, M. 2018. The Association between E326K of GBA and the Risk of Parkinson's Disease. *Parkinsons Dis,* 2018**,** 1048084.

HUEBECKER, M., MOLONEY, E. B., VAN DER SPOEL, A. C., PRIESTMAN, D. A., ISACSON, O., HALLETT, P. J. & PLATT, F. M. 2019. Reduced

sphingolipid hydrolase activities, substrate accumulation and ganglioside decline in Parkinson's disease. *Molecular Neurodegeneration,* 14**,** 40.

HUH, Y. E., CHIANG, M. S. R., LOCASCIO, J. J., LIAO, Z., LIU, G., CHOUDHURY, K., KURAS, Y. I., TUNCALI, I., VIDENOVIC, A., HUNT, A. L., SCHWARZSCHILD, M. A., HUNG, A. Y., HERRINGTON, T. M., HAYES, M. T., HYMAN, B. T., WILLS, A. M., GOMPERTS, S. N., GROWDON, J. H., SARDI, S. P. & SCHERZER, C. R. 2020. beta-Glucocerebrosidase activity in GBA-linked Parkinson disease: The type of mutation matters. *Neurology,* 95**,** e685-e696.

IOANNOU, M. S., LIU, Z. & LIPPINCOTT-SCHWARTZ, J. 2019. A Neuron-Glia Co-culture System for Studying Intercellular Lipid Transport. *Current Protocols in Cell Biology,* 84**,** e95.

ISONAKA, R., GOLDSTEIN, D. S., ZHU, W., YOON, E., EHRLICH, D., SCHINDLER, A. B., KOKKINIS, A. D., SABIR, M. S., SCHOLZ, S. W., BANDRES-CIGA, S., BLAUWENDRAAT, C., GONZALEZ-ALEGRE, P., LOPEZ, G., SIDRANSKY, E. & NARENDRA, D. P. 2021. alpha-Synuclein Deposition in Sympathetic Nerve Fibers in Genetic Forms of Parkinson's Disease. *Mov Disord*.

IWATSUBO, T. 2003. Aggregation of α-synuclein in thepathogenesis of Parkinson's disease. *Journal of Neurology,* 250**,** iii11-iii14.

IYER, A. & CLAESSENS, M. 2019. Disruptive membrane interactions of alpha-synuclein aggregates. *Biochim Biophys Acta Proteins Proteom,* 1867**,** 468-482.

IZCO, M., BLESA, J., SCHLEEF, M., SCHMEER, M., PORCARI, R., AL-SHAWI, R., ELLMERICH, S., DE TORO, M., GARDINER, C., SEOW, Y., REINARES-SEBASTIAN, A., FORCEN, R., SIMONS, J. P., BELLOTTI,

V., COOPER, J. M. & ALVAREZ-ERVITI, L. 2019. Systemic Exosomal Delivery of shRNA Minicircles Prevents Parkinsonian Pathology. *Mol Ther,* 27**,** 2111-2122.

JEBBINK, J. M., BOOT, R. G., KEIJSER, R., MOERLAND, P. D., ATEN, J., VEENBOER, G. J. M., VAN WELY, M., BUIMER, M., VAN THEMAAT, E. V. L., AERTS, J. M. F. G., VAN DER POST, J. A. M., AFINK, G. B. & RIS-STALPERS, C. 2015. Increased glucocerebrosidase expression and activity in preeclamptic placenta. *Placenta,* 36**,** 160-169.

JEWETT, K. A., THOMAS, R. E., PHAN, C. Q., LIN, B., MILSTEIN, G., YU, S., BETTCHER, L. F., NETO, F. C., DJUKOVIC, D., RAFTERY, D., PALLANCK, L. J. & DAVIS, M. Y. 2021. Glucocerebrosidase reduces the spread of protein aggregation in a Drosophila melanogaster model of neurodegeneration by regulating proteins trafficked by extracellular vesicles. *PLoS Genet,* 17**,** e1008859.

JO, J., YANG, L., TRAN, H. D., YU, W., SUN, A. X., CHANG, Y. Y., JUNG, B. C., LEE, S. J., SAW, T. Y., XIAO, B., KHOO, A. T. T., YAW, L. P., XIE, J. J., LOKMAN, H., ONG, W. Y., LIM, G. G. Y., LIM, K. L., TAN, E. K., NG, H. H. & JE, H. S. 2021. Lewy Body-like Inclusions in Human Midbrain Organoids Carrying Glucocerebrosidase and alpha-Synuclein Mutations. *Ann Neurol*.

JUNG, O., PATNAIK, S., MARUGAN, J., SIDRANSKY, E. & WESTBROEK, W. 2016. Progress and potential of non-inhibitory small molecule chaperones for the treatment of Gaucher disease and its implications for Parkinson disease. *Expert Rev Proteomics,* 13**,** 471-9.

KACHER, Y., BRUMSHTEIN, B., BOLDIN-ADAMSKY, S., TOKER, L., SHAINSKAYA, A., SILMAN, I., SUSSMAN, J. L. & FUTERMAN, A. H.

2008. Acid beta-glucosidase: insights from structural analysis and relevance to Gaucher disease therapy. *Biol Chem,* 389**,** 1361-9.

KARATAŞ, M., DOĞAN, Ş., SPAHIU, E., AŠIĆ, A., BEŠIĆ, L. & TURAN, Y. 2020. Enzyme Kinetics and Inhibition Parameters of Human Leukocyte Glucosylceramidase. *bioRxiv***,** 2020.02.23.961599.

KAUFMAN, R. J. 2000. Overview of vector design for mammalian gene expression. *Molecular Biotechnology,* 16**,** 151-160.

KAUSHIK, S., MASSEY, A. C. & CUERVO, A. M. 2006. Lysosome membrane lipid microdomains: novel regulators of chaperone-mediated autophagy. *The EMBO journal,* 25**,** 3921-3933.

KEATINGE, M., BUI, H., MENKE, A., CHEN, Y. C., SOKOL, A. M., BAI, Q., ELLETT, F., DA COSTA, M., BURKE, D., GEGG, M., TROLLOPE, L., PAYNE, T., MCTIGHE, A., MORTIBOYS, H., DE JAGER, S., NUTHALL, H., KUO, M. S., FLEMING, A., SCHAPIRA, A. H., RENSHAW, S. A., HIGHLEY, J. R., CHACINSKA, A., PANULA, P., BURTON, E. A., O'NEILL, M. J. & BANDMANN, O. 2015. Glucocerebrosidase 1 deficient Danio rerio mirror key pathological aspects of human Gaucher disease and provide evidence of early microglial activation preceding alpha-synuclein-independent neuronal cell death. *Hum Mol Genet,* 24**,** 6640-52.

KHANNA, R., BENJAMIN, E. R., PELLEGRINO, L., SCHILLING, A., RIGAT, B. A., SOSKA, R., NAFAR, H., RANES, B. E., FENG, J., LUN, Y., POWE, A. C., PALLING, D. J., WUSTMAN, B. A., SCHIFFMANN, R., MAHURAN, D. J., LOCKHART, D. J. & VALENZANO, K. J. 2010. The pharmacological chaperone isofagomine increases the activity of the Gaucher disease L444P mutant form of beta-glucosidase. *FEBS J,* 277**,** 1618-38.

KHATCHADOURIAN, A., BOURQUE, S. D., RICHARD, V. R., TITORENKO, V. I. & MAYSINGER, D. 2012. Dynamics and regulation of lipid droplet formation in lipopolysaccharide (LPS)-stimulated microglia. *Biochim Biophys Acta,* 1821**,** 607-17.

KILPATRICK, B. S., EDEN, E. R., SCHAPIRA, A. H., FUTTER, C. E. & PATEL, S. 2013. Direct mobilisation of lysosomal Ca2+ triggers complex Ca2+ signals. *J Cell Sci,* 126**,** 60-6.

KILPATRICK, B. S., MAGALHAES, J., BEAVAN, M. S., MCNEILL, A., GEGG, M. E., CLEETER, M. W. J., BLOOR-YOUNG, D., CHURCHILL, G. C., DUCHEN, M. R., SCHAPIRA, A. H. & PATEL, S. 2016. Endoplasmic reticulum and lysosomal Ca^{2+} stores are remodelled in GBA1-linked Parkinson disease patient fibroblasts. *Cell calcium,* 59**,** 12-20.

KIM, C., HO, D. H., SUK, J. E., YOU, S., MICHAEL, S., KANG, J., JOONG LEE, S., MASLIAH, E., HWANG, D., LEE, H. J. & LEE, S. J. 2013. Neuron-released oligomeric alpha-synuclein is an endogenous agonist of TLR2 for paracrine activation of microglia. *Nat Commun,* 4**,** 1562.

KIM, M. J., JEON, S., BURBULLA, L. F. & KRAINC, D. 2018a. Acid ceramidase inhibition ameliorates α-synuclein accumulation upon loss of GBA1 function. *Human Molecular Genetics,* 27**,** 1972-1988.

KIM, S., WONG, Y. C., GAO, F. & KRAINC, D. 2021. Dysregulation of mitochondria-lysosome contacts by GBA1 dysfunction in dopaminergic neuronal models of Parkinson's disease. *Nature communications,* 12**,** 1807-1807.

KIM, S., YUN, S. P., LEE, S., UMANAH, G. E., BANDARU, V. V. R., YIN, X., RHEE, P., KARUPPAGOUNDER, S. S., KWON, S.-H., LEE, H., MAO, X., KIM, D., PANDEY, A., LEE, G., DAWSON, V. L., DAWSON, T. M. & KO,

H. S. 2018b. GBA1 deficiency negatively affects physiological α-synuclein tetramers and related multimers. *Proceedings of the National Academy of Sciences,* 115**,** 798-803.

KINGHORN, K. J., GRÖNKE, S., CASTILLO-QUAN, J. I., WOODLING, N. S., LI, L., SIRKA, E., GEGG, M., MILLS, K., HARDY, J., BJEDOV, I. & PARTRIDGE, L. 2016. A Drosophila Model of Neuronopathic Gaucher Disease Demonstrates Lysosomal-Autophagic Defects and Altered mTOR Signalling and Is Functionally Rescued by Rapamycin. *The Journal of Neuroscience,* 36**,** 11654-11670.

KLEPPE, R., UHLEMANN, K., KNAPPSKOG, P. M. & HAAVIK, J. 1999. Urea-induced denaturation of human phenylalanine hydroxylase. *J Biol Chem,* 274**,** 33251-8.

KLIONSKY, D. J. & EMR, S. D. 2000. Autophagy as a regulated pathway of cellular degradation. *Science,* 290**,** 1717-21.

KLUCKEN, J., POEHLER, A.-M., EBRAHIMI-FAKHARI, D., SCHNEIDER, J., NUBER, S., ROCKENSTEIN, E., SCHLÖTZER-SCHREHARDT, U., HYMAN, B. T., MCLEAN, P. J., MASLIAH, E. & WINKLER, J. 2012. Alpha-synuclein aggregation involves a bafilomycin A(1)-sensitive autophagy pathway. *Autophagy,* 8**,** 754-766.

KOCH, H. G., MOSER, M. & MULLER, M. 2003. Signal recognition particle-dependent protein targeting, universal to all kingdoms of life. *Rev Physiol Biochem Pharmacol,* 146**,** 55-94.

KORDOWER, J. H., CHU, Y., HAUSER, R. A., FREEMAN, T. B. & OLANOW, C. W. 2008. Lewy body-like pathology in long-term embryonic nigral transplants in Parkinson's disease. *Nat Med,* 14**,** 504-6.

KORKOTIAN, E., SCHWARZ, A., PELLED, D., SCHWARZMANN, G., SEGAL, M. & FUTERMAN, A. H. 1999. Elevation of intracellular glucosylceramide levels results in an increase in endoplasmic reticulum density and in functional calcium stores in cultured neurons. *J Biol Chem,* 274**,** 21673-8.

KOUNDOUROS, N. & POULOGIANNIS, G. 2020. Reprogramming of fatty acid metabolism in cancer. *British Journal of Cancer,* 122**,** 4-22.

KOVALEVICH, J. & LANGFORD, D. 2013. Considerations for the use of SH-SY5Y neuroblastoma cells in neurobiology. *Methods in molecular biology (Clifton, N.J.),* 1078**,** 9-21.

KRIKS, S., SHIM, J. W., PIAO, J., GANAT, Y. M., WAKEMAN, D. R., XIE, Z., CARRILLO-REID, L., AUYEUNG, G., ANTONACCI, C., BUCH, A., YANG, L., BEAL, M. F., SURMEIER, D. J., KORDOWER, J. H., TABAR, V. & STUDER, L. 2011. Dopamine neurons derived from human ES cells efficiently engraft in animal models of Parkinson's disease. *Nature,* 480**,** 547-51.

KUEHN, M. J., HERRMANN, J. M. & SCHEKMAN, R. 1998. COPII-cargo interactions direct protein sorting into ER-derived transport vesicles. *Nature,* 391**,** 187-90.

KUO, C.-L., KALLEMEIJN, W. W., LELIEVELD, L. T., MIRZAIAN, M., ZOUTENDIJK, I., VARDI, A., FUTERMAN, A. H., MEIJER, A. H., SPAINK, H. P., OVERKLEEFT, H. S., AERTS, J. M. F. G. & ARTOLA, M. 2019. In vivo inactivation of glycosidases by conduritol B epoxide and cyclophellitol as revealed by activity-based protein profiling. *The FEBS Journal,* 286**,** 584-600.

KUROCHKA, A. S., YUSHCHENKO, D. A., BOUR, P. & SHVADCHAK, V. V. 2021. Influence of Lipid Membranes on alpha-Synuclein Aggregation. *ACS Chem Neurosci,* 12**,** 825-830.

KURZAWA-AKANBI, M., HANSON, P. S., BLAIN, P. G., LETT, D. J., MCKEITH, I. G., CHINNERY, P. F. & MORRIS, C. M. 2012. Glucocerebrosidase Mutations alter the endoplasmic reticulum and lysosomes in Lewy body disease. *Journal of Neurochemistry,* 123**,** 298-309.

KURZAWA-AKANBI, M., TAMMIREDDY, S., FABRIK, I., GLIAUDELYTE, L., DOHERTY, M. K., HEAP, R., MATECKO-BURMANN, I., BURMANN, B. M., TROST, M., LUCOCQ, J. M., GHERMAN, A. V., FAIRFOUL, G., SINGH, P., BURTE, F., GREEN, A., MCKEITH, I. G., HARTLOVA, A., WHITFIELD, P. D. & MORRIS, C. M. 2021. Altered ceramide metabolism is a feature in the extracellular vesicle-mediated spread of alpha-synuclein in Lewy body disorders. *Acta Neuropathol,* 142**,** 961-984.

LASHUEL, H. A., OVERK, C. R., OUESLATI, A. & MASLIAH, E. 2013. The many faces of alpha-synuclein: from structure and toxicity to therapeutic target. *Nat Rev Neurosci,* 14**,** 38-48.

LEE, A. S. 2005. The ER chaperone and signaling regulator GRP78/BiP as a monitor of endoplasmic reticulum stress. *Methods,* 35**,** 373-81.

LEE, E. J., WOO, M. S., MOON, P. G., BAEK, M. C., CHOI, I. Y., KIM, W. K., JUNN, E. & KIM, H. S. 2010. Alpha-synuclein activates microglia by inducing the expressions of matrix metalloproteinases and the subsequent activation of protease-activated receptor-1. *J Immunol,* 185**,** 615-23.

LEE, H.-J., BAE, E.-J. & LEE, S.-J. 2014. Extracellular α-synuclein—a novel and crucial factor in Lewy body diseases. *Nature Reviews Neurology,* 10**,** 92-98.

LEE, H. J., CHOI, C. & LEE, S. J. 2002. Membrane-bound alpha-synuclein has a high aggregation propensity and the ability to seed the aggregation of the cytosolic form. *J Biol Chem,* 277**,** 671-8.

LEE, H. J., PATEL, S. & LEE, S. J. 2005. Intravesicular localization and exocytosis of alpha-synuclein and its aggregates. *J Neurosci,* 25**,** 6016-24.

LEE, J., HOMMA, T., KURAHASHI, T., KANG, E. S. & FUJII, J. 2015. Oxidative stress triggers lipid droplet accumulation in primary cultured hepatocytes by activating fatty acid synthesis. *Biochem Biophys Res Commun,* 464**,** 229-35.

LEE, S. J., ZHANG, J., CHOI, A. M. & KIM, H. P. 2013. Mitochondrial dysfunction induces formation of lipid droplets as a generalized response to stress. *Oxid Med Cell Longev,* 2013**,** 327167.

LEITMAN, J., BARAK, B., BENYAIR, R., SHENKMAN, M., ASHERY, U., HARTL, F. U. & LEDERKREMER, G. Z. 2014. ER stress-induced eIF2-alpha phosphorylation underlies sensitivity of striatal neurons to pathogenic huntingtin. *PLoS One,* 9**,** e90803.

LEKKA, M. 2016. Discrimination Between Normal and Cancerous Cells Using AFM. *Bionanoscience,* 6**,** 65-80.

LESAGE, S., ANHEIM, M., CONDROYER, C., POLLAK, P., DURIF, F., DUPUITS, C., VIALLET, F., LOHMANN, E., CORVOL, J. C., HONORE, A., RIVAUD, S., VIDAILHET, M., DURR, A., BRICE, A. & FRENCH PARKINSON'S DISEASE GENETICS STUDY, G. 2011. Large-scale screening of the Gaucher's disease-related glucocerebrosidase gene in Europeans with Parkinson's disease. *Hum Mol Genet,* 20**,** 202-10.

LEUNG, D. T. H. & CHU, S. 2018. Measurement of Oxidative Stress: Mitochondrial Function Using the Seahorse System. *In:* MURTHI, P. & VAILLANCOURT, C. (eds.) *Preeclampsia : Methods and Protocols.* New York, NY: Springer New York.

LEVINE, H., 3RD 1999. Quantification of beta-sheet amyloid fibril structures with thioflavin T. *Methods Enzymol,* 309**,** 274-84.

LI, H., HAM, A., MA, T. C., KUO, S.-H., KANTER, E., KIM, D., KO, H. S., QUAN, Y., SARDI, S. P., LI, A., ARANCIO, O., KANG, U. J., SULZER, D. & TANG, G. 2019. Mitochondrial dysfunction and mitophagy defect triggered by heterozygous GBA mutations. *Autophagy,* 15**,** 113-130.

LI, J., UVERSKY, V. N. & FINK, A. L. 2001. Effect of familial Parkinson's disease point mutations A30P and A53T on the structural properties, aggregation, and fibrillation of human alpha-synuclein. *Biochemistry,* 40**,** 11604-13.

LI, J. Y., ENGLUND, E., HOLTON, J. L., SOULET, D., HAGELL, P., LEES, A. J., LASHLEY, T., QUINN, N. P., REHNCRONA, S., BJORKLUND, A., WIDNER, H., REVESZ, T., LINDVALL, O. & BRUNDIN, P. 2008. Lewy bodies in grafted neurons in subjects with Parkinson's disease suggest host-to-graft disease propagation. *Nat Med,* 14**,** 501-3.

LI, W., LESUISSE, C., XU, Y., TRONCOSO, J. C., PRICE, D. L. & LEE, M. K. 2004. Stabilization of alpha-synuclein protein with aging and familial parkinson's disease-linked A53T mutation. *J Neurosci,* 24**,** 7400-9.

LI, X., RYDZEWSKI, N., HIDER, A., ZHANG, X., YANG, J., WANG, W., GAO, Q., CHENG, X. & XU, H. 2016. A molecular mechanism to regulate lysosome motility for lysosome positioning and tubulation. *Nat Cell Biol,* 18**,** 404-17.

LIEBERMAN, R. L. 2011. A Guided Tour of the Structural Biology of Gaucher Disease: Acid-beta-Glucosidase and Saposin C. *Enzyme Res,* 2011**,** 973231.

LIEBERMAN, R. L., D'AQUINO J, A., RINGE, D. & PETSKO, G. A. 2009. Effects of pH and iminosugar pharmacological chaperones on lysosomal glycosidase structure and stability. *Biochemistry,* 48**,** 4816-27.

LIEBERMAN, R. L., WUSTMAN, B. A., HUERTAS, P., POWE, A. C., JR., PINE, C. W., KHANNA, R., SCHLOSSMACHER, M. G., RINGE, D. & PETSKO, G. A. 2007. Structure of acid beta-glucosidase with pharmacological chaperone provides insight into Gaucher disease. *Nat Chem Biol,* 3**,** 101-7.

LIEDTKE, H. & LEGLER, G. Splenic Glucocerebrosidase and Its Cytosolic Activator Protein: Effects on Substrate Hydrolysis and Covalent Inhibition by Conduritol B Epoxides. *In:* SALVAYRE, R., DOUSTE-BLAZY, L. & GATT, S., eds. Lipid Storage Disorders, 1988// 1988 Boston, MA. Springer US, 353-358.

LIOU, B. & GRABOWSKI, G. A. 2012. Is E326K glucocerebrosidase a polymorphic or pathological variant? *Molecular Genetics and Metabolism,* 105**,** 528-529.

LIOU, B., HAFFEY, W. D., GREIS, K. D. & GRABOWSKI, G. A. 2014. The LIMP-2/SCARB2 binding motif on acid beta-glucosidase: basic and applied implications for Gaucher disease and associated neurodegenerative diseases. *J Biol Chem,* 289**,** 30063-74.

LIOU, B., KAZIMIERCZUK, A., ZHANG, M., SCOTT, C. R., HEGDE, R. S. & GRABOWSKI, G. A. 2006. Analyses of variant acid beta-glucosidases: effects of Gaucher disease mutations. *J Biol Chem,* 281**,** 4242-53.

LIU, L., MACKENZIE, K. R., PUTLURI, N., MALETIC-SAVATIC, M. & BELLEN, H. J. 2017. The Glia-Neuron Lactate Shuttle and Elevated ROS Promote Lipid Synthesis in Neurons and Lipid Droplet Accumulation in Glia via APOE/D. *Cell Metab,* 26**,** 719-737 e6.

LIU, L., ZHANG, K., SANDOVAL, H., YAMAMOTO, S., JAISWAL, M., SANZ, E., LI, Z., HUI, J., GRAHAM, B. H., QUINTANA, A. & BELLEN, H. J. 2015. Glial lipid droplets and ROS induced by mitochondrial defects promote neurodegeneration. *Cell,* 160**,** 177-90.

LIU, Y. F. & YE, Y. H. 2011. Proteostasis regulation at the endoplasmic reticulum: a new perturbation site for targeted cancer therapy. *Cell Research,* 21**,** 867-883.

LOBB, R. J., BECKER, M., WEN, S. W., WONG, C. S. F., WIEGMANS, A. P., LEIMGRUBER, A. & MÖLLER, A. 2015. Optimized exosome isolation protocol for cell culture supernatant and human plasma. *Journal of extracellular vesicles,* 4**,** 27031-27031.

LORIA, F., VARGAS, J. Y., BOUSSET, L., SYAN, S., SALLES, A., MELKI, R. & ZURZOLO, C. 2017. alpha-Synuclein transfer between neurons and astrocytes indicates that astrocytes play a role in degradation rather than in spreading. *Acta Neuropathol,* 134**,** 789-808.

LOVING, B. A. & BRUCE, K. D. 2020. Lipid and Lipoprotein Metabolism in Microglia. *Frontiers in Physiology,* 11.

LU, J., CHIANG, J., IYER, R. R., THOMPSON, E., KANESKI, C. R., XU, D. S., YANG, C., CHEN, M., HODES, R. J., LONSER, R. R., BRADY, R. O. & ZHUANG, Z. 2010. Decreased glucocerebrosidase activity in Gaucher disease parallels quantitative enzyme loss due to abnormal interaction with TCP1 and c-Cbl. *Proc Natl Acad Sci U S A,* 107**,** 21665-70.

LU, J., YANG, C., CHEN, M., YE, D. Y., LONSER, R. R., BRADY, R. O. & ZHUANG, Z. 2011. Histone deacetylase inhibitors prevent the degradation and restore the activity of glucocerebrosidase in Gaucher disease. *Proceedings of the National Academy of Sciences,* 108**,** 21200-21205.

LUK, K. C., KEHM, V., CARROLL, J., ZHANG, B., O'BRIEN, P., TROJANOWSKI, J. Q. & LEE, V. M. Y. 2012. Pathological α-synuclein transmission initiates Parkinson-like neurodegeneration in nontransgenic mice. *Science (New York, N.Y.),* 338**,** 949-953.

LUK, K. C., SONG, C., O'BRIEN, P., STIEBER, A., BRANCH, J. R., BRUNDEN, K. R., TROJANOWSKI, J. Q. & LEE, V. M. 2009. Exogenous alpha-synuclein fibrils seed the formation of Lewy body-like intracellular inclusions in cultured cells. *Proc Natl Acad Sci U S A,* 106**,** 20051-6.

LWIN, A., ORVISKY, E., GOKER-ALPAN, O., LAMARCA, M. E. & SIDRANSKY, E. 2004. Glucocerebrosidase mutations in subjects with parkinsonism. *Molecular Genetics and Metabolism,* 81**,** 70-73.

MAEGAWA, G. H. B., TROPAK, M. B., BUTTNER, J. D., RIGAT, B. A., FULLER, M., PANDIT, D., TANG, L. I., KORNHABER, G. J., HAMURO, Y., CLARKE, J. T. R. & MAHURAN, D. J. 2009. Identification and Characterization of Ambroxol as an Enzyme Enhancement Agent for Gaucher Disease. *Journal of Biological Chemistry,* 284**,** 23502-23516.

MAGALHAES, J., GEGG, M. E., MIGDALSKA-RICHARDS, A., DOHERTY, M. K., WHITFIELD, P. D. & SCHAPIRA, A. H. V. 2016. Autophagic lysosome reformation dysfunction in glucocerebrosidase deficient cells: relevance to Parkinson disease. *Human molecular genetics,* 25**,** 3432-3445.

MAGALHAES, J., GEGG, M. E., MIGDALSKA-RICHARDS, A. & SCHAPIRA, A. H. 2018. Effects of ambroxol on the autophagy-lysosome pathway and mitochondria in primary cortical neurons. *Sci Rep,* 8**,** 1385.

MAHUL-MELLIER, A.-L., BURTSCHER, J., MAHARJAN, N., WEERENS, L., CROISIER, M., KUTTLER, F., LELEU, M., KNOTT, G. W. & LASHUEL, H. A. 2020. The process of Lewy body formation, rather than simply α-synuclein fibrillization, is one of the major drivers of neurodegeneration. *Proceedings of the National Academy of Sciences,* 117**,** 4971-4982.

MAHUL-MELLIER, A. L., VERCRUYSSE, F., MACO, B., AIT-BOUZIAD, N., DE ROO, M., MULLER, D. & LASHUEL, H. A. 2015. Fibril growth and seeding capacity play key roles in α-synuclein-mediated apoptotic cell death. *Cell Death & Differentiation,* 22**,** 2107-2122.

MALEK, N., WEIL, R. S., BRESNER, C., LAWTON, M. A., GROSSET, K. A., TAN, M., BAJAJ, N., BARKER, R. A., BURN, D. J., FOLTYNIE, T., HARDY, J., WOOD, N. W., BEN-SHLOMO, Y., WILLIAMS, N. W., GROSSET, D. G., MORRIS, H. R. & CONSORTIUM, P. R. C. 2018. Features of GBA-associated Parkinson's disease at presentation in the UK Tracking Parkinson's study. *J Neurol Neurosurg Psychiatry,* 89**,** 702-709.

MALEY, F., TRIMBLE, R. B., TARENTINO, A. L. & PLUMMER, T. H., JR. 1989. Characterization of glycoproteins and their associated oligosaccharides through the use of endoglycosidases. *Anal Biochem,* 180**,** 195-204.

MALINI, E., GROSSI, S., DEGANUTO, M., ROSANO, C., PARINI, R., DOMINISINI, S., CARIATI, R., ZAMPIERI, S., BEMBI, B., FILOCAMO, M. & DARDIS, A. 2014. Functional analysis of 11 novel GBA alleles. *Eur J Hum Genet,* 22**,** 511-6.

MALLETT, V., ROSS, J. P., ALCALAY, R. N., AMBALAVANAN, A., SIDRANSKY, E., DION, P. A., ROULEAU, G. A. & GAN-OR, Z. 2016. GBA p.T369M substitution in Parkinson disease: Polymorphism or association? A meta-analysis. *Neurol Genet,* 2**,** e104.

MANNING-BOĞ, A. B., SCHÜLE, B. & LANGSTON, J. W. 2009. Alpha-synuclein-glucocerebrosidase interactions in pharmacological Gaucher models: A biological link between Gaucher disease and parkinsonism. *NeuroToxicology,* 30**,** 1127-1132.

MAOR, G., CABASSO, O., KRIVORUK, O., RODRIGUEZ, J., STELLER, H., SEGAL, D. & HOROWITZ, M. 2016. The contribution of mutant GBA to the development of Parkinson disease in Drosophila. *Hum Mol Genet,* 25**,** 2712-2727.

MAOR, G., RAPAPORT, D. & HOROWITZ, M. 2019. The effect of mutant GBA1 on accumulation and aggregation of alpha-synuclein. *Hum Mol Genet*.

MAOR, G., RENCUS-LAZAR, S., FILOCAMO, M., STELLER, H., SEGAL, D. & HOROWITZ, M. 2013. Unfolded protein response in Gaucher disease: from human to Drosophila. *Orphanet Journal of Rare Diseases,* 8**,** 140.

MARQUES, A. R., MIRZAIAN, M., AKIYAMA, H., WISSE, P., FERRAZ, M. J., GASPAR, P., GHAUHARALI-VAN DER VLUGT, K., MEIJER, R., GIRALDO, P., ALFONSO, P., IRÚN, P., DAHL, M., KARLSSON, S., PAVLOVA, E. V., COX, T. M., SCHEIJ, S., VERHOEK, M., OTTENHOFF, R., VAN ROOMEN, C. P., PANNU, N. S., VAN EIJK, M., DEKKER, N., BOOT, R. G., OVERKLEEFT, H. S., BLOMMAART, E., HIRABAYASHI, Y. & AERTS, J. M. 2016. Glucosylated cholesterol in mammalian cells and tissues: formation and degradation by multiple cellular β-glucosidases. *J Lipid Res,* 57**,** 451-63.

MARSCHALLINGER, J., IRAM, T., ZARDENETA, M., LEE, S. E., LEHALLIER, B., HANEY, M. S., PLUVINAGE, J. V., MATHUR, V., HAHN, O., MORGENS, D. W., KIM, J., TEVINI, J., FELDER, T. K., WOLINSKI, H., BERTOZZI, C. R., BASSIK, M. C., AIGNER, L. & WYSS-CORAY, T. 2020. Lipid-droplet-accumulating microglia represent a dysfunctional and proinflammatory state in the aging brain. *Nature Neuroscience,* 23**,** 194-208.

MARSDEN, C. D. 1990. Parkinson's disease. *Lancet,* 335**,** 948-52.

MARTINEZ-VICENTE, M. & CUERVO, A. M. 2007. Autophagy and neurodegeneration: when the cleaning crew goes on strike. *Lancet Neurol,* 6**,** 352-61.

MARTINEZ, Z., ZHU, M., HAN, S. & FINK, A. L. 2007. GM1 specifically interacts with alpha-synuclein and inhibits fibrillation. *Biochemistry,* 46**,** 1868-77.

MATA, I. F., SAMII, A., SCHNEER, S. H., ROBERTS, J. W., GRIFFITH, A., LEIS, B. C., SCHELLENBERG, G. D., SIDRANSKY, E., BIRD, T. D., LEVERENZ, J. B., TSUANG, D. & ZABETIAN, C. P. 2008. Glucocerebrosidase gene mutations: a risk factor for Lewy body disorders. *Arch Neurol,* 65**,** 379-82.

MATSUI, H., SATO, F., SATO, S., KOIKE, M., TARUNO, Y., SAIKI, S., FUNAYAMA, M., ITO, H., TANIGUCHI, Y., UEMURA, N., TOYODA, A., SAKAKI, Y., TAKEDA, S., UCHIYAMA, Y., HATTORI, N. & TAKAHASHI, R. 2013. ATP13A2 deficiency induces a decrease in cathepsin D activity, fingerprint-like inclusion body formation, and selective degeneration of dopaminergic neurons. *FEBS Letters,* 587**,** 1316-1325.

MAZZULLI, J. R., XU, Y. H., SUN, Y., KNIGHT, A. L., MCLEAN, P. J., CALDWELL, G. A., SIDRANSKY, E., GRABOWSKI, G. A. & KRAINC, D.

2011. Gaucher disease glucocerebrosidase and alpha-synuclein form a bidirectional pathogenic loop in synucleinopathies. *Cell,* 146**,** 37-52.

MAZZULLI, J. R., ZUNKE, F., ISACSON, O., STUDER, L. & KRAINC, D. 2016. alpha-Synuclein-induced lysosomal dysfunction occurs through disruptions in protein trafficking in human midbrain synucleinopathy models. *Proc Natl Acad Sci U S A,* 113**,** 1931-6.

MCFADDEN, J. W., AJA, S., LI, Q., BANDARU, V. V. R., KIM, E.-K., HAUGHEY, N. J., KUHAJDA, F. P. & RONNETT, G. V. 2014. Increasing Fatty Acid Oxidation Remodels the Hypothalamic Neurometabolome to Mitigate Stress and Inflammation. *PLOS ONE,* 9**,** e115642.

MCKERAN, R. O., BRADBURY, P., TAYLOR, D. & STERN, G. 1985. Neurological involvement in type 1 (adult) Gaucher's disease. *J Neurol Neurosurg Psychiatry,* 48**,** 172-5.

MCNEILL, A., DURAN, R., HUGHES, D. A., MEHTA, A. & SCHAPIRA, A. H. 2012. A clinical and family history study of Parkinson's disease in heterozygous glucocerebrosidase mutation carriers. *J Neurol Neurosurg Psychiatry,* 83**,** 853-4.

MCNEILL, A., MAGALHAES, J., SHEN, C., CHAU, K. Y., HUGHES, D., MEHTA, A., FOLTYNIE, T., COOPER, J. M., ABRAMOV, A. Y., GEGG, M. & SCHAPIRA, A. H. 2014. Ambroxol improves lysosomal biochemistry in glucocerebrosidase mutation-linked Parkinson disease cells. *Brain,* 137**,** 1481-95.

MELNIKOVA, A., POZDYSHEV, D., BARINOVA, K., KUDRYAVTSEVA, S. & MURONETZ, V. I. 2020. α-Synuclein Overexpression in SH-SY5Y Human Neuroblastoma Cells Leads to the Accumulation of Thioflavin S-positive

Aggregates and Impairment of Glycolysis. *Biochemistry (Moscow),* 85**,** 604-613.

MELO, F., CABALLERO, L., ZAMORANO, E., VENTURA, N., NAVARRO, C., DOLL, I., ZAMORANO, P. & CORNEJO, A. 2021. The Cytotoxic Effect of alpha-Synuclein Aggregates. *Chemphyschem,* 22**,** 526-532.

MELO, T. Q., VAN ZOMEREN, K. C., FERRARI, M. F. R., BODDEKE, H. W. G. M. & COPRAY, J. C. V. M. 2017. Impairment of mitochondria dynamics by human A53T α-synuclein and rescue by NAP (davunetide) in a cell model for Parkinson's disease. *Experimental brain research,* 235**,** 731-742.

MERCADO, G., VALDES, P. & HETZ, C. 2013. An ERcentric view of Parkinson's disease. *Trends Mol Med,* 19**,** 165-75.

METZ, S. W., TIAN, S., HOEKSTRA, G., YI, X., STONE, M., HORVATH, K., MILEY, M. J., DESIMONE, J., LUFT, C. J. & DE SILVA, A. M. 2016. Precisely Molded Nanoparticle Displaying DENV-E Proteins Induces Robust Serotype-Specific Neutralizing Antibody Responses. *PLoS neglected tropical diseases,* 10**,** e0005071-e0005071.

MIAKE, H., MIZUSAWA, H., IWATSUBO, T. & HASEGAWA, M. 2002. Biochemical characterization of the core structure of alpha-synuclein filaments. *J Biol Chem,* 277**,** 19213-9.

MICHIORRI, S., GELMETTI, V., GIARDA, E., LOMBARDI, F., ROMANO, F., MARONGIU, R., NERINI-MOLTENI, S., SALE, P., VAGO, R., ARENA, G., TOROSANTUCCI, L., CASSINA, L., RUSSO, M. A., DALLAPICCOLA, B., VALENTE, E. M. & CASARI, G. 2010. The Parkinson-associated protein PINK1 interacts with Beclin1 and promotes autophagy. *Cell Death & Differentiation,* 17**,** 962-974.

MIGDALSKA-RICHARDS, A., DALY, L., BEZARD, E. & SCHAPIRA, A. H. 2016. Ambroxol effects in glucocerebrosidase and alpha-synuclein transgenic mice. *Ann Neurol,* 80**,** 766-775.

MIGDALSKA-RICHARDS, A., KO, W. K., LI, Q., BEZARD, E. & SCHAPIRA, A. H. 2017a. Oral ambroxol increases brain glucocerebrosidase activity in a nonhuman primate. *Synapse*.

MIGDALSKA-RICHARDS, A. & SCHAPIRA, A. H. V. 2016. The relationship between glucocerebrosidase mutations and Parkinson disease. *Journal of Neurochemistry,* 139**,** 77-90.

MIGDALSKA-RICHARDS, A., WEGRZYNOWICZ, M., HARRISON, I. F., VERONA, G., BELLOTTI, V., SPILLANTINI, M. G. & SCHAPIRA, A. H. V. 2020. L444P Gba1 mutation increases formation and spread of alpha-synuclein deposits in mice injected with mouse alpha-synuclein pre-formed fibrils. *PLoS One,* 15**,** e0238075.

MIGDALSKA-RICHARDS, A., WEGRZYNOWICZ, M., RUSCONI, R., DEANGELI, G., DI MONTE, D. A., SPILLANTINI, M. G. & SCHAPIRA, A. H. V. 2017b. The L444P Gba1 mutation enhances alpha-synuclein induced loss of nigral dopaminergic neurons in mice. *Brain : a journal of neurology,* 140**,** 2706-2721.

MISTRY, P. K., LIU, J., YANG, M., NOTTOLI, T., MCGRATH, J., JAIN, D., ZHANG, K., KEUTZER, J., CHUANG, W. L., MEHAL, W. Z., ZHAO, H., LIN, A., MANE, S., LIU, X., PENG, Y. Z., LI, J. H., AGRAWAL, M., ZHU, L. L., BLAIR, H. C., ROBINSON, L. J., IQBAL, J., SUN, L. & ZAIDI, M. 2010. Glucocerebrosidase gene-deficient mouse recapitulates Gaucher disease displaying cellular and molecular dysregulation beyond the macrophage. *Proc Natl Acad Sci U S A,* 107**,** 19473-8.

MOLONEY, E. B., MOSKITES, A., FERRARI, E. J., ISACSON, O. & HALLETT, P. J. 2018. The glycoprotein GPNMB is selectively elevated in the substantia nigra of Parkinson's disease patients and increases after lysosomal stress. *Neurobiol Dis,* 120**,** 1-11.

MONTFORT, M., CHABÁS, A., VILAGELIU, L. & GRINBERG, D. 2004. Functional analysis of 13 GBA mutant alleles identified in Gaucher disease patients: Pathogenic changes and “modifier” polymorphisms. *Human Mutation,* 23**,** 567-575.

MOORS, T. E., PACIOTTI, S., INGRASSIA, A., QUADRI, M., BREEDVELD, G., TASEGIAN, A., CHIASSERINI, D., EUSEBI, P., DURAN-PACHECO, G., KREMER, T., CALABRESI, P., BONIFATI, V., PARNETTI, L., BECCARI, T. & VAN DE BERG, W. D. J. 2019. Characterization of Brain Lysosomal Activities in GBA-Related and Sporadic Parkinson's Disease and Dementia with Lewy Bodies. *Mol Neurobiol,* 56**,** 1344-1355.

MU, H. & HØY, C.-E. 2001. Intestinal absorption of specific structured triacylglycerols. *Journal of Lipid Research,* 42**,** 792-798.

MU, T. W., FOWLER, D. M. & KELLY, J. W. 2008. Partial restoration of mutant enzyme homeostasis in three distinct lysosomal storage disease cell lines by altering calcium homeostasis. *PLoS Biol,* 6**,** e26.

MULLIN, S., SMITH, L., LEE, K., D'SOUZA, G., WOODGATE, P., ELFLEIN, J., HALLQVIST, J., TOFFOLI, M., STREETER, A., HOSKING, J., HEYWOOD, W. E., KHENGAR, R., CAMPBELL, P., HEHIR, J., CABLE, S., MILLS, K., ZETTERBERG, H., LIMOUSIN, P., LIBRI, V., FOLTYNIE, T. & SCHAPIRA, A. H. V. 2020. Ambroxol for the Treatment of Patients With Parkinson Disease With and Without Glucocerebrosidase Gene Mutations: A Nonrandomized, Noncontrolled Trial. *JAMA Neurol*.

MURILLO, J. R., GOTO-SILVA, L., SÁNCHEZ, A., NOGUEIRA, F. C. S., DOMONT, G. B. & JUNQUEIRA, M. 2017. Quantitative proteomic analysis identifies proteins and pathways related to neuronal development in differentiated SH-SY5Y neuroblastoma cells. *EuPA Open Proteomics,* 16**,** 1-11.

MURPHY, K. E., GYSBERS, A. M., ABBOTT, S. K., TAYEBI, N., KIM, W. S., SIDRANSKY, E., COOPER, A., GARNER, B. & HALLIDAY, G. M. 2014. Reduced glucocerebrosidase is associated with increased alpha-synuclein in sporadic Parkinson's disease. *Brain,* 137**,** 834-848.

MURUGESAN, V., LIU, J., YANG, R., LIN, H., LISCHUK, A., PASTORES, G., ZHANG, X., CHUANG, W. L. & MISTRY, P. K. 2018. Validating glycoprotein non-metastatic melanoma B (gpNMB, osteoactivin), a new biomarker of Gaucher disease. *Blood Cells Mol Dis,* 68**,** 47-53.

NAGATA, M., IZUMI, Y., ISHIKAWA, E., KIYOTAKE, R., DOI, R., IWAI, S., OMAHDI, Z., YAMAJI, T., MIYAMOTO, T., BAMBA, T. & YAMASAKI, S. 2017. Intracellular metabolite β-glucosylceramide is an endogenous Mincle ligand possessing immunostimulatory activity. *Proceedings of the National Academy of Sciences,* 114**,** E3285-E3294.

NAIKI, H., HIGUCHI, K., HOSOKAWA, M. & TAKEDA, T. 1989. Fluorometric determination of amyloid fibrils in vitro using the fluorescent dye, thioflavin T1. *Anal Biochem,* 177**,** 244-9.

NAKAJIMA, S., GOTOH, M., FUKASAWA, K., MURAKAMI-MUROFUSHI, K. & KUNUGI, H. 2019. Oleic acid is a potent inducer for lipid droplet accumulation through its esterification to glycerol by diacylglycerol acyltransferase in primary cortical astrocytes. *Brain Res,* 1725**,** 146484.

NAPHATSAMON, U., OHASHI, T., MISAKI, R. & FUJIYAMA, K. 2018. The Production of Human β-Glucocerebrosidase in Nicotiana benthamiana Root Culture. *International journal of molecular sciences,* 19**,** 1972.

NARHI, L., WOOD, S. J., STEAVENSON, S., JIANG, Y., WU, G. M., ANAFI, D., KAUFMAN, S. A., MARTIN, F., SITNEY, K., DENIS, P., LOUIS, J. C., WYPYCH, J., BIERE, A. L. & CITRON, M. 1999. Both familial Parkinson's disease mutations accelerate alpha-synuclein aggregation. *J Biol Chem,* 274**,** 9843-6.

NEUMANN, J., BRAS, J., DEAS, E., O'SULLIVAN, S. S., PARKKINEN, L., LACHMANN, R. H., LI, A., HOLTON, J., GUERREIRO, R., PAUDEL, R., SEGARANE, B., SINGLETON, A., LEES, A., HARDY, J., HOULDEN, H., REVESZ, T. & WOOD, N. W. 2009. Glucocerebrosidase mutations in clinical and pathologically proven Parkinson's disease. *Brain,* 132**,** 1783-94.

NEUMANN, M., KAHLE, P. J., GIASSON, B. I., OZMEN, L., BORRONI, E., SPOOREN, W., MÜLLER, V., ODOY, S., FUJIWARA, H., HASEGAWA, M., IWATSUBO, T., TROJANOWSKI, J. Q., KRETZSCHMAR, H. A. & HAASS, C. 2002. Misfolded proteinase K-resistant hyperphosphorylated alpha-synuclein in aged transgenic mice with locomotor deterioration and in human alpha-synucleinopathies. *The Journal of clinical investigation,* 110**,** 1429-1439.

NGUYEN, T. B., LOUIE, S. M., DANIELE, J. R., TRAN, Q., DILLIN, A., ZONCU, R., NOMURA, D. K. & OLZMANN, J. A. 2017. DGAT1-Dependent Lipid Droplet Biogenesis Protects Mitochondrial Function during Starvation-Induced Autophagy. *Dev Cell,* 42**,** 9-21.e5.

NICHOLS, W. C., PANKRATZ, N., MAREK, D. K., PAUCIULO, M. W., ELSAESSER, V. E., HALTER, C. A., RUDOLPH, A., WOJCIESZEK, J., PFEIFFER, R. F., FOROUD, T. & PARKINSON STUDY GROUP, P. I. 2009. Mutations in GBA are associated with familial Parkinson disease susceptibility and age at onset. *Neurology,* 72**,** 310-6.

NILSSON, O. & SVENNERHOLM, L. 1982. Accumulation of glucosylceramide and glucosylsphingosine (psychosine) in cerebrum and cerebellum in infantile and juvenile Gaucher disease. *J Neurochem,* 39**,** 709-18.

NISHIOKA, K., ROSS, O. A., VILARINO-GUELL, C., COBB, S. A., KACHERGUS, J. M., MANN, D. M., SNOWDEN, J., RICHARDSON, A. M., NEARY, D., ROBINSON, C. A., RAJPUT, A., PAPAPETROPOULOS, S., MASH, D. C., PAHWA, R., LYONS, K. E., WSZOLEK, Z. K., DICKSON, D. W. & FARRER, M. J. 2011. Glucocerebrosidase mutations in diffuse Lewy body disease. *Parkinsonism Relat Disord,* 17**,** 55-7.

NIXON, R. A. 2013. The role of autophagy in neurodegenerative disease. *Nat Med,* 19**,** 983-97.

NUNES, D. S., GONZAGA, H. T., RIBEIRO, V. S., CUNHA-JÚNIOR, J. P. & COSTA-CRUZ, J. M. 2017. Usefulness of gel filtration fraction as potential biomarker for neurocysticercosis in serum: towards a new diagnostic tool. *Parasitology,* 144**,** 426-435.

OFFMAN, M. N., KROL, M., ROST, B., SILMAN, I., SUSSMAN, J. L. & FUTERMAN, A. H. 2011. Comparison of a molecular dynamics model with the X-ray structure of the N370S acid-beta-glucosidase mutant that causes Gaucher disease. *Protein Eng Des Sel,* 24**,** 773-5.

OFFMAN, M. N., KROL, M., SILMAN, I., SUSSMAN, J. L. & FUTERMAN, A. H. 2010. Molecular basis of reduced glucosylceramidase activity in the most common Gaucher disease mutant, N370S. *J Biol Chem,* 285**,** 42105-14.

OGAWA, K., FUJIWARA, Y., SUGAMATA, K. & ABE, T. 1988. Thin-layer chromatography of neutral glycosphingolipids: an improved simple method for the resolution of GlcCer, GalCer, LacCer and Ga2Cer. *Journal of Chromatography B: Biomedical Sciences and Applications,* 426**,** 188-193.

OHASHI, T., HONG, C. M., WEILER, S., TOMICH, J. M., AERTS, J. M., TAGER, J. M. & BARRANGER, J. A. 1991. Characterization of human glucocerebrosidase from different mutant alleles. *J Biol Chem,* 266**,** 3661-7.

OLIVEIRA, L. M. A., FALOMIR-LOCKHART, L. J., BOTELHO, M. G., LIN, K. H., WALES, P., KOCH, J. C., GERHARDT, E., TASCHENBERGER, H., OUTEIRO, T. F., LINGOR, P., SCHÜLE, B., ARNDT-JOVIN, D. J. & JOVIN, T. M. 2015. Elevated α-synuclein caused by SNCA gene triplication impairs neuronal differentiation and maturation in Parkinson's patient-derived induced pluripotent stem cells. *Cell death & disease,* 6**,** e1994-e1994.

ONG, D. S., MU, T. W., PALMER, A. E. & KELLY, J. W. 2010. Endoplasmic reticulum Ca2+ increases enhance mutant glucocerebrosidase proteostasis. *Nat Chem Biol,* 6**,** 424-32.

ORENSTEIN, S. J., KUO, S. H., TASSET, I., ARIAS, E., KOGA, H., FERNANDEZ-CARASA, I., CORTES, E., HONIG, L. S., DAUER, W., CONSIGLIO, A., RAYA, A., SULZER, D. & CUERVO, A. M. 2013. Interplay of LRRK2 with chaperone-mediated autophagy. *Nat Neurosci,* 16**,** 394-406.

ORVISKY, E., PARK, J. K., LAMARCA, M. E., GINNS, E. I., MARTIN, B. M., TAYEBI, N. & SIDRANSKY, E. 2002. Glucosylsphingosine accumulation in tissues from patients with Gaucher disease: correlation with phenotype and genotype. *Mol Genet Metab,* 76**,** 262-70.

OSELLAME, L. D. & DUCHEN, M. R. 2013. Defective quality control mechanisms and accumulation of damaged mitochondria link Gaucher and Parkinson diseases. *Autophagy,* 9**,** 1633-5.

OSELLAME, L. D., RAHIM, A. A., HARGREAVES, I. P., GEGG, M. E., RICHARD-LONDT, A., BRANDNER, S., WADDINGTON, S. N., SCHAPIRA, A. H. & DUCHEN, M. R. 2013. Mitochondria and quality control defects in a mouse model of Gaucher disease--links to Parkinson's disease. *Cell Metab,* 17**,** 941-53.

OUTEIRO, T. F. & LINDQUIST, S. 2003. Yeast cells provide insight into alpha-synuclein biology and pathobiology. *Science (New York, N.Y.),* 302**,** 1772-1775.

PAPADOPOULOS, V. E., NIKOLOPOULOU, G., ANTONIADOU, I., KARACHALIOU, A., ARIANOGLOU, G., EMMANOUILIDOU, E., SARDI, S. P., STEFANIS, L. & VEKRELLIS, K. 2018. Modulation of β-glucocerebrosidase increases α-synuclein secretion and exosome release in mouse models of Parkinson's disease. *Human Molecular Genetics,* 27**,** 1696-1710.

PARK, S., AHN, E. S. & KIM, Y. 2015. Neuroblastoma SH-SY5Y cell-derived exosomes stimulate dendrite-like outgrowths and modify the differentiation of A375 melanoma cells. *Cell Biology International,* 39**,** 379-387.

PARKKINEN, L., NEUMANN, J., O'SULLIVAN, S. S., HOLTON, J. L., REVESZ, T., HARDY, J. & LEES, A. J. 2011. Glucocerebrosidase mutations do not

cause increased Lewy body pathology in Parkinson's disease. *Mol Genet Metab,* 103**,** 410-2.

PARNETTI, L., CHIASSERINI, D., PERSICHETTI, E., EUSEBI, P., VARGHESE, S., QURESHI, M. M., DARDIS, A., DEGANUTO, M., DE CARLO, C., CASTRIOTO, A., BALDUCCI, C., PACIOTTI, S., TAMBASCO, N., BEMBI, B., BONANNI, L., ONOFRJ, M., ROSSI, A., BECCARI, T., EL-AGNAF, O. & CALABRESI, P. 2014. Cerebrospinal fluid lysosomal enzymes and alpha-synuclein in Parkinson's disease. *Mov Disord,* 29**,** 1019-27.

PARODI, A. J. 2000. Protein glucosylation and its role in protein folding. *Annu Rev Biochem,* 69**,** 69-93.

PARZYCH, K. R. & KLIONSKY, D. J. 2014. An overview of autophagy: morphology, mechanism, and regulation. *Antioxid Redox Signal,* 20**,** 460-73.

PASTORES, G. M. & HUGHES, D. A. 1993. Gaucher Disease. *In:* PAGON, R. A., ADAM, M. P., ARDINGER, H. H., WALLACE, S. E., AMEMIYA, A., BEAN, L. J. H., BIRD, T. D., FONG, C. T., MEFFORD, H. C., SMITH, R. J. H. & STEPHENS, K. (eds.) *GeneReviews(R).* Seattle (WA).

PATEL, G. K., KHAN, M. A., ZUBAIR, H., SRIVASTAVA, S. K., KHUSHMAN, M. D., SINGH, S. & SINGH, A. P. 2019. Comparative analysis of exosome isolation methods using culture supernatant for optimum yield, purity and downstream applications. *Scientific Reports,* 9**,** 5335.

PATNAIK, S., ZHENG, W., CHOI, J. H., MOTABAR, O., SOUTHALL, N., WESTBROEK, W., LEA, W. A., VELAYATI, A., GOLDIN, E., SIDRANSKY, E., LEISTER, W. & MARUGAN, J. J. 2012. Discovery, structure-activity relationship, and biological evaluation of noninhibitory small molecule

chaperones of glucocerebrosidase. *Journal of medicinal chemistry,* 55**,** 5734-5748.

PAUL, A., JACOBY, G., LAOR BAR-YOSEF, D., BECK, R., GAZIT, E. & SEGAL, D. 2021. Glucosylceramide Associated with Gaucher Disease Forms Amyloid-like Twisted Ribbon Fibrils That Induce alpha-Synuclein Aggregation. *ACS Nano*.

PEMBERTON, K., MERSMAN, B. & XU, F. 2018. Using ImageJ to Assess Neurite Outgrowth in Mammalian Cell Cultures: Research Data Quantification Exercises in Undergraduate Neuroscience Lab. *Journal of undergraduate neuroscience education : JUNE : a publication of FUN, Faculty for Undergraduate Neuroscience,* 16**,** A186-A194.

PENG, C., GATHAGAN, R. J. & LEE, V. M. Y. 2018. Distinct α-Synuclein strains and implications for heterogeneity among α-Synucleinopathies. *Neurobiology of disease,* 109**,** 209-218.

PENG, C., SHI, C., CAO, X., LI, Y., LIU, F. & LU, F. 2019. Factors Influencing Recombinant Protein Secretion Efficiency in Gram-Positive Bacteria: Signal Peptide and Beyond. *Frontiers in Bioengineering and Biotechnology,* 7.

PENTCHEV, P. G., BRADY, R. O., HIBBERT, S. R., GAL, A. E. & SHAPIRO, D. 1973. Isolation and characterization of glucocerebrosidase from human placental tissue. *J Biol Chem,* 248**,** 5256-61.

PETRUCCI, S., GINEVRINO, M., TREZZI, I., MONFRINI, E., RICCIARDI, L., ALBANESE, A., AVENALI, M., BARONE, P., BENTIVOGLIO, A. R., BONIFATI, V., BOVE, F., BONANNI, L., BRUSA, L., CEREDA, C., COSSU, G., CRISCUOLO, C., DATI, G., DE ROSA, A., ELEOPRA, R., FABBRINI, G., FADDA, L., GARBELLINI, M., MINAFRA, B., ONOFRJ, M.,

PACCHETTI, C., PALMIERI, I., PELLECCHIA, M. T., PETRACCA, M., PICILLO, M., PISANI, A., VALLELUNGA, A., ZANGAGLIA, R., DI FONZO, A., MORGANTE, F., VALENTE, E. M. & GROUP, I.-G.-P. S. 2020. GBA-Related Parkinson's Disease: Dissection of Genotype-Phenotype Correlates in a Large Italian Cohort. *Mov Disord,* 35**,** 2106-2111.

POL-FACHIN, L., SIEBERT, M., VERLI, H. & SARAIVA-PEREIRA, M. L. 2016. Glycosylation is crucial for a proper catalytic site organization in human glucocerebrosidase. *Glycoconjugate Journal,* 33**,** 237-244.

PRESGRAVES, S. P., AHMED, T., BORWEGE, S. & JOYCE, J. N. 2004. Terminally differentiated SH-SY5Y cells provide a model system for studying neuroprotective effects of dopamine agonists. *Neurotox Res,* 5**,** 579-98.

RAJU, D., SCHONAUER, S., HAMZEH, H., FLYNN, K. C., BRADKE, F., VOM DORP, K., DÖRMANN, P., YILDIZ, Y., TRÖTSCHEL, C., POETSCH, A., BREIDEN, B., SANDHOFF, K., KÖRSCHEN, H. G. & WACHTEN, D. 2015. Accumulation of glucosylceramide in the absence of the beta-glucosidase GBA2 alters cytoskeletal dynamics. *PLoS Genet,* 11**,** e1005063.

RALHAN, I., CHANG, C. L., LIPPINCOTT-SCHWARTZ, J. & IOANNOU, M. S. 2021. Lipid droplets in the nervous system. *J Cell Biol,* 220.

RAN, C., BRODIN, L., FORSGREN, L., WESTERLUND, M., RAMEZANI, M., GELLHAAR, S., XIANG, F., FARDELL, C., NISSBRANDT, H., SÖDERKVIST, P., PUSCHMANN, A., YGLAND, E., OLSON, L., WILLOWS, T., JOHANSSON, A., SYDOW, O., WIRDEFELDT, K., GALTER, D., SVENNINGSSON, P. & BELIN, A. C. 2016. Strong

association between glucocerebrosidase mutations and Parkinson's disease in Sweden. *Neurobiol Aging,* 45**,** 212.e5-212.e11.

RAN, F. A., HSU, P. D., WRIGHT, J., AGARWALA, V., SCOTT, D. A. & ZHANG, F. 2013. Genome engineering using the CRISPR-Cas9 system. *Nature Protocols,* 8**,** 2281-2308.

RECZEK, D., SCHWAKE, M., SCHRÖDER, J., HUGHES, H., BLANZ, J., JIN, X., BRONDYK, W., VAN PATTEN, S., EDMUNDS, T. & SAFTIG, P. 2007. LIMP-2 Is a Receptor for Lysosomal Mannose-6-Phosphate-Independent Targeting of β-Glucocerebrosidase. *Cell,* 131**,** 770-783.

REYES, J. F., OLSSON, T. T., LAMBERTS, J. T., DEVINE, M. J., KUNATH, T. & BRUNDIN, P. 2015. A cell culture model for monitoring alpha-synuclein cell-to-cell transfer. *Neurobiol Dis,* 77**,** 266-75.

ROCHA, E. M., SMITH, G. A., PARK, E., CAO, H., BROWN, E., HALLETT, P. & ISACSON, O. 2015a. Progressive decline of glucocerebrosidase in aging and Parkinson's disease. *Ann Clin Transl Neurol,* 2**,** 433-8.

ROCHA, E. M., SMITH, G. A., PARK, E., CAO, H., BROWN, E., HAYES, M. A., BEAGAN, J., MCLEAN, J. R., IZEN, S. C., PEREZ-TORRES, E., HALLETT, P. J. & ISACSON, O. 2015b. Glucocerebrosidase gene therapy prevents alpha-synucleinopathy of midbrain dopamine neurons. *Neurobiol Dis,* 82**,** 495-503.

ROCHA, E. M., SMITH, G. A., PARK, E., CAO, H., GRAHAM, A.-R., BROWN, E., MCLEAN, J. R., HAYES, M. A., BEAGAN, J., IZEN, S. C., PEREZ-TORRES, E., HALLETT, P. J. & ISACSON, O. 2015c. Sustained Systemic Glucocerebrosidase Inhibition Induces Brain α-Synuclein Aggregation, Microglia and Complement C1q Activation in Mice. *Antioxidants & Redox Signaling,* 23**,** 550-564.

RON, I., DAGAN, A., GATT, S., PASMANIK-CHOR, M. & HOROWITZ, M. 2005. Use of fluorescent substrates for characterization of Gaucher disease mutations. *Blood Cells, Molecules, and Diseases,* 35**,** 57-65.

RON, I. & HOROWITZ, M. 2005. ER retention and degradation as the molecular basis underlying Gaucher disease heterogeneity. *Hum Mol Genet,* 14**,** 2387-98.

RON, I., RAPAPORT, D. & HOROWITZ, M. 2010. Interaction between parkin and mutant glucocerebrosidase variants: a possible link between Parkinson disease and Gaucher disease. *Human Molecular Genetics,* 19**,** 3771-3781.

ROSENBLOOM, B., BALWANI, M., BRONSTEIN, J. M., KOLODNY, E., SATHE, S., GWOSDOW, A. R., TAYLOR, J. S., COLE, J. A., ZIMRAN, A. & WEINREB, N. J. 2011. The incidence of Parkinsonism in patients with type 1 Gaucher disease: Data from the ICGG Gaucher Registry. *Blood Cells, Molecules, and Diseases,* 46**,** 95-102.

RUSKEY, J. A., GREENBAUM, L., RONCIÈRE, L., ALAM, A., SPIEGELMAN, D., LIONG, C., LEVY, O. A., WATERS, C., FAHN, S., MARDER, K. S., CHUNG, W., YAHALOM, G., ISRAELI-KORN, S., LIVNEH, V., FAY-KARMON, T., ALCALAY, R. N., HASSIN-BAER, S. & GAN-OR, Z. 2019. Increased yield of full GBA sequencing in Ashkenazi Jews with Parkinson's disease. *Eur J Med Genet,* 62**,** 65-69.

RYU, E. J., HARDING, H. P., ANGELASTRO, J. M., VITOLO, O. V., RON, D. & GREENE, L. A. 2002. Endoplasmic reticulum stress and the unfolded protein response in cellular models of Parkinson's disease. *The Journal of neuroscience : the official journal of the Society for Neuroscience,* 22**,** 10690-10698.

SABATY, M., GROSSE, S., ADRYANCZYK, G., BOIRY, S., BIASO, F., ARNOUX, P. & PIGNOL, D. 2013. Detrimental effect of the 6 His C-terminal tag on YedY enzymatic activity and influence of the TAT signal sequence on YedY synthesis. *BMC Biochem,* 14**,** 28.

SABERIANFAR, R., SATTARZADEH, A., JOENSUU, J. J., KOHALMI, S. E. & MENASSA, R. 2016. Protein Bodies in Leaves Exchange Contents through the Endoplasmic Reticulum. *Frontiers in plant science,* 7**,** 693-693.

ŞAHIN, M., ÖNCÜ, G., YıLMAZ, M. A., ÖZKAN, D. & SAYBAŞıLı, H. 2021. Transformation of SH-SY5Y cell line into neuron-like cells: Investigation of electrophysiological and biomechanical changes. *Neuroscience Letters,* 745**,** 135628.

SALVIOLI, R., TATTI, M., SCARPA, S., MOAVERO, S. M., CIAFFONI, F., FELICETTI, F., KANESKI, C. R., BRADY, R. O. & VACCARO, A. M. 2005. The N370S (Asn370-->Ser) mutation affects the capacity of glucosylceramidase to interact with anionic phospholipid-containing membranes and saposin C. *The Biochemical journal,* 390**,** 95-103.

SANCHEZ-MARTINEZ, A., BEAVAN, M., GEGG, M. E., CHAU, K. Y., WHITWORTH, A. J. & SCHAPIRA, A. H. 2016. Parkinson disease-linked GBA mutation effects reversed by molecular chaperones in human cell and fly models. *Sci Rep,* 6**,** 31380.

SANG, J. C., HIDARI, E., MEISL, G., RANASINGHE, R. T., SPILLANTINI, M. G. & KLENERMAN, D. 2021. Super-resolution imaging reveals alpha-synuclein seeded aggregation in SH-SY5Y cells. *Commun Biol,* 4**,** 613.

SARDI, P. S., SHIHABUDDIN, L. S., SIDMAN, R. L. & CHENG, S. H. 2013. Augmenting CNS Glucocerebrosidase Activity as a Therapeutic Strategy

for Parkinsonism and Other Gaucher-Related Synucleinopathies. *Molecular Therapy,* 21**,** S14-S15.

SARDI, S. P., CLARKE, J., KINNECOM, C., TAMSETT, T. J., LI, L., STANEK, L. M., PASSINI, M. A., GRABOWSKI, G. A., SCHLOSSMACHER, M. G., SIDMAN, R. L., CHENG, S. H. & SHIHABUDDIN, L. S. 2011. CNS expression of glucocerebrosidase corrects alpha-synuclein pathology and memory in a mouse model of Gaucher-related synucleinopathy. *Proc Natl Acad Sci U S A,* 108**,** 12101-6.

SARDI, S. P., VIEL, C., CLARKE, J., TRELEAVEN, C. M., RICHARDS, A. M., PARK, H., OLSZEWSKI, M. A., DODGE, J. C., MARSHALL, J., MAKINO, E., WANG, B., SIDMAN, R. L., CHENG, S. H. & SHIHABUDDIN, L. S. 2017. Glucosylceramide synthase inhibition alleviates aberrations in synucleinopathy models. *Proc Natl Acad Sci U S A,* 114**,** 2699-2704.

SAWKAR, A. R., SCHMITZ, M., ZIMMER, K.-P., RECZEK, D., EDMUNDS, T., BALCH, W. E. & KELLY, J. W. 2006. Chemical Chaperones and Permissive Temperatures Alter the Cellular Localization of Gaucher Disease Associated Glucocerebrosidase Variants. *ACS Chemical Biology,* 1**,** 235-251.

SCHAPIRA, A. H. 2008. Mitochondria in the aetiology and pathogenesis of Parkinson's disease. *Lancet Neurol,* 7**,** 97-109.

SCHAPIRA, A. H., COOPER, J. M., DEXTER, D., CLARK, J. B., JENNER, P. & MARSDEN, C. D. 1990. Mitochondrial complex I deficiency in Parkinson's disease. *J Neurochem,* 54**,** 823-7.

SCHAPIRA, A. H., COOPER, J. M., DEXTER, D., JENNER, P., CLARK, J. B. & MARSDEN, C. D. 1989. Mitochondrial complex I deficiency in Parkinson's disease. *Lancet,* 1**,** 1269.

SCHAPIRA, A. H. & GEGG, M. 2011. Mitochondrial contribution to Parkinson's disease pathogenesis. *Parkinsons Dis,* 2011**,** 159160.

SCHIESLING, C., KIEPER, N., SEIDEL, K. & KRÜGER, R. 2008. Review: Familial Parkinson's disease--genetics, clinical phenotype and neuropathology in relation to the common sporadic form of the disease. *Neuropathol Appl Neurobiol,* 34**,** 255-71.

SCHLAGER, B., STRAESSLE, A. & HAFEN, E. 2012. Use of anionic denaturing detergents to purify insoluble proteins after overexpression. *BMC Biotechnology,* 12**,** 95.

SCHMITZ, M., ALFALAH, M., AERTS, J. M., NAIM, H. Y. & ZIMMER, K. P. 2005. Impaired trafficking of mutants of lysosomal glucocerebrosidase in Gaucher's disease. *Int J Biochem Cell Biol,* 37**,** 2310-20.

SCHÖNDORF, D. C., AURELI, M., MCALLISTER, F. E., HINDLEY, C. J., MAYER, F., SCHMID, B., SARDI, S. P., VALSECCHI, M., HOFFMANN, S., SCHWARZ, L. K., HEDRICH, U., BERG, D., SHIHABUDDIN, L. S., HU, J., PRUSZAK, J., GYGI, S. P., SONNINO, S., GASSER, T. & DELEIDI, M. 2014. iPSC-derived neurons from GBA1-associated Parkinson’s disease patients show autophagic defects and impaired calcium homeostasis. *Nature Communications,* 5**,** 4028.

SCHÖNDORF, D. C., IVANYUK, D., BADEN, P., SANCHEZ-MARTINEZ, A., DE CICCO, S., YU, C., GIUNTA, I., SCHWARZ, L. K., DI NAPOLI, G., PANAGIOTAKOPOULOU, V., NESTEL, S., KEATINGE, M., PRUSZAK, J., BANDMANN, O., HEIMRICH, B., GASSER, T., WHITWORTH, A. J. & DELEIDI, M. 2018. The NAD+ Precursor Nicotinamide Riboside Rescues Mitochondrial Defects and Neuronal Loss in iPSC and Fly Models of Parkinson’s Disease. *Cell Reports,* 23**,** 2976-2988.

SCHÖNFELD, P. & REISER, G. 2013. Why does brain metabolism not favor burning of fatty acids to provide energy? Reflections on disadvantages of the use of free fatty acids as fuel for brain. *J Cereb Blood Flow Metab,* 33**,** 1493-9.

SCHOTT, M. B., WELLER, S. G., SCHULZE, R. J., KRUEGER, E. W., DRIZYTE-MILLER, K., CASEY, C. A. & MCNIVEN, M. A. 2019. Lipid droplet size directs lipolysis and lipophagy catabolism in hepatocytes. *Journal of Cell Biology,* 218**,** 3320-3335.

SENTHILKUMAR, R. & SHARMA, K. K. 2002. Effect of chaotropic agents on the structure-function of recombinant acylpeptide hydrolase. *J Protein Chem,* 21**,** 323-32.

SHAHMORADIAN, S. H., LEWIS, A. J., GENOUD, C., HENCH, J., MOORS, T. E., NAVARRO, P. P., CASTANO-DIEZ, D., SCHWEIGHAUSER, G., GRAFF-MEYER, A., GOLDIE, K. N., SUTTERLIN, R., HUISMAN, E., INGRASSIA, A., GIER, Y., ROZEMULLER, A. J. M., WANG, J., PAEPE, A., ERNY, J., STAEMPFLI, A., HOERNSCHEMEYER, J., GROSSERUSCHKAMP, F., NIEDIEKER, D., EL-MASHTOLY, S. F., QUADRI, M., VAN, I. W. F. J., BONIFATI, V., GERWERT, K., BOHRMANN, B., FRANK, S., BRITSCHGI, M., STAHLBERG, H., VAN DE BERG, W. D. J. & LAUER, M. E. 2019. Lewy pathology in Parkinson's disease consists of crowded organelles and lipid membranes. *Nat Neurosci,* 22**,** 1099-1109.

SHANMUGANATHAN, M. & BRITZ-MCKIBBIN, P. 2011. Inhibitor screening of pharmacological chaperones for lysosomal beta-glucocerebrosidase by capillary electrophoresis. *Anal Bioanal Chem,* 399**,** 2843-53.

SHEMESH, E., DEROMA, L., BEMBI, B., DEEGAN, P., HOLLAK, C., WEINREB, N. J. & COX, T. M. 2015. Enzyme replacement and substrate reduction therapy for Gaucher disease. *Cochrane Database Syst Rev***,** CD010324.

SHIPLEY, M. M., MANGOLD, C. A. & SZPARA, M. L. 2016. Differentiation of the SH-SY5Y Human Neuroblastoma Cell Line. *Journal of visualized experiments : JoVE***,** 53193-53193.

SIDRANSKY, E. 2004. Gaucher disease: complexity in a "simple" disorder. *Molecular Genetics and Metabolism,* 83**,** 6-15.

SIDRANSKY, E. 2012. Gaucher disease: insights from a rare Mendelian disorder. *Discov Med,* 14**,** 273-81.

SIDRANSKY, E. & LOPEZ, G. 2012. The link between the GBA gene and parkinsonism. *Lancet Neurol,* 11**,** 986-98.

SIDRANSKY, E., NALLS, M. A., AASLY, J. O., AHARON-PERETZ, J., ANNESI, G., BARBOSA, E. R., BAR-SHIRA, A., BERG, D., BRAS, J., BRICE, A., CHEN, C. M., CLARK, L. N., CONDROYER, C., DE MARCO, E. V., DÜRR, A., EBLAN, M. J., FAHN, S., FARRER, M., FUNG, H. C., GAN-OR, Z., GASSER, T., GERSHONI-BARUCH, R., GILADI, N., GRIFFITH, A., GUREVICH, T., JANUARIO, C., KROPP, P., LANG, A. E., LEE-CHEN, G. J., LESAGE, S., MARDER, K., MATA, I. F., MIRELMAN, A., MITSUI, J., MIZUTA, I., NICOLETTI, G., OLIVEIRA, C., OTTMAN, R., ORR-URTREGER, A., PEREIRA, L. V., QUATTRONE, A., ROGAEVA, E., ROLFS, A., ROSENBAUM, H., ROZENBERG, R., SAMII, A., SAMADDAR, T., SCHULTE, C., SHARMA, M., SINGLETON, A., SPITZ, M., TAN, E. K., TAYEBI, N., TODA, T., TROIANO, A., TSUJI, S., WITTSTOCK, M., WOLFSBERG, T. G., WU, Y. R., ZABETIAN, C. P., ZHAO, Y. & ZIEGLER, S. G. 2009. Multi-center analysis of

glucocerebrosidase mutations in Parkinson disease. *N Engl J Med,* 361**,** 1651-61.

SIMON, E. & KORNITZER, D. 2014. Chapter Six - Pulse-Chase Analysis to Measure Protein Degradation. *In:* LORSCH, J. (ed.) *Methods in Enzymology.* Academic Press.

SMITH, L., MULLIN, S. & SCHAPIRA, A. H. V. 2017. Insights into the structural biology of Gaucher disease. *Exp Neurol,* 298**,** 180-190.

SMITH, M. H., PLOEGH, H. L. & WEISSMAN, J. S. 2011. Road to ruin: targeting proteins for degradation in the endoplasmic reticulum. *Science,* 334**,** 1086-90.

SMITH, W. W., MARGOLIS, R. L., LI, X., TRONCOSO, J. C., LEE, M. K., DAWSON, V. L., DAWSON, T. M., IWATSUBO, T. & ROSS, C. A. 2005. Alpha-synuclein phosphorylation enhances eosinophilic cytoplasmic inclusion formation in SH-SY5Y cells. *J Neurosci,* 25**,** 5544-52.

SOUFFRANT, M. G., YAO, X.-Q., MOMIN, M. & HAMELBERG, D. 2020. N-Glycosylation and Gaucher Disease Mutation Allosterically Alter Active-Site Dynamics of Acid-β-Glucosidase. *ACS Catalysis,* 10**,** 1810-1820.

SPENCER, B., POTKAR, R., TREJO, M., ROCKENSTEIN, E., PATRICK, C., GINDI, R., ADAME, A., WYSS-CORAY, T. & MASLIAH, E. 2009. Beclin 1 gene transfer activates autophagy and ameliorates the neurodegenerative pathology in alpha-synuclein models of Parkinson's and Lewy body diseases. *J Neurosci,* 29**,** 13578-88.

SPILLANTINI, M. G., CROWTHER, R. A., JAKES, R., CAIRNS, N. J., LANTOS, P. L. & GOEDERT, M. 1998. Filamentous alpha-synuclein inclusions link multiple system atrophy with Parkinson's disease and dementia with Lewy bodies. *Neurosci Lett,* 251**,** 205-8.

SPILLANTINI, M. G., SCHMIDT, M. L., LEE, V. M., TROJANOWSKI, J. Q., JAKES, R. & GOEDERT, M. 1997. Alpha-synuclein in Lewy bodies. *Nature,* 388**,** 839-40.

SPRIESTERSBACH, A., KUBICEK, J., SCHAFER, F., BLOCK, H. & MAERTENS, B. 2015. Purification of His-Tagged Proteins. *Methods Enzymol,* 559**,** 1-15.

SPRINGER, S. & SCHEKMAN, R. 1998. Nucleation of COPII vesicular coat complex by endoplasmic reticulum to Golgi vesicle SNAREs. *Science,* 281**,** 698-700.

STEET, R. A., CHUNG, S., WUSTMAN, B., POWE, A., DO, H. & KORNFELD, S. A. 2006. The iminosugar isofagomine increases the activity of N370S mutant acid beta-glucosidase in Gaucher fibroblasts by several mechanisms. *Proc Natl Acad Sci U S A,* 103**,** 13813-8.

STEYN, F. J., LI, R., KIRK, S. E., TEFERA, T. W., XIE, T. Y., TRACEY, T. J., KELK, D., WIMBERGER, E., GARTON, F. C., ROBERTS, L., CHAPMAN, S. E., COOMBES, J. S., LEEVY, W. M., FERRI, A., VALLE, C., RENÉ, F., LOEFFLER, J.-P., MCCOMBE, P. A., HENDERSON, R. D. & NGO, S. T. 2020. Altered skeletal muscle glucose–fatty acid flux in amyotrophic lateral sclerosis. *Brain Communications,* 2.

STOJKOVSKA, I. & MAZZULLI, J. R. 2021. Detection of pathological alpha-synuclein aggregates in human iPSC-derived neurons and tissue. *STAR Protoc,* 2**,** 100372.

STOKER, T. B., CAMACHO, M., WINDER-RHODES, S., LIU, G., SCHERZER, C. R., FOLTYNIE, T., BARKER, R. A. & WILLIAMS-GRAY, C. H. 2020a. A common polymorphism in SNCA is associated with accelerated motor

decline in GBA-Parkinson's disease. *J Neurol Neurosurg Psychiatry,* 91**,** 673-674.

STOKER, T. B., CAMACHO, M., WINDER-RHODES, S., LIU, G., SCHERZER, C. R., FOLTYNIE, T., EVANS, J., BREEN, D. P., BARKER, R. A. & WILLIAMS-GRAY, C. H. 2020b. Impact of GBA1 variants on long-term clinical progression and mortality in incident Parkinson's disease. *J Neurol Neurosurg Psychiatry*.

STOKER, T. B., TORSNEY, K. M. & BARKER, R. A. 2018. Pathological Mechanisms and Clinical Aspects of GBA1 Mutation-Associated Parkinson's Disease. *In:* STOKER, T. B. & GREENLAND, J. C. (eds.) *Parkinson's Disease: Pathogenesis and Clinical Aspects.* Brisbane (AU).

STRASBERG, P. M., LOWDEN, J. A. & MAHURAN, D. 1982. Purification of glucosylceramidase by affinity chromatography. *Can J Biochem,* 60**,** 1025-31.

STUENDL, A., KRAUS, T., CHATTERJEE, M., ZAPKE, B., SADOWSKI, B., MOEBIUS, W., HOBERT, M. A., DEUSCHLE, C., BROCKMANN, K., MAETZLER, W., MOLLENHAUER, B. & SCHNEIDER, A. 2021. alpha-Synuclein in Plasma-Derived Extracellular Vesicles Is a Potential Biomarker of Parkinson's Disease. *Mov Disord*.

SUPLATOV, D., VOEVODIN, V. & SVEDAS, V. 2015. Robust enzyme design: bioinformatic tools for improved protein stability. *Biotechnol J,* 10**,** 344-55.

SUZUKI, M., SANGO, K., WADA, K. & NAGAI, Y. 2018. Pathological role of lipid interaction with alpha-synuclein in Parkinson's disease. *Neurochem Int*.

SUZUKI, T., SHIMODA, M., ITO, K., HANAI, S., AIZAWA, H., KATO, T., KAWASAKI, K., YAMAGUCHI, T., RYOO, H. D., GOTO-INOUE, N., SETOU, M., TSUJI, S. & ISHIDA, N. 2015. Expression of Human Gaucher

Disease Gene GBA Generates Neurodevelopmental Defects and ER Stress in Drosophila Eye (vol 8, e69147, 2013). *Plos One,* 10.

TAGUCHI, Y. V., LIU, J., RUAN, J., PACHECO, J., ZHANG, X., ABBASI, J., KEUTZER, J., MISTRY, P. K. & CHANDRA, S. S. 2017. Glucosylsphingosine Promotes alpha-Synuclein Pathology in Mutant GBA-Associated Parkinson's Disease. *J Neurosci,* 37**,** 9617-9631.

TAKASAKI, S., MURRAY, G. J., FURBISH, F. S., BRADY, R. O., BARRANGER, J. A. & KOBATA, A. 1984. Structure of the N-asparagine-linked oligosaccharide units of human placental beta-glucocerebrosidase. *J Biol Chem,* 259**,** 10112-7.

TAN, Y. L., GENEREUX, J. C., PANKOW, S., AERTS, J. M., YATES, J. R., 3RD & KELLY, J. W. 2014. ERdj3 is an endoplasmic reticulum degradation factor for mutant glucocerebrosidase variants linked to Gaucher's disease. *Chem Biol,* 21**,** 967-76.

TANG, Y. T., HUANG, Y. Y., ZHENG, L., QIN, S. H., XU, X. P., AN, T. X., XU, Y., WU, Y. S., HU, X. M., PING, B. H. & WANG, Q. 2017. Comparison of isolation methods of exosomes and exosomal RNA from cell culture medium and serum. *Int J Mol Med,* 40**,** 834-844.

TANJI, K., MORI, F., MIMURA, J., ITOH, K., KAKITA, A., TAKAHASHI, H. & WAKABAYASHI, K. 2010. Proteinase K-resistant alpha-synuclein is deposited in presynapses in human Lewy body disease and A53T alpha-synuclein transgenic mice. *Acta Neuropathol,* 120**,** 145-54.

TANSEY, M. G. & GOLDBERG, M. S. 2010. Neuroinflammation in Parkinson's disease: its role in neuronal death and implications for therapeutic intervention. *Neurobiol Dis,* 37**,** 510-8.

TAYEBI, N., CALLAHAN, M., MADIKE, V., STUBBLEFIELD, B. K., ORVISKY, E., KRASNEWICH, D., FILLANO, J. J. & SIDRANSKY, E. 2001. Gaucher disease and parkinsonism: A phenotypic and genotypic characterization. *Molecular Genetics and Metabolism,* 73**,** 313-321.

TAYEBI, N., WALKER, J., STUBBLEFIELD, B., ORVISKY, E., LAMARCA, M. E., WONG, K., ROSENBAUM, H., SCHIFFMANN, R., BEMBI, B. & SIDRANSKY, E. 2003. Gaucher disease with parkinsonian manifestations: does glucocerebrosidase deficiency contribute to a vulnerability to parkinsonism? *Molecular Genetics and Metabolism,* 79**,** 104-109.

TEKOAH, Y., TZABAN, S., KIZHNER, T., HAINRICHSON, M., GANTMAN, A., GOLEMBO, M., AVIEZER, D. & SHAALTIEL, Y. 2013. Glycosylation and functionality of recombinant beta-glucocerebrosidase from various production systems. *Bioscience Reports,* 33**,** 771-U272.

TEVES, J. M. Y., BHARGAVA, V., KIRWAN, K. R., CORENBLUM, M. J., JUSTINIANO, R., WONDRAK, G. T., ANANDHAN, A., FLORES, A. J., SCHIPPER, D. A., KHALPEY, Z., SLIGH, J. E., CURIEL-LEWANDROWSKI, C., SHERMAN, S. J. & MADHAVAN, L. 2018. Parkinson's Disease Skin Fibroblasts Display Signature Alterations in Growth, Redox Homeostasis, Mitochondrial Function, and Autophagy. *Frontiers in neuroscience,* 11**,** 737-737.

THOMAS, R., MOLONEY, E. B., MACBAIN, Z. K., HALLETT, P. J. & ISACSON, O. 2021. Fibroblasts from idiopathic Parkinson's disease exhibit deficiency of lysosomal glucocerebrosidase activity associated with reduced levels of the trafficking receptor LIMP2. *Mol Brain,* 14**,** 16.

THOMAS, R. E., VINCOW, E. S., MERRIHEW, G. E., MACCOSS, M. J., DAVIS, M. Y. & PALLANCK, L. J. 2018. Glucocerebrosidase deficiency promotes

protein aggregation through dysregulation of extracellular vesicles. *PLoS Genet,* 14**,** e1007694.

THOME, A. D., HARMS, A. S., VOLPICELLI-DALEY, L. A. & STANDAERT, D. G. 2016. microRNA-155 Regulates Alpha-Synuclein-Induced Inflammatory Responses in Models of Parkinson Disease. *J Neurosci,* 36**,** 2383-90.

TORRALBA, M. A., PÉREZ-CALVO, J. I., PASTORES, G. M., CENARRO, A., GIRALDO, P. & POCOVí, M. 2001. Identification and Characterization of a Novel Mutation c.1090G>T (G325W) and Nine Common Mutant Alleles Leading to Gaucher Disease in Spanish Patients. *Blood Cells, Molecules, and Diseases,* 27**,** 489-495.

TOSETTI, P., TAGLIETTI, V. & TOSELLI, M. 1998. Functional changes in potassium conductances of the human neuroblastoma cell line SH-SY5Y during in vitro differentiation. *J Neurophysiol,* 79**,** 648-58.

TURPIN, J. C., DUBOIS, G., BRICE, A., MASSON, M., NADAUD, M. C., BOUTRY, J. M., SCHRAM, A. W., TAGER, J. M. & BAUMANN, N. Parkinsonian Symptomatology in a Patient with Type I (Adult) Gaucher's Disease. 1988 Boston, MA. Springer US, 103-105.

ULLOA-AGUIRRE, A., JANOVICK, J. A., BROTHERS, S. P. & CONN, P. M. 2004. Pharmacologic rescue of conformationally-defective proteins: implications for the treatment of human disease. *Traffic,* 5**,** 821-37.

UNGER, R. H. & ORCI, L. 2002. Lipoapoptosis: its mechanism and its diseases. *Biochim Biophys Acta,* 1585**,** 202-12.

USENOVIC, M., TRESSE, E., MAZZULLI, J. R., TAYLOR, J. P. & KRAINC, D. 2012. Deficiency of ATP13A2 leads to lysosomal dysfunction, alpha-synuclein accumulation, and neurotoxicity. *J Neurosci,* 32**,** 4240-6.

VAN DEN BERGE, N., FERREIRA, N., MIKKELSEN, T. W., ALSTRUP, A. K. O., TAMGUNEY, G., KARLSSON, P., TERKELSEN, A. J., NYENGAARD, J. R., JENSEN, P. H. & BORGHAMMER, P. 2021. Ageing promotes pathological alpha-synuclein propagation and autonomic dysfunction in wild-type rats. *Brain,* 144**,** 1853-1868.

VANDELL, V. E. & LIMBACH, P. A. 2010. Overview of Biochemical Applications of Mass Spectrometry*. *In:* LINDON, J. C. (ed.) *Encyclopedia of Spectroscopy and Spectrometry (Second Edition).* Oxford: Academic Press.

VARELA, A. R., VENTURA, A. E., CARREIRA, A. C., FEDOROV, A., FUTERMAN, A. H., PRIETO, M. & SILVA, L. C. 2016. Pathological levels of glucosylceramide change the biophysical properties of artificial and cell membranes. *Phys Chem Chem Phys,* 19**,** 340-346.

VELÁZQUEZ, A. P., TATSUTA, T., GHILLEBERT, R., DRESCHER, I. & GRAEF, M. 2016. Lipid droplet-mediated ER homeostasis regulates autophagy and cell survival during starvation. *J Cell Biol,* 212**,** 621-31.

VERMILYEA, S. C., BABINSKI, A., TRAN, N., TO, S., GUTHRIE, S., KLUSS, J. H., SCHMIDT, J. K., WIEPZ, G. J., MEYER, M. G., MURPHY, M. E., COOKSON, M. R., EMBORG, M. E. & GOLOS, T. G. 2020. In Vitro CRISPR/Cas9-Directed Gene Editing to Model LRRK2 G2019S Parkinson's Disease in Common Marmosets. *Scientific Reports,* 10**,** 3447.

VIEIRA, D. B., THUR, K., SULTANA, S., PRIESTMAN, D. & VAN DER SPOEL, A. C. 2015. Verification and refinement of cellular glycosphingolipid profiles using HPLC. *Biochem Cell Biol,* 93**,** 581-6.

VISANJI, N. P., BROTCHIE, J. M., KALIA, L. V., KOPRICH, J. B., TANDON, A., WATTS, J. C. & LANG, A. E. 2016. α-Synuclein-Based Animal Models of

Parkinson's Disease: Challenges and Opportunities in a New Era. *Trends Neurosci,* 39**,** 750-762.

VITNER, E. B., FARFEL-BECKER, T., EILAM, R., BITON, I. & FUTERMAN, A. H. 2012. Contribution of brain inflammation to neuronal cell death in neuronopathic forms of Gaucher's disease. *Brain,* 135**,** 1724-35.

VITNER, E. B., SALOMON, R., FARFEL-BECKER, T., MESHCHERIAKOVA, A., ALI, M., KLEIN, A. D., PLATT, F. M., COX, T. M. & FUTERMAN, A. H. 2014. RIPK3 as a potential therapeutic target for Gaucher's disease. *Nat Med,* 20**,** 204-8.

VOLPICELLI-DALEY, L. A., LUK, K. C. & LEE, V. M. 2014. Addition of exogenous α-synuclein preformed fibrils to primary neuronal cultures to seed recruitment of endogenous α-synuclein to Lewy body and Lewy neurite-like aggregates. *Nat Protoc,* 9**,** 2135-46.

VOLPICELLI-DALEY, L. A., LUK, K. C., PATEL, T. P., TANIK, S. A., RIDDLE, D. M., STIEBER, A., MEANEY, D. F., TROJANOWSKI, J. Q. & LEE, V. M. 2011. Exogenous alpha-synuclein fibrils induce Lewy body pathology leading to synaptic dysfunction and neuron death. *Neuron,* 72**,** 57-71.

WAJNER, M. & AMARAL, A. U. 2015. Mitochondrial dysfunction in fatty acid oxidation disorders: insights from human and animal studies. *Bioscience reports,* 36**,** e00281-e00281.

WAKABAYASHI, K., TANJI, K., ODAGIRI, S., MIKI, Y., MORI, F. & TAKAHASHI, H. 2013. The Lewy body in Parkinson's disease and related neurodegenerative disorders. *Mol Neurobiol,* 47**,** 495-508.

WANG, F., SONG, W., BRANCATI, G. & SEGATORI, L. 2011. Inhibition of endoplasmic reticulum-associated degradation rescues native folding in

loss of function protein misfolding diseases. *The Journal of biological chemistry,* 286**,** 43454-43464.

WANG, H., WEI, E., QUIROGA, A. D., SUN, X., TOURET, N. & LEHNER, R. 2010. Altered lipid droplet dynamics in hepatocytes lacking triacylglycerol hydrolase expression. *Molecular biology of the cell,* 21**,** 1991-2000.

WANG, X., YAN, M. H., FUJIOKA, H., LIU, J., WILSON-DELFOSSE, A., CHEN, S. G., PERRY, G., CASADESUS, G. & ZHU, X. 2012. LRRK2 regulates mitochondrial dynamics and function through direct interaction with DLP1. *Human Molecular Genetics,* 21**,** 1931-1944.

WARD, O. P. & MOO-YOUNG, M. 1988. Thermostable enzymes. *Biotechnol Adv,* 6**,** 39-69.

WATT, M. J., CLARK, A. K., SELTH, L. A., HAYNES, V. R., LISTER, N., REBELLO, R., PORTER, L. H., NIRANJAN, B., WHITBY, S. T., LO, J., HUANG, C., SCHITTENHELM, R. B., ANDERSON, K. E., FURIC, L., WIJAYARATNE, P. R., MATZARIS, M., MONTGOMERY, M. K., PAPARGIRIS, M., NORDEN, S., FEBBRAIO, M., RISBRIDGER, G. P., FRYDENBERG, M., NOMURA, D. K. & TAYLOR, R. A. 2019. Suppressing fatty acid uptake has therapeutic effects in preclinical models of prostate cancer. *Sci Transl Med,* 11.

WEI, R. R., HUGHES, H., BOUCHER, S., BIRD, J. J., GUZIEWICZ, N., VAN PATTEN, S. M., QIU, H., PAN, C. Q. & EDMUNDS, T. 2011. X-ray and biochemical analysis of N370S mutant human acid beta-glucosidase. *J Biol Chem,* 286**,** 299-308.

WEISH, P., LÁZARO, D. F., PALMARES, L., SANTOS, P. I., STADELMANN, C., HÖGLINGER, G. U., RIZZOLI, S. O. & OUTEIRO, T. F. 2021. Super-resolution microscopy informs on the molecular architecture of alpha-

synuclein inclusions in model systems and in the human brain. *bioRxiv*, 2021.04.25.441304.

WENGER, D. A., CLARK, C., SATTLER, M. & WHARTON, C. 1978. Synthetic substrate beta-glucosidase activity in leukocytes: a reproducible method for the identification of patients and carriers of Gaucher's disease. *Clin Genet,* 13**,** 145-53.

WESTBROEK, W., GUSTAFSON, A. M. & SIDRANSKY, E. 2011. Exploring the link between glucocerebrosidase mutations and parkinsonism. *Trends in Molecular Medicine,* 17**,** 485-493.

WINDER-RHODES, S. E., EVANS, J. R., BAN, M., MASON, S. L., WILLIAMS-GRAY, C. H., FOLTYNIE, T., DURAN, R., MENCACCI, N. E., SAWCER, S. J. & BARKER, R. A. 2013. Glucocerebrosidase mutations influence the natural history of Parkinson's disease in a community-based incident cohort. *Brain,* 136**,** 392-9.

WINFIELD, S. L., TAYEBI, N., MARTIN, B. M., GINNS, E. I. & SIDRANSKY, E. 1997. Identification of three additional genes contiguous to the glucocerebrosidase locus on chromosome 1q21: Implications for Gaucher disease. *Genome Research,* 7**,** 1020-1026.

WONG, K., SIDRANSKY, E., VERMA, A., MIXON, T., SANDBERG, G. D., WAKEFIELD, L. K., MORRISON, A., LWIN, A., COLEGIAL, C., ALLMAN, J. M. & SCHIFFMANN, R. 2004. Neuropathology provides clues to the pathophysiology of Gaucher disease. *Mol Genet Metab,* 82**,** 192-207.

WONG, Y. C. & KRAINC, D. 2016. Lysosomal trafficking defects link Parkinson's disease with Gaucher's disease. *Mov Disord,* 31**,** 1610-1618.

WONG, Y. C. & KRAINC, D. 2017. α-synuclein toxicity in neurodegeneration: mechanism and therapeutic strategies. *Nature Medicine,* 23**,** 1.

WOOD, P. L., TIPPIREDDY, S., FERIANTE, J. & WOLTJER, R. L. 2018. Augmented frontal cortex diacylglycerol levels in Parkinson's disease and Lewy Body Disease. *PLOS ONE,* 13**,** e0191815.

WOODARD, C. M., CAMPOS, B. A., KUO, S. H., NIRENBERG, M. J., NESTOR, M. W., ZIMMER, M., MOSHAROV, E. V., SULZER, D., ZHOU, H. Y., PAULL, D., CLARK, L., SCHADT, E. E., SARDI, S. P., RUBIN, L., EGGAN, K., BROCK, M., LIPNICK, S., RAO, M., CHANG, S., LI, A. Q. & NOGGLE, S. A. 2014. iPSC-Derived Dopamine Neurons Reveal Differences between Monozygotic Twins Discordant for Parkinson's Disease. *Cell Reports,* 9**,** 1173-1182.

WU, Q., TAKANO, H., RIDDLE, D. M., TROJANOWSKI, J. Q., COULTER, D. A. & LEE, V. M. Y. 2019. α-Synuclein (αSyn) Preformed Fibrils Induce Endogenous αSyn Aggregation, Compromise Synaptic Activity and Enhance Synapse Loss in Cultured Excitatory Hippocampal Neurons. *The Journal of Neuroscience,* 39**,** 5080.

XIA, W., XU, X., QIAN, L., SHI, P., BAI, Y., LUO, H., MA, R. & YAO, B. 2016. Engineering a highly active thermophilic β-glucosidase to enhance its pH stability and saccharification performance. *Biotechnology for Biofuels,* 9**,** 147.

XICOY, H., WIERINGA, B. & MARTENS, G. J. M. 2017. The SH-SY5Y cell line in Parkinson's disease research: a systematic review. *Molecular Neurodegeneration,* 12**,** 10.

XIE, H. R., HU, L. S. & LI, G. Y. 2010. SH-SY5Y human neuroblastoma cell line: in vitro cell model of dopaminergic neurons in Parkinson's disease. *Chinese Medical Journal,* 123**,** 1086-1092.

XU, Y. H., SUN, Y., RAN, H., QUINN, B., WITTE, D. & GRABOWSKI, G. A. 2011. Accumulation and distribution of alpha-synuclein and ubiquitin in the CNS of Gaucher disease mouse models. *Mol Genet Metab,* 102**,** 436-47.

XU, Y. H., XU, K., SUN, Y., LIOU, B., QUINN, B., LI, R. H., XUE, L., ZHANG, W., SETCHELL, K. D., WITTE, D. & GRABOWSKI, G. A. 2014. Multiple pathogenic proteins implicated in neuronopathic Gaucher disease mice. *Hum Mol Genet,* 23**,** 3943-57.

XUE, C., LIN, T. Y., CHANG, D. & GUO, Z. 2017. Thioflavin T as an amyloid dye: fibril quantification, optimal concentration and effect on aggregation. *Royal Society open science,* 4**,** 160696-160696.

YANG, J., HERTZ, E., ZHANG, X., LEINARTAITE, L., LUNDIUS, E. G., LI, J. & SVENNINGSSON, P. 2016. Overexpression of alpha-synuclein simultaneously increases glutamate NMDA receptor phosphorylation and reduces glucocerebrosidase activity. *Neurosci Lett,* 611**,** 51-8.

YANG, L., LIANG, J., LAM, S. M., YAVUZ, A., SHUI, G., DING, M. & HUANG, X. 2020a. Neuronal lipolysis participates in PUFA-mediated neural function and neurodegeneration. *EMBO reports,* 21**,** e50214.

YANG, S. Y., BEAVAN, M., CHAU, K. Y., TAANMAN, J. W. & SCHAPIRA, A. H. 2017. A Human Neural Crest Stem Cell-Derived Dopaminergic Neuronal Model Recapitulates Biochemical Abnormalities in GBA1 Mutation Carriers. *Stem Cell Reports,* 8**,** 728-742.

YANG, S. Y., GEGG, M., CHAU, D. & SCHAPIRA, A. 2020b. Glucocerebrosidase activity, cathepsin D and monomeric alpha-synuclein interactions in a stem cell derived neuronal model of a PD associated GBA1 mutation. *Neurobiol Dis,* 134**,** 104620.

YAP, T. L., GRUSCHUS, J. M., VELAYATI, A., SIDRANSKY, E. & LEE, J. C. 2013a. Saposin C Protects Glucocerebrosidase against α-Synuclein Inhibition. *Biochemistry,* 52**,** 10.1021/bi401191v.

YAP, T. L., GRUSCHUS, J. M., VELAYATI, A., WESTBROEK, W., GOLDIN, E., MOAVEN, N., SIDRANSKY, E. & LEE, J. C. 2011. Alpha-synuclein interacts with Glucocerebrosidase providing a molecular link between Parkinson and Gaucher diseases. *J Biol Chem,* 286**,** 28080-8.

YAP, T. L., JIANG, Z., HEINRICH, F., GRUSCHUS, J. M., PFEFFERKORN, C. M., BARROS, M., CURTIS, J. E., SIDRANSKY, E. & LEE, J. C. 2015. Structural features of membrane-bound glucocerebrosidase and alpha-synuclein probed by neutron reflectometry and fluorescence spectroscopy. *J Biol Chem,* 290**,** 744-54.

YAP, T. L., VELAYATI, A., SIDRANSKY, E. & LEE, J. C. 2013b. Membrane-bound alpha-synuclein interacts with glucocerebrosidase and inhibits enzyme activity. *Mol Genet Metab,* 108**,** 56-64.

YEOMAN, C. H., Y; DODD, D; SCHROEDER, C; MACKIE, R; CANN, I; 2010. *Advances in Applied Microbiology*.

YILDIZ, Y., HOFFMANN, P., VOM DAHL, S., BREIDEN, B., SANDHOFF, R., NIEDERAU, C., HORWITZ, M., KARLSSON, S., FILOCAMO, M., ELSTEIN, D., BECK, M., SANDHOFF, K., MENGEL, E., GONZALEZ, M. C., NÖTHEN, M. M., SIDRANSKY, E., ZIMRAN, A. & MATTHEISEN, M. 2013. Functional and genetic characterization of the non-lysosomal glucosylceramidase 2 as a modifier for Gaucher disease. *Orphanet Journal of Rare Diseases,* 8**,** 151.

YOSHIDA, H., MATSUI, T., YAMAMOTO, A., OKADA, T. & MORI, K. 2001. XBP1 mRNA is induced by ATF6 and spliced by IRE1 in response to ER stress to produce a highly active transcription factor. *Cell,* 107**,** 881-91.

YUN, S. P., KIM, D., KIM, S., KIM, S., KARUPPAGOUNDER, S. S., KWON, S.-H., LEE, S., KAM, T.-I., LEE, S., HAM, S., PARK, J. H., DAWSON, V. L., DAWSON, T. M., LEE, Y. & KO, H. S. 2018. α-Synuclein accumulation and GBA deficiency due to L444P GBA mutation contributes to MPTP-induced parkinsonism. *Molecular neurodegeneration,* 13**,** 1-1.

ZHANG, C. K., STEIN, P. B., LIU, J., WANG, Z. H., YANG, R. H., CHO, J. H., GREGERSEN, P. K., AERTS, J. M. F. G., ZHAO, H. Y., PASTORES, G. M. & MISTRY, P. K. 2012. Genome-wide association study of N370S homozygous Gaucher disease reveals the candidacy of CLN8 gene as a genetic modifier contributing to extreme phenotypic variation. *American Journal of Hematology,* 87**,** 377-383.

ZHANG, W., WANG, T., PEI, Z., MILLER, D. S., WU, X., BLOCK, M. L., WILSON, B., ZHANG, W., ZHOU, Y., HONG, J. S. & ZHANG, J. 2005. Aggregated alpha-synuclein activates microglia: a process leading to disease progression in Parkinson's disease. *FASEB J,* 19**,** 533-42.

ZHANG, X. F., YANG, G. Y., ZHANG, Y., XIE, Y., WITHERS, S. G. & FENG, Y. 2016. A general and efficient strategy for generating the stable enzymes. *Sci Rep,* 6**,** 33797.

ZHANG, Y., SUN, Q. Y., ZHAO, Y. W., SHU, L., GUO, J. F., XU, Q., YAN, X. X. & TANG, B. S. 2015. Effect of GBA Mutations on Phenotype of Parkinson's Disease: A Study on Chinese Population and a Meta-Analysis. *Parkinsons Dis,* 2015**,** 916971.

ZHAO, F., BI, L., WANG, W., WU, X., LI, Y., GONG, F., LU, S., FENG, F., QIAN, Z., HU, C., WU, Y. & SUN, Y. 2016. Mutations of glucocerebrosidase gene and susceptibility to Parkinson's disease: An updated meta-analysis in a European population. *Neuroscience,* 320**,** 239-46.

ZHAO, Y., REN, J., PADILLA-PARRA, S., FRY, E. E. & STUART, D. I. 2014. Lysosome sorting of β-glucocerebrosidase by LIMP-2 is targeted by the mannose 6-phosphate receptor. *Nature Communications,* 5**,** 4321.

ZHENG, H., XIE, Z., ZHANG, X., MAO, J., WANG, M., WEI, S., FU, Y., ZHENG, H., HE, Y., CHEN, H. & XU, Y. 2021. Investigation of alpha-Synuclein Species in Plasma Exosomes and the Oligomeric and Phosphorylated alpha-Synuclein as Potential Peripheral Biomarker of Parkinson's Disease. *Neuroscience,* 469**,** 79-90.

ZIEGLER, S. G., EBLAN, M. J., GUTTI, U., HRUSKA, K. S., STUBBLEFIELD, B. K., GOKER-ALPAN, O., LAMARCA, M. E. & SIDRANSKY, E. 2007. Glucocerebrosidase mutations in Chinese subjects from Taiwan with sporadic Parkinson disease. *Mol Genet Metab,* 91**,** 195-200.

ZIMMER, K. P., LE COUTRE, P., AERTS, H. M., HARZER, K., FUKUDA, M., O'BRIEN, J. S. & NAIM, H. Y. 1999. Intracellular transport of acid beta-glucosidase and lysosome-associated membrane proteins is affected in Gaucher's disease (G202R mutation). *J Pathol,* 188**,** 407-14.

ZIMRAN, A., ALTARESCU, G. & ELSTEIN, D. 2013. Pilot study using ambroxol as a pharmacological chaperone in type 1 Gaucher disease. *Blood Cells Mol Dis,* 50**,** 134-7.

ZUNKE, F., MOISE, A. C., BELUR, N. R., GELYANA, E., STOJKOVSKA, I., DZAFERBEGOVIC, H., TOKER, N. J., JEON, S., FREDRIKSEN, K. & MAZZULLI, J. R. 2018. Reversible Conformational Conversion of α-

Synuclein into Toxic Assemblies by Glucosylceramide. *Neuron,* 97**,** 92-107.e10.